This document is:

Ikegami, H., ed. *Third International Conference on Cold Fusion, "Frontiers of Cold Fusion"*. 1992, Universal Academy Press, Inc., Tokyo, Japan: Nagoya Japan. 698.

The printed book is in one volume, but this version has been split into two parts to facilitate downloading.

This is Part 1, title page to page 252:

http://lenr-canr.org/acrobat/IkegamiHthirdinter.pdf

Part 2, page 253 to page 698, is here:

http://lenr-canr.org/acrobat/IkegamiHthirdintera.pdf

FRONTIERS SCIENCE SERIES NO. 4

Proceedings of the Third International Conference on Cold Fusion

Frontiers of Cold Fusion

October 21 – 25, 1992
Nagoya, Japan

Edited by
H. Ikegami
National Institute for Fusion Science, Japan

Universal Academy Press, Inc.
Tokyo, Japan

Universal Academy Press,Inc.
International Publishers in Science & Technology
Publishing Tomorrow's Technologies Today


The Third International Conference on Cold Fusion
October 21-25, 1992, Nagoya, Japan

Frontiers of Cold Fusion

Proceedings of the Third International Conference on Cold Fusion
October 21 – 25, 1992, Nagoya, Japan

Edited by H. Ikegami

Frontiers Science Series No. 4 (FSS-4)
ISSN 0915-8502

Published by
Universal Academy Press, Inc.

Postal Address: C.P.O. Box 235, Tokyo 100-91, JAPAN
Address for Visitors: BR-Hongo-5 Bldg., 6–16–2, Hongo, Bunkyo-ku, Tokyo 113, JAPAN
Telephone: + 81 3 3813 7232
Facsimile: + 81 3 3813 5932

ISBN 4-946443-12-6

Printed in Japan

Preface

These proceedings of the Third International Conference on Cold Fusion (ICCF3), Frontiers of Cold Fusion, document the beginning of a new field of science, now in its fourth year. The five-day conference, held in Nagoya, Japan at the Nagoya Congress Center, from October 21 through 25, 1992, was the third such affair. In 1990, the first cold fusion conference took place in Salt Lake City, Utah, in the United States and the second, in 1991 was held in Como, Italy. A comparison of the proceedings from these conferences, shows that not only is evidence for the existence associated to cold fusion, unassailable, but that there are now substantial interdisciplinary research efforts in many countries, probing cold fusion phenomena in depth.

In planning ICCF3, the Organizing Committee sought to cover the broadest topics relevant to this new research field, including nuclear physics, electrochemistry, solid state physics, and materials science, so that this conference was cosponsored by the Physical Society of Japan, the Japan Society of Applied Physics, the Atomic Energy Society of Japan, the Institute of Electrical Engineers of Japan, the Chemical Society of Japan, the Electrochemical Society of Japan, and the Japan Society of Plasma Science and Nuclear Fusion Research.

Aside from press and other visitors, there were 346 registered participants at the Conference from 18 countries. Of course, the largest number, 229, was resident in Japan. One hundred and forty-eight abstracts were originally submitted, of which 137 were presented at poster sessions.

At the Conference, there were 27 invited lectures and three panel discussions, incorporating comments from the International Advisory Committee. The first panel, on the Takahashi Method, included several scientists who successfully replicated Takahashi's experiment, and one who could not. The second panel was on the Theoretical Models, and included a broad diversity of opinion, including differences on whether the production of excess heat is nuclear or not, and whether "cold fusion" is actually a fusion event, or reflects some other process. The concluding session, addressed the question of the Next Step for the direction of researches in this new field.

The Conference was organized to allow maximum time at poster sessions for small group's discussions on every poster paper, which included additional discussion time even for those already presented orally in the plenary sessions, while some would have still preferred more discussions at the oral sessions. It was clear to me, as the Chairman of the Organizing committee, that the heated discussion which occurred during the conference could have continued for longer than one week.

The proceedings consist of two parts: one for the invited papers and the other for the contributed papers. For purposes of publication, the format has been changed to reflect the subject under discussion, rather than the order of the presentations at the Conference. The number of papers contained in the proceedings, is in total, 102 out of the 148 abstract titles as listed in the program.

It was not an easy task to peer review each of the submitted papers to this Conference. The editorial board of the Organizing Committee accepted a lenient standard for publication. Most papers presented at the Conference were accepted so long as they satisfied a minimum standard. Sixteen papers, though submitted, were either not presented at the Conference, or withdrawn thereafter, and these were not published. Their titles, however, have been left in the attached program, with an asterisk to denote this. Likewise, other 30 titles, for which the Secretariat did not receive papers before the publication deadline, are marked with a dagger (†).

At the Conference, the video produced by Drs. Fleischmann and Pons allowed us to see that a controllable excess heat generator was already in hand. These remarkable results were confirmed thanks to the efforts of Dr. McKubre, Dr. Takahashi, Dr. Kunimatsu and Dr. Storms, who along with Drs. Fleischmann and Pons, reported on their work at the Conference and offered extensive documentation of their experiments.

Positive heat results were also presented on several light water experiments, which may be closely related to the mechanisms of excess heat generation that we see in heavy water experiments.

There is still no evidence to prove that the heat produced is nuclear in origin. The participation of main-line scientists who are not themselves working in this field, is indispensable in stimulating discussions and exchanging ideas. For this reason we found the critical contributions by Dr. Fukai at the Conference to be of great value.

A number of still indefinite but important new results were reported at the Conference, to do with the detection of nuclear products from "cold fusion" cells. The most important among these, was the report by Drs. Yamaguchi and Nishioka, that they detected helium and energetic alpha particles, which may be a possible energy carrier for excess heat. Their results, along with other interesting nuclear experiments reported by Dr. Kasagi, and Drs. Iida and Takahashi, were extremely provocative in this regard. Whatever the relation of excess heat to the occurrence of nuclear reactions, nuclear events have been demonstrated and this raises the question for theorists, of what can explain them.

These findings are extremely important even though we do not yet understand what physics exists behind these phenomena. The one thing we can say positively, is that what we have here is no ordinary nuclear reaction. Many theorists are now trying to find mechanisms that will allow them to avoid any direct handling of the coulomb barrier. What is being created is an entirely new field of research from that of traditional nuclear sciences. Probably we should no longer call this field "cold fusion," but "fusion in solid state."

It is my belief that cold fusion will become one of the most important subjects in science, one for which we have been working so patiently, with dedication and with courage, for future generations, for those who will live in the twenty-first century. In order to achieve our goal, our ultimate goal, we must continue and extend our interdisciplinary and international collaboration.

We regret deeply the untimely death of Dr. Andrew Riley of SRI International. Recently one of the most generous sponsors of our work, Mr. Minoru Toyoda passed away. At the banquet held during the Nagoya Conference, Mr. Toyoda expressed the philosophy that led him to promote cold fusion as a science. I would like to cite the last part of his message. There he said, "Cold fusion is not a matter to be studied by one single enterprise or nation. I have confidence that it will become the greatest asset as an eventual energy for mankind, to be shared among the world." This is our dream, our common understanding and the reason why we are so intensely and patiently working on cold fusion.

I would like to take this opportunity to express my sincere gratitude to the members of the International Advisory Committee and the Organizing Committee, and to all of those who participated in the Conference. It was their cooperation that made the Conference so fruitful. On behalf of the Organizing Committee, I would like to thank the Japan Society for the Promotion of Science and all the contributors for their generous financial support. I would particularly like to express my deep appreciation to Mr. Koichi Takashima, President of Kyoei Steel Ltd. for his extremely generous contribution to this Conference.

It is also my privilege to thank the Tokyo Club for the full support which they gave to the publication of these proceedings, Frontiers of Cold Fusion.

Finally I thank Miss S. Saito and Mrs. M. Tsubaki for their dedicated work for the Conference on behalf of the Secretariat . They not only helped to make the Conference itself successful, but they were active in forwarding the arrangements for this publication.

Hideo Ikegami, Editor
National Institute for Fusion Science
March 1993

Contents

Nuclear Products

Materials and Hydrogen Behavior

Theory and Modeling

Activity Review

II Contributed Papers

Chapter I : Excess Heat

Chapter II : Nuclear Products

Chapter III : Materials and Hydrogen Behavior

Chapter IV : Theory and Modeling

I. Invited Papers

Excess Heat

Excess Power Observations in Electrochemical Studies of the D/Pd System; the Influence of Loading

M. C. H. McKUBRE, S. CROUCH-BAKER, A. M. RILEY,
S. I. SMEDLEY and F. L. TANZELLA

Energy Research Centre,
SRI International,
Menlo Park, CA 94025
U. S. A.

ABSTRACT

Excess power measurements have been carried out on a deuterium-based electrochemical system of novel design. The excess power generation is reported as a function of electrochemical current and cathode loading. A phenomenological model for excess power production is introduced and briefly discussed.

INTRODUCTION

An experimental programme was undertaken to test the hypothesis that anomalous thermal processes occur when deuterium is loaded by electrochemical means into palladium to high atomic (*D / Pd*) ratios. Based on calorimetric results obtained to date,[1-3] it appears that one criterion (amongst others) for the observation of anomalous power generation is the attainment of average deuterium loadings of approximately 0.9 or greater. In view of the importance attached to the loading-related aspects of excess power production, a considerable amount of effort has been expended thus far on the characterization of the kinetic features of the loading process and means to achieve, maintain and measure *in situ* high deuterium loadings. Some aspects of these studies have been reported previously;[4] additional aspects are discussed further below.

FRONTIERS OF COLD FUSION

Here, the results of calorimetric measurements on an electrochemical cell of novel design are reported. These results enable apparent correlations to be established between the excess power generation, the electrochemical current and the average deuterium loading. These correlations are discussed in terms of the phenomenological model for excess power generation introduced previously [2,3].

EXPERIMENTAL METHODS

Maintenance of high deuterium loading

The ability to maintain a high steady-state loading is determined essentially by the extent to which the rates of the reactions which lead to the loss of deuterium from the cathode can be suppressed. Important in this regard is the imposition of a uniform current density distribution over as much of the cathode surface as practical. This is partly achievable with suitable cell design; in particular, appropriate relative cathode / anode disposition. In addition, the production of cracks on the cathode surface (either directly or via the expansion of internal voids) inevitably leads to a disruption of the local current density and loss of deuterium. Thus processes likely to result in cracking, for example repeated cycling through the α / β phase transition in the case of palladium, should be avoided.

Classically, a number of so-called "recombination poisons" (typically, sulphur-containing compounds, e.g. thiourea) have been employed to retard the rate of gaseous hydrogen evolution from the cathode surface, and thereby enhance the net loading rate. However, such electrolyte additives have little effect on the maintenance of high loadings due to their volatility or electrochemical decomposition over long time-periods. As a possible solution to this problem, we have observed that the addition of small amounts (typically 200 ppm) of non-classical additives, such as aluminium or silicon (in metallic and oxide form, respectively), to the electrolyte, results in the ability to maintain high loadings for longer periods, without impeding the initial attainment of high loadings. In this context, it should be mentioned that, in cells which utilize glass components, silicon-containing species will accumulate in basic electrolytes over extended time-periods.

Electrochemical cell design

The following cell design, Figure 1, was employed in this study. The cell body was made of stainless steel for convenience in manufacture and to ensure good thermal contact between the cell and the heat transfer fluid. A PTFE liner was employed in order to prevent the highly corrosive electrolyte, 1 M LiOD + 200 ppm Al, from making contact with the metal cell body.

Two concentric-cylinder palladium sheet anodes were used. These were 25 μ thick, approximately 5 cm high, 2 and 4 cm diameter, respectively. A 1 mm diameter vacuum-annealed palladium wire cathode, approximately 45 cm long (with 36 cm submerged in the electrolyte), was secured by four PTFE pegs from below and mounted between the concentric anodes in the manner shown in Figure 1. The anodes were mounted between two parallel PTFE plates which were themselves held in position by a PTFE pillar placed inside the inner anode, and a series of PTFE posts placed outside the outer anode.

Recombination of the evolved deuterium and oxygen was achieved using porous, platinum coated alumina spheres held within a wide-mesh platinum cage. The cage was suspended below a PTFE plate at the top of the cell. The collapse of deuterium and oxygen bubbles above the electrolyte surface projects liquid a considerable vertical distance during the operation of the cell at high current. In the absence of suitable precautions, the head space of the cell would fill with LiOD-saturated mist, possibly affecting the recombiner function. In order to prevent this, a PTFE cone was mounted between the electrodes and the recombiner. The center of the cone was removed and a static mixer inserted in order to remove LiOD-containing droplets from the gas stream reaching the recombiner. Small holes were drilled in the periphery of the cone in order that recombined D_2O could drip back into the electrolyte.

A pressure pipe connected the inside of the cell to a pressure transducer mounted above the calorimeter. The cell body was sheathed with a brass cylinder containing a resistive heater. In order to ensure good thermal contact with the calorimetric fluid, cooling fins were brazed to the outside of the brass cylinder.

Once assembled, approximately 200 cm^3 of electrolyte was added to the cell, reaching a level just below the bottom of the PTFE cone. The residual head-space within the cell was approximately 100 cm^3.

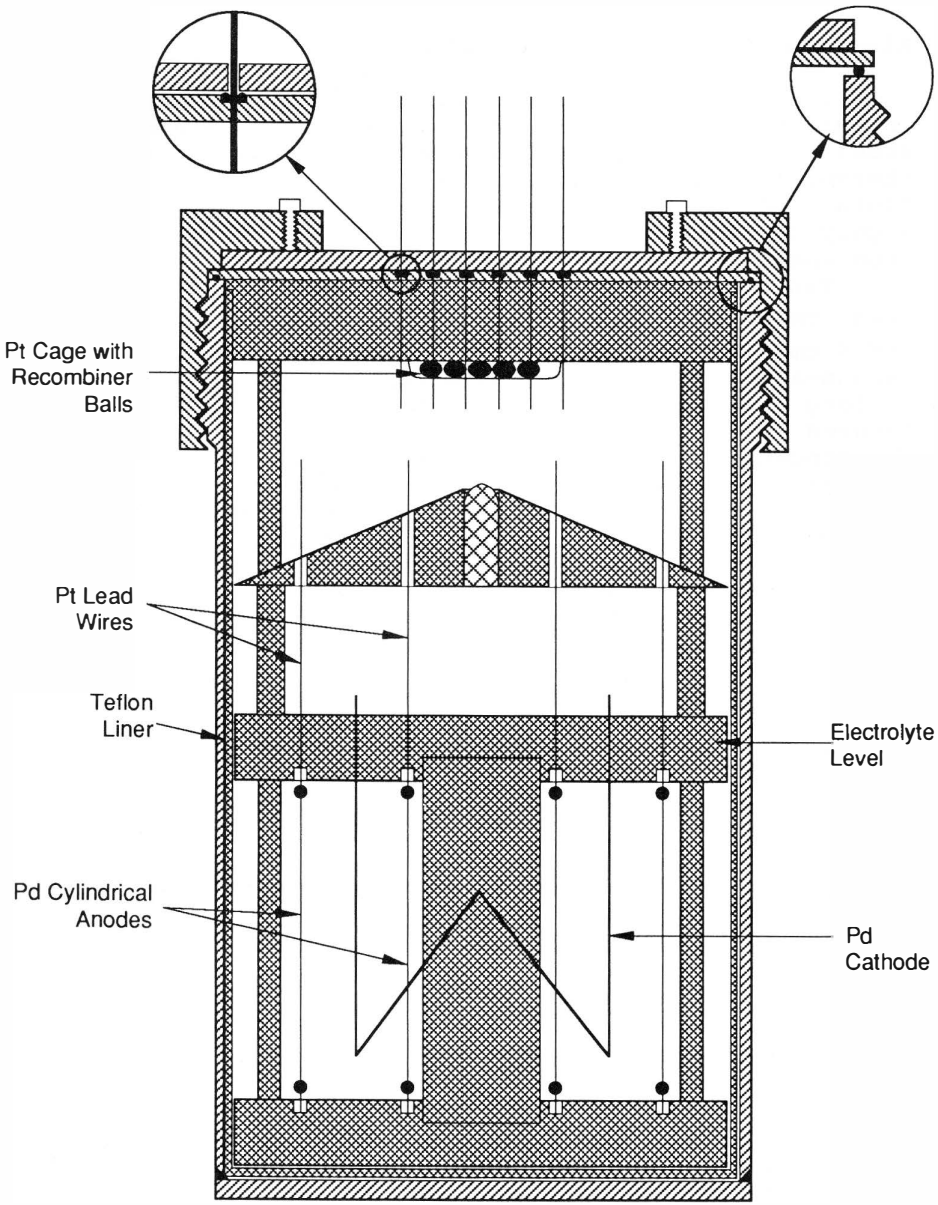

Fig. 1. Electrochemical cell design

Initially, before sealing, the cell was filled with deuterium gas at approximately 1 atm pressure.

Calorimetry

The electrochemical cell described above was contained within a mass flow calorimeter, Figure 2, the design and operation of which have been described previously.[2,3] Briefly, the calorimeter consisted of an approximately adiabatic enclosure - comprised largely of a silvered, evacuated Dewar - which contained the electrochemical cell and through which the calorimetric fluid (water) was pumped. The calorimeter was situated in a constant temperature bath, maintained at 30 ± 0.003°C, which also served as the source of the calorimetric fluid. The mass flow rate of the calorimetric fluid was determined gravimetrically, using an auto-siphon device mounted on an electronic balance, after passing through the calorimeter. The internal heater, described above, permitted operation at constant total input power, so as to maintain approximately constant the mean electrochemical cell temperature. The power output from the calorimeter was determined essentially by the mass flow rate, the change in the temperature of the calorimetric fluid on its transit through the calorimeter, and a power loss term, discussed further below. Experimental control and data acquisition were achieved with a Macintosh microcomputer.

Data analysis

The difference between the output power and the power input to the calorimeter (both electrochemical and heater) may be referred to as an "excess power", P_{xs}. For the calorimetric system employed here, this quantity is given by

$$P_{xs} = (C_p \frac{\delta m}{\delta t} + k') (T_{out} - T_{in}) - P_{el} - P_h$$

where C_p is the heat capacity of water, $\delta m / \delta t$ the mass flow rate, T_{out} the outlet temperature of the calorimetric fluid, T_{in} the corresponding inlet temperature, P_{el} the input electrochemical power and P_h the input heater power. The power loss term k' is retained in order to account for the fact that the adiabatic calorimeter boundary is inevitably imperfect, and some conductive heat loss is expected. The methods employed both for the determination of k' at the outset

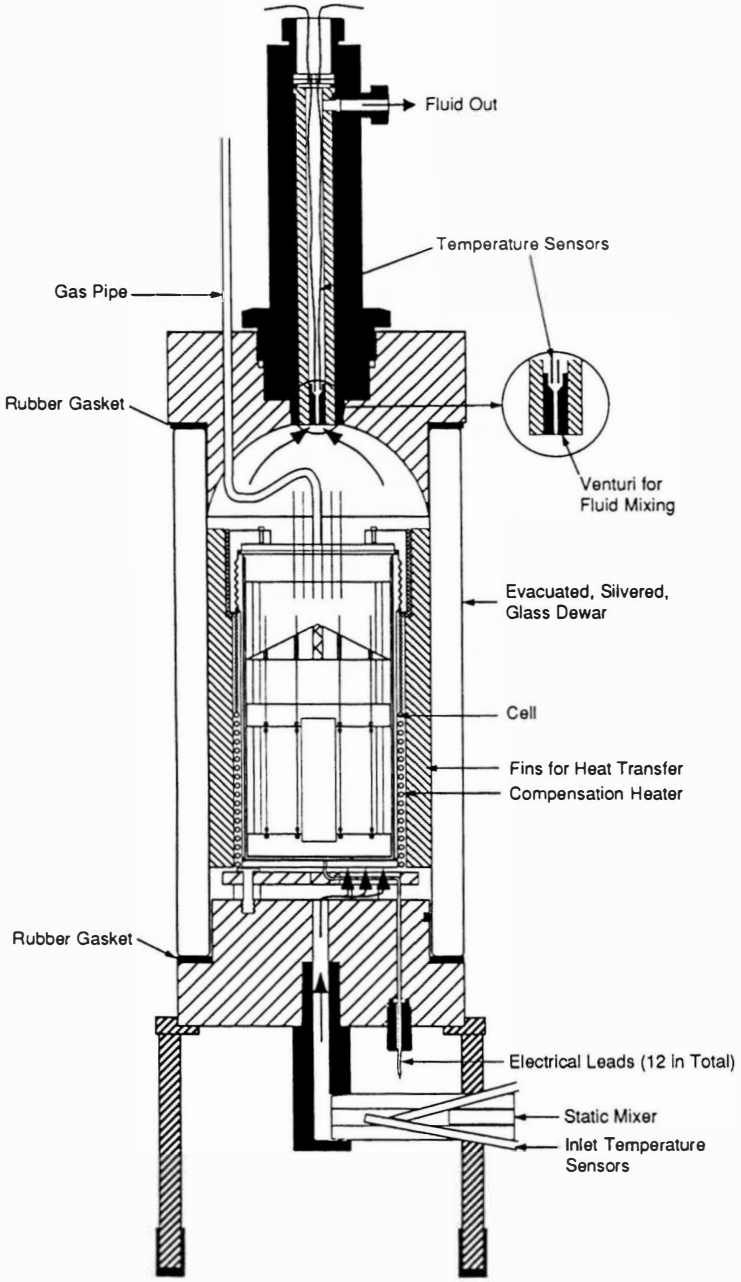

Fig. 2. Calorimeter containing electrochemical cell

of an experiment, and for the confirmation of its constancy during the course of an experiment, have been described.[2,3] Similarly, the exact means employed for the measurement of the other quantities in the above equation, and the steps taken to reduce systematic errors in their respective measurements, have been discussed [2,3]. The measurement uncertainty in the excess power, treated as an example of a single-sample measurement,[5] was calculated as described previously[3] and is quoted (approximately) at the 95% confidence level ($\pm$ 2 σ).

RESULTS

Electrochemical and calorimetric data for the experiment described here during the time period 300 - 780 h are presented in Figures 3 to 5. Prior to 300 h, either statistically significant quantities of excess power were not produced, or complete calorimetric data were not obtained (due to a bath malfunction). For the calorimeter employed in this experiment, k' was 0.46 $\pm$ 0.05 W K^{-1}. Figure 3 shows the variation of input electrochemical and heater powers, and the resulting total input power. Figure 4 describes the measured cell voltage and the electrochemical current during the time period 300 - 780 h. Note that a cell current of, for example, 5 A is equivalent to a current density of 0.44 A cm^{-2}. The calculated excess power with its associated measurement uncertainty and the average cathode loading are shown in Figure 5. Figures 6 and 7 depict the variation of excess power with electrochemical current and average cathode loading, respectively.

DISCUSSION

During the time period of interest, excess power up to approximately 1.2 W was produced. Although significant with respect to the measurement uncertainty, the excess power in this particular experiment was relatively small, in particular when compared to the total input power. The excess energy produced *during the time period of interest* was 1.2 $\pm$ 0.3 MJ or approximately 4.3 MJ cm^{-3} of palladium cathode. During this period, the total input electrochemical and heater energies were 36.3 $\pm$ 0.07 and 12.6 $\pm$ 0.03 MJ, respectively.

In common with previous experiments,[2,3] the excess power production observed here appears to conform to a certain phenomenology, discussed below. In addition,

Fig. 3. Variation of input powers with time

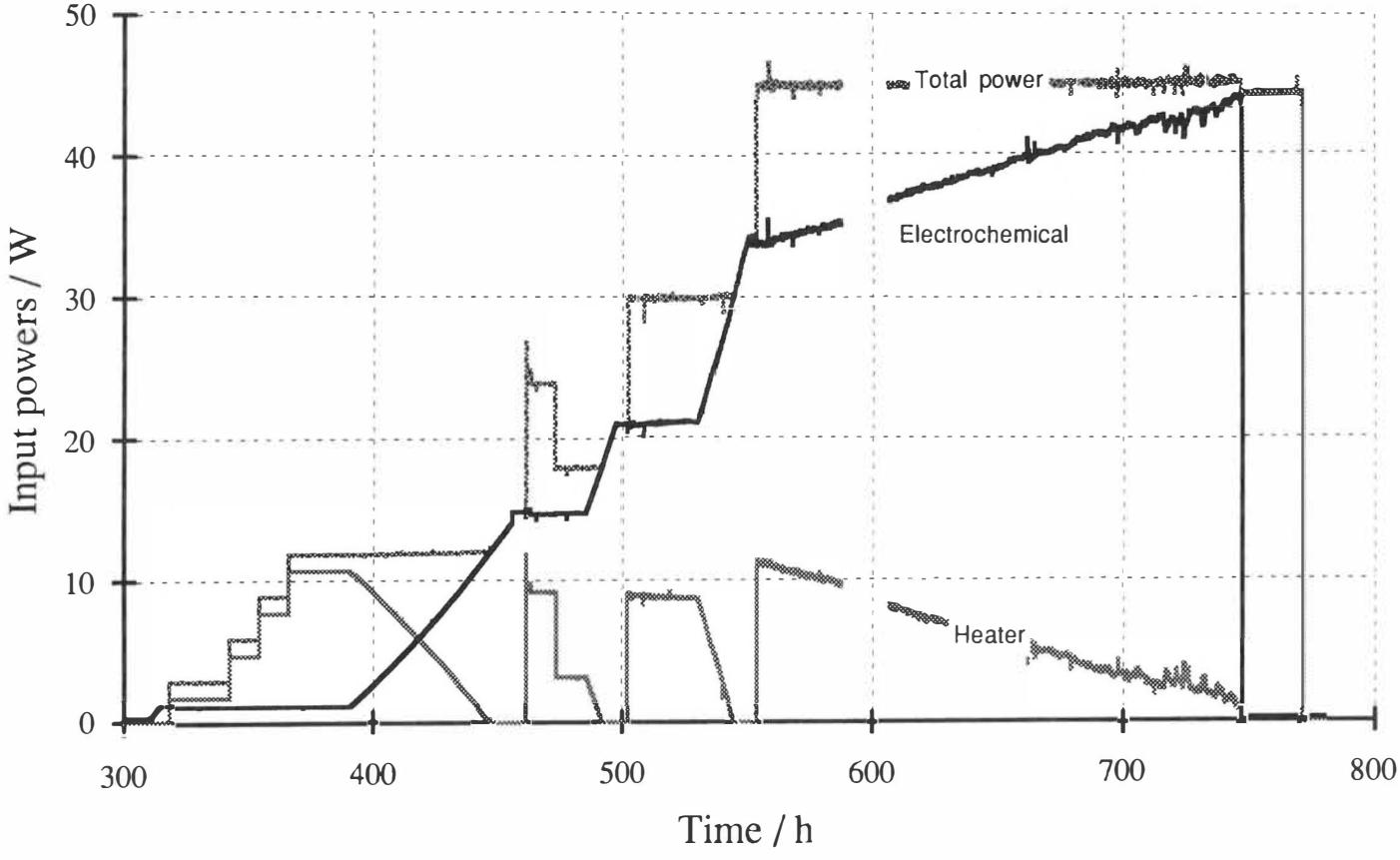

Fig. 4. Variation of cell voltage and current with time

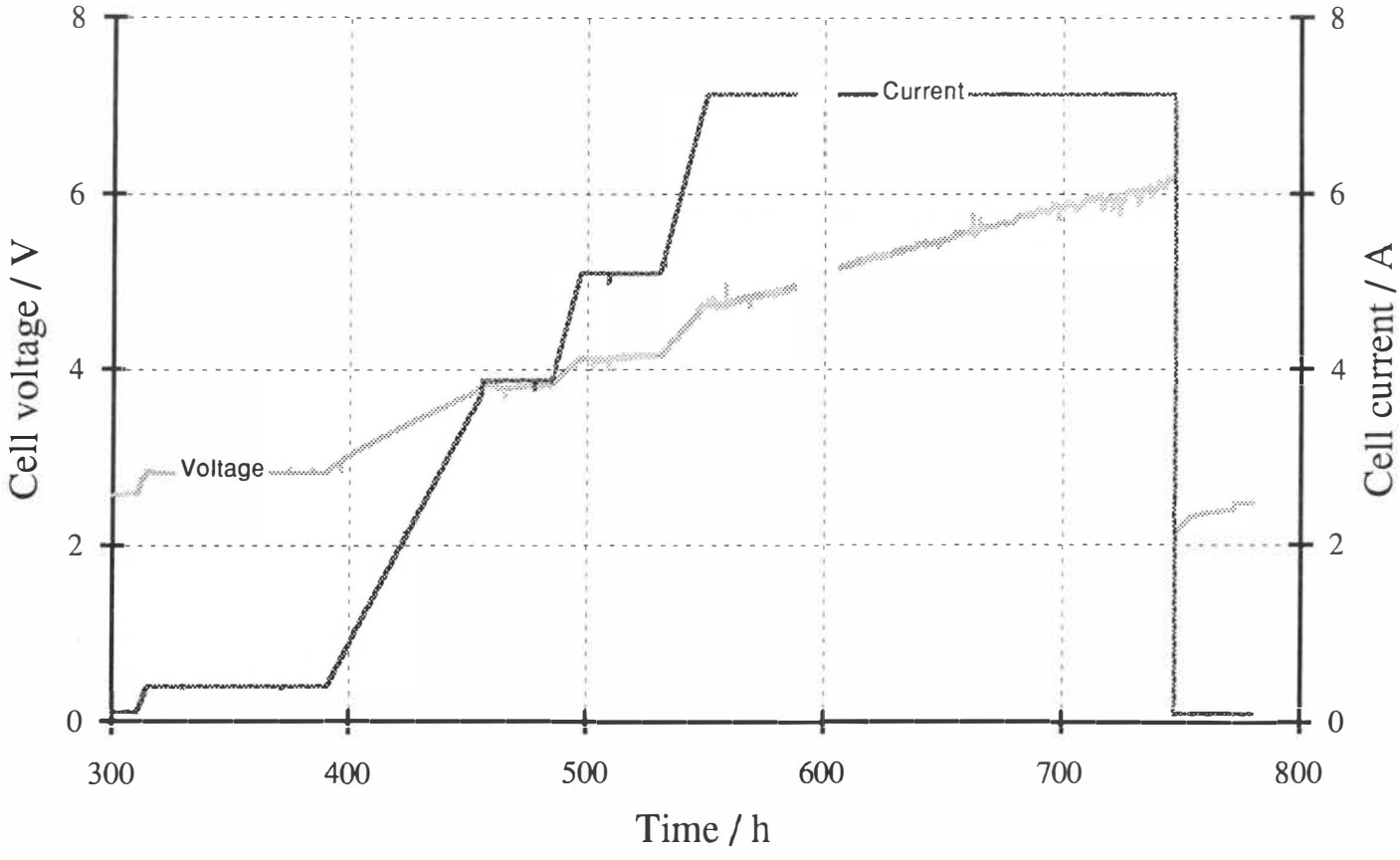

Fig. 5. Variation of excess power, uncertainty and loading

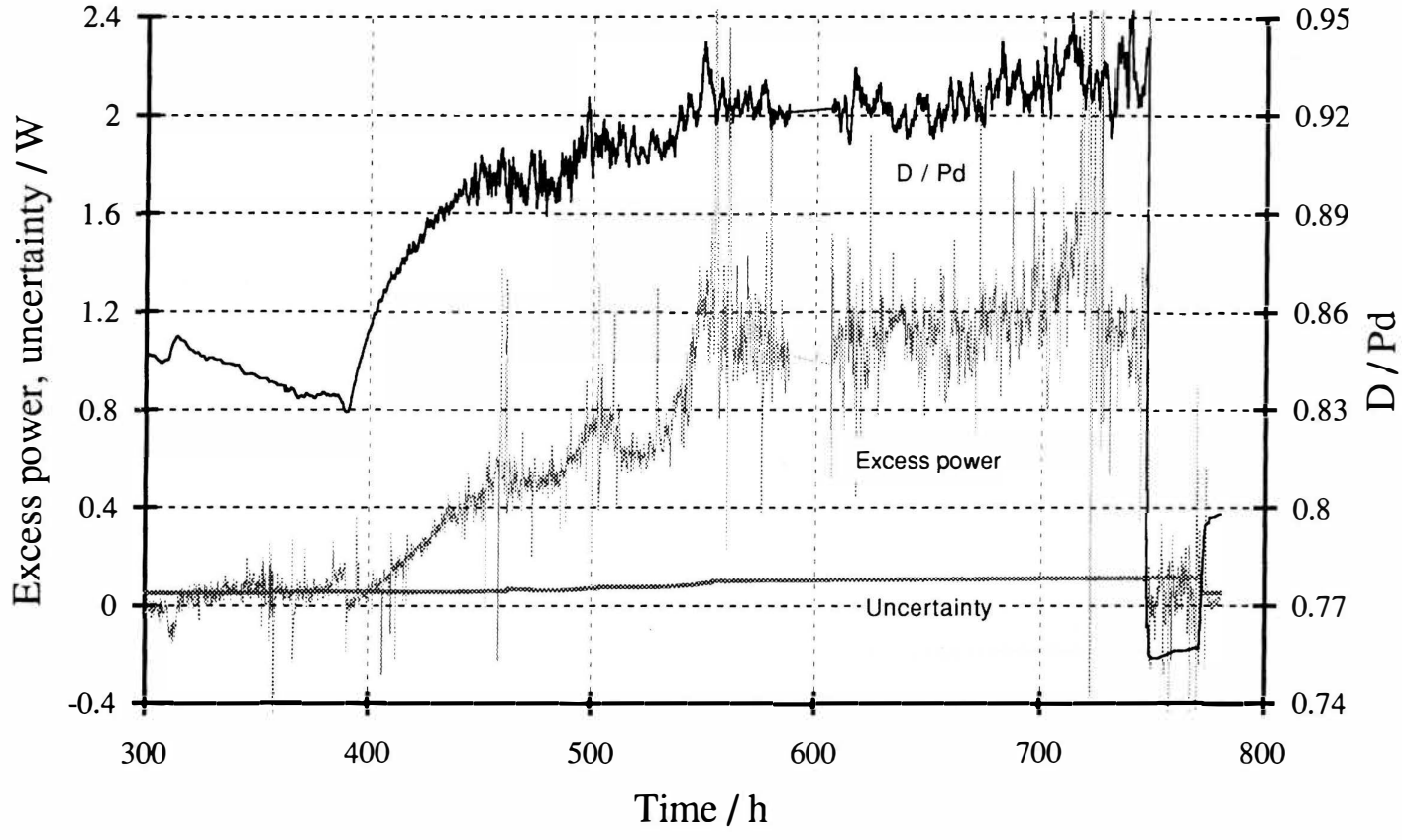

Fig. 6. Variation of excess power with cell current

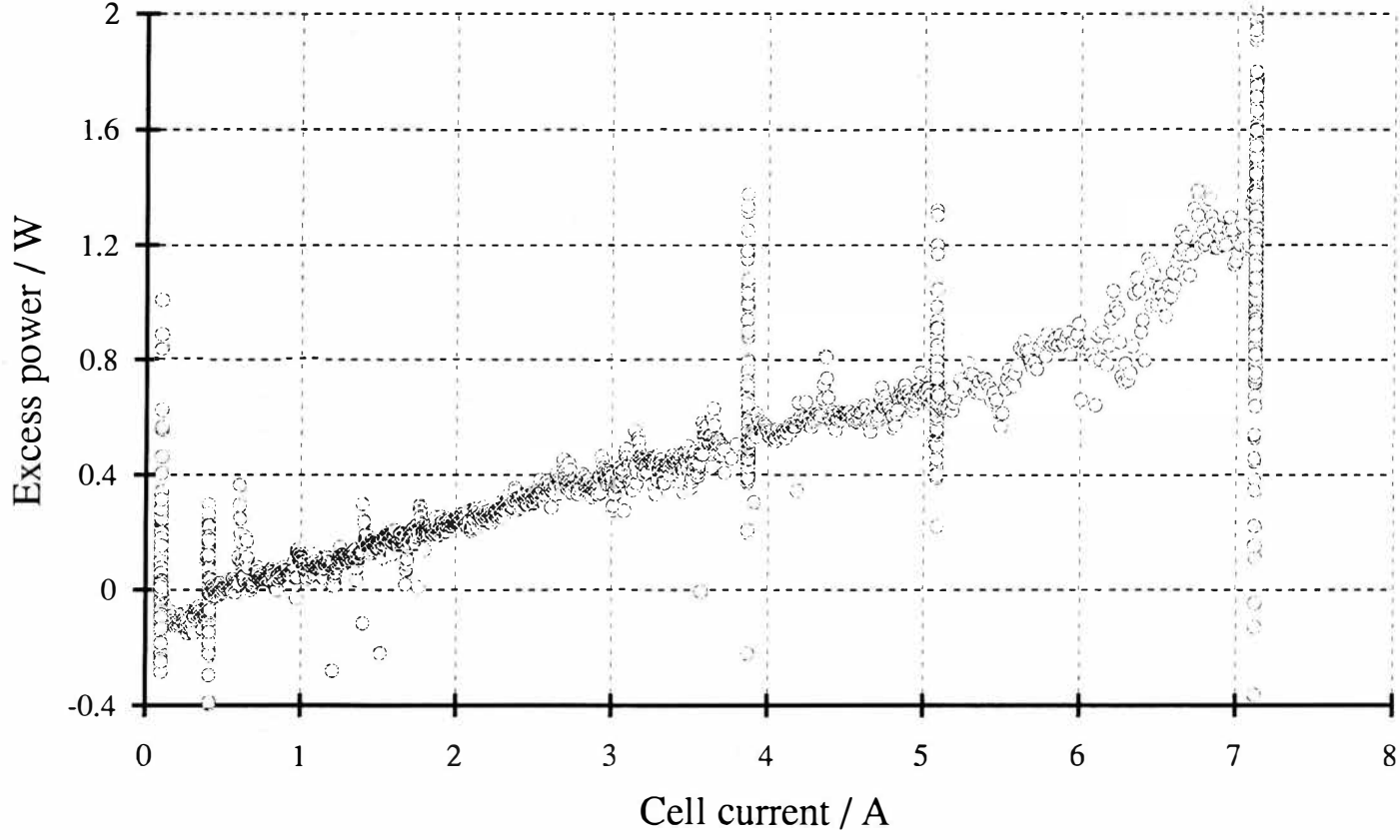

Fig. 7. Variation of excess power with loading

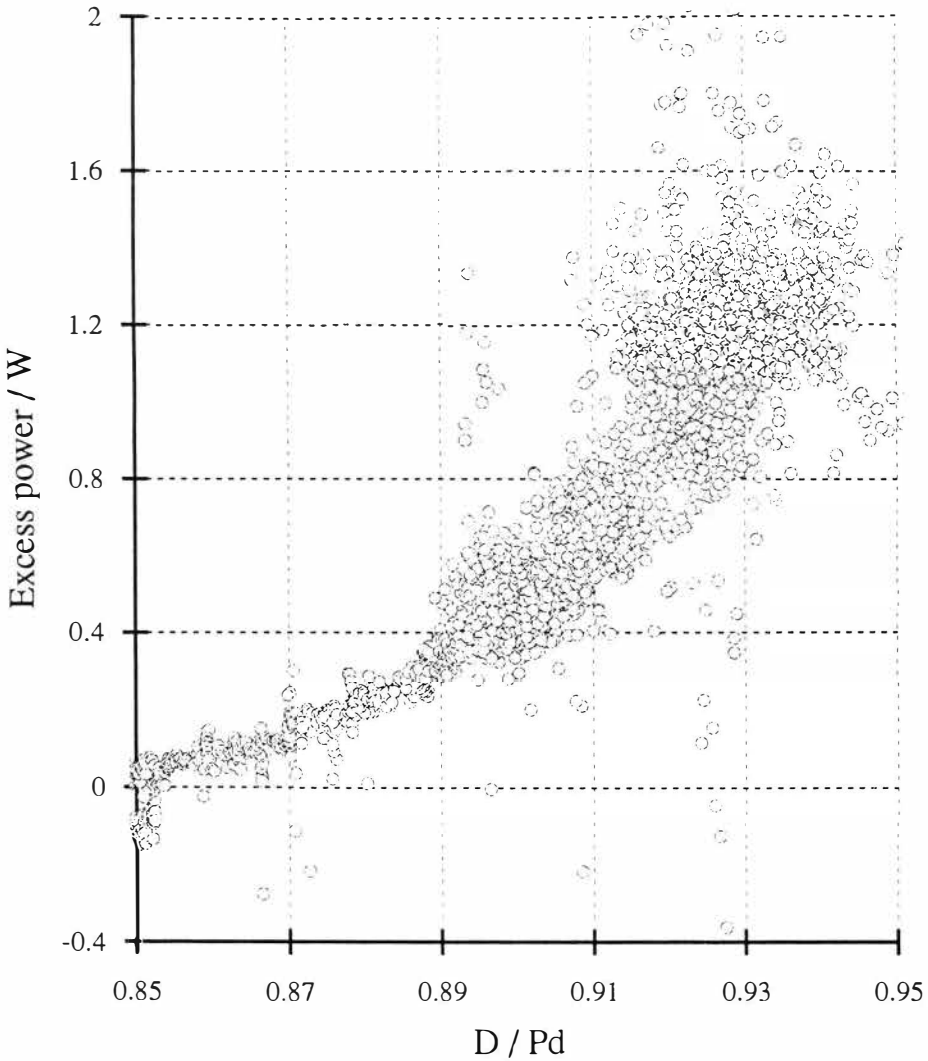

for the experimental configuration utilized here, the excess power is observed to vary systematically with current and in an second order manner (approximately) with average loading, above a loading threshold.

Using a different calorimetric system, a higher than first order dependence has been reported previously[6] for the variation of excess power with electrochemical current. An important distinction between this previous study and the results reported here is that, in the former case, the calorimetric system was not operated, as here, at constant total input power with an efficient heat removal mechanism, thereby ensuring an approximately constant mean cell temperature. Instead the system was operated at constant electrochemical current in a heat-retaining calorimeter design, thereby forcing the mean cell temperature to increase with increasing current. Clearly, further work is required in order to elucidate the nature of this apparent temperature dependence of the excess power. The approximately quadratic dependence of excess power on average cathode loading reported here serves to reinforce the remarks made above concerning the need for care in cell design and operation, if high loading are to be realized. At present, since the origin of the excess power production phenomenon in electrochemical systems utilizing deuterated palladium cathodes is unknown, the significance, if any, of the data in Figure 7, remains unclear. The data are, nonetheless, intriguing.

Phenomenological model

Based on our calorimetric studies carried out to-date, we may construct a phenomenological model for excess power production from deuterium-based electrochemical systems employing palladium cathodes. For an (initially) unalloyed cathode, the following three factors (at least) are associated with the observation of excess power production: i) The average cathode loading should exceed (approximately) 0.9; ii) an initiation time (typically, several hundred hours) is required which is long when compared with the time required for initial deuterium loading; iii) changes in the excess power level are usually associated with departures from the electrochemical steady-state, caused primarily by varying the current. Although the mechanistic significance, if any, and interdependence of these factors are presently unknown, the following supplementary, necessarily somewhat speculative, suggestions may be noted:

Firstly, due to current density inhomogeneities on the cathode surface, it is likely that regions exist within the cathode where the loading exceeds the average value, perhaps significantly. Thus, it may be possible for the local loading, in certain regions, to approach unity in a cathode with a high average loading. In this connection, the development of new methods to further increase and maintain loading may be important. In addition, techniques for the accurate characterization of loading inhomogeneities may prove useful.

In the studies carried out here, the cathode dimensions were such that deuterium loading was achieved on the time-scale of hours, certainly much sooner than the several hundred hours required for the production of excess power. This observation raises the interesting possibility that one or more species, other than deuterium, are required to be present in the cathode in order to observe excess power, species which are not present initially and are thus required to diffuse into the cathode, presumably from the electrolyte. Analyses of used cathodes have revealed the presence of several light elements in the near-surface region (to a depth of several microns); in particular, lithium. Clearly, calorimetric experiments involving the use of selectively pre-alloyed cathodes are of interest.

For a cathode initially in the steady-state (with respect to loading), a departure from this state will lead to the modification of the deuterium fluxes within the electrode. Since it has been observed that excess power levels generally increase with increasing current density, the possible role of the interplay between the ionic and electronic fluxes within the metal merits consideration, particularly with respect to its influence on the (local) loading.

In order to understand the origin and/or mechanism of the excess power phenomenon, it is clearly essential to identify either the fuel(s) or the product(s) (preferably both) of the energy producing process, assuming, for the moment, that it is non-artifactual in nature. This task is made easier if the excess power (and, hence, the integrated excess energy) levels are caused to increase intensively. We are presently investigating the utilization of the phenomenological model described here, to achieve the intensive scale-up of the excess power effect.

Approximately 70 hours after the excess power event described here, an accident occurred which caused termination of the experiment. The cause of this accident is discussed in a paper published elsewhere in these Proceedings.

ACKNOWLEDGEMENT

We gratefully acknowledge the financial support of the Electric Power Research Institute.

REFERENCES

1. M. C. H. McKubre, R. C. Rocha - Filho, S. I. Smedley, F. L. Tanzella, J. Chao, B. Chexal, T. O. Passell and J. Santucci, in *Proceedings of the First Annual Conference on Cold Fusion,* National Cold Fusion Institute, Salt Lake City, p. 20 (1990).

2. M. C. H. McKubre, R. C. Rocha - Filho, S. I. Smedley, F. L. Tanzella, S. Crouch - Baker, T. O. Passell and J. Santucci, in *The Science of Cold Fusion*, eds. T. Bressani, E. Del Giudice and G. Preparata, Conference Proceedings Vol. 33, Italian Physical Society, Bologna, p. 419 (1992).

3. M. C. H. McKubre, S. Crouch - Baker, R. C. Rocha - Filho, S. I. Smedley, F. L. Tanzella, T. O. Passell and J. Santucci, submitted to J. Electroanal. Chem.

4. M. C. H. McKubre, S. Crouch - Baker, A. M. Riley, R. C. Rocha - Filho, M. Schreiber, S. I. Smedley and F. L. Tanzella, in *Proceedings of the Symposium on Hydrogen Storage Materials, Batteries, and Electrochemistry,* eds. D. A. Corrigan and S. Srinivasan, Electrochemical Soc. Inc., p. 269 (1992).

5. S. J. Kline and F. A. McClintock, Mech. Eng., Jan. 1953; R. J. Moffat, J. Fluids Eng., 104 (1982) 253.

6. M. Fleischmann, S. Pons, M. W. Anderson, L. J. Li and M. Hawkins, J. Electroanal. Chem. 287 (1990) 293.

Measurement of Excess Heat from a Pons-Fleischmann Type Electrolytic Cell

Edmund STORMS

NMT Division, MS-C348, Los Alamos, National Laboratory,
Los Alamos, NM, 87545, USA

ABSTRACT

Two samples of Pd were obtained from Tanaka Kikinzoku Kogyo K. K. (Japan). One sample gave 20 % excess heat before the run was prematurely terminated and the other sample gave no excess heat. The sample giving excess energy contained only 0.8% excess volume while the nonproductive sample had 13.5 % excess volume.

The calorimeter is closed in an energy sense, pressured with D_2, and stirred. Calibration was done before, during and after heat measurement. Four different calibration procedures were used including a blank using a platinum cathode. Temperature gradients were monitored and found to change when excess heat was produced. This change strongly suggests that normal electrolysis releases energy mainly at the anode while excess heat is released mainly at the cathode. The bulk D/Pd ratio was measured during initial charging and was found to reach 0.82. Voltage difference between cathode and reference electrode was measured and indicates that the deuterium concentration gradient is small during initial charging at $0.02 A/cm^2$.

Excess volume in each palladium cathode was measured after each study. Heat production is proposed to be prevented if excess volume is too large.

FRONTIERS OF COLD FUSION

1. Introduction

A computer controlled, sealed, isoperibol-type calorimeter has been constructed and was used to study palladium sheets supplied by Tanaka Kikinzoku Kogyo K. K. (Japan). Single samples of palladium sheet from two different batches were studied[1].

Takahashi has reported[2] the production of excess power that exceeded 100 watts/cm^3 (average 1.7 x input power) from a Pons-Fleischmann-type electrolytic cell using similar material. In addition to this extraordinary energy production, low level neutron emission was measured that was roughly proportional to the magnitude of heat production when cell current was changed but decreased with time.

In addition to using this potentially unique palladium, Takahashi has suggested two procedures for success. The arrangement between the cathode and anode should produce uniform loading with deuterium, and the cathode should be subjected to periodic changes in cell current. He reports that excess energy increased with time when these procedures were used.

In addition to this recent success, excess heat production has also been reported by a significant number of studies[3] using a variety of procedures and calorimeter designs, and these studies found, in most cases, many positive results. Rods of palladium were studied in most of this work in contrast to the plate shaped cathode used here.

A calorimeter design having simplicity of operation and calibration was used in order to counter various objections raised by critics of similar measurements. Active stirring and temperature readings at two levels within the cell were used to eliminate the effect of possible temperature gradients. Four different calibration procedures were used and these were applied before, during and after the production of excess energy. The primary calibration used electrolytic heating of the LiOD electrolyte with a platinum cathode and anode. Except for chemical heat that might be associated with palladium, this method has the same bubble pattern, heat distribution and chemical effects within the electrolyte as would be found in the cold fusion cell. In addition, this method produced a similar calibration constant to that determined when "dead" palladium was used as the cathode. Consequently, most of the objections raised to discount excess heat production are eliminated because they are canceled out by the calibration procedure.

Because the calorimeter contained a recombiner, it could be completely sealed, pressurized with deuterium gas, and the internal pressure could be monitored. In this way, no material entered or left the cell under normal conditions. Significant excess heat was observed using these methods.

This work concentrates on the verification of excess heat and the measurement of various physical and chemical factors that are thought to be associated with excess energy production. No data or theories are pre-

sented about the possible source of heat or associated nuclear products other than to note that no tritium was produced.

2. Methods

2. A. Calorimeter

Figure 1 shows the cathode-anode assembly and Fig. 2 shows a cross-section of the closed, pyrex-glass calorimeter. A teflon plug is held into a standard taper by a spring that allows pressure release should the internal pressure rise above 1.5 atm. Tapered ports through this plug give access for various probes. The calorimeter is attached to a sealed gas handling system that maintains an overpressure of D_2 and allows the pressure to be monitored. An additional sheet of platinum (counter electrode) within the electrolyte provides means to calibrate the cell without disturbing the palladium and to conduct heat generated at the recombiner into the electrolyte. Later in the study, this feature was eliminated without producing a change in the calibration constant. The recombiner is carbon cloth impregnated with teflon and platinum. Active stirring by a teflon covered magnet is used.

Temperature is measured at two points in the surrounding constant temperature jacket and at two points within the interior of the cell, one near the top and the other at the bottom. The difference between the average of the two inner and the two outer temperatures is used to obtain the temperature difference across the glass wall of the cell. After calibration, this difference is used to determine total power production within the cell.

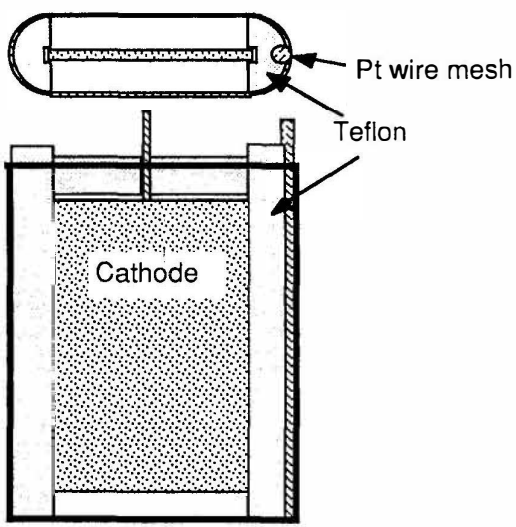

Figure 1. View of cathode-anode assembly.

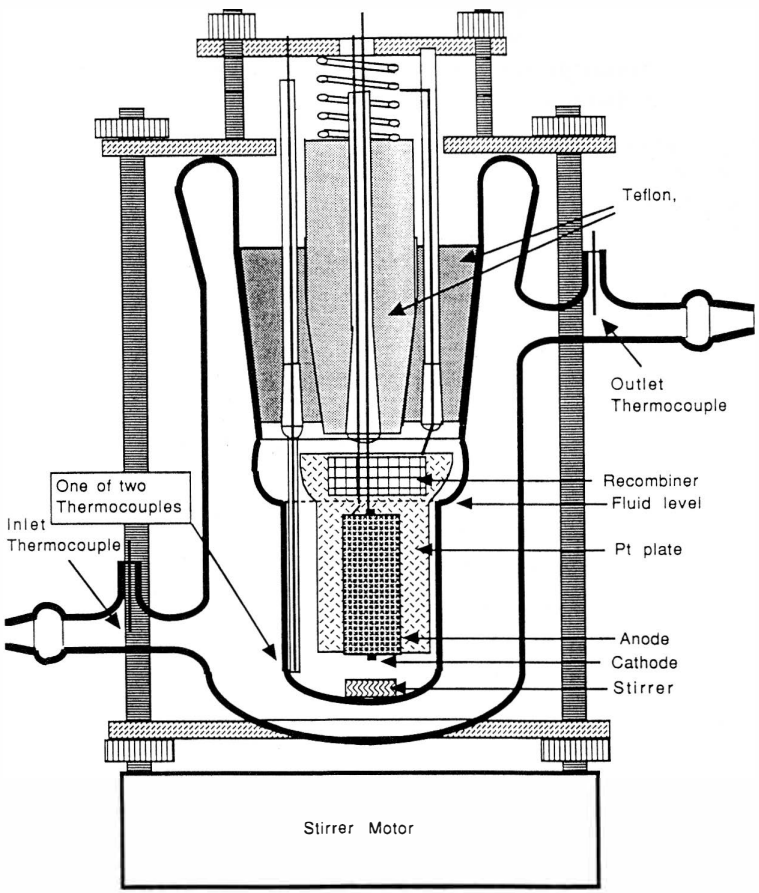

Figure 2. Cross-section of Calorimeter

Calibration is done using four methods.

1. Current is passed through an internal, glass covered, immersion heater to give simple joule heat,
2. A Pt sheet is substituted for the palladium cathode and electrolytic heat is created using the normal anode-cathode configuration.
3. Electrolytic current is passed between the normal Pt anode and a Pt sheet that holds the recombiner.
4. The current is cycled between two values over an extended period of time using either a Pt cathode or an inactive Pd cathode. This technique is called " bivalue" in subsequent discussion.

Several of these methods contribute heat to different positions within the cell, thus testing the effect of potential temperature gradients. The time stability of the calibration is tested by the bivalue mode. A comparison between electrolytic and joule heat tests the effect of heat being produced at the recombiner in the former case. It is important to note that method 2 has the same heat distribution, bubble pattern, and recombiner heat as when palladium is studied. This method is used to calibrate the cell before and after each cell modification. Method 1 is used to detect changes in the calibration constant while palladium is being electrolyzed but is not used to provide an absolute calibration because of a small heat loss through the wires. A small charging current is applied to the palladium electrode during this calibration to prevent loss of deuterium. This additional power is taken into account. Method 4 tests the effects of the recommended bivalued mode of charging on the calibration constant. Platinum is used as the cathode or, when excess heat is not being produced, palladium is used. However, this calibration method is less accurate when using palladium because fewer points must be taken in order not to alter the charging conditions too much. Figure 3 compares typical calibrations using methods 1 and 2 and shows typical scatter within data sets as well as the difference between calibrations.

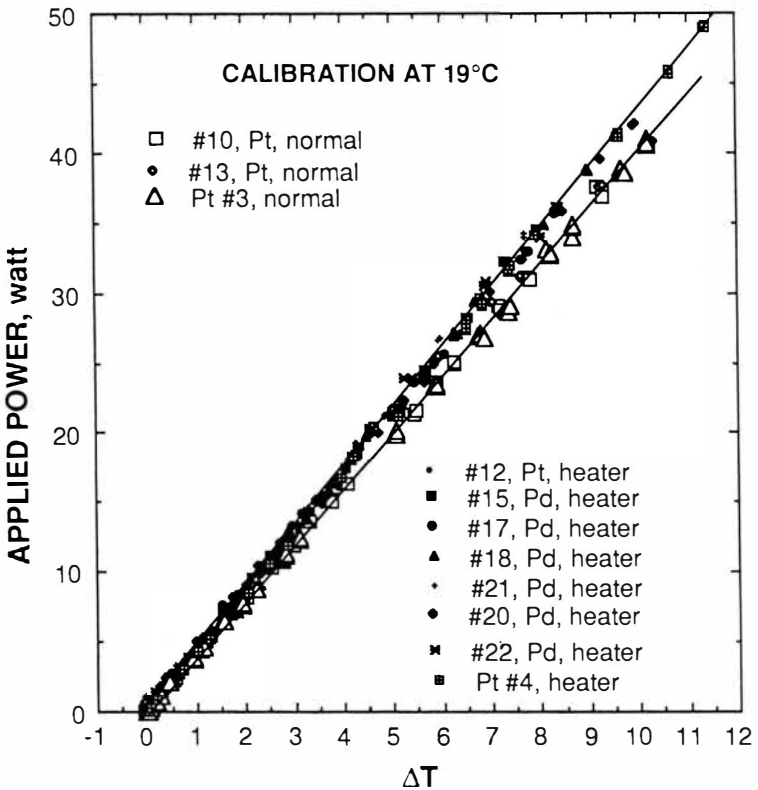

Figure 3. Comparison between calibrations using normal electrolysis with a Pt cathode and the immersion heater. Linear least-squares fits to the data are shown. Jacket temperature is near 19° C, and the electrolyte is 0.3 N LiOD.

Figure 4 compares the slope of lines shown in Figure 3 with values obtained using the bivalue mode at various jacket temperatures.

The product of current flowing through the cell times the voltage across the cell, measured where the wires enter the active region of the calorimeter, is used as the applied power. The difference between total power and applied power is taken as excess power. Many measurements of excess power under a variety of applied currents and calibrations give uncertainties of ±1 W at 40 W of applied power and ±0.3 W when the applied power is near zero. Therefore, excess power is not claimed unless the value is above 1 W.

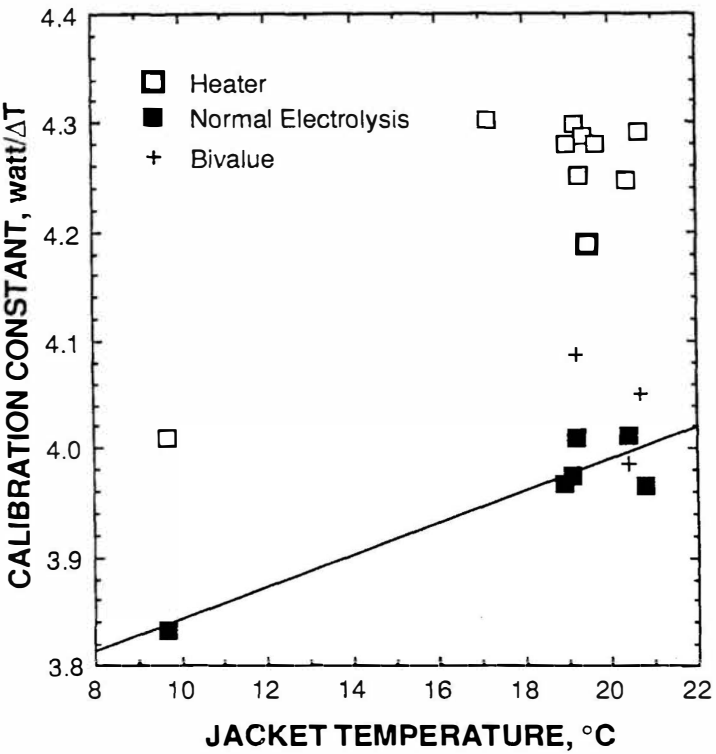

Figure 4. Effect of jacket temperature on the calibration constant when calibration is done using the immersion heater, normal electrolysis with a platinum cathode and bivalue using a palladium cathode.

2. B. Additional Measurements

The D/Pd ratio is measured during initial charging using the system volume, the decrease in D_2 pressure within the system, and the weight of the palladium cathode. Figure 5 shows this quantity as a function of time for Pd sample #1. Up to ≈150 min, nearly every deuterium atom released by electrolysis dissolves in the palladium. The apparent decrease in deuterium composition after 650 min is not thought to be real. The charging behavior of Pd sample #2 shows a lower efficiency for deuterium dissolution.

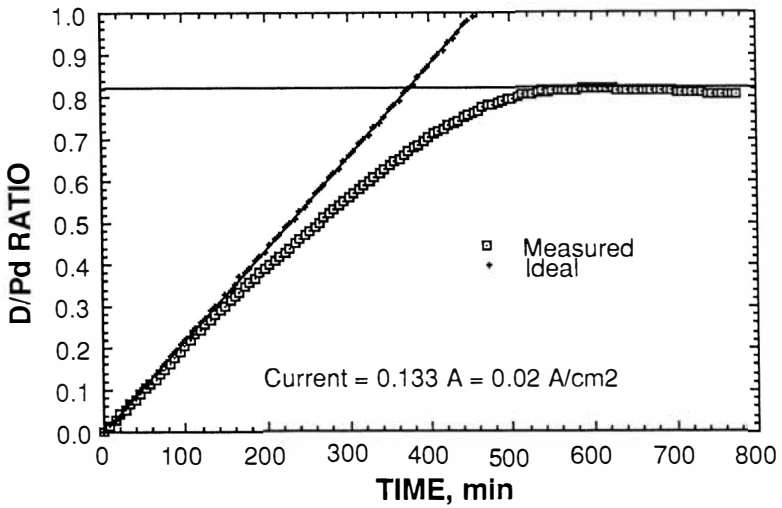

Figure 5. D/Pd ratio as a function of time during the initial charging of Pd #1. The ideal line shows the expected composition if every atom of electrolyzed D dissolved in the palladium.

An exterior platinum electrode is connected, using an electrolyte bridge, to a capillary located about 0.5 mm from the cathode surface. The voltage between this electrode and the cathode is monitored and found to change by 0.34 V when the cathode changed from pure Pd to $PdD_{0.82}$.

The volume of the cathode is measured using a micrometer. The measured change in volume when the deuteride formed is compared to the expected change based on the known lattice parameter change. Samples of palladium deuteride always show a variable volume that is in excess of the expected value[4] owing to cracks and other distortions to the lattice. The palladium that produced excess heat had an excess volume of 0.8% while the palladium that did not produce excess heat had an excess volume of 13.5% at D/Pd=0.75.

3. Results

After initial charging, the sample is ramped for 64 hr between 0.133 A and 2.77 A using various cycle times. No excess heat is observed at 0.133 A. After bivalued charging between 0.133 A and 2.77 A was initiated, excess heat between 1 and 2 W is seen at 2.77 A after 30 additional hours. After a total time of 159 hr the cell was opened to repair the recombiner that had stopped working at 145 hr. During this repair, the cathode was

exposed to air for 47 min. After reassembly, the cell was calibrated and the bivalue mode was resumed. The resulting excess heat is plotted in Fig. 6. After about 5 hr, a small burst of heat is observed which is typical of earlier behavior. This is followed by a steady increase over the next 55 hr. A calibration using the immersion heater was run between 304 hr and 312 hr while 1.0 A was applied to the cathode. Periodically, excess power measurements are made at various lower currents. Not only is the excess absent at 2.0 A and below, but these periodic interruptions do not seem to alter the steady rise once 2.8 A is resumed. At 295 hr, the recombiner began to fail again, owing to attack by lithium from the electrolyte, and the measured excess power is seen to decrease.

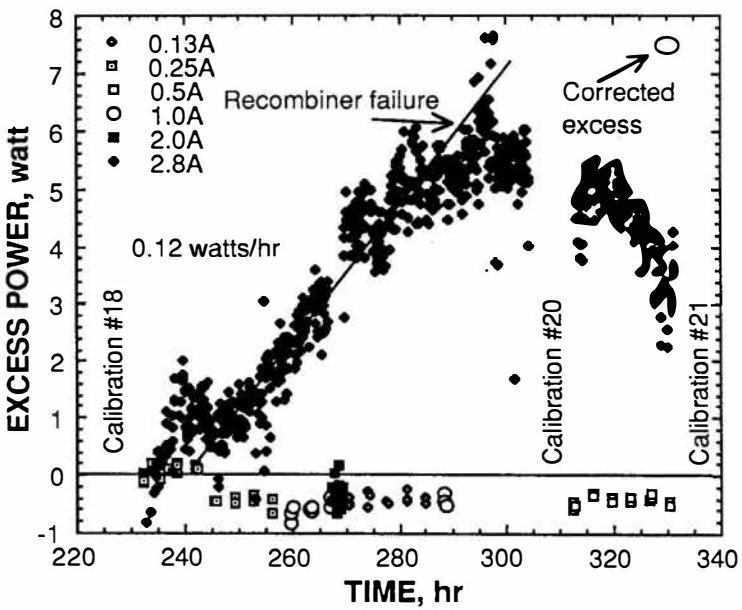

Figure 6. Excess power at various cell currents during Phase 2. The "corrected excess" value is the maximum excess power expected if the recombiner had worked properly.

If no oxygen is being recombined in the cell at 330 hr, 4.3 watts (2.8 A x 1.54 V) must be added to the measured excess to give the actual excess power. When this is done, the value falls on the upward trend created by earlier data. Thus, the upward trend in power generation apparently is continuing up to the time when the cell is again turned off. After repair, heat at the 2-3 W level is observed for 6 hrs before additional problems re-

quire the experiment to be terminated.

4. Conclusions

Excess power has been made in an electrolytic cell using palladium similar to that used by A. Takahashi (Japan). After 90 hr of electrolysis, small amounts of excess heat were observed. After the cathode was exposed to air for 47 min and electrolyzed for ≈30 additional hours, excess power started to increase and reached ≈20 % of applied power (≈7.5 watts) before the study had to be interrupted. This power increased with time only while the palladium was electrolyzed at 0.42 A/cm^2. No measurable excess power was seen at or below 0.38A/cm^2. This excess is about 75% of the amount expected at 0.42 A/cm^2 as proposed by Storms[3] based on a variety of calorimetric measurements. The excess heat originates from a different position within the cell than does electrolytic heat. This position is proposed to be the palladium cathode. The palladium produced heat in spite of being exposed to air after loading with deuterium, being placed in liquid nitrogen for a short time, and the electrolyte being saturated with CO_2. However, no excess was produced after deloading to D/Pd=0.73 had occurred. The bivalued mode of charging, as used by Prof. Takahashi, does not appear to be a requirement for continued heat production once production starts. The palladium (Pd#1) that produced excess heat loaded to D/Pd=0.82 and the deuteride contained no significant excess volume. On the other hand, the palladium (Pd#2) that failed to show excess power loaded to only D/Pd=0.75 and had 13.5% excess volume. One explanation is that the second piece of palladium contained internal defects that caused the formation of cracks during loading with the result that a sufficiently high D/Pd ratio could not be achieved.

References

[1] More detail about this work can be found in the March 1993 issue of Fusion Technology.

[2] A. Takahashi, T. Iida, T. Takeuchi and A. Mega, "Excess Heat and Nuclear Products by D_2O/Pd Electrolysis and Multibody Fusion", Submitted to Applied Electromagnetics in Materials, 1992.

[3] E. Storms, "Review of Experimental Observations About the Cold Fusion Effect", Fusion Tech. **20** (1991) 433.

[4] E. Storms and C. Talcott-Storms, "The Effect of Hydriding on the Physical Structure of Palladium and on the Release of Contained Tritium", Fusion Tech. **20**, (1991) 246.

Deuterium Loading Ratio and Excess Heat Generation during Electrolysis of Heavy Water by a Palladium Cathode in a Closed Cell Using a Partially Immersed Fuel Cell Anode

K.Kunimatsu, N.Hasegawa, A.Kubota, N.Imai, M.Ishikawa, H.Akita and Y.Tsuchida.

IMRA JAPAN CO.,LTD.
3-6 Techno Park 2 cho-me,Shimonopporo,Atsubetsu-ku,Sapporo 004 JAPAN

ABSTRACT

We have developed a novel electrolytic cell pressurized by D_2 in which deuterium loading ratio in a palladium cathode can be determined in-situ during the calorimetric measurements of excess heat. A gas diffusion type fuel cell anode is partially immersed in the electrolyte solution to act as a counter electrode, at which electrochemical oxidation of deuterium gas molecules to deuterium ions takes place instead of electrolytic decomposition of water molecules to generate oxygen gas.

Factors controlling the loading ratio such as electrolyte composition, hydrogen overvoltage at the palladium cathode,current density,isotope effect,have been examined.

Dependence of the excess heat generation at the palladium cathode on the loading ratio as well as on the current density shows that the critical loading ratio and the current density to generate excess heat are ca. 0.83 and 100mA/cm^2,respectively.

The maximum D/Pd of 0.89 has been achieved in the present study, at which excess heat generation of ca. 35% with respect to the input electrolytic power has been observed.

INTRODUCTION

The difficulty in replicating the Pons/Fleischmann type electrolytic excess heat generation [1],[2] during electrolysis of heavy water has caused strong criticism on their experiments,and the reality of the so-called cold fusion has been questioned. However,to date very few studies have been reported on the fundamental factors controlling the deuterium loading ratio in the palladium cathode which has been believed to be the key factor to control the excess heat generation. The NCFI final report [3] contains some data on the loading ratio under various conditions but they are too preliminary to suggest important factors controlling the loading ratio. Will et al.[4] reported loading ratio higher than 0.85 as key factor for tritium production,while Mackbure et al.[5],[6] reported the critical loading ratio around 0.9 to give rise to the excess heat generation. The loading ratio was determined by

FRONTIERS OF COLD FUSION

conducting the electrolysis in a closed cell utilizing a fuel cell anode by Will et al.and by monitoring the electrical resistance by Mackbure et al.

Electrolysis in a closed cell utilizing a fuel cell anode offers a direct method to determine the loading ratio by monitoring the deuterium pressure during electrolysis while measurement of the electrical resistance is an indirect one which relies on the resistivity data as a function of loading ratio observed in gas phase[7].The structure of the electrolysis cell utilizing fuel cell anode proposed by Will[4] is difficult to conduct calorimetry and to carry out long term electrolysis.

The purpose of the present study is firstly to develop a novel new electrolysis cell utilizing a fuel cell anode which allows us simultaneously to carry out calorimetry and to conduct in-situ determination of loading ratio and secondly to examine the factors controlling the loading ratio and thirdly to investigate the relation between the excess heat generation and the loading ratio.

EXPERIMENTALS

Determination of hydrogen/deuterium loading ratio in a palladium cathode was done first in a closed cell developed in our laboratory which is shown schematically in Fig.1. The pressure vessel made from SUS316 filled with deuterium gas of 5–10 atm has an electrolyte container made from PTFE or glass with four windows at which gas diffusion electrodes are attached with their reaction layers in contact with electrolyte solution. A platinized platinum electrode(Pt/Pt) was placed in the electrolyte and acted as a reference electrode(RHE) to measure hydrogen overvoltage at the palladium cathode.

The cathode and anode reactions in alkaline solutions are given respectively by,

$$\text{Cathode reaction: } 2D_2O + 2e^- \dashrightarrow 2D(\text{ads.}) + 2OD^- \qquad (1)$$

$$2D(\text{ads.}) \dashrightarrow \begin{cases} D_2 \\ 2D(Pd) \end{cases} \qquad (2)$$

$$\text{Anode reaction: } D_2 \dashrightarrow 2D^+ + 2e^- \qquad (3)$$

where,D(ads.)and D(Pd) denote deuterium atom adsorbed on the cathode surface and absorbed into the cathode respectively.

From (1),(2) and (3),the over-all cell reaction for the electrolysis with a Pd cathode and a fuel cell anode is given by:

$$D_2 \dashrightarrow 2D(Pd) \qquad (4)$$

Therefore,pressure of D_2 gas decreases as electrolysis proceeds due to deuterium absorption into the Pd cathode. We have,

$$(P_O - P)V = (n_O - n)RT, \qquad (5)$$

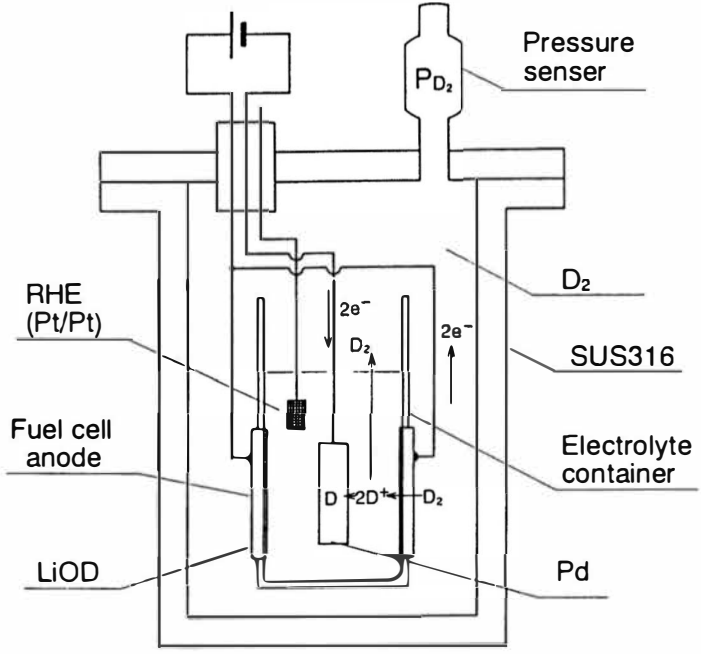

Fig. 1 Electrolysis cell using an fuel cell anode.

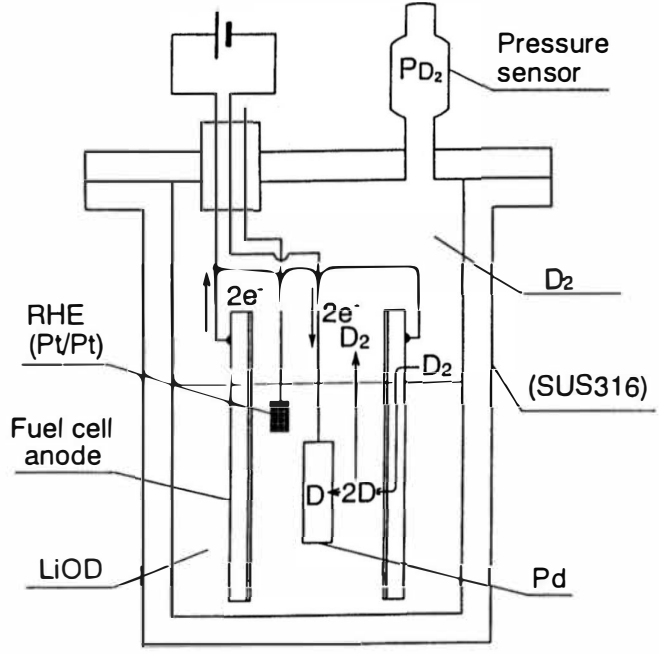

Fig. 2 Electrolysis cell using a partially immersed fuel cell anode.

where, P_O and n_O are the pressure and total number of moles of D_2 gas in the pressure vessel at the onset of electrolysis, and P and n are the pressure and the number of moles of D_2 gas at a given time of electrolysis, respectively, while V is the free volume of the vessel which is measured before electrolysis and is taken constant. The loading ratio at a given time is calculated from the pressure decrease by the relation

$$D/Pd = 2V(P_O - P)/RT/n_{Pd}, \quad (6)$$

where n_{Pd} is the number of gram atoms of Pd in the cathode.

The calculation of D/Pd needs corrections; however, for the change in vapor pressure of D_2O in the gas phase due to the temperature change during electrolysis, change in the solubility of D_2 gas in the electrolyte solution as well as in PTFE materials in the vessel due to the temperature as well as pressure change in the vessel. These corrections are usually small, 1–2%, but the loading ratio reported in the present study have been corrected for them.

There is another advantage of using a fuel cell anode; because no electrolytic decomposition of D_2O takes place, less input power is required for electrolysis and further more, the input power, W_{input}, is given simply by a product of electrolysis current I and cell voltage E_{cell} as,

$$W_{input} = I \times E_{cell} \quad (7)$$

Performance of the cell shown in Fig.1 was excellent for determination of the loading ratio at low current densities. It turned out, however, that the cell has a serious problem when operated at high current densities. Substantial amount of solvent is lost from the electrolyte container when electrolysis is conducted at high current densities for a long period. The solvent tends to condense at the bottom of the pressure vessel and the electrolysis was no longer possible in that case.

In view of the problems described above, we further have developed a new type of closed cell schematically shown in Fig.2. The fuel cell anode is directly immersed in the electrolyte leaving some portion of it in the gas phase. The gas diffusion layer of the fuel cell anode above the electrolyte served as inlet of D_2 gas into the fuel cell anode. The supply of deuterium gas through the gas diffusion layer partially immersed in the electrolyte is greatly reduced, however, compared to the configuration shown in Fig.1. Figure 3 shows relation between the current density and the overvoltage for the anode reaction, i.e., $H_2 \rightarrow 2H^+ + 2e^-$, observed in 1M LiOH at various hydrogen pressures. The similar relation for an unimmersed gas diffusion electrode is compared in the same figure. The overvoltage for the immersed electrode is much higher than the one not immersed and depends strongly on the hydrogen pressure. This indicates that the overvoltage is primarily governed by the supply of hydrogen gas through the gas diffusion layer.

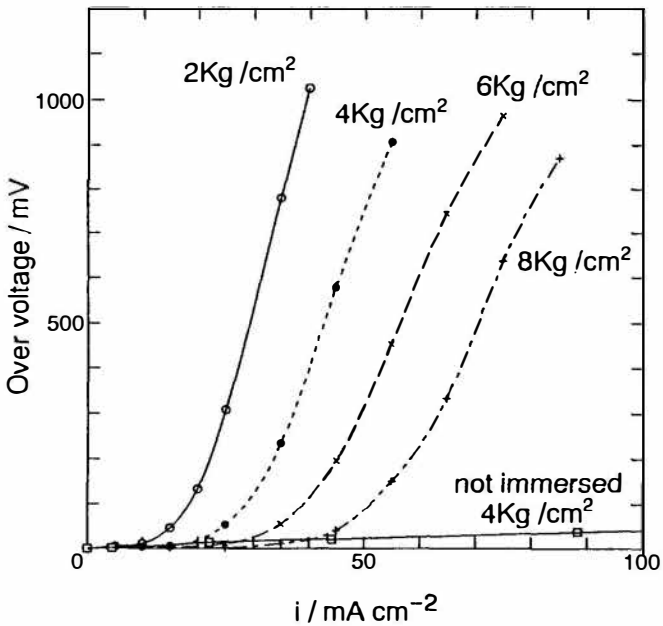

Fig. 3 Polarization curves of the immersed electrode.

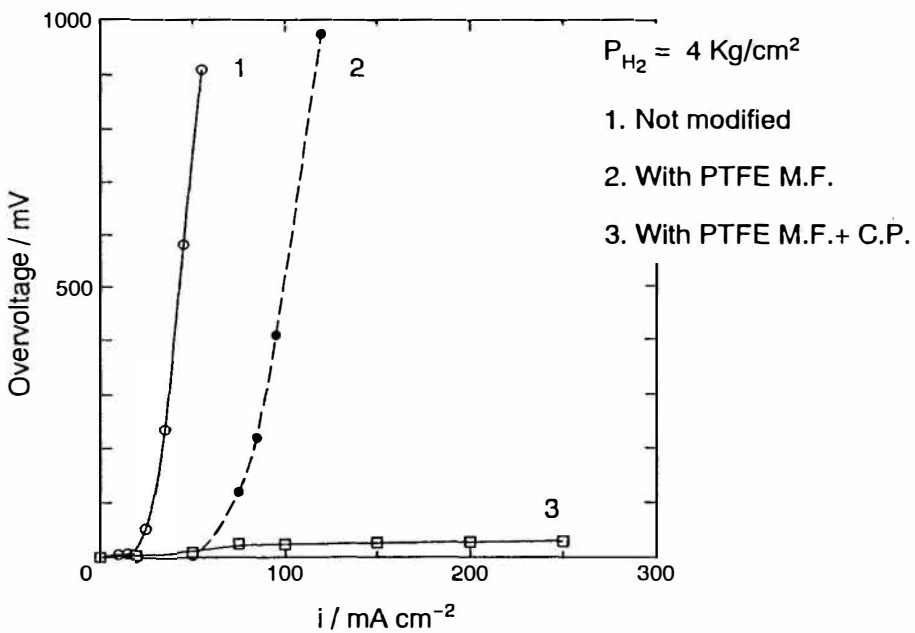

Fig. 4 Polarization curves of the modified electrodes.

We then modified the gas diffusion layer by adding firstly a PTFE membrane filter and then a carbon paper/PTFE membrane filter composite layer in order to establish a gas supplying route to the gas diffusion layer.Figure 4 shows results of such modification of the gas diffusion layer. The overvoltage is greatly reduced by applying the composite layer. Electrolysis using the configuration shown in Fig.2 has become feasible by the improvement of the performance of the partially immersed gas diffusion electrode. All the experiments described hereafter have been conducted in the cell shown in Fig.2.

Palladium cathodes were rods of 2mm,4mm or 5mm in diameters, of 99.99% purity obtained from Tanaka Kikinzoku and also from IMRA Materials co.,Ltd. Two palladium wires of 0.5mm in diameter were spot welded to the palladium rods and then the rods were etched in conc.HNO_3. They were then degassed in vacuum at 200 ℃ for three hours.

The chemicals LiOH,H_2SO_4,D_2SO_4 were all reagent grade and used without further purification. LiOD solutions were made from D_2O(Isotech,99.9% isotopic purity) and Li metal of 99.9% obtained from Johnson Matthey. The lithium metal kept in paraffin oil was washed by propanol and then it was put into D_2O to prepare 1M LiOD solution. Preparation of the electrolyte and its filling into the cell were conducted in a glove box purged continuously by dry air. After the filling the cell was purged by hydrogen or deuterium gas for half an hour and then pressurized by the respective gas. It was necessary to wait for some time,typically a day,for the pressure to be stabilized due to absorption of hydrogen or deuterium gas into the electrolyte solution and the electrolyte container made from PTFE. One ml of PTFE absorbs approximately 0.7 ml of hydrogen or deuterium gas at 1 atm at 20° C with diffusion constant of $2.6 \times 10^{-7} cm^2 sec^{-1}$[8].Potential of the palladium electrode was kept at 1.0V with respect to the RHE during the waiting period to prevent absorption of hydrogen or deuterium gas into the palladium electrode. After the purging,cyclic voltammogram of the Pd electrode was taken between 0.4V and 1.5V/RHE in order to clean the Pd surface. Finally the palladium electrode was polarized at 1.5V/RHE for 15 min. in order to clean its surface just before starting electrolysis when the pressure in the vessel is stabilized.

A pressure vessel used for most of the loading experiments is shown schematically in Fig.5. The inner wall of the vessel is coated by a thin ceramic layer resistant to acids and bases.

The pressure vessel which had been carefully checked for its pressure leakage by helium leak detector has several Ag wires of 1mm diameter for electrical leads and k-type thermocouples sealed through a sealing ground. All the wires and thermocouples were insulated by PTFE tubing. Electrolysis was conducted with the pressure vessel totally submerged in the water bath regulated at a constant temperature typically 10° C. The content of light water in the electrolyte when using

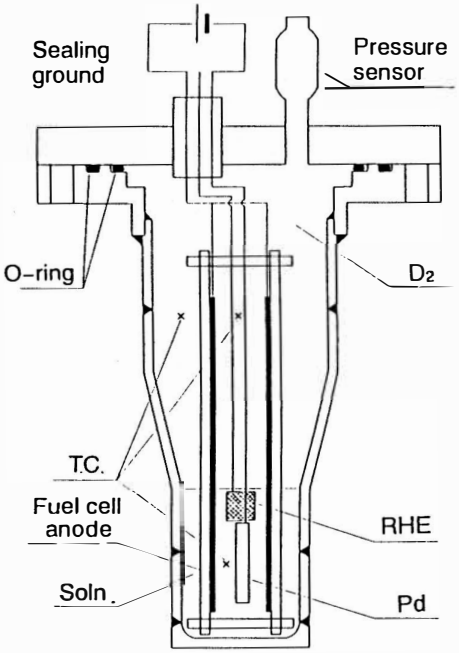

Fig. 5 Electrolysis cell for loading experiments

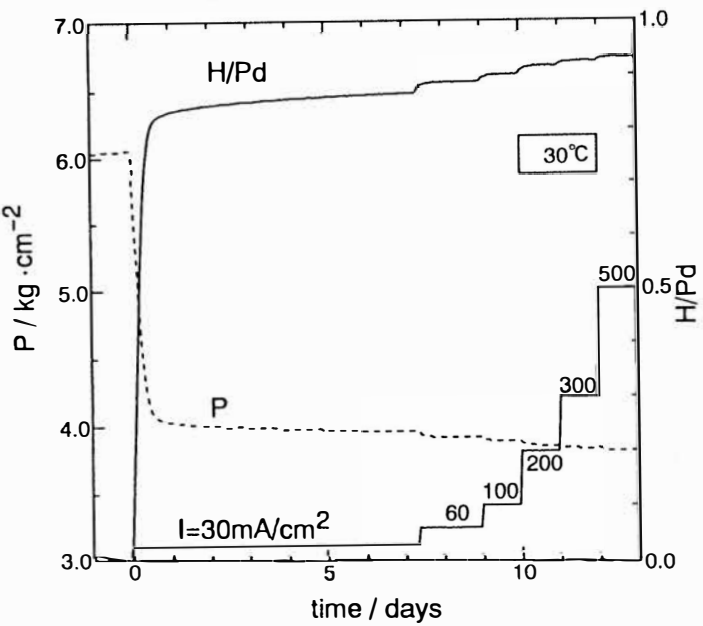

Fig. 6 Change of H/Pd with current density in 1M LiOH.

D_2O was checked by NMR after a two months electrolysis period but no change in the light water content was detected.

The cell shown in Fig.5 has a low thermal cell constant, ca. 1 ° C/W, when submerged in the water bath, therefore the temperature of the electrolyte remained almost constant during the loading experiments.

Electrolysis was conducted at constant currents supplied by a DC power supply for each cell. The power supplies were controlled by a computer, by which data acquisition was also conducted throughout the electrolysis period.

Calorimetry was conducted in another type of cell with higher thermal cell constants,5–8° C/W. The experimental details is given elsewhere[9].

Most of the loading experiments were conducted in a constant temperature room regulated at 20 ±0.1° C.

RESULTS AND DISCUSSION

I. Factors controlling loading ratio

We investigated firstly factors controlling the loading ratio in order to find optimum loading conditions.

1.Dependence on overvoltage and current density in acids and bases.

A typical example of a loading experiment in 1M LiOH is shown in Fig.6,in which change of pressure and loading ratio are displayed as a function of electrolysis time. The electrolysis was started at 30mA/cm^2 and then current density was increased up to 500mA/cm^2 nearly every 24 hours in a stepwise manner. The loading ratio increases systematically in response to the change in current density and reaches 0.930 at 500mA/cm^2.The example shows clearly that loading ratio can be controlled by current density. Figure 7 shows initial stage of the loading at 30mA/cm^2 which is compared to the line showing the loading ratio change for 100% current efficiency. We can see that the loading proceeds almost at 100% current efficiency up to H/Pd=0.5. In general the current efficiency of loading increases at lower current densities. Figure 8 shows that loading at 3mA/cm^2 proceeds linearly with time at current efficiency slightly higher than 100% throughout the entire loading period. The linear increase of D/Pd with time implies that the loading process is totally governed by supply of D to the Pd surface,and the current efficiency higher than 100% is most likely due to direct absorption of D_2 dissolved in the electrolyte into the Pd electrode.

Effect of hydrogen overvoltage at Pd cathode on the loading ratio was compared in acids and bases for the light water as well as for the heavy water system. Figure 9 shows H/Pd as a function of overvoltage observed in 2.8M H_2SO_4,and 1M LiOH. The results show clearly that loading ratio increases systematically with overvoltage increase and that the data in both media almost coincide. It should be particularly

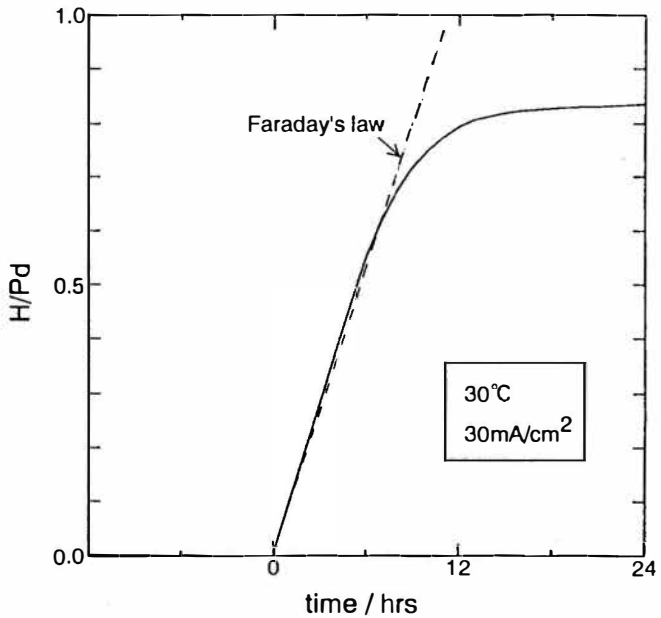

Fig. 7 Change of H/Pd with time in 1M LiOH

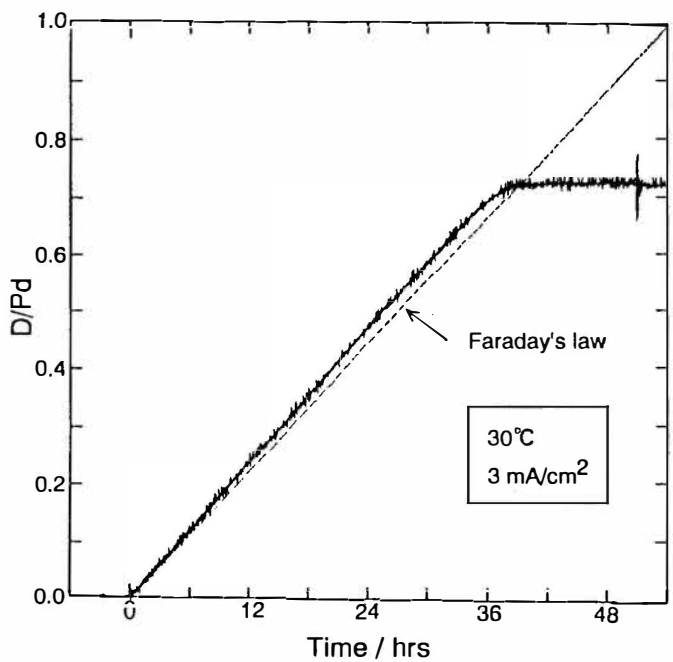

Fig. 8 Change of D/Pd with time in 1M LiOD

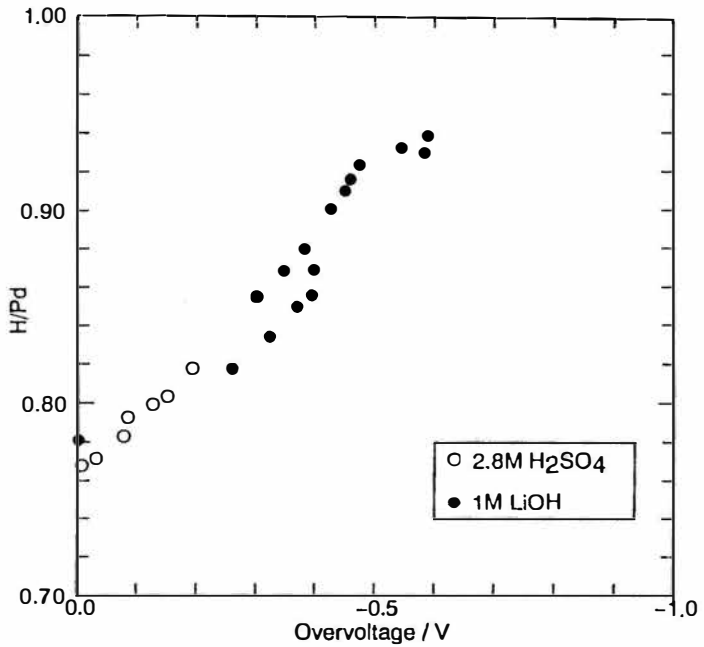

Fig. 9 Dependence of H/Pd on overvoltage in acid and base.

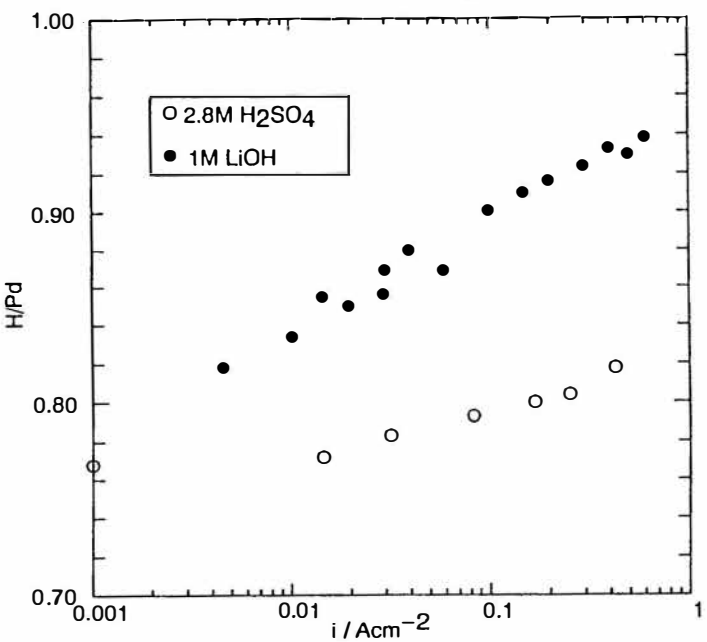

Fig.10 Dependence of H/Pd on current density.

noted that the highest H/Pd achieved in acidic solutions is much lower than in alkaline solution. This is simply because the hydrogen overvoltage in acids is usually much lower than in bases for a given current density. Therefore the difference between acid and base becomes clear when H/Pd is plotted as a function of current density as shown in Fig.10.

The loading ratio in acid and base was compared also for deuterium in 1M LiOD and 2.8M D_2SO_4 at 10° C and the result is shown in Fig. 11.The loading ratio in the common overvoltage region below −500mV coincides in the two media but the difference between the two media becomes evident when D/Pd is plotted as a function of current density as shown in Fig.12.

We can conclude from the data in Figs. 9−12 that alkaline media is a better choice than acids to realize higher loading ratio.
On the other hand, the fact that the loading ratio appears to be controlled by total hydrogen overvoltage and is almost independent of electrolytic medium looks strange in view of kinetic analysis of the so−called equivalent hydrogen pressure acting on the palladium electrode. Enyo and Maoka [10] related the equivalent pressure to the overvoltage of the Tafel step [2H(ads.)−−−>H_2];

$$P^* = P_{H_2} \exp(-2F\eta_2/RT) \qquad (8)$$

where P^* and P_{H_2} are the equivalent pressure and the actual pressure of hydrogen in the electrolysis cell, respectively, and η_2 is the overvoltage of the Tafel step. The equation becomes the so−called Nernst equation if η_2 is replaced by the total overvoltage.
Analysis of the data in Figs. 9 and 11 based on the equation (8) leads to a conclusion that the overvoltage of the Tafel step is common in the acid and base for a given total overvoltage. The validity of the conclusion and hence of equation (8) could be tested by measurements of the component overvoltage of the Tafel step or that of the Volmer step in various media.

2. Isotope effect

Isotope effect on the loading ratio has been investigated elsewhere [11] for both acidic and alkaline media. The lower loading ratio for deuterium can be interpreted in terms of the higher plateau pressure in p−c−T curve of Pd/D_2 system in gas phase than Pd/H_2 system. It makes rather difficult to conduct excess heat measurements at D/Pd close to 1. Our excess heat measurement was conducted up to D/Pd=0.89 as shown in the following section.

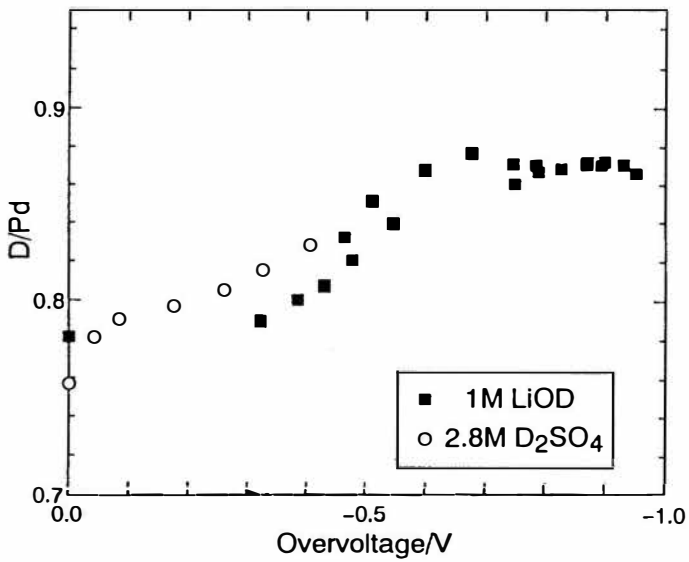

Fig.11 Dependence of D/Pd on overvoltage in 1M LiOD and 2.8M D_2SO_4 at 10℃.

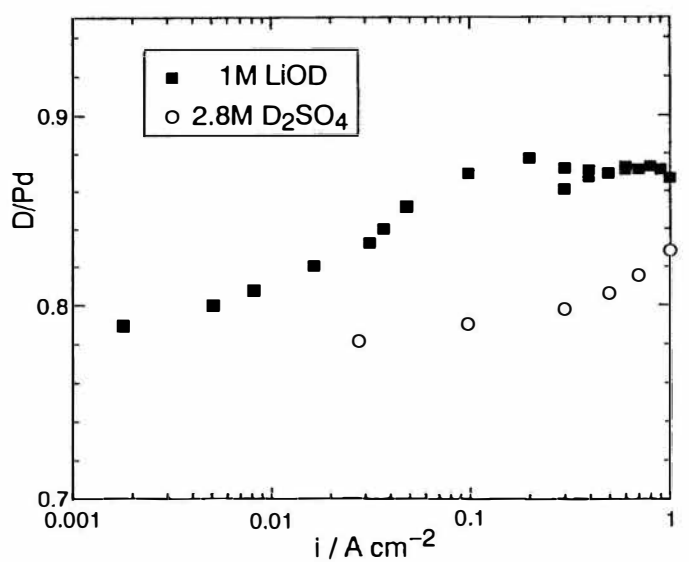

Fig.12 Dependence of D/Pd on current density in 1M LiOD and 2.8M D_2SO_4 at 10℃.

II. Excess heat measurement

The details of excess heat measurement has been described elsewhere [9].

The relation between the excess heat and D/Pd in 1M LiOD is plotted in Fig.13, which suggests that the critical loading ratio to give rise to the excess heat is ca.0.83. Unfortunately the highest loading ratio achieved in the present study is 0.89 and we cannot predict the dependence of excess heat on D/Pd at higher loading ratios.

The critical D/Pd which is ca. 0.83 found in the present study is well compared to the results reported by Mckubre et al.[6].

We derived relation between the excess heat and current density from the data described in the preceeding part and the result is shown in Fig.14. The figure suggests that excess heat is almost proportional to current density and that the critical current density to give rise to excess heat is close to 100mA/cm^2. The data is in agreement with those reported by Pons and Fleischmann in 1990[2]. The role of high current density needed to produce excess heat is obvious from Fig.12 which shows the current density dependence of D/Pd.Below 100mA/cm^2,D/Pd decreases sharply and current density higher than 100mA/cm^2 is necessary to maintain high loading ratio.

III.Conclusion

A new method of electrolysis in a closed cell pressurized by D_2 gas has been developed utilizing a partially immersed fuel cell anode modified by a composite layer of PTFE and carbon paper. The cell allows us to conduct simultaneous measurement of excess heat and D/Pd during electrolysis. We can summarize the following conclusions:

(1) Loading ratio is primarily controlled by hydrogen overvoltage at the Pd cathode.
(2) D/Pd is lower than H/Pd by 5–10% for a given overvoltage.
(3) Excess heat generation increases at higher D/Pd between 0.83 and 0.89.
(4) Excess heat is proportional to the current density above 100mA/cm^2, the role of the current density being to maintain high D/Pd.

Confirmation of these conclusions by repeated investigations and improvement of D/Pd will be necessary in future experiments. They are currently in progress in our lab and will be reported in due course.

IV. Acknowledgement

Financial supports for the present study by Aisin AW Co.,Ltd. and by Technova Inc. is greatly acknowledged. Supply of Pd from IMRA Materials Co.,Ltd. and discussion with Prof. N.Furuya are also greatly acknowledged.

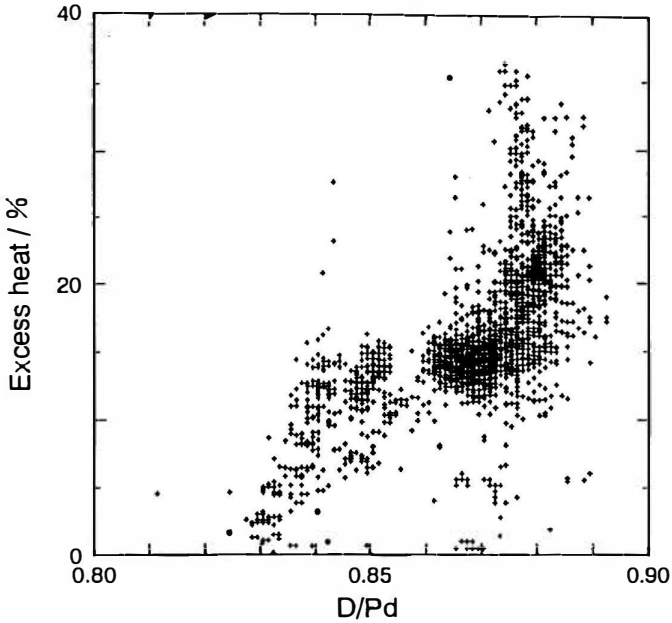

Fig.13 Dependence of excess heat generation on D/Pd.

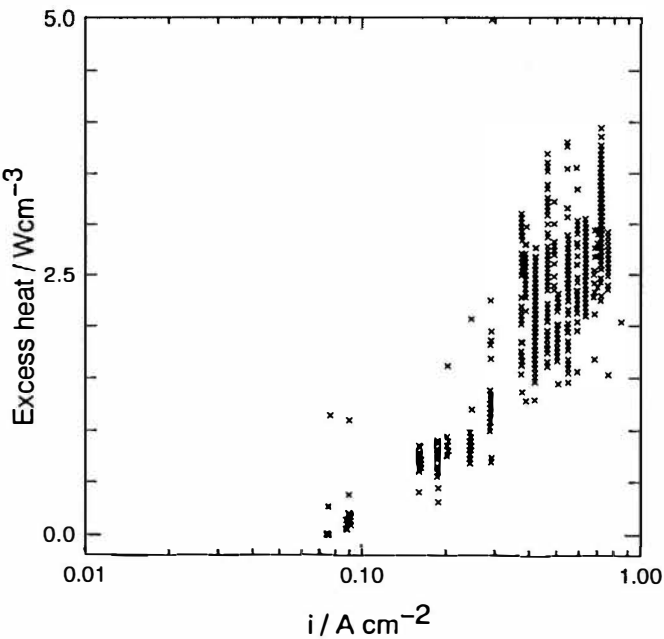

Fig.14 Dependence of specific excess heat on current density.

REFERENCES

1. M.Fleischmann, S.Pons and M.Hawkins : J. Electroanal. Chem., **261**(1989)301. Erratum,**263**(1989)187.

2. M.Fleischmann, S.Pons, M.W.Anderson, L.J.Li and M.Hawkins : J. Electroanal. Chem.,**287**(1990)293.

3. A.M.Riley, J.D.Seader, D.W.Pershing, D.C.Linton and S.Shimizu : NCFI Final Report ***Vol.II***(1991)123.

4. F.G.Will, K.Cedzynska and C.Linton : NCFI Final Report **Vol.I**(1990)131.

5. M.C.H.Mckubre, R.Rocha-Filho, S.I.Smedley, F.L.Tanzella, S.Crouch-Baker, T.O.Passel, J.Santucci : The Science of Cold Fusion, Proceedings of **ICCF2**(1991)419.

6. M.C.H.Mckubre : Review of Fatal Accident at SRI January 2(1992).

7. J.C.Barton, F.A.Lewis and I.Woodward : Trans. Faraday Soc.,**59**(1963)1201.

8. A.Ya.Kupryazhkin, I.A.Korolev, P.V.Bolobuev and P.E.Suetin : Sov. Phys. Tech. Phys.,**22**(1977)1406.

9. N.Hasegawa, K.Kunimatsu, T.Ohi and T.Terasawa : Proceedings of **ICCF3**(1992).

10. T.Maoka and M.Enyo : Electrochim. Acta,**26**(1981)607.

11. A.Kubota, H.Akita, Y.Tsuchida, T.Saito, Akiko Kubota, N.Hasegawa, N.Imai, N.Hayakawa and K.Kunimatsu : Proceedings of **ICCF3**(1992).

Calorimetry of the PD ED_2O System: from Simplicity via Complications to Simplicity .

Martin FLEISCHMANN
Dept. of Chemistry, Univ. of Southampton, Southampton, U.K.

Stanley PONS
IMRA Europe, Sophia Antipolis, 06560 Valbonne, FRANCE

ABSTRACT

We present here one aspect of our recent research on the calorimetry of the Pd/D_2O system which has been concerned with high rates of specific excess enthalpy generation ($> 1kWcm^{-3}$) at temperatures close to (or at) the boiling point of the electrolyte solution. This has led to a particularly simple method of deriving the rate of excess enthalpy production based on measuring the times required to boil the cells to dryness, this process being followed by using time-lapse video recordings.

Our use of this simple method as well as our investigations of the results of other research groups prompts us to present also other simple methods of data analysis which we have used in the preliminary evaluations of these systems.

General Features of our Calorimetry

Our approach to the measurement of excess enthalpy generation in Pd and Pd-alloy cathodes polarised in D_2O solutions has been described in detail elsewhere (see especially [1-5]; see also [6]). The form of the calorimeter which we currently use is illustrated in Fig 1. The following features are of particular importance:

(i) at low to intermediate temperatures (say 20-50°C) heat transfer from the cell is dominated by radiation across the vacuum gap of the lower, unsilvered, portion of the Dewar vessel to the surrounding water bath (at a cell current of 0.5A and atmospheric pressure of 1 bar, the cooling due to evaporation of D_2O reaches 10% of that due to radiation at typically 95-98°C for Dewar cells of the design shown in Fig 1).

(ii) the values of the heat transfer coefficients determined in a variety of ways (see below) both with and without the calibrating resistance heater (see Fig 2 for an example of the temperature-time and cell potential-time transients) are close to those given by the product of the Stefan-Boltzmann coefficient and the radiant surface areas of the cells.

(iii) the variations of the heat transfer coefficients with time (due to the progressive fall of the level of the electrolyte) may be neglected at the first level of approximation (heat balances to within 99%) as long as the liquid level remains in the upper, silvered

FRONTIERS OF COLD FUSION

portions of the calorimeters.

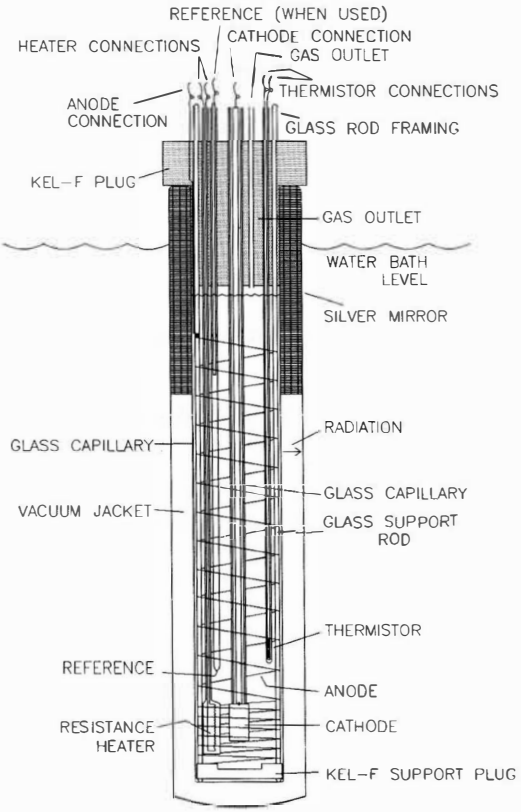

Figure 1. Schematic diagram of the single compartment open vacuum Dewar calorimeter cells used in this work.

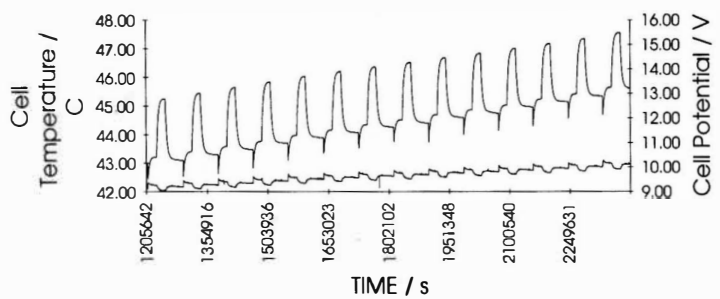

Figure 2. Segment of a temperature-time/cell potential-time response (with 0.250 W heat calibration pulses) for a cell containing a 12.5 × 1.5mm platinum electrode polarised in 0.1M LiOD at 0.250A.

(iv) the room temperature is controlled and set equal to that of the water baths which contain secondary cooling circuits; this allows precise operation of the calorimeters at low to intermediate temperatures (thermal balances can be made to within 99.9% if this is required).

(v) heat transfer from the cells becomes dominated by evaporation of D_2O as the cells are driven to the boiling point.

(vi) the current efficiencies for the electrolysis of D_2O (or H_2O) are close to 100%.

Modelling of the Calorimeters

The temperature-time variations of the calorimeters have been shown to be determined by the differential equation [1]

$$\underbrace{C_{P,D_2O,\ell}M^0\left[1-\frac{(1+\beta)It}{2FM^0}\right]\frac{d\Delta\theta}{dt}-C_{P,D_2O,\ell}M^0\frac{(1+\beta)I\Delta\theta}{2FM^0}}_{\text{change in the enthalpy content of the calorimeter}}$$

$$=\underbrace{\left[E_{cell}(t)-E_{thermoneutral,cell}\right]I}_{\text{enthalpy input due to electrolysis}}$$

$$-\frac{I}{F}\underbrace{\left\{\left[0.5C_{P,D_2}+0.25C_{P,O_2}+0.75\left(\frac{P}{P^\star-P}\right)C_{P,D_2O,g}\right]\Delta\theta+0.75\left(\frac{P}{P^\star-P}\right)L\right\}}_{\text{enthalpy content of the gas stream}}$$

$$+\underbrace{Q_f(t)}_{\text{excess enthalpy}}+\underbrace{\Delta QH[t-t_1]-\Delta QH[t-t_2]}_{\text{calibration pulse}}$$

$$-\underbrace{k_R^0\theta_{bath}^3\left[1-\left(\frac{(1+\lambda)It}{2FM^0}\right)\right]}_{\substack{\text{time dependent}\\ \text{heat transfer coefficient}}}\left\{\underbrace{\left[\frac{(\theta_{bath}+\Delta\theta)^4-\theta_{bath}^4}{\theta_{bath}^3}\right]}_{\text{effect of radiation}}+\underbrace{4\Phi\Delta\theta}_{\text{effect of conduction}}\right\} \qquad [1]$$

In equation [1] the term $\left[1-\frac{(1+\beta)It}{2FM^0}\right]$ allows for the change of the water equivalent with time; the term β was introduced to allow for a more rapid decrease than would be given by electrolysis alone (exposure of the solid components of the cell contents, D_2O vapour carried off in the gas stream). As expected, the effects of β on Q_f and k_R^0 can be neglected if the cells are operated below 60°C. Furthermore, significant changes in the enthalpy contents of the calorimeters are normally only observed following the refilling of the cells with D_2O (to make up for losses due to electrolysis and evaporation) so that it is usually sufficient to use the approximation

$$C_{P,D_2O,\ell}M^0\left[1-\frac{(1+\beta)It}{2FM^0}\right]\frac{d\Delta\theta}{dt} \simeq C_{P,D_2O,\ell}M^0\frac{d\Delta\theta}{dt} \qquad [2]$$

The term $\left[1-\frac{(1+\lambda)It}{2FM^0}\right]$ allows for the decrease of the radiant surface area with time but, as we have already noted, this term may be neglected for calorimeters silvered in the top portion (however, this term is significant for measurements made in unsilvered Dewars [1]; see also [7]). Similarly, the effects of conductive heat transfer are small. We have therefore set $\Phi = 0$ and have made a small increase in the radiative heat transfer coefficient k_R^0 to k'_R to allow for this assumption. We have shown (see Appendix 2 of [1]) that this leads to a small underestimate of $Q_f(t)$; at the same time the random errors of the estimations are decreased because the number of parameters to be determined is reduced by one.

We have also throughout used the temperature of the water bath as the reference value and arrive at the simpler equation which we have used extensively in our work:

$$\begin{aligned} C_{P,D_2O,\ell}M^0\frac{d\Delta\theta}{dt} &= \left[E_{cell}(t) - E_{thermoneutral,bath}\right]I + Q_f(t) \\ &+ \Delta Q\,H(t-t_1) - \Delta Q\,H(t-t_2) - \frac{3I}{4F}\left[\frac{P}{P^\star - P}\right]\left[\left(C_{P,D_2O,g} - C_{P,D_2O,\ell}\right)\Delta\theta + L\right] \\ &- k'_R\left[(\theta_{bath}+\Delta\theta)^4 - \theta_{bath}^4\right] \end{aligned} \qquad [3]$$

Methods of Data Evaluation: the Precision and Accuracy of the Heat Transfer Coefficients

A very useful first guide to the behaviour of the systems can be obtained by deriving a lower bound of the heat transfer coefficients (designated by $(k'_R)_6$ and/or $(k'_R)_{11}$ in our working manuals and reports) which is based on the assumption that there is zero excess enthalpy generation within the calorimeters:

$$(k'_R)_{11} = \frac{\left\{\left[E_{cell} - E_{thermoneutral,bath}\right]I - \frac{3I}{4F}\left[\frac{P}{P^\star - P}\right]\left[(C_{P,D_2O,g} - C_{P,D_2O,\ell})\Delta\theta + L\right] - C_{P,D_2O,\ell}M^0\frac{d\Delta\theta}{dt}\right\}}{(\theta_{bath}+\Delta\theta)^4 - \theta_{bath}^4} \qquad [4]$$

The reason why $(k'_R)_{11}$ is a lower bound is because the inclusion of any process leading to the generation of heat within the cells (specifically the heat of absorption of D (or H) within the lattice or the generation of excess enthalpy within the electrodes) would increase the derived value of this heat transfer coefficient: $(k'_R)_{11}$ will be equal to the true value of the coefficient only if there is no such source of excess enthalpy in the cells as would be expected to hold, for example, for the polarisation of Pt in D_2O solutions, Fig 2. The simplest procedure is to evaluate these coefficients at a set of

fixed times following the addition of D_2O to make up for losses due to electrolysis and/or evaporation. Convenient positions are just before the times, t_1, at which the calibrating heating pulses are applied to the resistive heaters, Fig 3. For the particular experiment illustrated in Fig 2, the mean value of $(k'_R)_{11}$ for 19 such measurements is $0.7280 \times 10^{-9} WK^{-4}$ with a standard deviation $\sigma_{(k'_R)_{11}} = 0.0013 WK^{-4}$ or 0.17% of the mean.

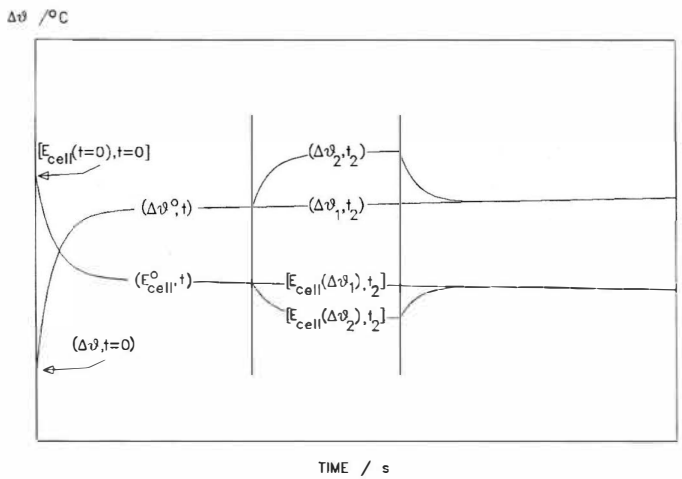

Figure 3. Schematic diagram of the methodology used for the calculations.

It is evident therefore that even such simple procedures can give precise values of the heat transfer coefficients but, needless to say, it is also necessary to investigate their accuracy. We have always done this at the next level of complication by applying heater pulses lying in the time range $t_1 < t < t_2$ and by making a thermal balance just before the termination of this pulse at $t = t_2$. This time is chosen so that

$$t_2 - t_1 \geq 6\tau \qquad [5]$$

where τ is the thermal relaxation time

$$\tau = \frac{M^0 C_{P,D_2O,\ell}}{4k'_R \; \theta^3_{bath}} \qquad [6]$$

The scheme of the calculation is illustrated in Fig 3: we determine the temperatures and cell potentials at t_2 as well as the interpolated values $(\Delta\theta_1, t_2)$ and $[E_{cell}(\Delta\theta_1, t_2)]$ which would apply at these times in the absence of the heater calibration pulse. We derive the heat transfer coefficient which we have designated as $(k'_R)_2$ using

$$(k'_R)_2 = \frac{\Delta Q - \left\{[E_{cell}(\Delta\theta_1), t_2] - [E_{cell}(\Delta\theta_2), t_2]I\right\} - \frac{3I}{4F}\left\{\left(\frac{P_2}{P^\star - P_2}\right)\left[(C_{P,D_2O,g} - C_{P,D_2O,\ell})\Delta\theta_2 + L\right] - \left(\frac{P_1}{P^\star - P_1}\right)\left[(C_{P,D_2O,g} - C_{P,D_2O,\ell})\Delta\theta_1 + L\right]\right\}}{[(\theta_{bath} + \Delta\theta_2)^4 - (\theta_{bath} + \Delta\theta_1)^4]} \quad [7]$$

The mean value of $(k'_R)_2$ for the set of 19 measurements is $0.7264 WK^{-4}$ with a standard deviation $\sigma_{(k'_R)_2} = 0.0099 WK^{-4}$ or 1.4% of the mean.

The comparison of the means and standard deviations of $(k'_R)_2$ and $(k'_R)_{11}$ leads to several important conclusions:

(i) in the first place, we note that the mean of $(k'_R)_{11}$ is accurate as well as precise for such blank experiments: the mean of $(k'_R)_{11}$ is within $0.2\sigma_{(k'_R)_2}$ of the independently calibrated mean values of $(k'_R)_2$; indeed, the mean of $(k'_R)_2$ is also within $\sim 1\sigma_{(k'_R)_{11}}$ of the mean of $(k'_R)_{11}$ so that the differences between $(k'_R)_2$ and $(k'_R)_{11}$ are probably not significant.

(ii) as expected, the precision of $(k'_R)_2$ is lower than that of $(k'_R)_{11}$. This is due mainly to the fact that $(k'_R)_2$ (and other similar values) are derived by dividing by the differences between two comparably large quantities $(\theta_{bath} + \Delta\theta_2)^4 - (\theta_{bath} + \Delta\theta_1)^4$, equation [7]. The difference $(\theta_{bath} + \Delta\theta)^4 - \theta^4_{bath}$ used in deriving $(k'_R)_{11}$, equation [4], is known at a higher level of precision.

(iii) the lowering of the precision of $(k'_R)_2$ as compared to that of $(k'_R)_{11}$ can be avoided by fitting the integrals of equation [1] (for successive cycles following the refilling of the cells) directly to the experimental data (in view of the inhomogeneity and non-linearity of this differential equation, this integration has to be carried out numerically[1] although it is also possible to apply approximate algebraic solutions at high levels of precision [8]). Since the fitting procedures use all the information contained in each single measurement cycle, the precision of the estimates of the heat transfer coefficients, designated as $(k'_R)_5$, can exceed that of the coefficients $(k'_R)_{11}$. We have carried out these fitting procedures by using non-linear regression techniques [1–5] which have the advantage that they give direct estimates of $\sigma_{(k'_R)_5}$ (as well as of the standard deviations of the other parameters to be fitted) for each measurement cycle rather than requiring the use of repeated cycles as in the estimates of $\sigma_{(k'_R)_{11}}$ or $\sigma_{(k'_R)_2}$. While this is not of particular importance for the estimation of k'_R for the cell types illustrated in Fig 1 (since the effects of the irreproducibility of refilling the cells is small in view of the silvering of the upper portions of the Dewars) it is of much greater importance for the measurements carried out with the earlier designs[1] which were not silvered in this part; needless to say, it is important for estimating the variability of Q_f for measurements with all cell designs.

Estimates of k'_R have also been made by applying low pass filtering techniques

(such as the Kalman filter[6] and [8]); these methods have some special advantages as compared to the application of non-linear regression analysis and these advantages will be discussed elsewhere.[8] The values of the heat transfer coefficients derived are closely similar to those of $(k'_R)_5$.

Low pass filtering and non-linear regression are two of the most detailed (and complicated) methods which we have applied in our investigation. Such methods have the special advantage that they avoid the well-known pitfalls of making point-by-point evaluations based on the direct application of the differential equation modelling the system. These methods can be applied equally to make estimates of the lower bound heat transfer coefficient, $(k'_R)_{11}$. However, in this case the complexity of such calculations is not justified because the precision and accuracy of $(k'_R)_{11}$ evaluated point-by-point is already very high for blank experiments, see (i) and (ii) above. Instead, the objective of our preliminary investigations has been to determine what information can be derived for the Pd – H_2O and Pd – D_2O systems using $(k'_R)_{11}$ evaluated point-by-point and bearing in mind the precision and accuracy for blank experiments using Pt cathodes. As we seek to illustrate this pattern of investigation, we will not discuss the methods outlined in this subsection (iii) further in this paper.

(iv) we do, however, draw attention once again to the fact that in applying the heat transfer coefficients calibrated with the heater pulse $\Delta QH(t - t_1) - \Delta QH(t - t_2)$ we have frequently used the coefficient defined by

$$(k'_R)_4 = \frac{\Delta Q - \frac{3I}{4F}\left\{\left(\frac{P_2}{P^*-P_2}\right)\left[(C_{P,D_2O,g} - C_{P,D_2O,\ell})\Delta\theta_2 + L\right] - \left(\frac{P_1}{P^*-P_1}\right)\left[(C_{P,D_2O,g} - C_{P,D_2O,\ell})\Delta\theta_1 + L\right]\right\}}{[(\theta_{bath} + \Delta\theta_2)^4 - (\theta_{bath} + \Delta\theta_1)^4]} \quad [8]$$

and determined at $t = t_2$ to make thermal balances at the point just before the application of the calibrating heater pulse, Fig 3. The differences between the application of $(k'_R)_2$ and $(k'_R)_4$ are negligible for blank experiments which has not been understood by some authors e.g.,[9]. However, for the Pd – D_2O and Pd alloy – D_2O systems, the corresponding rate of excess enthalpy generation, $(Q_f)_2$, is significantly larger than is $(Q_f)_4$ for fully charged electrodes. As we have always chosen to underestimate Q_f, we have preferred to use $(Q_f)_4$ rather than $(Q_f)_2$.

The fact that $(Q_f)_2 > (Q_f)_4$ as well as other features of the experiments, shows that there is an element of "positive feedback" between the increase of temperature and the rate of generation of excess enthalpy. This topic will be discussed elsewhere[8]; we note here that the existence of this feedback has been a major factor in the choice of our calorimetric method and especially in the choice of our experimental protocols. As will be shown below, these provide systems which can generate excess enthalpy at rates above $1 kWcm^{-3}$.

Applications of Measurements of the Lower Bound Heat Transfer Coefficients to the Investigation of the Pd – D_2O System

In our investigations of the Pd – D_2O and Pd alloy – D_2O systems we have found that a great deal of highly diagnostic qualitative and semi-quanitative information can be rapidly obtained by examining the time-dependence of the lower bound

heat transfer coefficient, $(k'_R)_{11}$. The qualitative information is especially useful in this regard as it provides the answer to the key question: "is there generation of excess enthalpy within (or at the surface) of Pd cathodes polarised in D_2O solutions?"

We examine first of all the time-dependence of $(k'_R)_{11}$ in the initial time region for the blank experiment of a Pt cathode polarised in D_2O solution which has been illustrated by Fig 2. Fig 4 shows that $(k'_R)_{11}$ rapidly approaches the true steady state value $0.728 \times 10^{-9} WK^{-4}$ which applies to this particular cell. We conclude that there is no source of excess enthalpy for this system and note that this measurement in itself excludes the possibility of significant re-oxidation of D_2 at the anode or re-reduction of O_2 at the cathode.

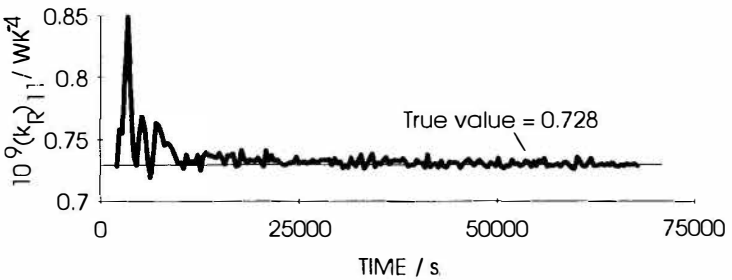

Figure 4. Plot of the heat transfer coefficient for the first day of electrolysis of the experiment described in Fig 2.

We examine next the behaviour of a Pd cathode in H_2O, Fig 5. The lower bound heat transfer coefficient again approaches the true value $0.747 WK^{-4}$ for the particular cell used with increasing time but there is now a marked decrease of $(k'_R)_{11}$ from this value at short times. As we have noted above, such decreases show the presence of a source of excess enthalpy in the system which evidently decreases in accord with the diffusional relaxation time of H^+ in the Pd cathode: this source can be attributed to the heat of absorption of H^+ within the lattice. We also note that the measurement of $(k'_R)_{11}$ in the initial stages is especially sensitive to the presence of such sources of excess enthalpy because $(\theta_{bath} + \Delta\theta)^4 - \theta^4_{bath} \rightarrow 0$ as $t \rightarrow 0$, equation [4]. Furthermore, in the absence of any such source of excess enthalpy the terms $[E_{cell} - E_{thermoneutral,bath}]I$ and $C_{P,D_2O,\ell} M^0 \frac{d\Delta\theta}{dt}$ will balance. The exclusion of the unknown enthalpy source must therefore give a decrease of $(k'_R)_{11}$ from the true value of the heat transfer coefficient. We see that this decrease is so marked for the $Pd - H_2O$ that $(k'_R)_{11}$ is initially negative! The measurements of $(k'_R)_{11}$ are highly sensitive to the exact conditions in the cell in this region of time, so that minor deviations from the true value (as for the $Pt - D_2O$ system, Fig 4) are not significant.

We observe also that measurements of $(k'_R)_{11}$ in the initial stages of the experiments provide an immediate answer to the vexed question: "do the electrodes charge with D^+ (or H^+)?" It is a common experience of research groups working in this field that some samples of Pd do not give cathodes which charge with D^+ (or, at least, which do not charge satisfactorily). A library of plots of $(k'_R)_{11}$ versus time is a useful tool in predicting the outcome of any given experiment!

We examine next the results for one Pd cathode polarised in D_2O solution out of a set of four whose behaviour we will discuss further in the next section. Fig 6B gives the overall temperature-time and cell potential-time data for the second electrode of the set. The overall objective of this part of our investigations has been to determine

the conditions required to produce high rates of excess enthalpy generation at the boiling point of the D_2O solutions. Our protocol for the experiment is based on the hypothesis that the further addition of D^+ to cathodes already highly loaded with deuterium will be endothermic. We therefore charge the electrodes at low to intermediate current densities and at temperatures below 50°C for prolonged periods of time; following this, the current densities are increased and the temperature is allowed to rise. The D^+ is then retained in the cathodes and we take advantage of the "positive feedback" between the temperature and the rate of excess enthalpy generation to drive the cells to the boiling point, Fig 6.

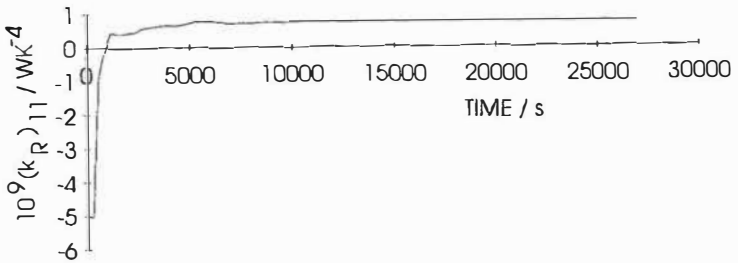

Figure 5. Plot of the heat transfer coefficient for the first day of electrolysis in a "blank" cell containing a 12.5 × 2mm palladium electrode polarised in 0.1M LiOH at 0.250mA.

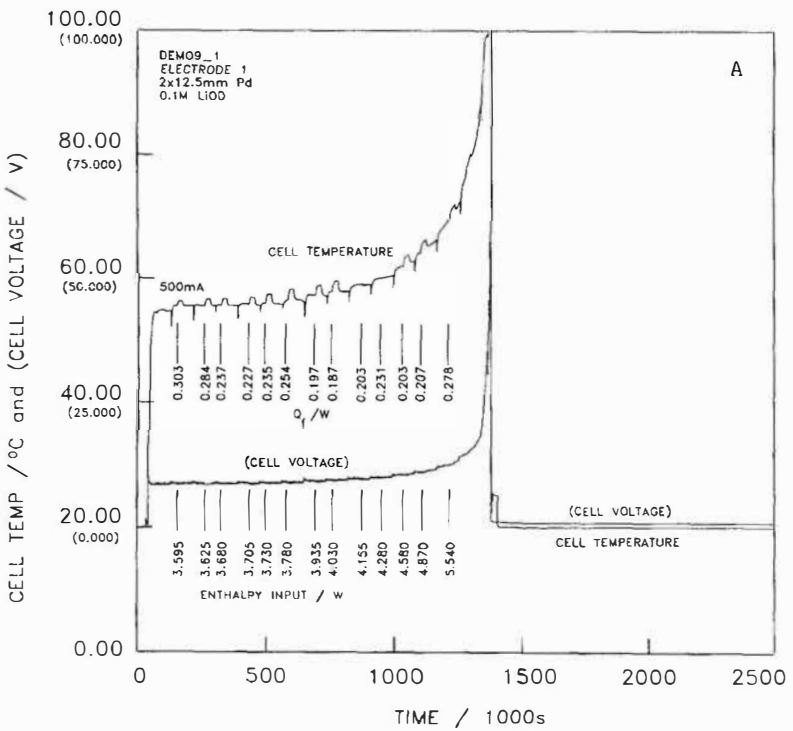

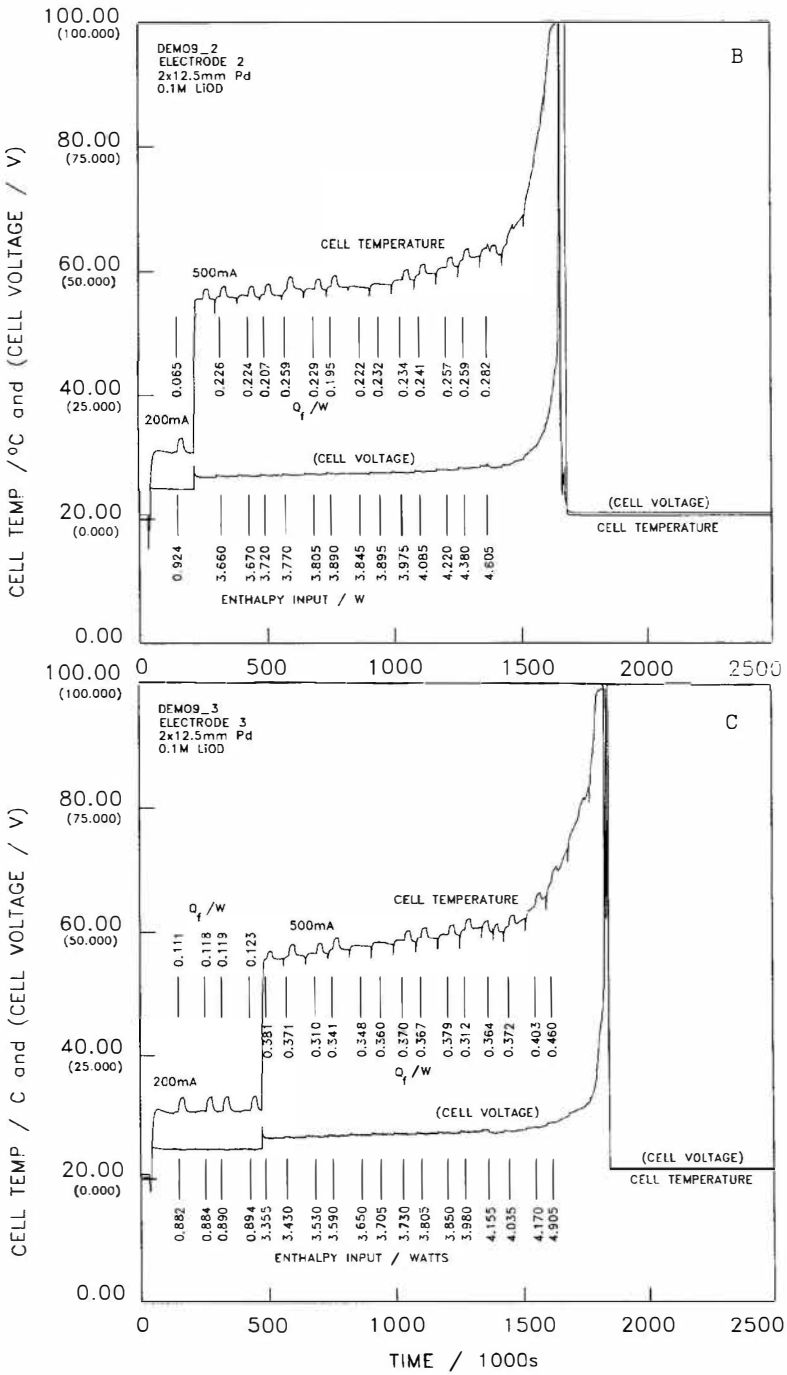
DEMO9_2
ELECTRODE 2
2x12.5mm Pd
0.1M LiOD
B
CELL TEMPERATURE
500mA
200mA
(CELL VOLTAGE)
(CELL VOLTAGE)
CELL TEMPERATURE
Q_f /W
0.065
0.226
0.224
0.207
0.259
0.229
0.195
0.222
0.232
0.234
0.241
0.257
0.259
0.282
0.924
3.660
3.670
3.720
3.770
3.805
3.890
3.845
3.895
3.975
4.085
4.220
4.380
4.605
ENTHALPY INPUT / W
CELL TEMP /°C and (CELL VOLTAGE / V)
100.00
(100.000)
80.00
(75.000)
60.00
(50.000)
40.00
(25.000)
20.00
(0.000)
0.00
0
500
1000
1500
2000
2500
DEMO9_3
ELECTRODE 3
2x12.5mm Pd
0.1M LiOD
C
Q_f /W
CELL TEMPERATURE
500mA
200mA
(CELL VOLTAGE)
(CELL VOLTAGE)
CELL TEMPERATURE
0.111
0.118
0.119
0.123
0.381
0.371
0.310
0.341
0.348
0.360
0.370
0.367
0.379
0.312
0.364
0.372
0.403
0.460
0.882
0.884
0.890
0.894
0.355
0.430
0.530
0.590
0.650
0.705
0.730
0.805
0.850
0.980
4.155
4.035
4.170
4.905
ENTHALPY INPUT / WATTS
CELL TEMP / C and (CELL VOLTAGE / V)
TIME / 1000s

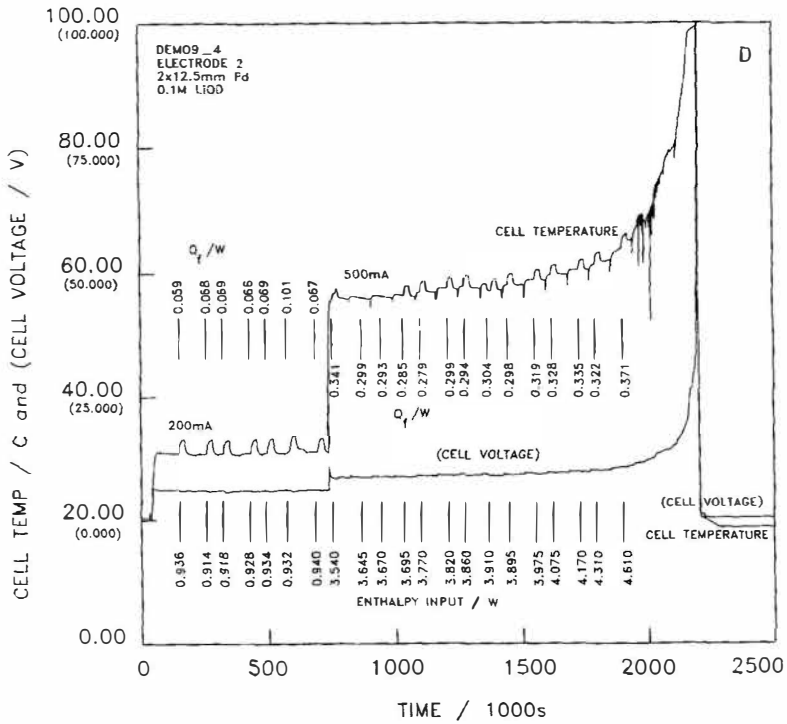

Figure 6. Temperature-time and potential-time profiles for four 12.5 × 2mm palladium electrodes polarised in heavy water (0.1M LiOD). Electrolysis was started at the same time for all cells. The input enthalpies and the excess enthalpy outputs at selected times are indicated on the diagrams. The current in the first cell was 0.500A. The initial current in each of the other 3 cells was 0.200A, which was increased to 0.500A at the beginning of days 3, 6, and 9, respectively.

We examine next the behaviour of the lower bound heat transfer coefficient as a function of time in three regions, Figs 7A-C. For the first day of operation, Fig 7A, $(k'_R)_{11}$ is initially markedly negative in view of the heat of dissolution of D^+ in the lattice. As for the case of dissolution of H^+ in Pd, this phenomenon decays with the diffusional relaxation time so that $(k'_R)_{11}$ increases towards the true value for this cell, $0.892 \times 10^{-9} WK^{-4}$. However, $(k'_R)_{11}$ never reaches this final value because a second exothermic process develops namely, the generation of excess enthalpy in the lattice. In view of this, $(k'_R)_{11}$ again decreases and we observe a maximum: these maxima may be strongly or weakly developed depending on the experimental conditions such as the diameter of the electrodes, the current density, the true heat transfer coefficients, the level of excess enthalpy generation etc.

We take note of an extremely important observation: although $(k'_R)_{11}$ never reaches the true value of the heat transfer coefficient, *the maximum values of this lower bound coefficient are the minimum values of* k'_R *which must be used in evaluating the thermal balances for the cells.* This maximum value is quite independent of other methods of calibration and, clearly, the use of this value will show that there is excess enthalpy generation both at short and at long times. These estimates in Q_f (which

we denote by $(Q_f)_{11}$ are the lower bounds of the excess enthalpy. The conclusion that there is excess enthalpy generation for Pd cathodes polarised in D_2O is inescapable and is independent of any method of calibration which may be adopted so as to put the study on a quantitative basis. It is worth noting that a similar observation about the significance of our data was made in the independent review which was presented at the 2nd Annual Conference on Cold Fusion.[6]

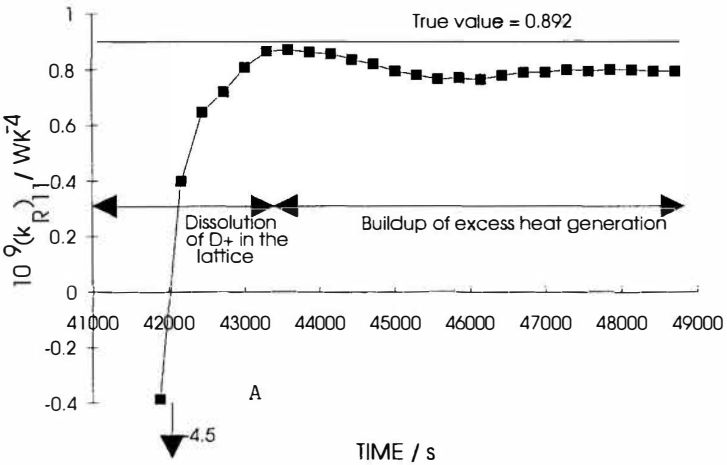

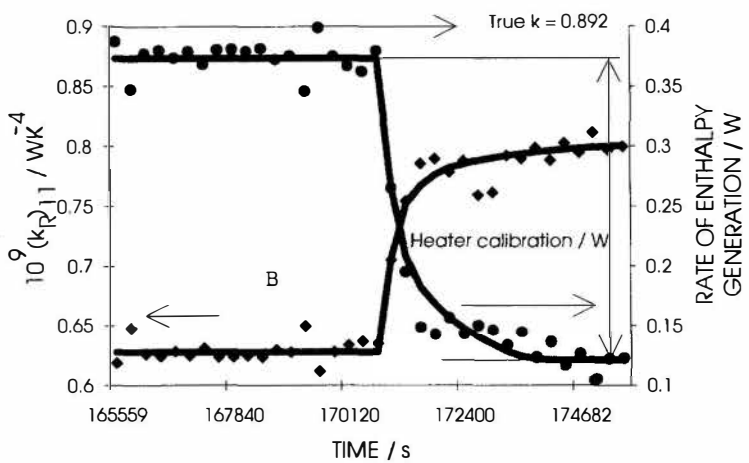

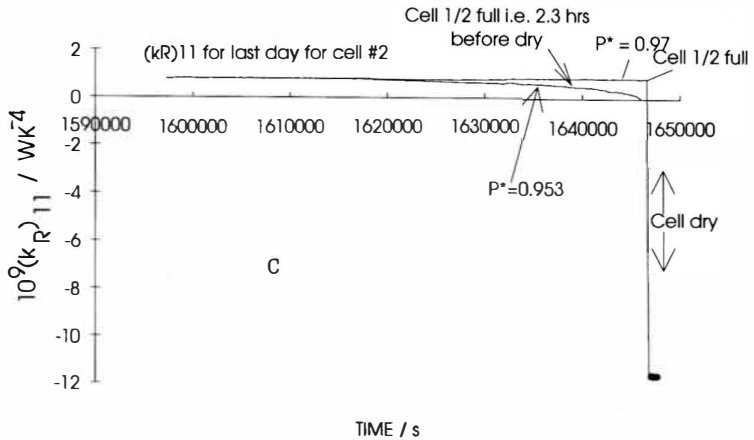

Figure 7. Plots of the lower bound heat transfer coefficient as a function of time for three different periods of the experiment described in Fig. 6B: (A) the first day of electrolysis, (B) during a period including the last part of the calibration cycle, and (C) the last day of electrolysis.

We comment next on the results for part of the second day of operation, Fig 7B. In the region of the first heater calibration pulse (see Fig 6), $(k_R')_{11}$ has decreased from the value shown in Fig 7A. This is due to the operation of the term ΔQ which is not taken into account in calculating $(k_R')_{11}$, see equation [4]. As we traverse the region of the termination of the pulse ΔQ, $t = t_2$, $(k_R')_{11}$ shows the expected increase. Fig 7B also illustrates that the use of the maximum value of $(k_R')_{11}$, Fig 7A, gives a clear indication of the excess enthalpy term ΔQ, here imposed by the resistive heater. We will comment elsewhere on the time dependencies of $(k_R')_{11}$ and of Q in the regions close to $t = t_1$ and $t = t_2$.[8]

The last day of operation is characterised by a rapid rise of temperature up to the boiling point of the electrolyte leading to a short period of intense evaporation/boiling Fig 8. The evidence for the time dependence of the cell contents during the last stages of operation is discussed in the next section. Fig 7C shows the values of $(k_R')_{11}$ calculated using two assumed atmospheric pressures, 0.953 and 0.97 bars. The first value has been chosen to give a smooth evaporation of the cell contents ($M^0 = 5.0$ D_2O) i.e., no boiling during the period up to the point when the cell becomes dry, 50,735 s. However, this particular mode of operation would have required the cell to have been half-full at a time 2.3 hrs before dryness. Furthermore, the ambient pressure at that time was 0.966 bars. We believe therefore that such a mode of operation must be excluded. For the second value of the pressure, 0.97 bars, the cell would have become half empty 11 minutes before dryness, as observed from the video recordings (see the next section) and this in turn requires a period of intense boiling during the last 11 minutes. It can be seen that the heat transfer coefficient $(k_R')_{11}$ decreases gradually for the assumed condition P = 0.953 bars whereas it stays more nearly constant for P = 0.97 up to the time at which the cell is half-full, followed by a very rapid fall to marked negative values. These marked negative values naturally are an expression of the high rates of enthalpy generation required to explain the rapid

boiling during the last 11 minutes of operation. The true behaviour must be close to that calculated for this value of the ambient pressure.

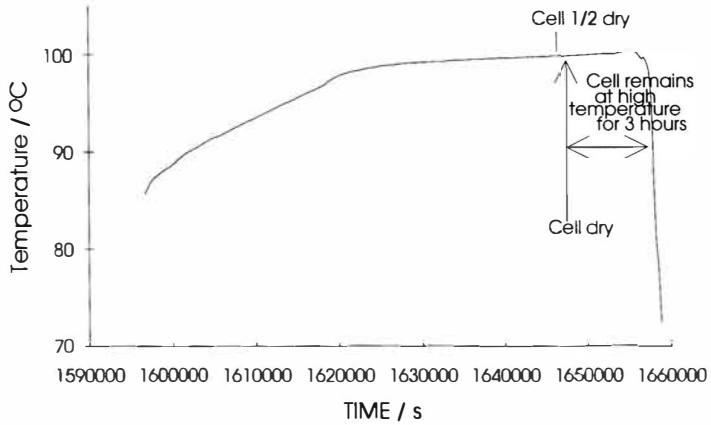

Figure 8. Expansion of the temperature-time portion of Fig 6B during the final period of rapid boiling and evaporation.

Figs 9A and B give the rates of the specific excess enthalpy generation for the first and last day corresponding to the heat transfer coefficients, Figs 7A and C. On the first day the specific rate due to the heat of dissolution of D^+ in the lattice falls rapidly in line with the decreasing rate of diffusion into the lattice coupled with the progressive saturation of the electrode. This is followed by a progressive build up of the long-time rate of excess enthalpy generation. The rates of the specific excess enthalpy generation for the last day of operation are given for the two assumed atmospheric pressures $P^*=0.953$ and 0.97 bars in Fig 9B. These rates are initially insensitive to the choice of the value of P^*. However, with increasing time, (Q_f) for the first condition increases reaching $\sim$300 watts cm^{-3} in the final stages. As we have noted above, this particular pattern of operation is not consistent with the ambient atmospheric pressure. The true behaviour must be close to that for $P^*=0.97$ bars for which (Q_f) remains relatively constant at $\sim$ 20W cm^{-3} for the bulk of the experiment followed by a rapid rise to $\sim$ 4kW cm^{-3} as the cell boils dry.

A Further Simple Method of Investigating the Thermal Balances for the Cells Operating in the Region of the Boiling Point

It will be apparent that for cells operating close to the boiling point, the derived values of Q_f and of $(k'_R)_{11}$ become sensitive to the values of the atmospheric pressure (broadly for $\theta_{cell} > 97.5°C$ e.g., see Fig 9B.) It is therefore necessary to develop independent means of monitoring the progressive evaporation/boiling of the D_2O. The simplest procedure is to make time-lapse video recordings of the operation of the cells which can be synchronised with the temperature-time and cell potential-time data. Figs 6A-D give the records of the operation of four such cells which are illustrated by four stills taken from the video recordings, Fig 10A-D. Of these, Fig 10A illustrates the initial stages of operation as the electrodes are being charged; Fig 10B shows the first cell being driven to boiling, the remaining cells being still at low to intermediate temperatures; Fig 10C shows the last cell being driven to boiling, the first three having boiled dry; finally, 10D shows all cells boiled dry.

As it is possible to repeatedly reverse and run forward the video recordings at

any stage of operation, it also becomes possible to make reasonably accurate estimates of the cell contents. We have chosen to time the evaporation/boiling of the last half of the D_2O in cells of this type and this allows us to make particularly simple thermal balances for the operation in the region of the boiling point. The enthalpy input is estimated from the cell potential-time record, the radiative output is accurately known (temperature measurements become unnecessary!) and the major enthalpy output is due to evaporation of the D_2O. We illustrate this with the behaviour of the cell, Fig 6D, Fig 10D.

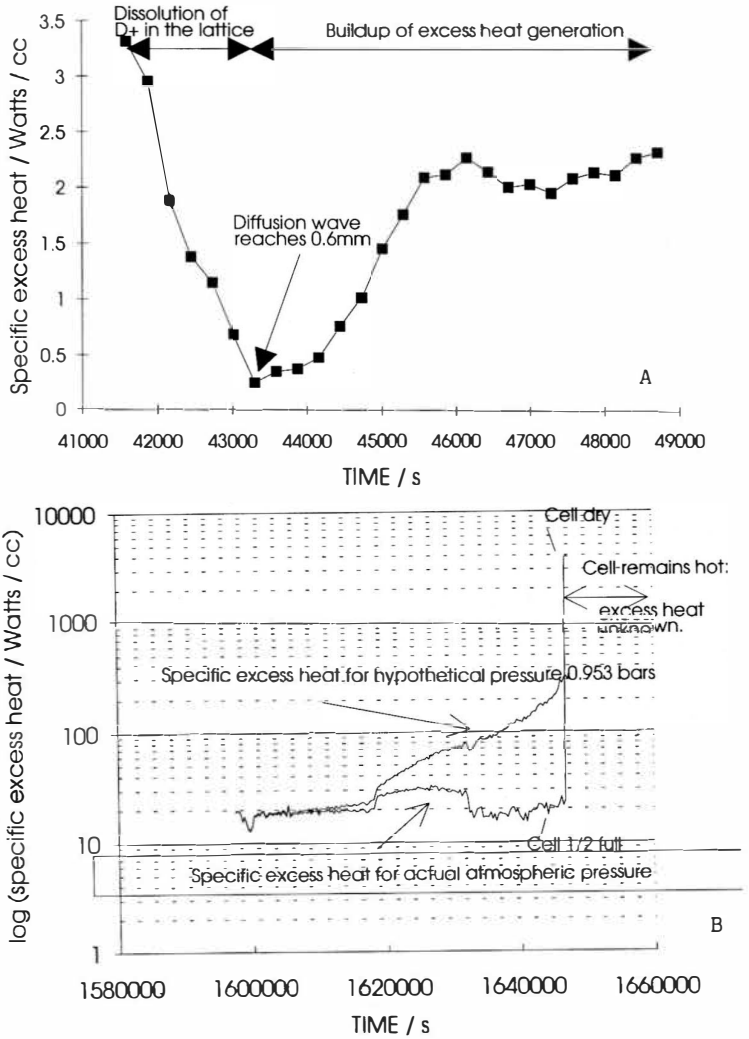

Figure 9. Plots of the specific excess enthalpy generation for (A) the first and (B) the last day of the experiment described in Fig 6B and using the heat transfer coefficients given in Figs 7A and 7C.

CALCULATION

Enthalpy Input

By electrolysis = $(E_{cell} - 1.54) \times$ Cell Current $\simeq$ 22,500J

Enthalpy Output

To Ambient $\simeq k'_R[(374.5°)^4 - (293.15°)^4] \times 600s = 6,700J$

In Vapour $\simeq$ (2.5 Moles $\times$ 41KJ/Mole) = 102,500J

Enthalpy Balance

Excess Enthalpy $\simeq$ 86,700J

Rate of Enthalpy Input

By Electrolysis, 22,500J/600s = 37.5W

Rate of Enthalpy Output

To Ambient, 6,600J/600s = 11W

In Vapour, 102,500J/600s $\simeq$ 171W

Balance of Enthalpy Rates

Excess Rate $\simeq$ 144.5W

Excess Specific Rate $\simeq 144.5W/0.0392cm^3 \simeq 3,700Wcm^{-3}$

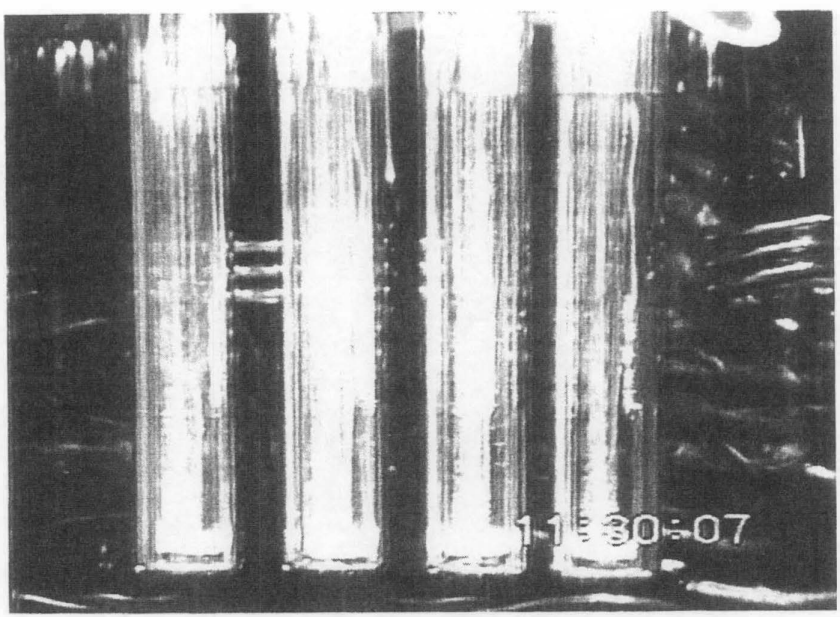

A

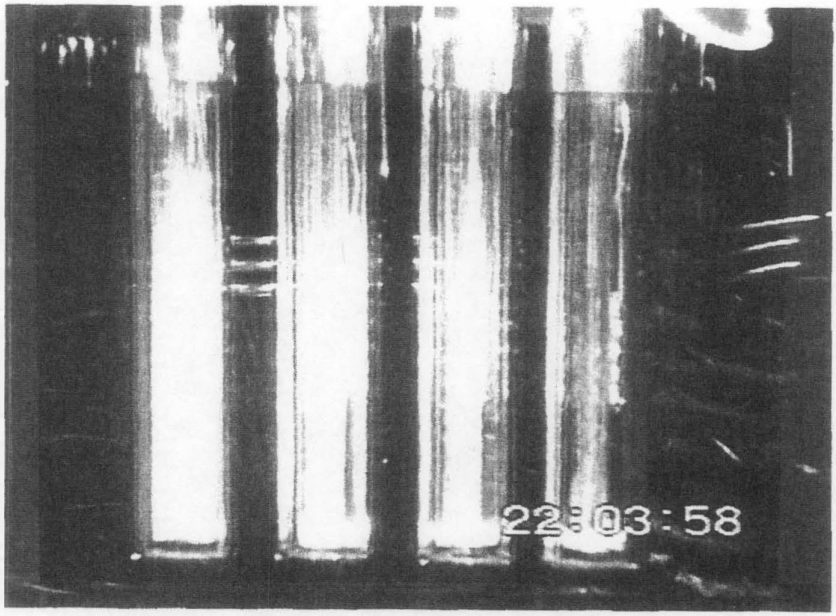

B

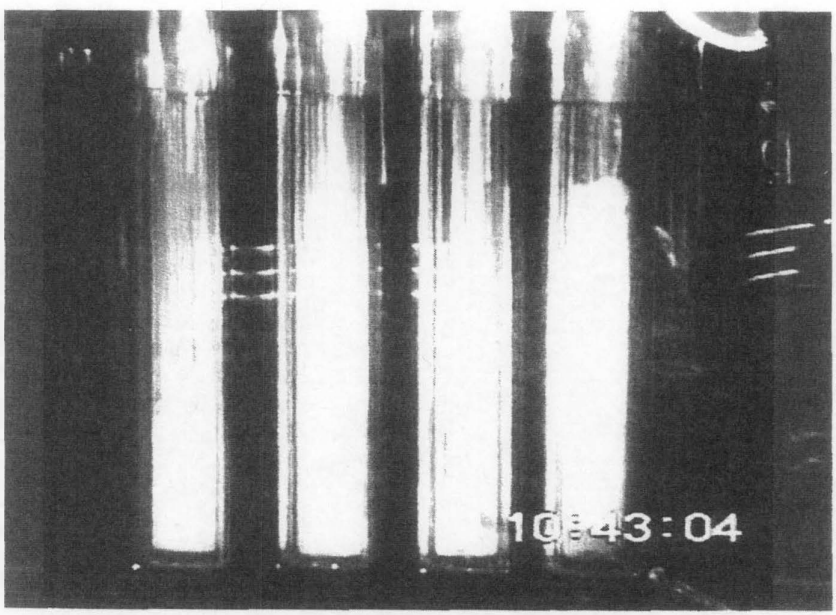

C

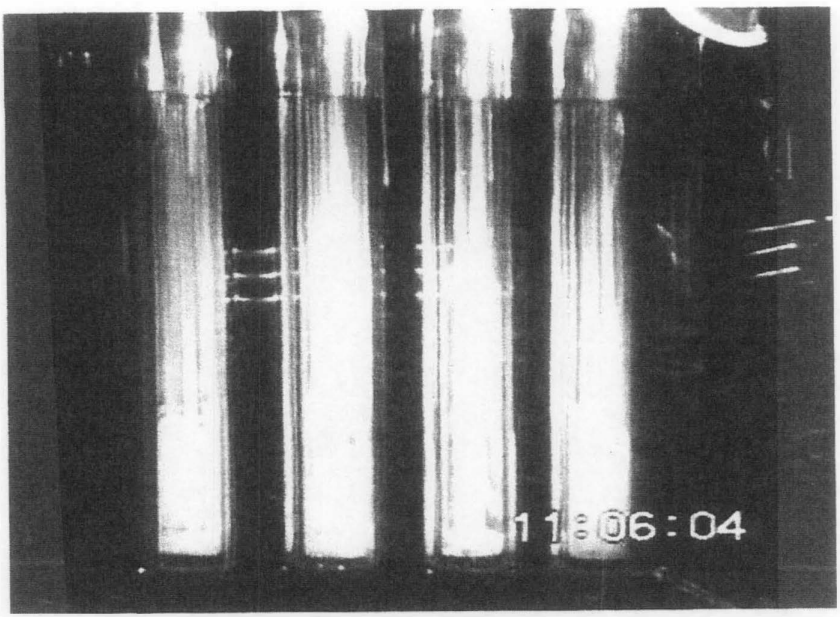

D

Figure 10. Stills of video recordings of the cells described in Fig 6 taken at increasing times. (A) Initial charging of the electrodes. (B) The first cell during the final period of boiling dry with the other cells at lower temperatures. (C) The last cell during the final boiling period, the other cells having boiled dry. (D) All the cells having boiled dry.

We note that excess rate of energy production is about four times that of the enthalpy input even for this highly inefficient system; the specific excess rates are broadly speaking in line with those achieved in fast breeder reactors. We also draw attention to some further important features: provided satisfactory electrode materials are used, the reproducibility of the experiments is high; following the boiling to dryness and the open-circuiting of the cells, the cells nevertheless remain at high temperature for prolonged periods of time, Fig 8; furthermore the Kel-F supports of the electrodes at the base of the cells melt so that the local temperature must exceed 300°C.

We conclude once again with some words of warning. A major cause of the rise in cell voltage is undoubtedly the gas volume between the cathode and anode as the temperature approaches the boiling point (i.e., heavy steam). The further development of this work therefore calls for the use of pressurised systems to reduce this gas volume as well as to further raise the operating temperature. Apart from the intrinsic difficulties of operating such systems it is also not at all clear whether the high levels of enthalpy generation achieved in the cells in Figs 10 are in any sense a limit or whether they would not continue to increase with more prolonged operation. At a specific excess rate of enthalpy production of 2kW cm^{-3}, the electrodes in the cells of Fig 10 are already at the limit at which there would be a switch from nucleate to film

boiling if the current flow were interrupted (we have shown in separate experiments that heat transfer rates in the range 1-10kW cm^{-2} can be achieved provided current flow is maintained i.e., this current flow extends the nucleate boiling regime). The possible consequences of a switch to film boiling are not clear at this stage. We have therefore chosen to work with "open" systems and to allow the cells to boil to dryness before interrupting the current.

GLOSSARY OF SYMBOLS USED

$C_{P,O_2,g}$
: Heat capacity of $O_2, JK^{-1}\text{mol}^{-1}$.

$C_{P,D_2,g}$
: Heat capacity of $D_2, JK^{-1}\text{mol}^{-1}$.

$C_{P,D_2O,\ell}$
: Heat capacity of liquid $D_2O, JK^{-1}\text{mol}^{-1}$.

$C_{P,D_2O,v}$
: Heat capacity of D_2O vapour, $JK^{-1}\text{mol}^{-1}$.

E_{cell}
: Measured cell potential,V.

$E_{cell,t=0}$
: Measured cell potential at the time when the initial values of the parameters are evaluated, V.

$E_{thermoneutral,bath}$
: Potential equivalent of the enthalpy of reaction for the dissociation of heavy water at the bath temperature, V.

F
: Faraday constant, 96484.56 C mol^{-1}.

H
: Heaviside unity function.

I
: Cell current, A.

k_R^0
: Heat transfer coefficient due to radiation at a chosen time origin, WK^{-4}

(k_R')
: Effective heat transfer coefficient due to radiation, WK^{-4}.

ℓ
: Symbol for liquid phase.

L
: Enthalpy of evaporation, $JK^{-1}\text{mol}^{-1}$.

M^0
: Heavy water equivalent of the calorimeter at a chosen time origin, mols.

P
: Partial pressure, Pa; product species.

$P^\star$
: Atmospheric pressure, Pa.

Q_f
: Rate of generation of excess enthalpy, W.

$Q_f(t)$
: Time dependent rate of generation of excess enthalpy, W.

t
: Time, s.

v
: Symbol for vapour phase.

ΔQ
: Rate of heat dissipation of calibration heater, W.

$\Delta\theta$
: Difference in cell and bath temperature, K.

θ Absolute temperature, K.

θ_{bath} Bath temperature, K.

λ Slope of the change in the heat transfer coefficient with time.

Φ Proportionality constant relating conductive heat transfer to the radiative heat transfer term.

References

1. Martin Fleischmann, Stanley Pons, Mark W. Anderson, Liang Jun Li and Marvin Hawkins, J. Electroanal. Chem., 287 (1990) 293.
2. Martin Fleischmann and Stanley Pons, Fusion Technology, 17 (1990) 669.
3. Stanley Pons and Martin Fleischmann, Proceedings of the First Annual Conference on Cold Fusion, Salt Lake City, Utah, U.S.A. (28-31 March, 1990).
4. Stanley Pons and Martin Fleischmann in T. Bressani, E. Del Guidice and G. Preparata (Eds), The Science of Cold Fusion: Proceedings of the II Annual Conference on Cold Fusion, Como, Italy, (29 June-4 July 1991), Vol. 33 of the Conference Proceedings, The Italian Physical Society, Bologna, (1992) 349, ISBN 887794-045-X.
5. M. Fleischmann and S. Pons, J. Electroanal. Chem., 332 (1992) 33.
6. W. Hansen, Report to the Utah State Fusion Energy Council on the Analysis of Selected Pons-Fleischmann Calorimetric Data, in T. Bressani, E. Del Guidice and G. Preparata (Eds), The Science of Cold Fusion: Proceedings of the II Annual Conference on Cold Fusion, Como, Italy, (29 June-4 July 1991), Vol. 33 of the Conference Proceedings, The Italian Physical Society, Bologna, (1992) 491, ISBN 887794-045-X.
7. D.E. Williams, D.J.S. Findlay, D.W. Craston, M.R. Sene, M. Bailey, S. Croft, B.W. Hooten, C.P. Jones, A.R.J. Kucernak, J.A. Mason and R.I. Taylor, Nature, 342 (1989) 375.
8. To be published.
9. R.H. Wilson, J.W. Bray, P.G. Kosky, H.B. Vakil and F.G. Will, J. Electroanal. Chem., 332 (1992) 1.

We dedicate this paper to the memory of our friend, Mr. Minoru Toyoda.

Electrochemical Calorimetry of D_2O Electrolysis Using a Palladium Cathode in a Closed Cell System

Noboru Oyama, Takashi Terashima, Seiji Kasahara, Osamu Hatozaki, Takeo Ohsaka and Tetsu Tatsuma
Department of Applied Chemistry, Tokyo University of Agriculture and Technology
2-24-16 Naka-machi, Koganei, Tokyo 184, Japan

ABSTRACT

Electrolysis of D_2O containing LiOD using palladium cathode was studied with a closed type calorimeter. The electric power input was kept constant, and all D_2 and O_2 generated and liberated to a gas phase were recombined on a catalyst, palladium black supported on a platinum wire. When the electric power of 0.2 W was employed, excess heat generation (2.4%) was observed once out of 5 experiments. No significant generation of excess heat was observed for $LiOH/H_2O$ electrolysis. In the case where the electric power of 0.3 W was employed, excess heat was observed (2.7%) for more than one month in the presence of 200 ppm aluminum. Depositon of aluminum onto the palladium surface was examined by means of in situ electrochemical quartz crystal microbalance.

1. Introduction

Since the observation of excess heat generation in D_2O electrolysis using a palladium cathode was reported (Fleischmann *et al.*, 1989), we have been addressed ourselves to the evaluation of excess heat. In the recent paper, we reported on the observation of excess heat generation in an open system (Oyama *et al.*, 1990). In the open system, however, the evaluation procedure for excess heat is complicated because several parameters must be considered and thus the evaluated value may contain some error (Balej and Divisek, 1989, Divisek *et al.*, 1990, Lewis and Skold, 1990 and Wilson *et al.*, 1992). That is, heat generation through the recombination of D_2 and O_2, the heat uptake through vaporization of D_2O, heat loss by radiation or conduction, and so forth must be taken into account. Thus we constructed a closed system in which D_2 (or H_2) and O_2 generated are recombined on a catalyst so that the errors contained in the open system are much smaller and excess heat can be evaluated more precisely in the present system.

2. Experimental

Electrolysis of D_2O containing LiOD (0.1 M) or H_2O containing LiOH (0.1 M)was performed with a two-electrode system in a twin cell (Figure 1). A palladium

rod (2.0 mm in diameter and 5.0 mm in length) of >99.9% purity (Tanaka Kikinzoku, Japan) and a platinum gauze were used as the cathode and anode, respectively. The product of the electrolytic current and the voltage was kept constant (0.200 or 0.300 W) by a computer (PC9801, NEC, Japan). The other twin cell as a reference was filled with a solution of the same amount and the same composition as was the electrolytic cell. Those twin cells were closed and set in a calorimeter (model MM 5111, Tokyo Riko, Japan) which is kept at 8.0°C. Difference in generated heat between the twin cells was measured and transferred to the computer every 10 seconds together with other parameters, applied voltage and current, for subsequent data processing and analysis. All D_2 (or H_2) and O_2 generated and liberated to a gas phase were recombined on a catalyst, palladium black supported on a platinum wire.

3. Results and Discussion

Calorimetry of LiOD/D_2O Electrolysis. In the case where electric power was kept at 0.200 W, excess heat generation was observed once out of 5 experiments. Figure 1 shows the time-course of the ratio of excess heat (W_{ex}) to input power (W_{in}). Continuous generation of excess heat was observed since the 12th day after beginning of D_2O electrolysis. The total energy produced for 27 days was 11.2 kJ, that means 2.4% of the power input. Excess heat per unit volume was 0.31 W cm^{-3}. Thus obtained excess heat was statistically examined and the value was certified to be larger than the error. Generation of ca. 4 ppm ^4He was observed by means of gas chromatography, though reproducibility and experimental error has not been examined. This value roughly agrees with that expected for the fusion of two D_2 molecules (Miles *et al.*, 1991). Then, another experiment was made with this palladium cathode and a newly prepared LiOD/D_2O solution, and slight excess heat (0.4% of the power input) was observed. On the other hand, no significant generation of excess heat has been observed for H_2O electrolysis.

Next the electric power was kept at 0.300 W to improve the reproducibility of excess heat generation. Further, aluminum (200 ppm) was added to the LiOD/D_2O solution. Aluminum is speculated to exist in the solution as AlO_2^-. In this case, continuous generation of excess heat was observed from the beginning of the electrolysis for more than one month. Figure 2A shows the time-course of the W_{ex}/W_{in} ratio. The total energy produced for 32 days was 22.7 kJ, which corresponds to 2.7% of the power input. Excess heat per unit volume was 0.52 W cm^{-3}. Addition of 50 ppm aluminum to a LiOD/D_2O solution resulted in observation of no significant excess heat generation (Figure 2B). Thus, it was found that aluminum content of the LiOD/D_2O solution might affect reproducibility of the excess heat generation.

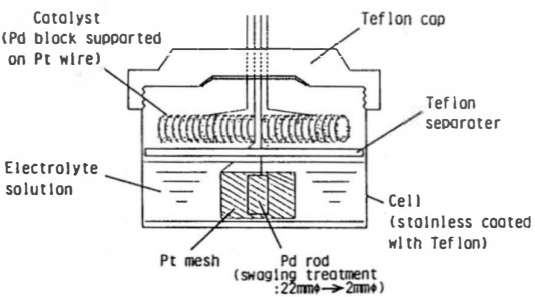

Fig. 1. Schematic depiction of the closed electrolytic cell.

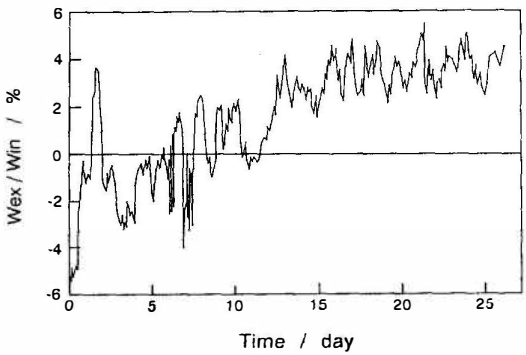

Fig. 2. Energy balance for the electrolysis of D_2O containing 0.1 M LiOD at a palladium cathode at 8.0°C. Input power = 0.20 W.

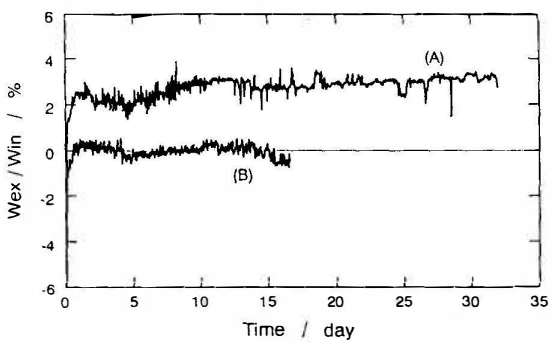

Fig. 3. Energy balance for the electrolysis of D_2O containing 0.1 M LiOD and 200 (A) or 50 (B) ppm aluminum at a palladium cathode at 8.0°C. Input power = 0.30 W.

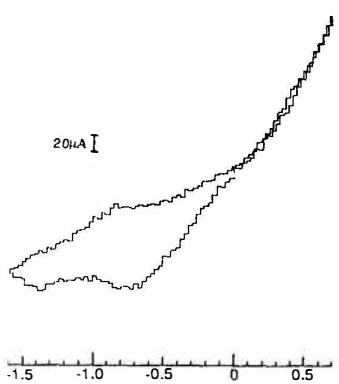

Fig. 4. Typical cyclic voltammogram obtained at palladium electrode in propylene carbonate containing 0.1 M tetrabutylammonium chloride as supporting electrolyte and 10 mM $AlCl_3$. Electrode area = 0.5 cm^2, scan rate = 20 mV s^{-1}.

Electrochemistry of Lithium and Aluminium on the Palladium Electrode. In the studies on calorimetry of $LiOD/D_2O$ or $LiOH/H_2O$ electrolysis, it is important to elucidate electrochemical behavior of lithium. In view of this, we have studied underpotential deposition of lithium by means of electrochemical quartz crystal microbalance (EQCM) (Oyama *et al.*, 1992). Lithium was found to be deposited at negative potential of -700 mV vs. Ag in propylene carbonate. In the present study, as mentioned above, aluminum may also play important role for the excess heat generation. Thus, EQCM technique was employed to study electrochemical behavior of aluminum. Palladium-coated quartz crystal oscillators and propylene carbonate containing 0.1 M tetrabutylammonium chloride as supporting electrolyte and 10 mM $AlCl_3$ were used here. The propylene carbonate solution is presumed to contain about 0.1% (vol) water. Resulted cyclic voltammogram was shown in Figure 4. Cathodic current was observed at a potential region more negative than 0 V vs. Ag and the current showed two peaks at about -0.8 V and -1.4 V. Anodic current increase was observed from 0 V. When the potential was swept between 0 V and -1.6 V, peak height of the cathodic peaks was decreased gradually. Resonant frequency of the quartz crystal was decreased with potential scanning; this indicates that mass of the electrode increased. Next the potential step measurements were performed. When the potential was stepped from 0 V to -1.6 V, mass increase was observed together with a cathodic current. Following step from -1.6 V to 0 V resulted in no significant change in mass, and further step from 0 V to 0.7 V caused mass decrease down to the initial value together with an anodic current. Thus, the cathodic and anodic currents were attributed to the electroreductive deposition and electrooxidative dissolution of aluminum, respectively. Similar behavior might be observed in an $LiOD/D_2O$ solution, though it will be examined elsewhere.

4. References

1. Balej, J. and Divisek, J., 1989, *J. Electroanal. Chem.*, 278, 85.
2. Divisek, J., Furst, L. and Balej, J., 1990, *J. Electroanal. Chem.*, 279, 99.
3. Fleischmann, M., Pons, S. and Hawkins, M., 1989, *J. Electroanal. Chem.*, 261, 301.
4. Lewis, D. and Skold, K., 1990, *J. Electroanal. Chem.*, 294, 275.
5. Miles, M. H., Bush, B. F., Ostrom, G. S. and Lagowski, J. J., 1991, In *The Science of Cold Fusion*, Italian Physical Society, pp. 363.
6. Oyama, N., Ohsaka, T., Hatozaki, O., Kurasawa, Y., Yamamoto, N., Kasahara, S., Ohta, N., Imai, Y., Oyama, Y., Nakamura, T., Shibata, T., Imamura, M., Uwamino, Y. and Shibata, S., 1990, *Bull. Chem. Soc. Jpn.*, 63, 2659.
7. Oyama, N., Yamamoto, N. and Tatsuma, T., 1992, *The 3rd International Conference on Cold Fusion*, Nagoya.
8. Wilson, R. H., Bray, J. W., Kosky, P. G., Vakil, H. B. and Will, F. G., 1992, *J. Electroanal. Chem.*, 332, 1.

Heat Production at the Heavy Water Electrolysis Using Mechanically Treated Pd Cathode

Ken-ichiro OTA, Masaki KURATSUKA,Kotoji ANDO,
Yoshihiro IIDA, Hideaki YOSHITAKE and Nobuyuki KAMIYA

Department of Energy Engineering,
Faculty of Engineering, Yokohama National University
156 Tokiwadai,Hotogaya-ku,Yokohama 240, Japan

ABSTRACT

The heat balances of the heavy water electrolysis by Pd were measured in the closed cell. The excess heat with burst was observed three times out of 13 runs when mechanically treated Pd cathodes were used in 1 M LiOD solution. One of these was for Pd-Ag alloy (90:10) which began at 1,155 h after the start of the electrolysis, lasting for 240 h. The average output power was 105 % of the input during that time. The integrated excess heat was calculated to be 185 MJ per cubic centimeter of palladium. In this case the maximum excess power was recorded for this Pd.

1. Introduction

The excess heat related with the cold fusion phenomena, originally reported by Fleischmann et al., was reproduced by some researching groups. Some reports have demonstrated that the output power was several times larger than the input power. The characteristics of Pd has been considered to be a key for these unusual phenomena in heavy water electrolysis. In this paper the electrolysis with mechanically treated Pd cathodes has been studied with measuring the heat balance and the influence of these treatment on the excess heat generation will be discussed.

FRONTIERS OF COLD FUSION

2. Experimental

The heat balance measurements have been carried out in the 50 cm^3 acrylic electrochemical cell equipped with the catalyst for the recombination of deuterium and oxygen evolved to keep the system thermochemically closed. The flow calorimetry technique was applied; copper tube surrounds the cell where cooling water flows and picking up the generated heat by the electrolysis. The increase of cooling water temperature was measured by CA thermocouples and the flow rate was measured by a measuring cylinder. The output power was calculated by the following equation where T_1 is the input water temperature, T_2 is the output temperature, G is the flow rate, C_p is the specific heat of water and d is the density of water.

$$W_{out} = 4.184/60 \times (T_1 - T_2) G C_p d$$

The electrolysis was operated at the constant power, normally at 10 W (the current density was varied from 200 to 1000 mA /cm^2) . The electrolytes used were 1 M LiOD heavy water solution which was prepared from Li and D_2O (99.9 atom%) in Ar atmosphere and 0.1M LiOH or 1M LiOH light water solution.

Several kinds of Pd were used for the cathode. Among thirteen runs in heavy water electrolysis, five runs were performed for mechanically treated Pd cathode. After the cold roll, Pd (2 mm or 5 mm in diameter with 10 to 20 mm length) was quenched from 1,023 K to get the fine grain size and compressed to promote the internal stress. The other samples were used as received.

3. Results and Discussion

Figure 1 shows the heat balance in the 1 M LiOD electrolysis by Ag-Pd alloy cathode with mechanical treatment. The average output power exceeded the input by ca. 5 % during 1,150 h < t < 1,395 h. That is, excess power of 0.5 W was observed. The power excess reached 13 % in one time. In the other period of this run, Wout/Win kept from 98 to 100 %. The integrated excess energy of this run was 185 MJ/cm^3 Pd for 2,000 h. The other results were summarized in Table 1. Run 17 also showed abnormal increase of electrolyte by 1.4 ℃ at 934 h < t < 935 h and excess power reached up to 9 % at the same time. The energy created in this period was 900 J/cm^3 Pd. Excess power was **never** observed for Pd without the treatment. And the light water electrolysis which is listed as runs No. 4, 7, 8 and 10 in Table 1 showed no unusual behavior as to power balance.

Although the reproducibility should be checked more, these mechanical treatments possibly promote the excess heat.

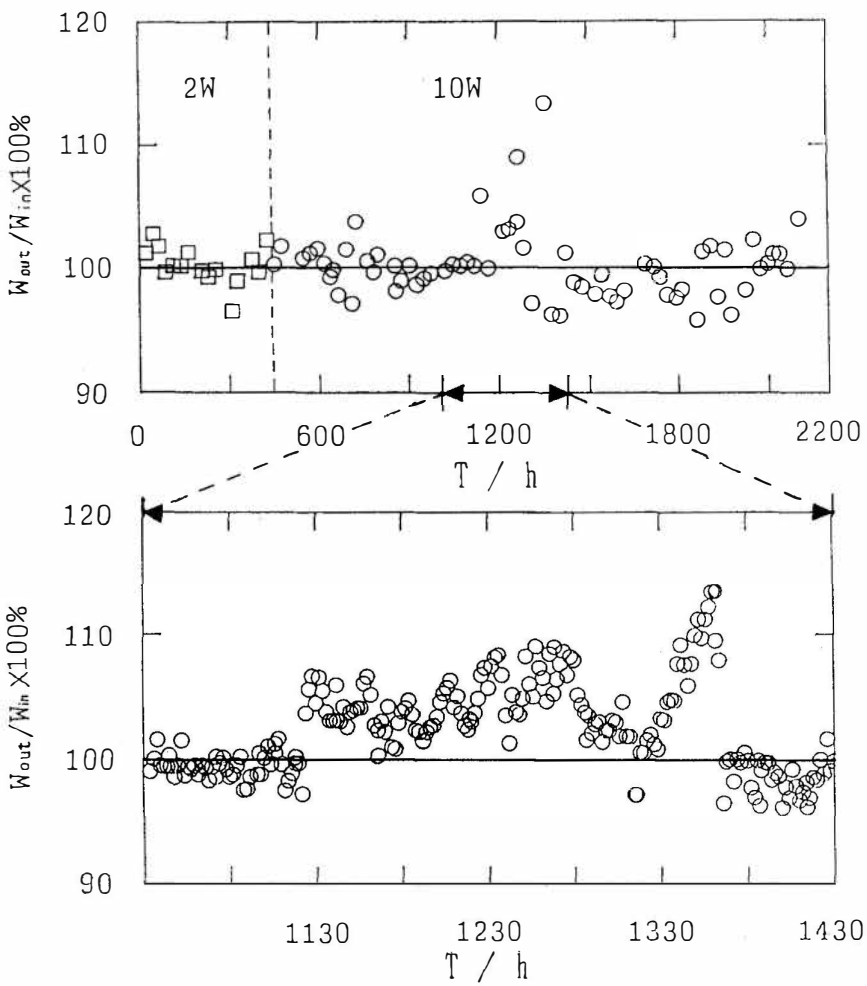

Figure1. Heat balance of electrolysis in 1M LiOD using mechanically treated Ag-Pd(10:90)

Table 1.The results of heat-balance measurement in power-stat electrolysis.

No	electrolyte	Pd dia. × long mm	oolant temp. ℃	current density mA/cm²	Win W	Wout/Win electrolysis max. %	electrolysis time h
1	0.1M LiOD	2 × 20	23	500	8.6	96.9	200
2	0.1M LiOD	2 × 20	23	600~400	8.6	97.6	600
3	0.1M LiOD	2 × 20	23	420	8.6	102.5	600
4	0.1M LiOH	2 × 20	23	500	8.6	95.5	200
5	1M LiOD	2 × 20	5	1260~770	10	101.8	1500
6	1M LiOD	5 × 20	5	630~460	10	99.5	3100
7	1M LiOH	2 × 20	5	1200~440	10	101.1	400
8	1M LiOH	2 × 20	5	1700~960	10	104.3	2000
9	1M LiOD	※5 × 20	5	600~300	10	108.6	2000
10	1M LiOH	Pt	23	-	10	99.8	200
11	1M LiOD	2×20(Ag25%)	23	1400~530	10	99.2	2200
12	1M LiOD	※5 × 20	23	1000~500	10	102.9	890
13	1M LiOD	2×20(Ag10%)	23	1500~900	10	98.7	1900
14	1M LiOD	※5 × 10	23	890~250	10	113.4	2200
15	1M LiOD	2×20(Ag10%)	23	990~430	5	99.6	710
16	1M LiOD	※ 5×10(Ag10%)	23	570~490	5	100.8	1500
17	1M LIOD	※ 5×10(Ag10%)	23	490~160	5	103.2	1500

※ mechanically treated Pd

4. Conclusions

Although these unusual phenomena were detected three times during the heavy water electrolysis with Pd cathodes and the importance of the mechanical treatment was noted , the results have not been yet reproduced enough. Further careful experiments were required.

Repeated Heat Bursts in the Electrolysis of D_2O

C.M. Wan, C.J. Lihn, Z.H. Chin, C.Y. Liang, S.K. Chen,
C.C. Wan, and T.P. Perng
Materials Science Center
National Tsing Hua University
Hsinchu, Taiwan, 30043, R.O.C.

ABSTRACT

Electrolysis of D_2O with Pd rod was performed under static or dynamic charging condition. The current densities were increased in steps in a long duration of electrolysis. During static charging, the Pd electrode was removed from the cell and partially outgassed in air. Resumption of the charging produced several repeated heat bursts. In the dynamic test, cyclic torsion was applied to the Pd electrode during the charging. No abnormal reaction was found during the torsion, but sometimes repeated occurrance of heat burst was observed after the cease of torsion. Possible causes for the heat bursts are proposed.

1. Introduction

"Cold Fusion" phenomenon has received much attention since the anouncement of Fleishmann and Pons in 1989 [1]. The excess heat has been reproduced by several research groups. The characteristics of Pd and the charging condition are considered to be the key factors for the abnormal phenomenon. In this paper, the electrolysis was performed under static or dynamic charging. A cyclic torsion was employed for the latter case. Some repeated heat bursts were observed under certain conditions. The phenomenon was correlated with the possible localized enrichment of deuterium in the defective structure produced during the test.

2. Experimental

A. Static Charging

An annealed palladium rod (99.95% purity, Tanaka) in a diameter of 3 mm was used as a cathode, which was surrounded by a wire-wound platinum anode. The Pd rod was annealed at 1100 K in vacuum for 2 hr before the electrolysis. The cell with 400 ml of electrolyte (0.1M LiOD in D_2O) was immersed in a 20-liter thermally insulated water tank. The experimental setup of the cell and tank has been reported previously [2]. The charging current densities were increased in steps from less than

0.1 to 1.8 A/cm^2 in a prolonged electrolysis. The electrolyte was automatically replenished to maintain a constant volume. The parameters monitored included the cell and tank temperatures and the cell current and voltage.

B. Dynamic charging

A cylindrical tensile specimen of Pd rod was mounted in a torsion testing machine. The gage section in a diameter of 3 mm and 3 cm long was enclosed in a glass cell for charging. The center of the cell bottom where the rod went through was sealed with silicon rubber so that cyclic torsion could be applied during the charging. The torsion amplitude was controlled at $\pm 3^{o}$ except higher ranges were used in the last run. The frequency was set at 0.1 Hz. The charging current density varied from 5 to 50 mA/cm^2. Cyclic torsion was applied after the specimen had been saturated with deuterium at a selected current density. The duration for each torsion was about 2 hr. After that, the charging current was increased and a similar sequence followed. Sometimes the charging current was also varied during the torsion to examine the effect of concentration gradient. Two thermocouples, one in the cell, the other one just outside of the cell, were used to monitor the temperature difference during the test.

3. Results

A. Static Charging

During the prolonged electrolysis, the temperature difference between the electrolyte and the tank water depended on the magnitude of charging current. A difference of 10 ^{o}C was observed for 1.8 A/cm^2. The cell temperature occasionally showed some abnormal fluctuation, but the fluctuation was always insignificant, less than 0.5^{o}C. There was no any abnormal temperature burst during the electrolysis for seven weeks. The experiment was then stopped, and both Pd cathode and Pt anode were removed from the cell. The Pd electrode was left in air to allow the outgassing of deuterium, whereas the Pt electrode was immersed in HNO_3 solution to get a cleaner surface. After 40 minutes of interruption of the experiment, both electrodes were put back to the cell assembly and the electrolysis was resumed. A series of cell temperature bursts, ranged from 1.0 to 2.5^{o}C were observed in the subsequent charging, as shown in Fig. 1. The first burst occurred at about 90 minutes after the restart of the experiment and lasted for 20 min. Similar events repeated more than

20 times within 5 days.

B. Dynamic charging

Since the cell was not insulated during the test, there was always a constant temperature difference between the cell and the ambient air. The difference increased with the charging current due to higher joule heating. No temperature burst was ever observed during the cyclic torsion. However, in one case, repeated bursts were observed after the cease of torsion. The first burst occurred about one hour after the torsion had been stopped. Subsequent bursts took place in a period of 13 hr, as shown in Fig. 2. The longest burst lasted for about one hour and the increase of temperature in the cell was about 1.5^{o}C. Further charging with or without torsion at higher current densities did not reproduce the same phenomenon. Even when the torsion amplitude was raised to $\pm 10^{o}$ and then $\pm 30^{o}$ in the final run, no abnormal burst was observed.

4. Discussion

The repeated heat bursts observed in static charging occurred only after the electrode had been partially outgassed. Since the lattice parameter of Pd increased from 3.89 Å to 4.02 Å after the formation of hydride (deuteride), the outgassing would cause some plastic strain in the surface layer, leading to a high concentration of dislocations. These dislocations could, in principle, provide an efficient trapping for deuterium atoms. Resumption of charging produced enrichment of deuterium around these dislocations. It has been frequently proposed that in order for the abnormal reaction to occur, a critical loading ratio of D/Pd has to be achieved. The localized enrichment of deuterium in the outgassed region might have contributed to the phenomenon.

Similar argument can also be applied to the dynamic charging. During the cyclic torsion, the degree of deformation in the outer layer was higher than that in the inner region. More dislocations were produced in the outer layer and more deuterium would segregate around these dislocations. Note that with a frequency of 0.1 Hz and an amplitude of $\pm\ 3^{o}$, the deformation rate was so high that dislocation sweep-in of deuterium would not occur. This explains why the bursts were observed only after the stop of torsion but not during the torsion. To examine whether transport of deuterium by dislocations can result in enrichment of deuterium at heterogeneous sites, a slower torsion rate or a slower extension rate tensile test should have been used.

Finally, it is reminded that the dynamic charging has one more advantage, i.e., the cyclic torsion could destroy the surface scale, allowing a regular flux of deuterium to diffuse into the electrode.

5. Conclusion

Repeated temperature bursts were observed in both static and dynamic electrolysis conditions. In static charging, the bursts occurred after partial outgassing of deuterium from the Pd electrode. In dynamic charging, the bursts occurred after the stop of torsion. The abnormal reaction could be correlated to the localized enrichment of deuterium at dislocations created by the test condition.

Acknowledgment

This research was supported by the National Science Council of Republic of China under Contract No. NSC 80-0405-E-007-26 and the Materials Science Center, National Tsing Hua University.

References

1. Fleishmann, M. and Pons, S., 1989, J. Electroanal. Chem., 261, 301.
2. Yang, C.-S., Liang, C.-Y., Perng, T.-P., Yuan, L.-J., Wan, C.-M., and Wan, C.-C., 1990, Special Symposium Proceedings on Cold Fusion, WHEC #8, P. 95.

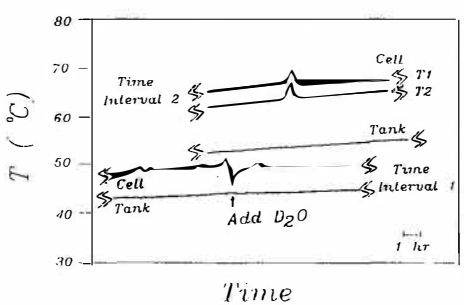

Fig. 1. Temperatures of the cell and tank in two different time intervals. In time interval 2, a higher charging current was applied and two thermocouples were used to monitor the cell temperatures at different locations.

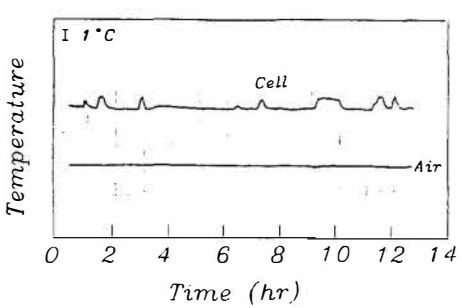

Fig. 2. Temperatures of the cell and the ambient air in one selected time interval after stop of torsion.

Anomalous Excess Heat by D_2O/Pd Cell under L-H Mode Electrolysis

Akito TAKAHASHI , Akimasa MEGA , Takayuki TAKEUCHI, Hiroyuki MIYAMARU and *Toshiyuki IIDA*

Department of Nuclear Engineering , Osaka University , 2-1 Yamadaoka , Suita , Osaka-565 , Japan

ABSTRACT

Using a plane symmetric configuration of centered Pd sheet cathode and Pt-wired anode in D_2O/LiOD electrolysis with the L-H mode pulse operation , anomalously large excess heat (32 watts in average for 2 months , 100~130 watts at peaks and averaged output/input power ratio 1.7) was once observed associating very few (~1 n/s) neutron emission . To investigate the reproducibility of this experiment , the second experiment with minor changes for cell was done for 4 months . We could reproduce excess heat , however with much smaller amounts (8 watts in average and 15 watts at peak) , and twice larger neutron emission rates . Discussions are given by speculating possible condition changes in two experiments , i.e. ,cell voltages and over-potentials , formation of thin MOS film on Pd cathode surface and mechanism enhancing D/Pd ratio . Excess power density per cm^2 of cathode surface showed systematic change as a function of surface current density . This trend is consistent with results by many other authors .

1. Introduction

The so called Fleischmann-Pons effect[1] , i.e. , unknown excess heat generation in Pd-cathode of D_2O/LiOD electrolysis has been confirmed by several groups[2),3)]. Some of critical conditions to meet excess heat , e.g. , unusual enhancement of D/Pd ratio (more than 0.85 in volume average) and critical current density (~200 mA/cm^2) are being clarified[2),4)] .

Results of many researches are converging onto an issue that the phenomenon occurs near surface of Pd cathode . To establish the reproducible excess heat effect , some key conditions are still missing . Those are conceived to be related to surface conditions of Pd cathode .

The dynamical electrolysis method used by present authors which once showed anomalously large excess heat[3] may realize the above mentioned critical conditions . The method is based on the adoption of Pd-sheet cathode (instead of thin rod adopted by other groups[1),3)]) centered in wired Pt anode and L-H mode pulse current operation with several hours repetition period . This "Takahashi method" is now being tried by many groups[5),6),7),8),9)] , many of which have been observing significant levels of excess heat , though what is going on is not well resolved .

The most important issue to be clarified is what the source of excess heat is , i.e. , nuclear origin or something else . Observation of close relations between excess heat and nuclear products (^{4}He,^{3}He,n,t,changed particles and photons) is the key to find underlying physics .

In this paper , we report the protocol of Takahashi method , major results of the first experiment (Experiment-D[3]) and our replication experiment (Experiment-D2) . Simultaneous measurements of excess heat and neutron emission have been done in this work . In addition , off-line monitoring of tritium level is shown . Discussions are given on critical conditions to reproduce the Fleischmann-Pons effect .

2. Experimental Method : Protocol

A detailed description is given in Ref.3 . The protocol is outlined as follows:

1) Setting-up : For cathode , 99.99% pure cold-worked Pd sheet with 1mm thick and 25mm square wide size is used . As shown in Fig.1, an electrodes-unit of centered Pd sheet cathode and plane-symmetrically wound Pt wire (0.5mm diameter , 7 turns with 5mm pitch) is made using polyethylene or acrylite supporter . Minimum cathode-anode distance is 10mm . This configuration of electrodes is expected to give uniform electrolytic current density on Pd cathode surfaces , hence to realize uniform deuteron loading into Pd sheet . A box-type or cylindrical cell container made of 5mm thick acrylite is used . The electrodes-unit is immersed into electrolyte of 700cc D_2O+0.3 mol/litter LiOD . An external cooling coil made of pyrex glass tube , through which temperature-regulated (20 °C±0.05 °C) light water is fed with 5~10 l/min flow rate (very

stable for long period), is also immersed in electrolyte . To stabilize the coolant temperature , a computerized chiller/heater equipment is used .

2) Procedure of electrolysis : For the beginning several days (typically one week), the sawtooth-current mode (repeated ramps from 0.25amp to 5.0amp with about 20min period) is tried to find generation of excess neutron counts above background level . Then we switch to the L-H current mode (typically , 0.2~0.4amp L-mode with 6 hours and 4.0~5.0 amp for H-mode with 6 hours) which is continued for 2~4 months to observe excess

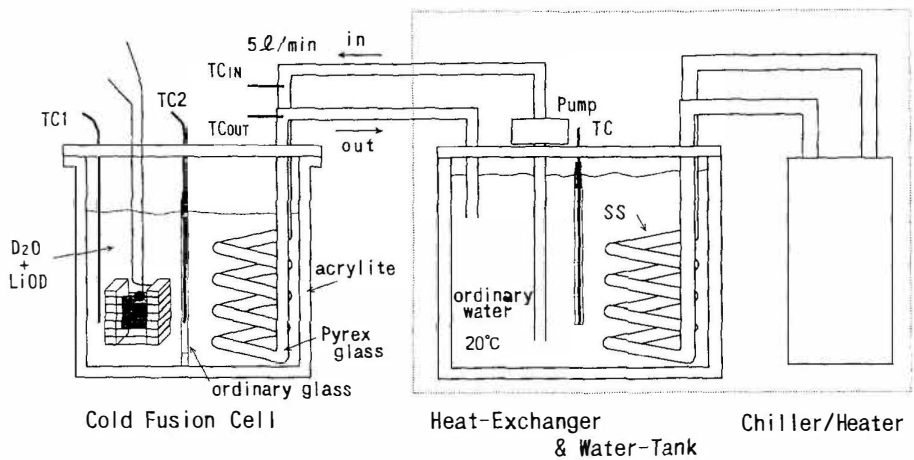

Fig.1 : Schematic view of electrolysis cell for L-H mode operation and cooling system .

heat , neutrons and tritium . We operate the electrolysis by current-controlled mode (constant current mode for L or H period). We monitor current and cell voltage . To compensate consumed D_2O by dissociation , we add fresh D_2O every several days (2~7 days depending on procedure) to the cell . Observation by oscilloscope found no AC power components during the L and H periods , except the beginning 10 min of switching .

3) Calorimetry: As shown in Fig.1 , we monitor cell temperatures by teflon coated thermocouples at 1 or 2 points (later we used 3~4 points[10]), and inlet (TCin) and outlet (TCout) temperatures of coolant . The calorimetry system is designed to cover a wide range of heat-power variation (1~200 watts) keeping linearity between heat-power level and temperature rises . We checked temperature variation in the electrolyte zone , and found it very uniform except the regions inside the

electrodes-unit and close to the cooling coil . Strong stirring effect by gas bubbling and convection current flow is attributed to uniforming cell temperature distribution . Due to high flow rate (5 l/min for Experiment-D2) of coolant , the cell reaches thermal equilibrium in 30 min when we switch the mode from L to H (or reverse), so that thermal energy balance of cell becomes simply $Q^{+}=kS(T_e-T_c)$, where Q^{+} is the heat source by joule-heating of electrolysis (+"nuclear" heating), T_e the equilibrium cell temperature , T_c the coolant temperature ($T_c=(T_{in}+T_{out})/2$), S the effective surface of cooling coil and k the heat conductivity of coil . We can ignore heat leak to (or from) ambient . Heat removal by coolant is $Q^{-}=4.2V_c(T_{out}-T_{in})$, where V_c is the coolant flow rate . Of course , it holds $Q^{+}=Q^{-}$. Correction for electrolyte level height is done using the former equation (7% at most for D_2O addition cycle of 7 days).

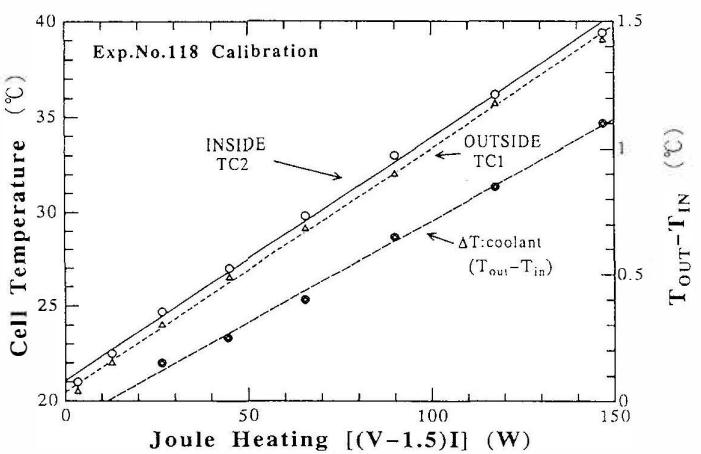

Fig.2 : Calibration for calorimetry for Exp.D2 .

For calorimetry calibration , we used a "dead" Pd plate (Exp.D) or a fresh Pd plate (Exp.D2 , regarding no excess heat at beginning). Calibration run was done by step-wise changing of current for every one hour . Calibration curves for Exp.D2 is shown in Fig.2 , which proves that the linear relation holds between heat-power level and temperature rise . We tried a gold plate cathode , instead of Pd , for calibration , but we found a slightly different slope , probably due to the change of bubbling on Au surface (electrochemical situation would be changed). Delta-T of coolant is a best monitor of calorimetry in principle , but the accuracy in the present system is not good due to a

small temperature rise (less than 1°C). Sensitivity of cell temperature is much higher . Difference of temperatures at inside and outside points is apparent due to the systematic shift of ambient-temperature compensation circuit of used data logger . We averaged temperatures of two points to make a calibration line . We obtained 7.0 watts per degree C as calorimetry constant for Exp.D2 . Estimated error for excess heat is ±1.0 watt , mostly due to the effect of turbulence flow of electrolyte .

4)Measurements of nuclear products : To monitor neutrons , we have been using a cross-checking system between an NE213 recoil proton spectrometer and a ^{3}He thermal neutron detector . The detailed circuit diagram and adjusting procedure are shown in Ref.11 . We record time history of neutron counts every 4 minutes , energy spectra of recoil protons (equivalently neutron spectra) in L and H periods and integrated sum peak area of $^{3}He(n,p)$reaction . All the time , we monitor continuously rise-time distribution of neutron signals to check any drift and contamination of gamma and noise signals ; no contamination was found in the series of this work . To monitor tritium level of electrolyte , we sample 1cc fresh D_2O before addition and 1cc electrolyte every week to be counted by a LSC (liquid scintillation counting) system .

3. Highlight of Exp.D

The detail of results is shown in Ref.3 . Here we pick up few results which are used for comparing with Exp.D2 later . Observed excess heat (average in 6 hours L or H period) and neutrons as a function of sweep number of L-H mode are shown in Fig.3-a&b , respectively for the first and the second month of runs . It looks that there are a bias-level of excess heat of 10-30 watts continuously and superposed heat bursts of 30-100 watts . This feature resembles with the results of Pons-Fleischmann[12] . For the two months run , total input energy was 250 MJ , total output energy 410 MJ and excess heat 160 MJ . The results destroy the 2nd law of thermodynamics unless we find a hidden free energy source which is 1000 times greater than any conceivable chemical heat sources in the cell[3] . Neutron emission is positive , but its rate is only about 1 n/s/source . However , we see correlations with the evolution of excess heat ;H-modes gave larger excess heats and larger neutron counts , compared with L-modes . In H-modes , when excess heat level increased , neutron count rates mostly decreased . If excess heats were generated by usual d-d fusions , we should

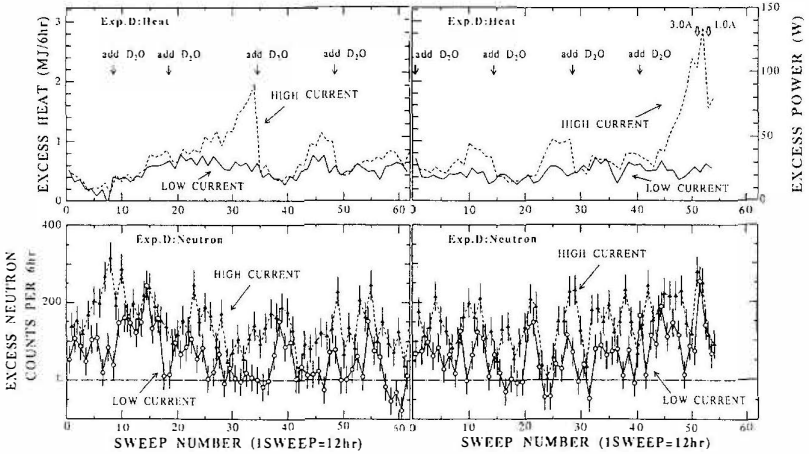

a) First one month b) Second one month
Fig.3 : Evolution of excess heat and neutron yield as a function of sweep cycle number of L-H mode electrolysis for Exp.D[3].

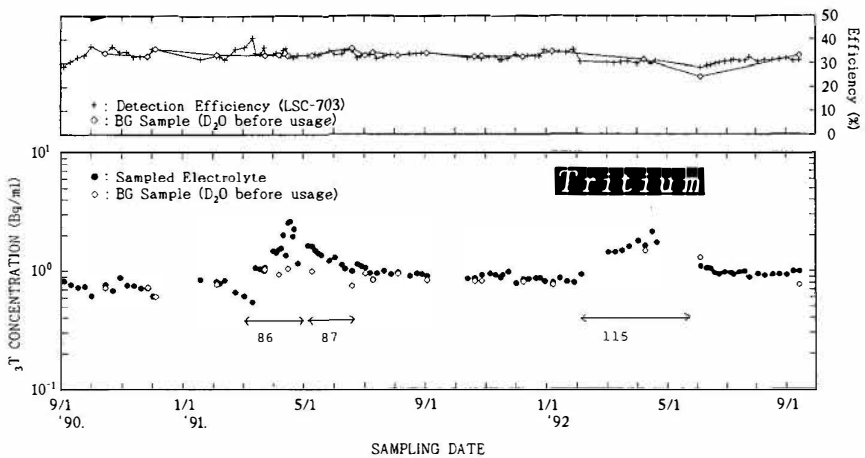

Fig.4 : Observed variation of tritium levels in electrolyte (solid points), compared with BG runs (white points) .

observe 10^{14}n/s/source so that observed excess heats could not be due to d-d fusions . A hypothetical interpretation[3] was given based on the multibody deuteron fusion reactions which emitted only high energy charged particles (α,d,t,^{3}He) as direct products and would produce very low level neutrons as secondary products . Fig.4 shows the results of tritium observation . We observed meaningful tritium generation in Exp.C[13](

No.86 & 87 runs) to give (n/t) ~10^{-5-6} . In Exp.D (No.115 run), we find increase of tritium level , but only one blank sample (fresh D_2O) also showed an increased level and we can not conclude tritium generation .

4. Replication Experiment : Exp.D2

Procedure of this replication experiment is shown in Table-1. To do this, we renewed electrolyte and Pd cathode sheet (same batch of Exp.D , batch No.1 from Tanaka Precious Metal Co.), added one thermocouple (see Fig.1) in electrolyte , put two thermocouples into inlet and outlet pipes of coolant and removed a thermocouple-support of soda glass . After about 10 hours of calibration run , we started the sawtooth run . After 2 days of the sawtooth run , we found clear increase of neutron count rates (see Fig.5), but we continued the sawtooth mode for 7 days . Time-dependent calorimetry within 20 min period of sawtooth is difficult since it takes 30 min for reaching thermal equilibrium , so that

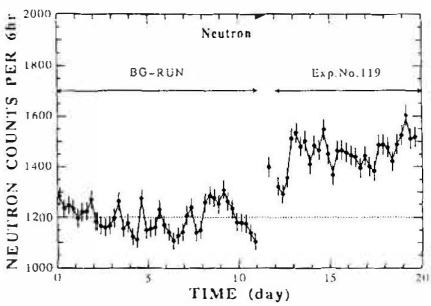

Fig.5 :Neutron generation by sawtooth current mode electrolysis

Table-1 : Procedure of Experiment D2

1) Calibration Run : Exp. No. 118
Beginning of electrolysis , renewed Pd sheet. (regarding no excess heat)
Stepup of electrolysis current for 9 steps: 0,1,2,3,4,5,6,7,8 amperes ; one hour per step .
2) Sawtooth Run : Pre-loading. Exp. No. 119
0.17 (minimum) to 5.0 (maximum) amperes.
20 minutes period. 7 days.
3) L/H Mode Run : Main Run. 6 hr / 6 hr
Exp.No.120;L/H = 0.17 A / 4.0 A (0.3 W / 44 W)20days
L/H = 0.4 A / 5.0 A14 days
L/H = 0.4 A / 6.0 A20 days
L/H = 1.0 A / 7.0 A20 days
Exp.No. 121 ;Step up Mode (same with Calibration)2 days
Exp.No. 122 ;L/H = 0.4 A / 3.0 A20 days
Exp.No. 123 ;L/H = 0.4 A / 4.0 A50 days

(Electricity in Campus was off for one day btw. Run-1 and Run-2 of Exp. 122.)

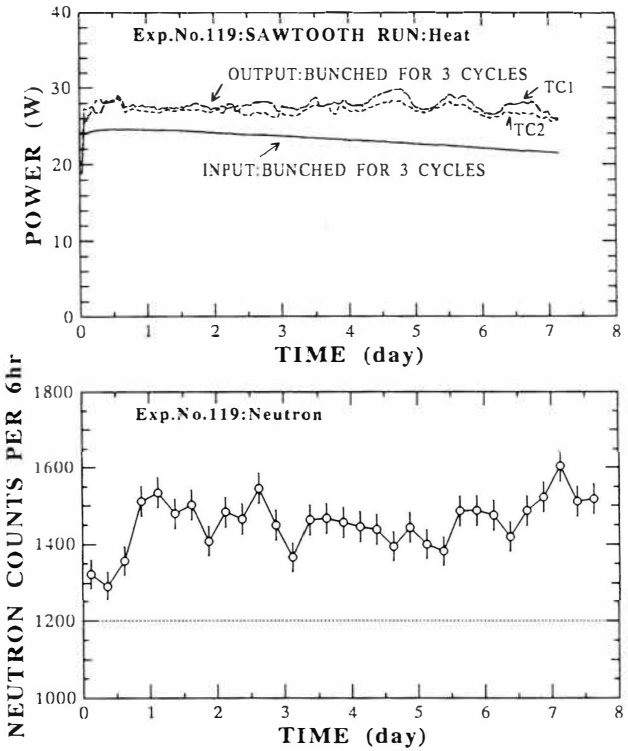

Fig.6 : Evolutions of excess heat and neutron yield by sawtooth current mode electrolysis ; 3 cycles data are bunched and averaged .

we averaged over 3 cycles of sawtooth-periods to reduce averaged input and output . The results are shown in Fig.6, compared with neutron emission rates . We saw excess heat in a day and excess heat increased gradually to reach 6 watts (29% of input) in 7 days .

From 8th day we started L-H mode run and continued for more than 3 months . For the first one month , excess heat level was rather constant (6~10 watts for H-mode and 2~4 watts for L-mode). We did not see rapid increase as in the case of Exp.D . Experiments were interrupted twice (in No.122 and No.123 runs), due to electric power shut down of Campus , for one day long each event . When we restarted electrolysis with L-mode , cell temperature increased slowly from 20.0 °C to higher value in 6 hours . Excess heats after restarts were about half of those before the power shut down ,

and recovered in 2~3 weeks . For about 3 months run of Exp.D2 , we changed currents for either L or H modes to take excess heat data for seeing if we found systematics between excess heat and current density . A typical data is shown in Fig.7 , which shows gradual increase of excess heat in a month . Corresponding excess neutron rates over background (B.G≈1200 counts per 6 hr) show higher count rates for H-modes and smaller for L-modes , as in the case of Exp.D , however absolute yields increased about twice of those in Exp.D , although average-excess heat level decreased to about 1/4 of that in Exp.D(average). This result is predicted by the multibody fusion theory[3]. Exp.D2 is still running the 4th month , and we have not observed big heat bursts like those in Exp.D .

Doubly increased neutron yields in Exp.D2 improved statistics of neutron spectroscopy , so that we could obtain neutron spectra having two components at 2.45 MeV and 3~7 MeV region as we observed in Exp.B and Exp.C[3], which were explained as the consequence of competing process of d-d and d-d-d fusions[13].

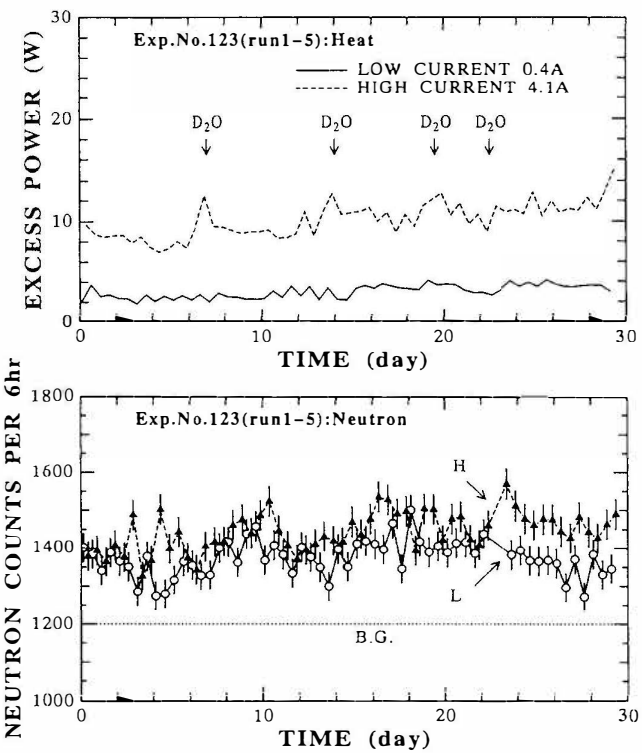

Fig.7 : Evolutions of excess heat and neutron yield for a month of No.123 runs of Exp.D2 .

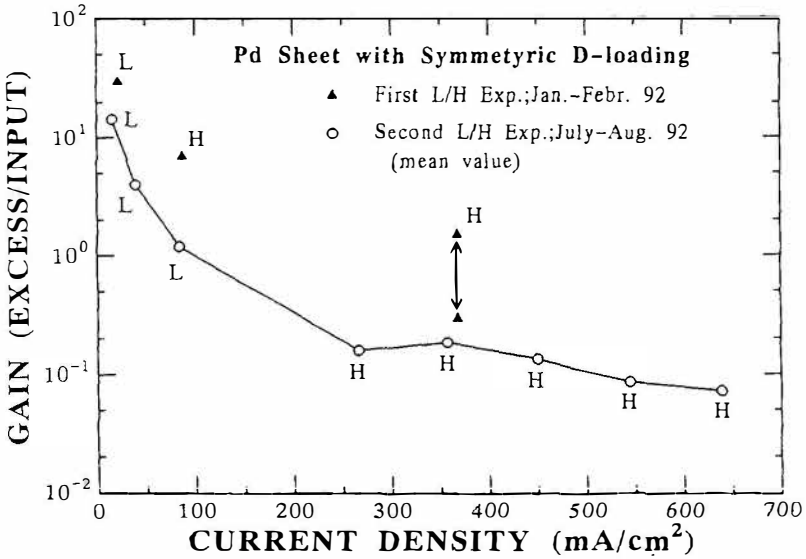

Fig.8 : Net gain (Output / Input - 1.0) of excess heat as a function of electrolytic current density .

5. Discussions

For summarizing observed excess heats in Exp.D and Exp.D2 , we plotted net gain (output / input - 1.0) as a function of electrolytic current density on Pd sheet surface (~11.5 cm²) , as shown in Fig.8 . Net gain of excess heat decreases as we increase current density , though absolute magnitude of excess heat increases , for both cases of Exp.D and Exp.D2 . We observed very high gain more than 10 for L-modes ; this feature is very different from results by other authors using continuous (DC) current mode operation . To compare our results with those by other groups , we deduced excess power per cm² of Pd surface to be plotted on the Storms' graph[14] , as shown in Fig.9 . Results from Exp.D2 follow the " limit " curve of Storms (solid curve) and look consistent with other results . This graph suggests us that excess heat phenomenon occurs near surface , not volumetric effect of Pd cathode . Much larger excess heats by Exp.D look consistent with Liaw's molten salt experiment[15] and burst data of Pons-Fleischmann[12] . It seems that the solid curve by Storms is not the limit . However , high power density (more than 10 watts/cm²) were observed as bursts and not controllable yet .

We could reproduce excess heat in Exp.D2 , but magnitudes were so different . It seems that we were not

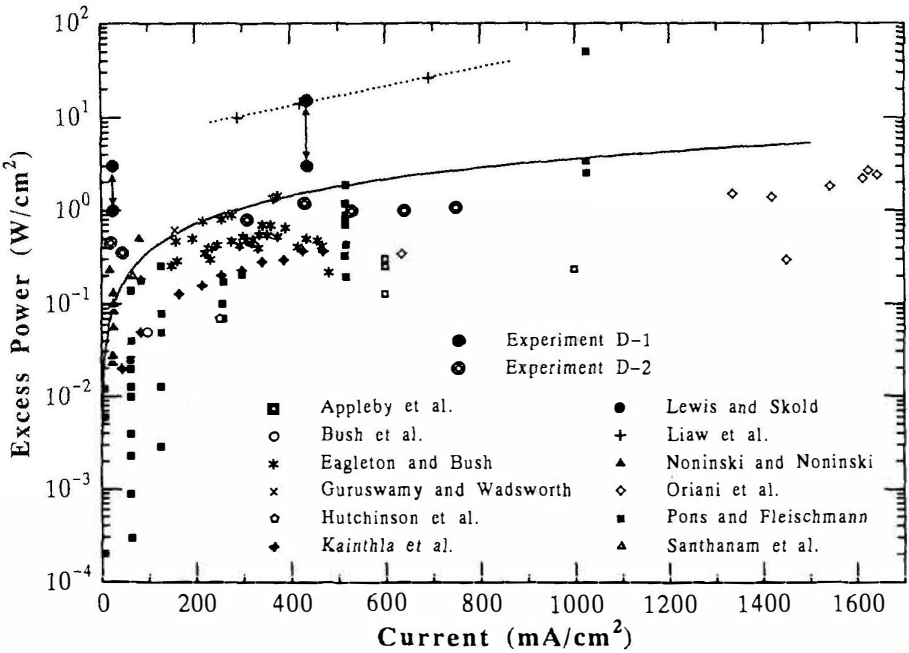

Fig.9 : Trends between excess power per surface area (cm²) and electrolytic current density . (see Ref.14)

aware of essential changes in two experiments . In Fig.10 , we compare histories of cell voltage for Exp.D and Exp.D2 . We notice that cell voltages in Exp.D are anomalously high (~25 volts in the beginning and increased to ~30 volts at the end) , compared with those in Exp.D2 (~14 volts in the beginning and very slowly increased to reach 20 volts after 3 months) . This fact shows that " effective " surface area of Exp.D Pd cathode was much smaller than that of Exp.D2 . What is the reason of this change ? We only renewed Pd sheet and electrolyte and took out a soda glass pipe . We made a surface analysis (~1 μm depth) by SIMS for the used Pd sheet of Exp.D , and found deposits of Al-27 and Ca-40 as comparable amounts as Li-7 . Ca-40 might come from pyrex glass . We do not know exactly from where Al-27 came . Anyway , we can conceive that thin MOS(metal oxide semiconductor)-like or MH(metal hydride) layers on both surfaces of Pd sheet were formed . It is interesting that McKubre pointed out the drastic effect of Al impurity in electrolyte to meet reproducible excess heat[16] . As shown in Fig.11 , we can speculate that the thin MOS film formation on Pd surface as " blocking layer " may play a role enhancing cathode over potential (hence cell voltage) and

suppressing deuteron diffusion-out from Pd to meet locally high D/Pd ratio near surface , because of depletion of free electrons in the MOS layer where atomic potential barrier is much higher than that in Pd zone . It seems a critical issue that reproducible MOS surface condition can reproduce excess heat phenomenon . In this respect , interests are on our recent experiment of deuteron-beam implantation into Pd or Ti foil with thin Al layer on surface which showed a drastic effect to emitted 8 MeV α-particles (by d-d-d fusion) , and other charged particles at 3 , 3.5 and about 4.5 MeV ; which , from the logic of experiment , should be regarded as " cold " nuclear reactions of deuterons[17] . We have to further resolve the role of " Takahashi method " , namely whether or not it satisfies the discussed critical condition , i.e. , locally high D/Pd region with the help of MOS surface film formation on Pd surface .

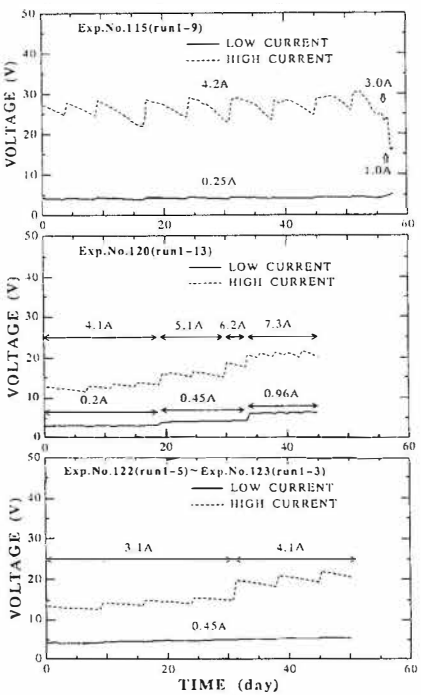

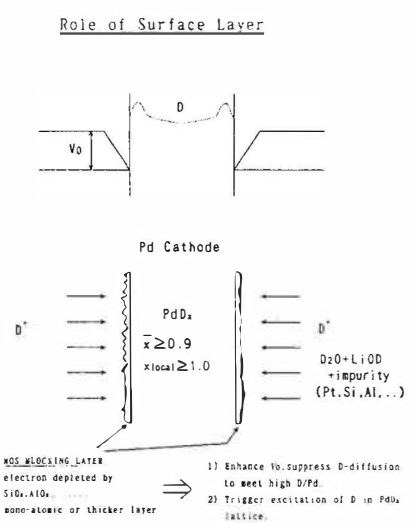

Fig.11 : Role of MOS (metal oxide semiconductor)-like film on surface of Pd cathode .

Fig.10 : Evolution of cell voltages ; for Exp.D (upper most graph), Exp.D2 (middle and lower graphs) .

[References]

1) M.Fleischmann and S.Pons : J. Electroanal. Chem. , 261 , 301 (1989)

2) C.H.McKubre , et al. : The Science of Cold Fusion , Proc. ACCF2 , Como , Italian Physical Soc. , p.419-444 , (1991)
3) A.Takahashi , et al. : Int. J. Appl. Electromag. Materials , 106 , 1-10 , (1992) , see also Proc. ISEM Nagoya , 1992 .
4) K.Kunimatsu : " Deuterium Loading Ratio and Excess Heat Generation During Electrolysis of Heavy Water by a Palladium Cathode in a Closed Cell Using a Partially Immersed Fuel Cell Anode " , this Conf. (ICCF3 , Nagoya , 1992)
5) E.Storms : " Measurements of Excess Heat from a Pons-Fleischmann Type Electrolytic Cell Using Palladium Sheet " , to be publ. in Fusion Technology , see also E.Storms , this Conf. (ICCF3 , Nagoya , 1992)
6) F.Celani , et al. : " Measurements of Excess Heat and Tritium during Self-biased Pulsed Electrolysis of Pd-D_2O " , this Conf. (ICCF3 , Nagoya ,1992)
7) L.Bertalot , et al. : " Study of Deuterium Charging in Palladium by the Electrolysis of Heavy Water : Search for Heat Excess and Nuclear Ashes " , this Conf. (ICCF3 , Nagoya , 1992)
8) T.Kusunoki , et al. : " Energy of the Neutrons Emitted in Heavy Water Electrolysis " , this Conf. (ICCF3 , Nagoya , 1992)
9) E.F.Mallove , et al. : " Calorimetry with an Electrolytic Cold Fusion Cell Based on the Design of A.Takahashi " , this Conf. (ICCF3 , Nagoya , 1992)
10) H.Miyamaru , et al. : " Periodically Current-Controlled Electrolysis of D_2O/Pd System for Excess Heat Production " , this Conf. (ICCF3 , Nagoya , 1992)
11) A.Takahashi , et al. : Fusion Technology , 19 , 380 ,(1991)
12) M.Fleischmann , et al. : J. Electroanal. Chem. , 287 , 293 (1990)
13) A.Takahashi , et al. : The Science of Cold Fusion , Proc. ACCF2 , Como. , Italian Phys. Soc. , pp.93-98 , (1991)
14) E.Storms : Fusion Technology , 20 , 443 , (1991)
15) Y.Liaw : The Science of Cold Fusion , Proc. ACCF2 , Como. , Italian Phys. Soc. , pp.55-64 (1991)
16) M.C.H.McKubre , et al. : " Excess Power Production in D_2O-Electrolysis Cells : A Comparison of Results from Differing Cell Designs " , this Conf. (ICCF3 , Nagoya , 1992)
17) T.Iida , et al. : " Deuteron Fusion Experiment with Ti & Pd Foils Implanted with Deuteron Beams " , this Conf. (ICCF3 , Nagoya , 1992)

Measurements of Excess Heat and Tritium during Self-Biased Pulsed Electrolysis of Pd-D_2O

Francesco CELANI, Antonio SPALLONE, Paolo TRIPODI, Anna NUVOLI

INFN, Laboratori Nazionali di Frascati, via E.Fermi, 00044 Frascati (Italy).

ABSTRACT

Following the Takahashi results about large excess heat by pulsed electrolysis, we built a gas-closed flow calorimeter to perform pulsed current electrolysis. Some blank tests, using Au plate cathode, were carried out to characterize the system. Four cold-worked Pd sheets were tested and two of them produced 7.5% and 6% of mean excess heat for many weeks. The others Pd sheets did not produce excess heat though one of them, after a deuterium re-loading, gave up to +25% of excess heat but only for few hours. Tritium analysis was carried out and some coincidence between tritium production and excess heat was found.

1. APPARATUS

We realized an electrolytic system [fig. 1] using a cylindric polyethylene vessel (12 cm of diameter, 7 cm height, 1 cm tickness) as an improved type of that reported by A.Takahashi [1].

We put, as cooler, a double turned copper coil (nickel coated and covered by acrylic resin) inside the vessel. A 1.2 Kw (maximum power) electrical heater was placed on the bottom of the vessel; like the cooler, it was nickel coated and covered by acrylic resin. The use of this particular insulation is required to avoid a contamination of the electrolytic solution due to the aggressivity of concentrated base(0.3M/l of LiOD or LiOH). The electrodes used were sheets (2.5 cm, 2.5 cm, 0.1 cm) as cathode and a Pt wire (100 cm long, 0.05 cm of diameter) turned around as anode. The electrodes were separated by 1 cm teflon bars and located at the center of

FRONTIERS OF COLD FUSION

the bottom of the vessel; a diagonal Pt wire (0.05 cm diameter), 0.3 cm far from the surface of the sheet, was used as the voltage reference electrode.

A 1 cm tick Ni rod, like inner temperature sensor, was put,very close to the electrodes. Three Pt short wires (1, 1.5 and 2.5 cm long) were put on the top of the vessel and are used for the purpose of solution level sensors.

All the materials used into the vessel were tested against unwanted poisoning of the solution.

The vessel was thermal insulated from environment by 5 cm tick polystyrene and 7 turns of alumined mylar.

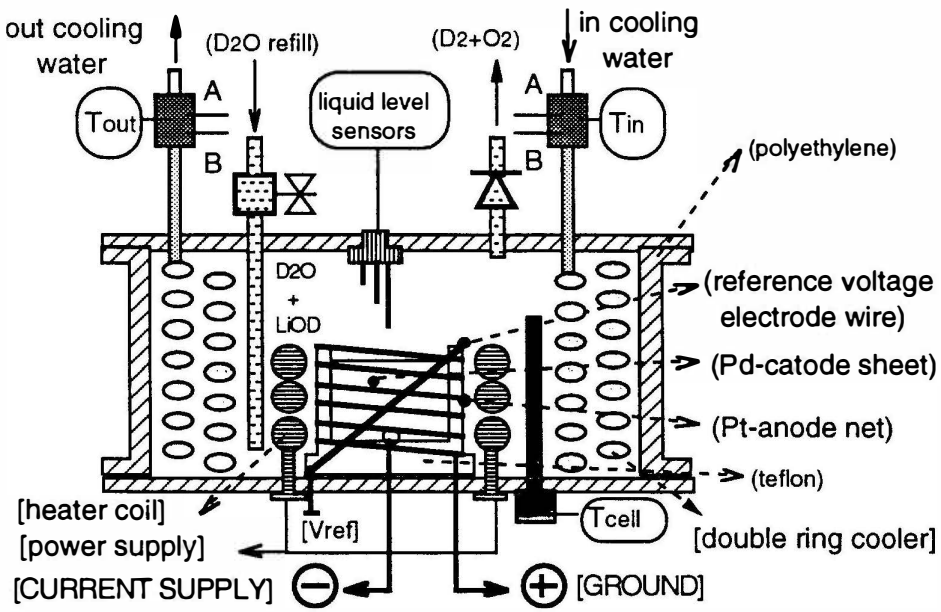

[Figure 1] Inner vessel.

The cooling system [fig. 2] consists of a inner coil, a peristaltic pump and a water bath; the cooling liquid is ordinary water.

The inner coil (0.5 cm of diameter and 4 m long) was overwhelmed to improve the cooling efficiency of the cooler fluid.The computer-controlled peristaltic pump was used to get a variable, constant cooling, flow ranging between 0.5 and 30 ml/s.

The water bath allows to get a 17 °C constant input temperature.

Seven temperature sensors (Si device AD590) are used and their sensitivity is 1 μA/°C. Using a 10 kΩ loading resistor in the circuit, we get, trough an operational

amplifier (OP227), a value of 10 mV/°C. The most important sensors placed outside the vessel, the input and output of the cooler, are doubled. This configuration allows to get a double independent control about the output thermal energy.

The outgoing gases from D_2O dissociation are sent into a close system as shown in fig. 3. A bottle is used to condense the vapors from the warm solution due to the electrolysis. Two optional large volume rubber balls are used to collect the gases and vacuum/over-pressure pump is used for pressure operating tests. A recombiner (gas diffusion electrode of E-TEK, USA), working at room temperature, is placed into a bottle to recombine the D_2 and O_2 gases into D_2O. The D_2O is routinely collected both for periodic tritium analysis and measurement of dissociated water (to check against self-recombination into the electrolyte vessel). Two pressure sensors (one analogic and one other digital) are used. Two in-line low-drop pressure valves are used to avoid a gas return to the vessel from the recombiner (mainly CO_2). A teflon tube entering into the vessel is used to refill the D_2O .

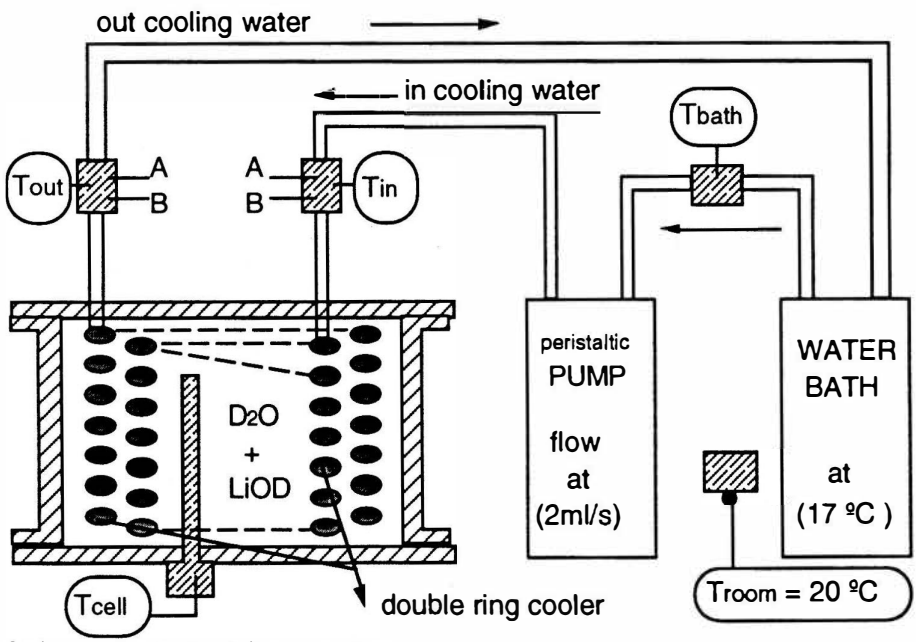

[Figure 2] Cooling system.

A specific home-made circuit [fig. 4] was used to control the constant-current generator in order to perform a time dependent electrolysis. The typical shapes used were a 20 minutes period, 0.25 to 5.1 A saw-tooth wave and

20 to 360 minutes half period, 0.25 to 7 A square wave. The wave controller is auto or manual, time and amplitude, selectable.

Two fast recovery-time high power diodes (mod. 40HFL80S05 by IR) were inserted between the generator and the electrodes to avoid a deuterium deloading from the Pd cathode during the fast transition current edge [3]: a reverse voltage polarization can occur for short time in this condition.

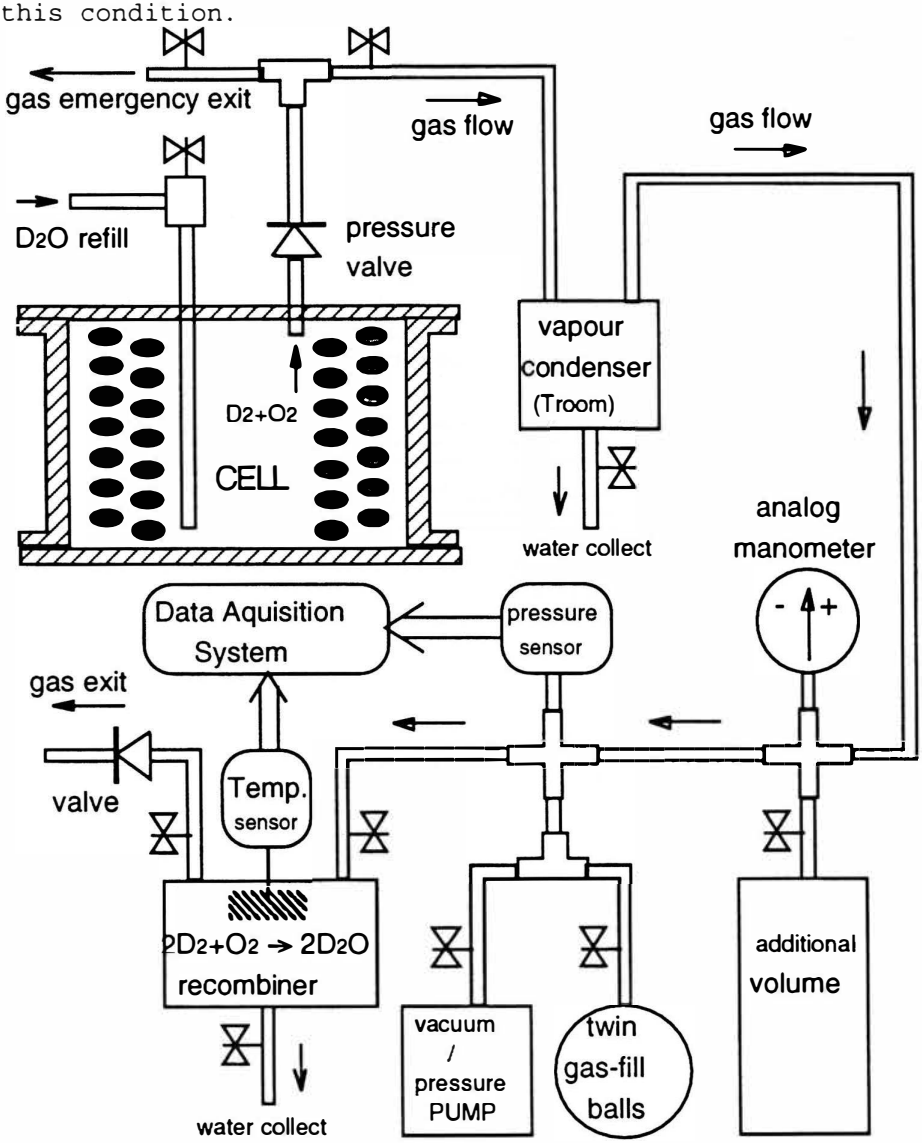

[Figure 3] Gas system.

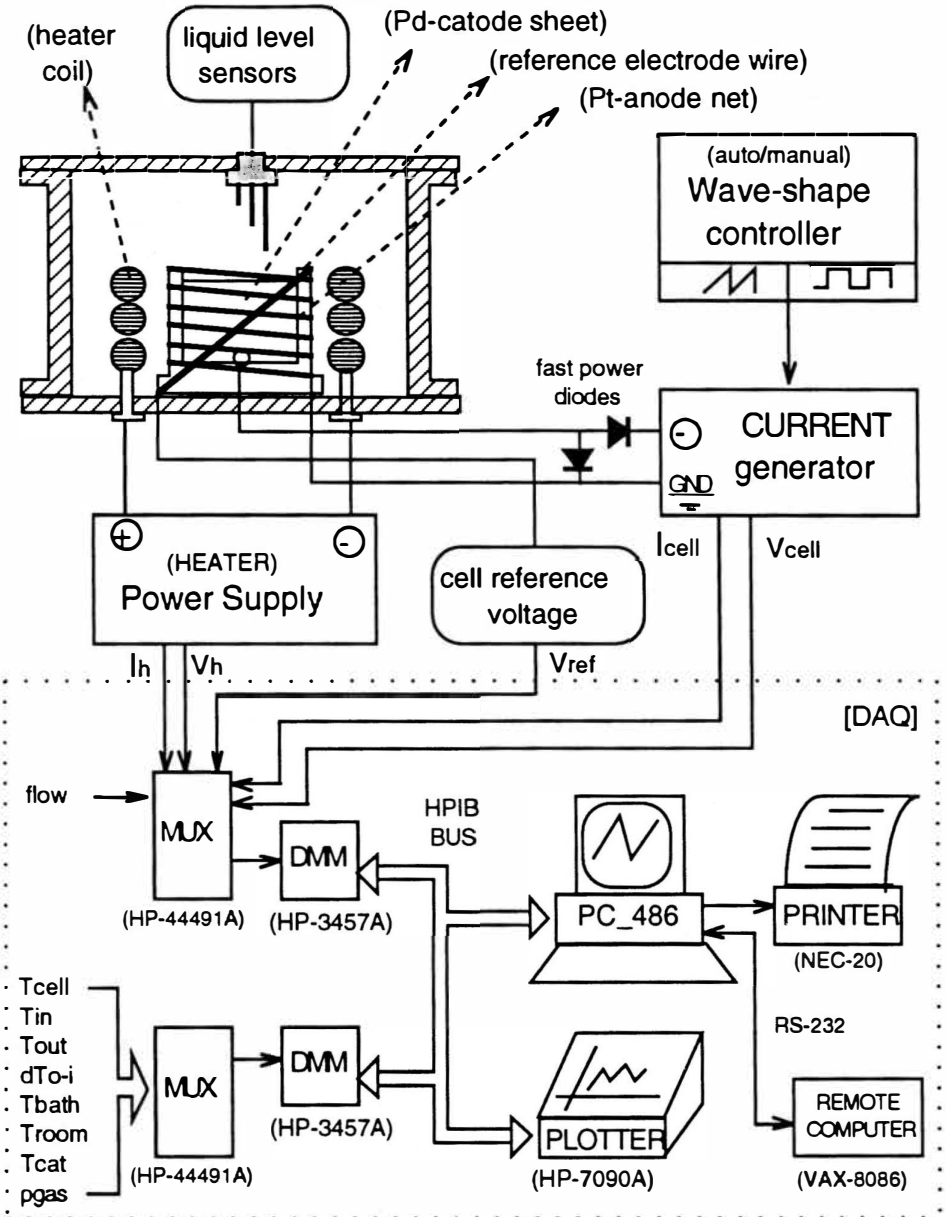

[Figure 4] Power supply and acquisition system.

An independent voltage generator is used to supply the inner heater for calorimetric calibration.

All the electric and thermal parameters were computer acquired by a IEEE488 bus connect to two 6.5 digits high

sensitivity DMM (HP-3457A) multiplexed. They are: seven temperatures (absolute and differential inlet and outlet cooling fluid, inner vessel, water bath, recombiner and room), current and voltage of the vessel, reference cathode voltage, outgoing gas pressure and peristaltic pump flow. Three of these parameters were independently selected and on-line plotted by a high resolution color graphics plotter (HP-7090A).

A PC-486 computer was used to monitor and acquire the parameters and linked to remote computer (VAX-8086) to store and off-line analyze the data.

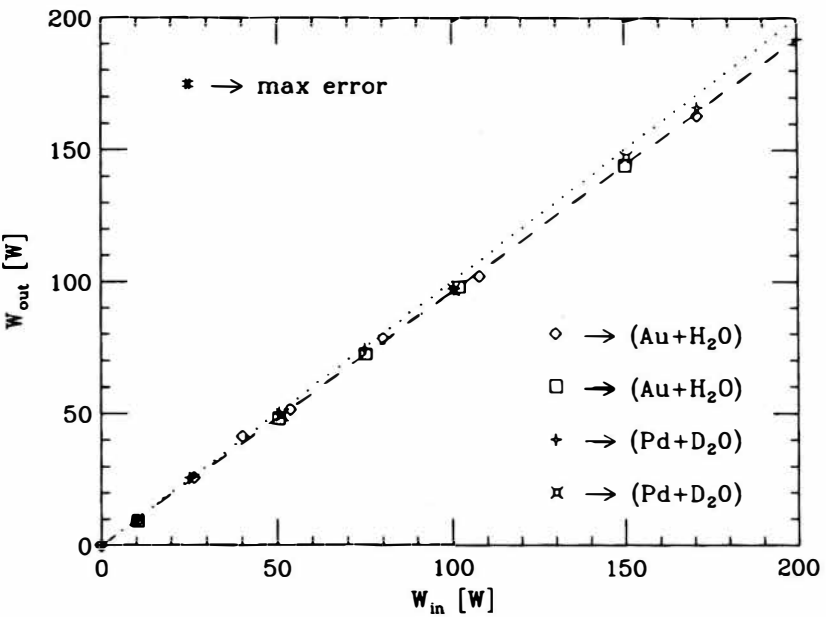

[Figure 5] Calorimeter thermal calibration.

2. CALIBRATION AND EXPERIMENTAL PROCEDURES

We performed two different types of thermal calibration: electric calibration, using the inner heater, and electrolytic calibration during the electrolysis with an Au plate cathode. Generally the calibration were performed before and after a measurement. In fig. 5 are shown electric calibration data ranging over 1 month performed in 4 different ways changing or the electrode (Au or Pd) or the electrolyte ($LiOH+H_2O$ or $LiOD+D_2O$).

The data show the linearity and stability of the calorimeter up to 180 W of input power, calculated as the product of the voltage times the current at the heater, in respect to the output power (in watt) calculated as (1):

$$W_{out} = K \cdot \phi \cdot \Delta T \qquad (1)$$

where, K= 4.184 J•/(ml•K) is a constant conversion factor taking into account the specific heat of cooling fluid (light water), ϕ is the cooling fluid flow in ml/s, ΔT is the temperature difference between the output and the input of the cooling fluid. The slope difference between the ideal curve (dotted in the plot), in the case of no heat lost by dissipation, and the straight interpolation curve of the data is 4 ±1% (because the thermal conductivity of vessel walls and water vapors). This slope difference is 5 ± 1% in case of electrolytic calibration (Au cathode and LiOD+D_2O solution) and the increase is almost due to the energy loss because outgoing gases. The sensitivity of the calorimeter, flow dependent, is 0.418 W/(ml/s) if cooling fluid is water; the resolution, dependent on thermometers sensitivity and flow stability, is estimated to be about 1.5%.

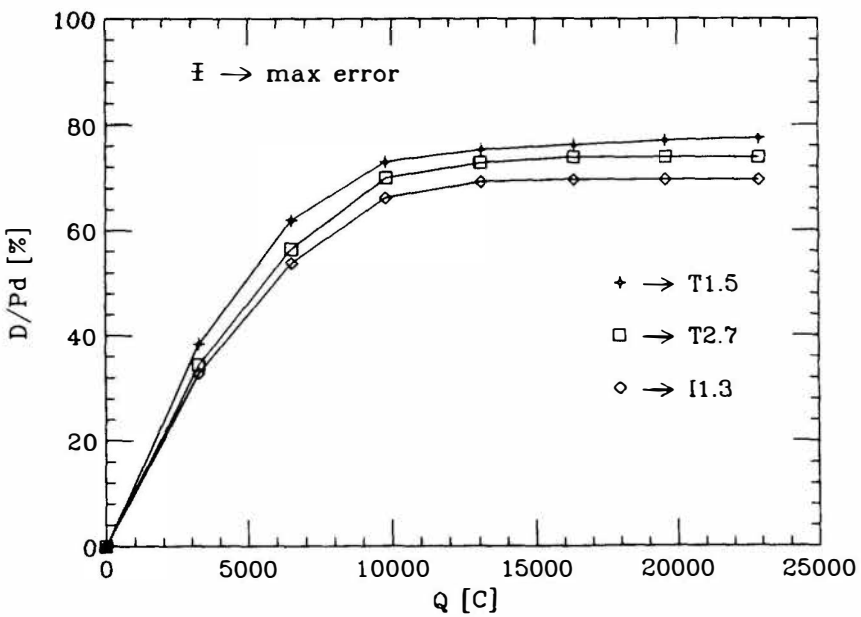

[Figure 6] D/Pd ratio for 3 different Pd sheets.

A specific procedure was adopted to measure the D adsorbed quantity into Pd cathode. During the 6 or 7 first current saw-teeth, the recombiner was excluded and the pressure of electrolytic gases (D_2+O_2) was collected into a well known volume. From the D_2 gas missing pressure, because D

adsorbed by cathode, we could calculate the charging ratio D/Pd. After the sixth current ramp the missing pressure measurement sensitivity becomes too low to estimate the D/Pd variation. After the tenth ramp we opened the recombiner to the gas system. In fig. 6 it is shown the D/Pd ratio versus the electric charge flowed between the electrodes for three different Pd sheets: each data point in the plot corresponds to the D/Pd value cumulated during a ramp. A later D/Pd independent check, based on D_2 gas evolution during Pd discharging at the end of the experiment (with no current applied to the electrode) gave a similar results; we supposed, in this last case, that the equilibrium ratio is 0.67 at STP.

Several tests were performed to study the electrolytic processes and characterize the calorimetric system.

Blank tests were performed using a Au cathode sheet and the electrolytic solution (0.3 M) was or H_2O+LiOH or D_2O+LiOD. The excitation used, as before described, was pulsed current: ramp current from the beginning of the test (until half a day maximum) and then square wave current (several days).

The D_2O from the recombiner was periodically collected and its Tritium contents was analyzed.

A neutron detector (REM counter) was located very close to the vessel to monitoring large neutron emissions just for safety reasons.

3. RESULTS

During two months of experimentation 4 cold-worked Pd sheets, by two different Japanese Firms, were tested: Tanaka Kikinzoku K.K. batch #1 (we call T1.2 and T1.5 which hardness is 155÷170 Vickers at 200g-10s) and batch #2 (T2.7) production (hardness: 145 Vickers), and IMRA Industries batch #1 (I1.3) production. Similar Pd sheets from Tanaka batch #1 and #2 were tested by E.Storm [2]. In tab. 1 is reported the list of all the tests performed.

No excess heat (±2%)was ever detected during the blank runs.

No excess tritium (±3%) was detected,during the blanks, apart the enrichment due to electrolysis, computed with a value of 2 for the isotopic separation factor.

The T1.2 Pd sheet gave excess heat up to about 12% maximum (≅4 W of ≈30 W mean input power), two days after the beginning of the run [fig. 7]. At the beginning, the current was ramped for 1 day and the excess heat occurred just some hours after the start run. During the following 5 days, with square wave current, the mean excess heat was about 7.5%. After that we retry to use ramp current, hoping to increase the excess heat by a D over-loading into the Pd, but the excess heat decreased sensitively.

TEST	DENSITY g/cm³	DATE d/m/y	CURRENT A	ΔE/E %	TRITIUM (excess)	NOTES
HEATER	----	2/8/92 3/8/92	DC	---	---	calib
Au/Pt LiOH+H2O	----	3/8/92 4/8/92	ramp+sqr max (4A)	---	---	blank
Au/Pt LiOD+D2O	----	4/8/92 6/8/92	ramp+sqr max (4A)	---	± 3%	blank
Pd/Pt [T1.2]	≈11.8	6/8/92 25/8/92	ramp+sqr max (5A)	12% max < 7.5% >	(26%)	D/Pd >0.75
Au/Pt LiOD+D2O	----	7/9/92 12/9/92	ramp+sqr max (5A)	---	± 3%	blank
Pd/Pt [I1.3]	11.99	12/9/92 22/9/92	ramp+sqr max (7A)	< 2% (25% peak)	(18%)	D/Pd=0.69 (≈0.84)
Pd/Pt [T2.7]	11.99	23/9/92 2/10/92	ramp+sqr max (7A)	< 2%	unknown	D/Pd=0.72
Pd/Pt [T1.5]	11.75	3/10/92 24/10/92	ramp+sqr max (7A)	8% max < 6% >	(36%)	D/Pd=0.79 running

[Table 1] List of the tests performed

After 3 days of ramp current we switched again on square wave current and the excess heat returned to a average value of 7.5%, lasting for 10 days. A long time main Laboratory black-out abruptly stopped the test. An overall excess heat of about 3 MJ were produced in 19 days. Because we did not measure at the beginning the maximum D/Pd charging value, we estimated this value (>0.75) when the plate was discharged. A total of +26% excess Tritium (+240 dpm/ml) was measured from the recombined D2O water collected, taking into account the enrichment factor (≅2) of the tritium in the solution.

The I1.3 Pd sheet did not produce relevant excess heat up to 7 days so we decided to stop the current supply for 12 hours letting the Pd electrode to deload the over-charged deuterium. After that we restarted the deuterium loading with some current ramps: the D/Pd reached the value of 0.84 ±0.04 starting from 0.67 (D/Pd value at equilibrium at STP); we note that the previous first charging up D/Pd value was 0.69. After this reloading, we used square current further increasing the high level from 5.1 up to 7.2 A. After this operation the excess heat

reached the 25% peak value lasting just some hours. During the 2 days following no relevant excess heat appeared [fig. 8]. The adding of borosilicate, to check if glass contamination can help the D adsorption on Pd surface, did not produced relevant effects. The overall excess Tritium produced was estimated be around +18% (+172 dpm/ml).

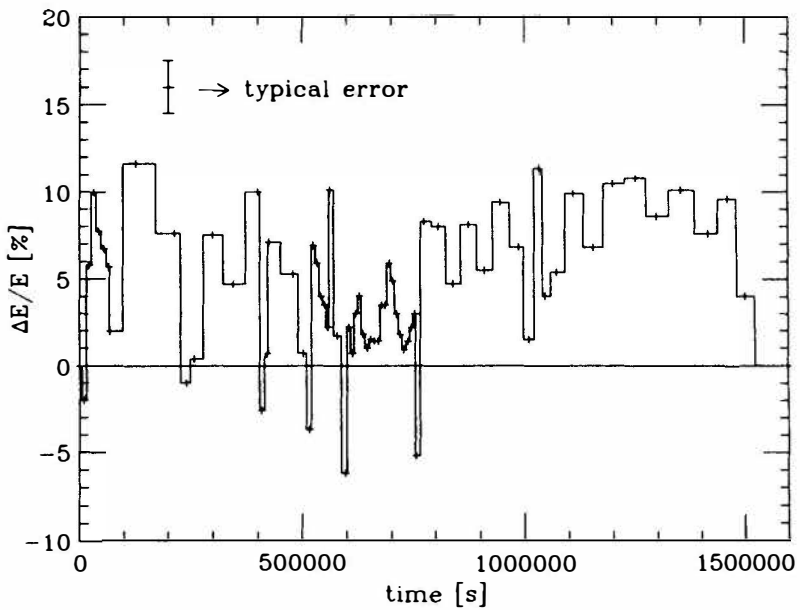

[Figure 7] The T1.2 Pd sheet gave excess heat up to +12%.

The T2.7 Pd sheet, operated in the same conditions of the previous sheets, produced no relevant excess heat (<2%) during 9 days of experiments.

The T1.5 Pd sheet gave the highest D/Pd value on the first charging up (D/Pd ≅0.79). After 2 days of current ramp, the current square wave was selected and the excess heat started from 4% (+2.5 W of about 60 W mean input power) increasing to about 6% in about 67 hours [fig. 9]. After this time a peristaltic pump failure occurred, so that the current was put to low value (0.25 A) for many hours. The excess Tritium measured,until the pump failure, was +36% (+340 dpm/ml).

After the fixing of the pump, the test restarted and the Pd sheet continued to produce about 5% mean excess heat for many days. This Pd sheet is still under run.

The reference voltage, from the diagonal Pt wire in front of the cathode, was always acquired and under study. It has been observed a sort of correlation between this parameter and the deuterium adsorption into the Pd.

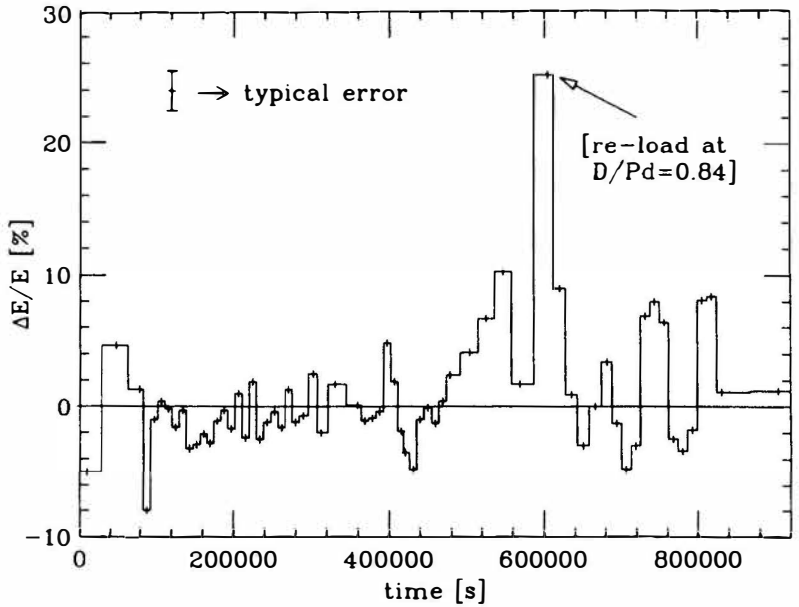

[Figure 8] The I1.3 Pd sheet gave once excess heat of +25% for short time

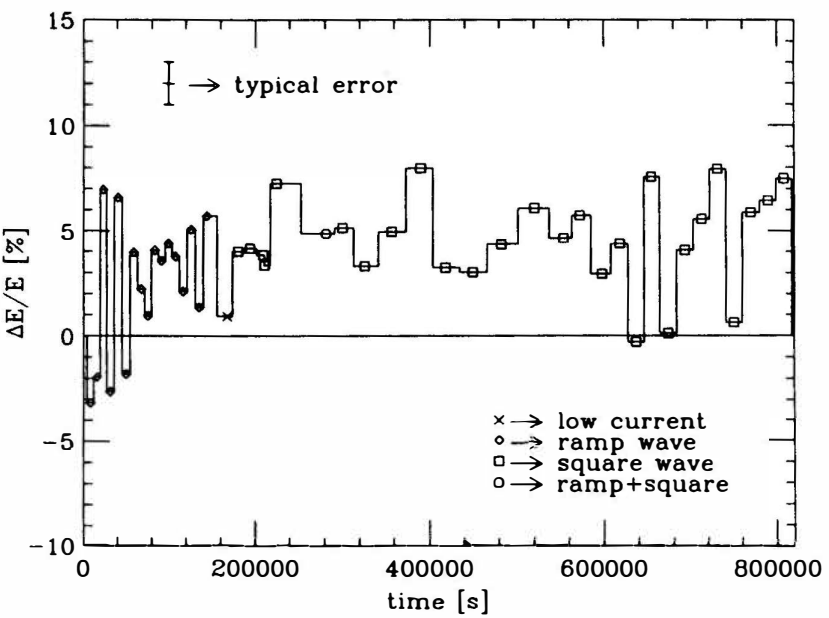

[Figure 9] The T1.5 Pd sheet gave excess heat of about +5% for long time.

Because this parameter involves the conductivity and the temperature of solution, apart the electric charge status of Pd-Pt pile, the correlation with the D/Pd parameter is not yet completely clear.

Looking at table 1, the D/Pd seems correlated to the mass density of the Pd sheet in this way: the D/Pd ratio increases if the mass density decreases.

4. CONCLUSIONS

By the tests performed, with our cold-worked Pd sheets, we can say that a high sensitivity flow calorimetry is required to observe, undoubtedly, excess heat even at low levels (5%).

The self-biased pulsed electrolysis, with a proper circuit,seems able to reduce the long deuterium charging time to a few hours and the excess heat generally appears some hours later; the excess heat is strictly correlate to high D/Pd charging ratio (> 0.75)

Looking at our data, it seems that there is a sort of correlation between excess heat and the low mass density (lower then the 12 g/cm^3 "standard" value) occurred to two Pd sheets.

The excess tritium (although low values) seems occur when excess heat is obtained.

In conclusion, we can say that the metallurgy of the Pd electrodes plays a very important role both for the high D/Pd ratios and large excess heat; moreover, the deuterium charging methods (pulsed current) strongly help the production of excess heat.

ACKNOWLEDGEMENTS

Most of the chemical and metallurgical aspects of these experiments were deeply discussed with S.Fortunati, P.Marini, V. Di Stefano and M.Tului of CSM,ILVA-IRI (Rome, Italy).

We are grate for invaluable skillful cooperation and technical assistance to F.Basti (INFN,LNF) .

We would like to thank profs. H.Ikegami and T. Tazima (NIFS, Nagoya,Japan) for their very important suggestions and continuos encouragements.

We thank: prof. A.Takahashi (Osaka Un.), prof. E.Storms (Los Alamos Lab.) prof. S.E.Jones (B.Y.U. Provo), prof. G.Preparata (Milan Un.) and S. Nezu (IMRA-Res.) for their stimulating discussions, criticism and suggestions.

We are grate to Drs F.Ferrarotto , M.Corradi and Prof. B.Stella (Rome Un.) for their criticisms.

The palladium plates were kindly provided from Tanaka K.K. and IMRA-Research, both from Japan.

This work is supported by grants from INFN and Italian Council of Research (CNR), "Comitato Nazionale per le Ricerche Tecnologiche e le Innovazioni".

REFERENCES

[1] A.Takahashi et al. "Excess Heat and Nuclear Products by D_2O/Pd Electrolysis and Multibody Fusion", Submitted to Applied Electromagnetics in Materials, (March 1992).

[2] E.K.Storms. "Measurements of Excess Heat From a Type Electrolytic Cell Using Palladium Sheet." Submitted to Fusion Technology (July 1992).

[3] F.Celani et al. "RESULT OF THE 1st GENERATION, AT GRAN SASSO UNDERGROUND LABORATORY, ON NUCLEAR COLD FUSION." Conference Proceedings, SIF Bologna 1989, Vol.24 pg.257 (1989).

"Quasi-Plasma" Transport Model in Deuterium Overloaded Palladium Cathodes

A. DE NINNO, V. VIOLANTE[a)]
ENEA - Area INN, Dip. Sviluppo Tecnologie di Punta, CRE
Frascati, C.P. 65 - 00044 Frascati, Rome, Italy
ITALY

ABSTRACT

The Pd-D system has been described assuming a two-population model. A "quasi-plasma" delocalized boson gas picture has been used for the deuterons exceeding the stoichiometric ratio in Pd-D compounds.

A mathematical model supported by a numerical computer code with distributed parameters has been developed in order to describe the evolution of the deuteron concentration profile inside a Pd cathode under pulsed electrolysis. Several boundary conditions have been taken into account.

A strong correlation has been found between the model system evolution and the experimental data[1].

1. Introduction

It is well established from experiments that (hydrogen or) deuterium can be loaded in the Pd lattice even above the so-called stoichiometric ratio, X = D/Pd = 0.7 (atoms of D per atom of Pd). Up to this value (hydrogen or) deuterium atoms are arranged in the lattice in the octahedral sites. A further increase in concentration (or loading ratio) can be described by assuming "guest" atoms delocalized arranged in shallow holes[2] corresponding to tetrahedal sites. The relative low energy barrier between two tetrahedral sites brings out to describe this population as almost free to move from a side to an other. We will refer only to D atoms.

In the following we will quote from the current literature two features of DPd compounds, showing that the D atoms exceeding the stoichiometric ratio have a very different kind of interaction with the lattice.

- It has been observed [3,4] that the diffusion coefficient of D in Pd increases steeply by almost two orders of magnitude above X=0.7.

FRONTIERS OF COLD FUSION

This effect can be explained by assuming that the energy variation, required for an atom to move from a lattice site to another, decreases as the concentration increases. The diffusion coefficient follows the Arrenius law

$$D = D_0 \exp(-E/kT)$$

where E is the energy barrier between two neighbour sites. Thus, the experimental data can be explained by assuming that the barrier is lowered when X exceeds 0.7.
- It is known [5,6] that the relative change of volume ($\Delta V/V$) of the Pd lattice cell as a function of loading ratio is a straight line, which shows a change in slope approximately at X = 0.7. This means that, for concentrations higher than this, the interaction between the D atoms and the Pd lattice changes.

These two features prompted us to propose a picture, in which the D atoms in the Pd lattice can be divided in two groups: localized atoms in the octahedral sites, and delocalized ones in the tetrahedral sites. The two groups have different kinds of interaction with the lattice. It has to be remembered that, even when X > 0.7, both groups are present: but, statistically, the delocalized fraction is negligible if octahedral sites are available, the latter's energy level being lower than for tetrahedral sites.

The model describes the behaviour of the latter population than it assumes a Pd lattice in which the octahedral sites are already filled. Since the particles are indistingushable exchanges between two population doesn't modifie the system status.

2. The model

Many experiments show that, when electrolytically charging D in Pd, the production of anomalous heat excess can be detected, if the loading ratio is in the range 0.8 - 1, or even larger. A typical feature of the first experiments was the need for a long pre-charging procedure, as long as weeks, or even months, in order for the anomalous effect to appear. More recently a pulsed technique has been used[7], consisting in either applying a sawtooth current (just at the beginning of the run), or alternating low currents to high currents with long periods ("lo-hi" technique), resulting in a much more efficient charging mechanism. This behaviour pushed us to study, from a theoretical point of view, the loading and the transport dynamics of D in Pd, for X > 0.7, in the framework of hi-lo electrolysis.

The model considers the Pd cathode as a membrane (with very high surface/thickness ratio), separating two regions. Two different instances have been considered:
A. The cathode is totally immersed in an electrolytic cell,
B. Only one of the sides of the cathode participates to electrolysis, while the other is exposed to an ambient containing D_2 gas.

It is well known that, during electrolysis, a strong electric field is present at the cathode-electrolyte interface. Furthermore, it is reasonable to assume a Thomas-Fermi like interaction between delocalized D atoms. Actually a dependence from the D concentration of the electronic shield has been assumed. We can then write an expression for the atom flow, depending both on concentration and local electric field:

$$J = -D(\nabla C + \frac{Fz^{*}E}{RT}C) \qquad (1)$$

where:
D diffusion coefficient, F Faraday constant, E total local electric field, C deuterium concentration , R gas constant, T temperature.

The local electric field can be considered as the algebraic sum of the applied electric field (due to electrolysis) and the reactional field due to the Thomas-Fermi like potential. The former is non-zero only at the cathode-electrolyte interface, while the latter can be calculated as a function of the loading ratio. Then. the mass transfer equation, in transient conditions, can be written as:

$$\frac{\partial C}{\partial t} = D\nabla^2 C + \frac{Fz^{*}}{RT}E\nabla C \qquad (2)$$

where: z* effective deuteron charge (electrotransport)[8-9].
where C is the concentration of delocalized deuterons, R is the gas constant, F is the Faraday constant, T is the temperature, and E is the local electric field.

The interaction potential between delocalized deuterons (in the Thomas-Fermi picture) is:

$$\Phi = \frac{q}{4\pi\varepsilon_0 r} exp(-\frac{r}{\lambda_D}) \qquad (3)$$

where r is the distance between a delocalized deuteron and the first neighbour (proportional to $1/N^{1/3}$), λ_D is the Debye distance, and q is the electric charge.

The initial and boundary conditions are:

$$C(x_1 t = 0) = 0$$

$$a)\quad C(x_0,t) = \begin{cases} C_1 & t_0 < t < (2n+1)t_s \\ C_2 & (2n+1)t_s < t < 2(n+1)t_s \end{cases} \qquad (n = 0,1,2,.....)$$

$$E(x_0,t) = E_0\delta(x_0)$$

b) $x = L; -D\frac{\partial C}{\partial x} = J_{ADS/DES}$

c) $x = \frac{L}{2}; \frac{\partial C}{\partial x} = 0$

Where: $2t_S$ is the period of the pulsed electrolysis, C_1 e C_2 are the surface concentration, on the electrolysis side, in low and high current respectively[10].

Condition (a) describes the electrolysis side of the electrode, condition (b) describes an electrode having one side in D gas ambient, condition (c) points a symmetric electrolysis (the membrane cathode is between two equal anodic plates).

In order to evaluate the flow, in the gas (JDES/ADS) it is necessary to write down a mass balance. Since the flow is a function of the surface concentration and of the deuterons concentration in the gas phase, we can write:

$$\frac{\partial C_{SUP}}{\partial t} = K_{ADS}C_{GAS} - K_{DES}C_{SUP} + J_{DIFF} \qquad (4)$$

where

$$J_{DIFF} = -D\frac{\partial C}{\partial x}; (x = L)$$

K_{DES} and K_{ADS} are the desorption and adsorption constants respectively, C_{GAS} and C_{SUP} are the D concentration on the gas phase cathode side and in the gas bulk respectively. The desorption rate has been approximated as a lumped first order kinetic.

The gas flux from/towards the cathode produces a variation of the number of D molecules in the gas phase producing a pressure variation:

$$\frac{\partial P}{\partial t} = \frac{RT}{V}\frac{\partial N_{GAS}}{\partial t} \qquad (5)$$

where P is the gas pressure, V is the gas volume and N_{GAS} is the number of D molecules within the gas (ideal behaviour is assumed).

The D concentration variation in the gas is:

$$\frac{\partial C_{GAS}}{\partial t} = \frac{1}{RT}\frac{\partial P}{\partial t} \qquad (6)$$

The model just described has been solved numerically by finite-difference method. For the adsorption/desorption constants, data from the literature have been used.

3. Results and conclusions

The main features emerging from this model are the following:
1. The period ($2t_S$) of hi-lo electrolysis affects the charging efficiency and the concentration profile (see Fig.1): with a proper period, strong concentration gradients are set up.

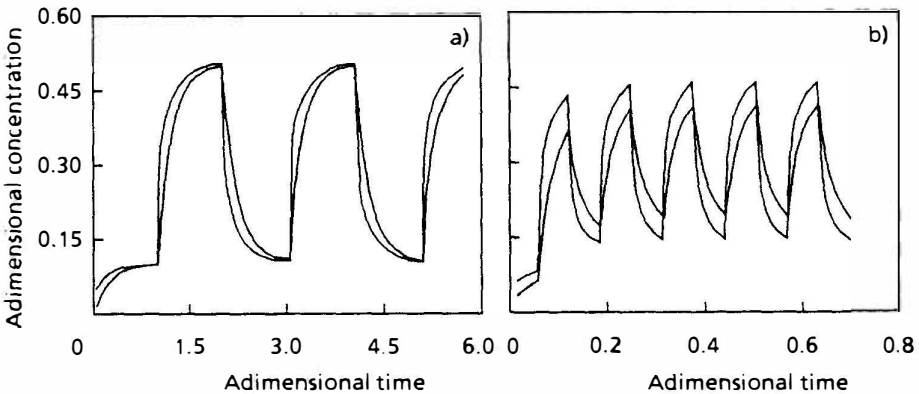

Figure 1. Concentration evolution in two contiguous slabs near the cathode surface in the electrolysis side. Profile in b) has been obtained with a period 4 times shorter than the one of a) case. Note the different time scale.

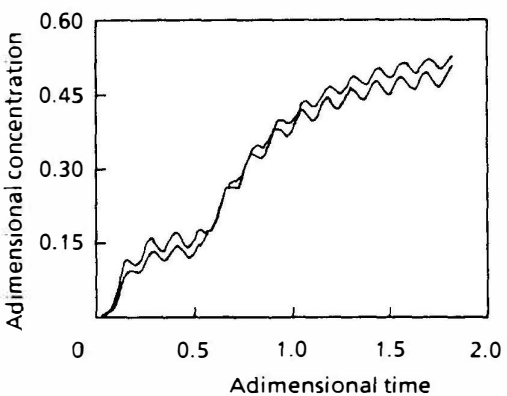

Figure 2. Concentration profiles evolution in two contiguous slabs near the cathode surface exposed to D2 gas. The perturbation simulates the inversionof the flow on the gas side.

2. A strong external electric field enhances the charging efficiency and the global loading ratio: it has been observed[6] that an increase in the potential across the cell (at constant current) announces the production of heat excess.

3. The inversion of flow on the gas side produces a compression on the delocalized deuterons (see Fig.2), and the rate of loading is increased.

The experiments performed at ENEA/Frascati[1] show that a strong D2 gas adsorption is detected when heat excess is produced. Thus, the model gives a satisfying description of the diffusion of deuterons in a Pd cathode under electrochemical loading: it was possible to establish a correlation between the deuterium dynamics within the cathode and the production of heat excess: the model analysis leads to the following consideration concerning the development of excess of heat oriented experiments. The electrode surface should be maintained active from the absorption point of view and an "ad hoc" poisoning on the surface, aimed to reduce the deuterium recombination and/or to enhance the cathodic over-potential, should be studied. In the geometry of the cell, particular care should be given to the evaluation of the currents distribution.

Footnote and References

a) ENEA - Dipartimento Fusione, CRE Frascati, C.P. 65 - 00044 Frascati, Rome, Italy

1) Bertalot L. et al. "Study of Deuterium Charging in PD....." This conference
2) Preparata G., Proc. of 1st Annual Conference on CF. Provo (USA 1990.
3) Mengoli G., et al. Surface and Bulk Effects in the Extraction of Hydrogen from Highly Pd Sheet Electrodes, Submitted to J. Electr. Anal. Chem.
4) Chernenko V.I. and Yakunina T.G., Diffusion of Hydrogen through Pd Membranes. Translated from Elektrokimiya Vol. 18, 7, (1982) 904-908
5) Peisl H., Lattice Strans due to Hydrogen in Metals, in Hydrogen in Metals I Ed. G. Alefeld & J. Volkl, Springer Verlag Berlin 1978, 53-73
6) Kittel C., Introduzione alla Fisica dello Stato Solido, Boringhieri 1971
7) Takahashi A. et al., Nuclear Products ..... Submitted to Int. J. of Appl. Electromagnetics in Mat. - May 1992
8) Wipf H., Electro and Thermo transport of Hydrogen in Metals. Hydrogen in Metals Vol. II, Cpa. 7 - Ed. G. Alefeld & J. Volkl, Springer Verlag Berlin 1978
9) Isengerg, I., Phys. Rev. Letts. 79 (1950) 736
10) Enyo M., Hydrogen-Electrode Reaction on Electro Catalytically Active Metals, pp. 241-250 in Comprehensive ..... of Electrochemistry Vol. 7, cap. 5, Plenum N.Y. 1983

Calorimetric Principles and Problems in Pd-D_2O Electrolysis

Melvin H. MILES and Benjamin F. BUSH
Chemistry Division, Research Department
Naval Air Warfare Center Weapons Division
China Lake, CA 93555-6001 USA

ABSTRACT

Most of the laboratories involved with the question of excess enthalpy in Pd-D_2O electrolysis experiments have employed isoperibolic calorimetric techniques. A careful re-examination of earlier results from several laboratories (California Institute of Technology, Massachusetts Institute of Technology, and Harwell Laboratory) is needed in terms of our present understanding of electrochemical calorimetry. Error sources in their experiments are discussed. There is possible evidence for excess power production in the Pd-D_2O electrolysis experiments at one of these laboratories.

A significant experimental problem in many isoperibolic calorimetric studies is the fact that the decrease in the electrolyte level due to electrolysis produces a significant decrease in the calorimetric cell constant if the temperature is measured in the electrolyte of the electrochemical cell. Furthermore, heat conduction pathways out of the top of the cell can produce large errors, especially at low power levels. There is no steady state in electrochemical calorimetry, hence acurate results require the evaluation of all terms in the differential equation governing the calorimeter.

1. Introduction

A critical assumption made by many laboratories is the steady state approximation for their isoperibolic calorimetric system. In point of fact there is no steady state during electrolysis experiments for either the cell voltage or the cell temperature. Exact calorimetric measurements, therefore, require the solution of the non-linear, inhomogeneous differential equation that governs the behavior of the calorimeter. Approximate solutions require, at the very least, an experimental evaluation of the terms involving the time-dependency of the cell temperature, cell voltage, and cell contents. This has not been done by most laboratories reporting electrochemical calorimetric results including studies by

FRONTIERS OF COLD FUSION

N. S. Lewis et. al., D. E. Williams et. al., D. Albagli et. al., and R. H. Wilson et. al.

Based on the isoperibolic calorimetric cells used at our laboratory, other major error sources arise from heat flow pathways through the top of the cell, room temperature changes, fluctuations in the cell voltage due to gas bubble effects, and changes in the liquid levels both within the cell and in the water bath. The convection-heat-transfer coefficient for air or other gases is 20-40 times smaller than for water according to L. C. Thomas.

Calorimetric accuracy is improved by systems of small volume with one short dimension and by intense stirring, thus long, thin, cylindrical calorimeters are favored by M. Fleischmann et. al. The significance of these calorimetric principles and problems were not obvious when several laboratories reported their failure to observe any excess power in 1989.

2. Methods

The sloping baseline is a significant problem in most isoperibolic calorimetric studies. The decrease in electrolyte level and the corresponding increase in gas volume in the headspace produces a calorimetric cell constant that decreases with time. We observed this major effect very early in our calorimetric studies (see D. E. Stilwell et. al.). An example of this large electrolyte-level effect is shown in Figure 1 for a Dewar-type calorimeter where the temperature is measured directly in the electrolyte. Other early investigators also noted this obvious effect including D. E. Williams et. al. and D. Albagli et. al., but it is a very surprising that no mention of this electrolyte-level effect was reported in the calorimetric studies by N. Lewis et. al. despite their extensive discussions of factors that may affect the calorimetric measurements. Calorimetric cell designs where the temperature is measured at a secondary liquid or solid phase at the outside surface of the electrochemical cell minimizes this sloping baseline problem as shown by D. E. Stilwell et. al. Our present calorimetric cell design and positions of the thermistors used for cell temperature measurements remains virtually unchanged from our previous reports (see M. H. Miles et. al.). In our experiments, the electrolyte level has very little effect on our calorimetric cell constant.

3. Results

The time dependence of cell potentials and cell temperatures for two simultaneous experiments (cells A and B) are shown in Figure 2. Since the bath temperature is constant, changes in ΔT reflect changes in the cell temperature. Note that there is never any steady state for either the cell temperature or cell voltage, although the changes in both are approximately linear with time. The additions of D_2O produces sudden changes in the cell voltages following which there would be no valid calorimetric measurements for several hours (the time constants for these calorimetric cells are about 25 minutes).

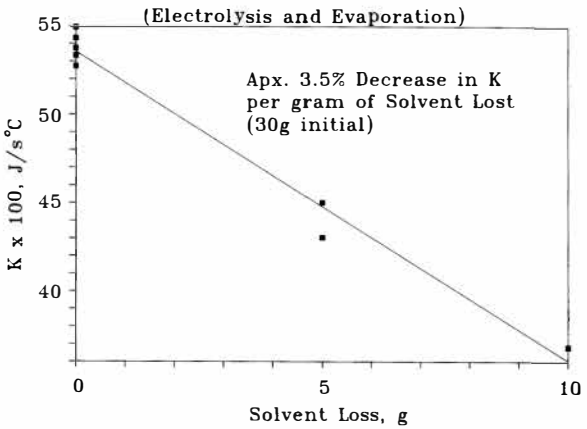

Figure 1. Decrease in the calorimetric cell constant due to solvent losses.

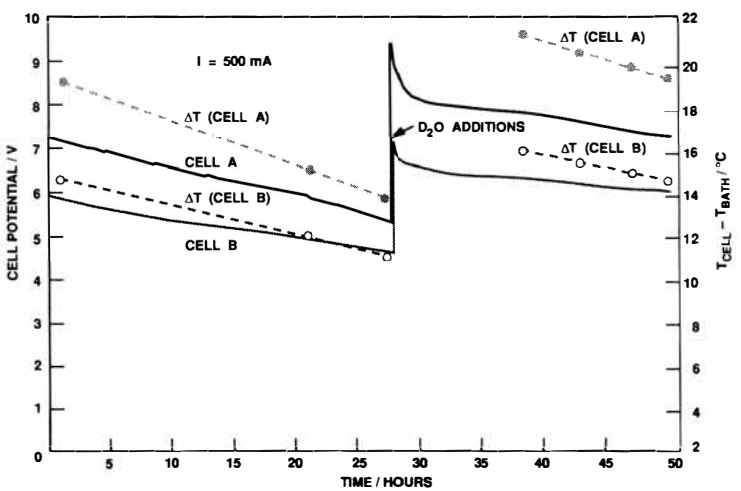

Figure 2. Time dependence of cell potentials and cell temperatures for cells A and B before and after D_2O additions.

The differential equation governing the behavior of our calorimeter can be expressed as

$$(E(t) - \gamma E_H) \bullet I + Px = a + K \bullet \Delta T + P_{gas} + P_{calor} \qquad (1)$$

where P_X represents any excess power. This equation also assumes that the bath and room temperatures are constant and that any power effects due to the

deuterium loading or deloading of the palladium are negligible. The rate of enthalpy transfer outside the cell due to the D_2, O_2, and D_2O gas stream (P_{gas}) is given by

$$P_{gas} = \frac{\gamma I}{F}\left\{\left[0.5\, C_{P,D_2} + 0.25\, C_{P,O_2} + 0.75\left(\frac{P}{P^* - P}\right)C_{P,D_2O(v)}\right]\Delta T + 0.75\left(\frac{P}{P^* - P}\right)L\right\} \quad (2)$$

and the time-dependence of the enthalpy of the calorimeter is given by

$$P_{calor.} = C_{P,D_2O(l)}\left[M^o - (1+\beta)\frac{\gamma I t}{2F}\right]\frac{d\Delta T}{dt} - (1+\beta)\frac{\gamma I}{2F}C_{P,D_2O(l)}\,\Delta T \quad (3)$$

These expressions are essentially the same as given by Fleischmann et. al.

For our calorimeter at typical conditions of 0.2 M LiOD and I = 500 mA, we calculate P_{gas}= 0.01 W and P_{cal} = -0.005 W using experimental measurements of ΔT and $d\Delta T/dt$. Although P_{gas} and P_{cal} vary significantly with I and the electrolyte concentration, their sum remains positive and less than 0.020 W for our range of experimental conditions. Therefore, the neglect of the sum $P_{gas} + P_{calor.}$ in Equation 1 will only underestimate our value for P_X. Furthermore, other error sources in our calorimetry, such as room temperature fluctuations, contribute to an estimated error of ±0.020 W. Calorimetric measurements of greater accuracy or over a wider range of experimental conditions, however, would require the solution of the differential equation (Eq. 1) as well as careful control of the bath and room temperatures.

It has been proposed by N. S. Lewis et. al. that a change in the rate and/or form of gas evolution can be a significant error source in electrochemical calorimetry. Therefore, our calorimetric cells were calibrated during electrolysis over a wide range of current densities (20-280 mA/cm^2). Results of these calibrations are presented in Figures 3 and 4. At low currents (I < 100 mA), stirring by the electrolysis may not be sufficient while at high currents, any errors due to the neglect of the $P_{gas} + P_{calor.}$ terms in Eq. 1 become larger. Nevertheless, the correlation coefficients of 0.999 or better for each thermistor show excellent heat recovery for these calorimetric cells over the entire calibration range. The rate of gas evolution is not a significant calorimetric error source as suggested by N. Lewis.

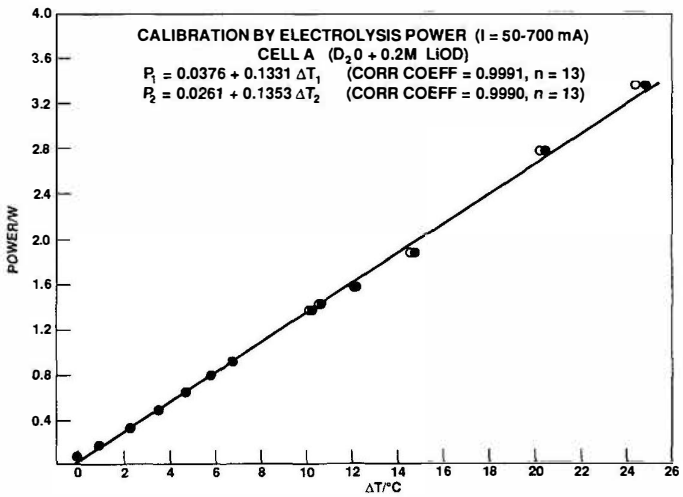

Figure 3. Calibrations for cell A by electrolysis power.

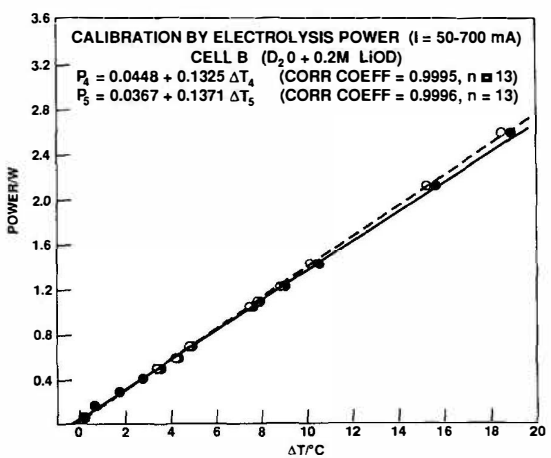

Figure 4. Calibrations for cell B by electrolysis power.

4. Discussion

For typical isoperibolic calorimetric cells, heat flows out of the top of the cell as well as into the constant temperature bath. Therefore, at constant bath and room temperature, it can be shown that

$$P = K_t (T_b - T_R) + K \bullet \Delta T = a + K \bullet \Delta T \qquad (4)$$

where $K = K_b + K_t$ (see M. H. Miles, R. A. Hollins et. al.). Thus there is a non-zero intercept for $\Delta T = 0$ as shown in Figures 3 and 4. The term $K_t(T_b - T_R)$ can become significant at low power levels, and the use of the approximate relationship $P \approx K \bullet \Delta T$ can produce large errors. This effect of the power level on the apparent cell constant (K) and heat transfer coefficient ($h = 1/k$) is shown in Figure 5 for our experimental results for thermistor 1 in cell A (Figure 3). The neglect of the intercept term in Equation 4 produces significant errors in the apparent cell constant for power levels below about 0.6 W. All of the calorimetric data reported by N. Lewis et. al. is near or below a total power level of 0.6 W, hence his use of the approximate relationship, $P \approx \Delta T/h$, is likely a large source of error. The schematic of the calorimetric cell design used at the California Institute of Technology as reported by G. M. Miskelly et. al. shows a relatively large area exposed to the ambient temperature, hence the problem of heat flow out of the cell top would be quite significant. Surprisingly, no mention of this large error source is discussed by N. S. Lewis.

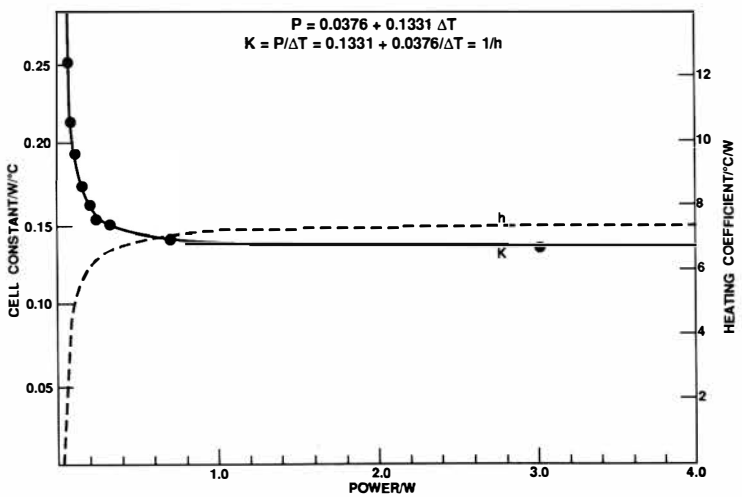

Figure 5. Effect of the power level on the apparent cell constant (K) and heat transfer coefficient (h).

A summary of our determinations of calorimetric cell constants over a three-year period is presented in Table 1. Except for the first three studies, these cell constants are based on Equation 4 rather than the approximate relationship, $P \approx K \bullet \Delta T$. There is no significant change of these cell constants over this time period. Calibrations were performed in D_2O as well as H_2O and by Joule heating (20-ohm resistor) as well as by electrolysis, yet excellent agreement is observed. The small differences in the measured cell constants could be attributed to the different methods of calibration and to differences in the insulation of the cell top from one experiment to another.

Table 1. Cell Constant Determinations.

Experiment	K_1 (W/°C)	K_2 (W/°C)	K_4 (W/°C)	K_5 (W/°C)	Date
Pd/D_2O	0.141	0.145	0.133	0.132	1989
Pd/H_2O	0.135	0.138	0.137	0.134	1989
Pd/D_2O	0.139	0.143	0.133	0.134	1990
Joule heating* (D_2O)	0.136	0.144	0.136	0.138	1990
Joule heating* (D_2O and H_2O)	0.141	0.148	0.132	0.133	1991
Pd/D_2O*	0.136	0.137	0.136	0.140	1991
Pd/D_2O*	0.143	0.143	0.141	0.141	1992
Mean	0.139 ±0.003	0.143 ±0.004	0.135 ±0.003	0.136 ±0.004	

* Calculated for P = 2.00 W.

In striking contrast to the stability of calorimetric cell constants in our experiments, N. Lewis et. al. report heat transfer coefficients that range from 12.6°C/W in H_2O to 15.9°C/W after 115 hours of D_2O electrolysis. This 26% increase in heating coefficients, based on our experience, is highly unusual. Closer examination, however, shows that N. Lewis et. al. erroneously define the heating coefficient as $h = \Delta T/P_T$ where the total power (P_T) is the sum of the electrolysis power + resistor power. According to the Newton law of cooling, the temperature difference, ΔT, defines the total output power from the cell to its surroundings, thus any excess power (P_X) must be included in defining the total power. This neglect of P_X by N. Lewis et. al. in the equation defining h would lead to an increase in the heating coefficient as the excess power increases. An analysis of this error in the N. Lewis study is presented in detail by M. H. Miles, R. A. Hollins et. al.

Table 2 presents an analysis of the results reported by N. Lewis et. al. when a constant heating coefficient of 14.0°C/W is assumed. Initially, there is no excess power. However, as electrolysis continues an excess power effect develops that becomes as large as 0.076 W after 161 hours of Pd/D_2O + LiOD electrolysis. The excess power density of 1.0 W/cm^3 Pd for this analysis of the N. Lewis study is in excellent agreement with our experiments (1.3 W/cm^3 Pd at 200 mA/cm^2) as well as with the results reported by M. Fleischmann et. al. in 1990.

In the calorimetric studies by N. Lewis et. al., a series of duplicate experiments (A, B, C, D, E) were conducted where a portion of the electrolysis power (P_{EL}) was replaced by resistor power (P_{Re}) in a manner that maintained the cell temperature essentially constant as shown in Table 2. Thus

$$P_T = P_{EL} + P_X \tag{5}$$

in one experiment where no resistor power is used ($P_{Re} = 0$), and

$$P_T' = P_{EL}' + P_X' + P_{Re}' \tag{6}$$

in the second experiment with $P_{EL}' < P_{EL}$ and $P_T' \approx P_T$. Thus

$$\Delta P_T = P_T - P_T' = P_{EL} - P_{EL}' + P_X - P_X' - P_{Re}' \tag{7}$$

For a constant cell temperature, the total output power must remain constant ($\Delta P_T = 0$), thus from simple algebra

$$P_X - P_X' = P_{EL}' + P_{Re}' - P_{EL} \tag{8}$$

The experimental observation by N. Lewis that $P_{EL}' + P_{Re}' \approx P_{EL}$ simply cannot prove that there is no excess power but only that $P_X - P_X' \simeq 0$, i.e., the change in P_X is small when a portion of the electrolysis power is replaced by resistor power. It is interesting to note from Table 2 that the input power ($P_{EL} + P_{Re}$) required to maintain a constant cell temperature in the Lewis study is always smaller for the experiment at the higher current density. This effect is consistent with the presence of an anomalous excess power that increases with the current density and is near the magnitude reported by Fleischmann et. al. A similar error analysis of the N. Lewis calorimetry has been previously provided by V. C. Noninski and C. I. Noninski.

Table 2. Analysis of Cal Tech Calorimetric Results.[a]

Pout = (T_{cell} -25.30)/h where h = 14.0°C/w

Exp.	Time (h)	Current Density (mA/cm^2)	T_{Cell} (°C)	P_{out} (W)	P_{in} (W)	P_X (W)
A-1	14.7	108	31.80	0.464	0.463	0.001[b]
A-2	16.0	74	31.82	0.466	0.467	-0.001
B-1	63.7	74	32.04	0.481	0.442	0.039
B-2	66.0	110	32.01	0.479	0.429	0.050[b]
C-1	88.7	110	34.69	0.671	0.619	0.052
C-2	94.5	140	34.64	0.667	0.607	0.060[b]
D-1	113.2	72	32.13	0.488	0.433	0.055
D-2	115.0	108	32.08	0.484	0.426	0.058[b]
E-1	161.0	140	34.69	0.671	0.595	0.076[b,c]
E-2	164.5	115	34.71	0.672	0.600	0.072

[a] N. S. Lewis, et. al., Nature, 340, 525 (1989).
[b] Higher current density.
[c] P_X/V_{Pd} = 0.076 W/0.073 cm^3 = 1.04 W/cm^3 (0.054 W/cm^2).

In contrast to the Lewis experiments, the calorimetric studies by D. E. Williams et. al. and D. Albagli et. al. identified the importance of the electrolyte level effect and the problem of the heat flow pathway through the top of the cell to the ambient atmosphere. However, both these studies invoke steady state approximations as well as questionable cell calibration procedures. The calorimetric error ranges of ±40 mW for the M.I.T. studies and ±15% excess power (±2σ) for the Harwell calorimetry fall far short of the ±1 mW accuracy reported by M. Fleischmann et. al. Both the Harwell and M.I.T. laboratories report calorimetric measurements over rather short time periods (100 hours for M.I.T. and one experiment lasting only 8 hours for Harwell). We have never observed any excess power in less that 6 days in our experiments involving Pd/D_2O + LiOD electrolysis.

A summary of additional error sources and problems for the study by D. E. Williams et. al. include their method of cell calibration during electrolysis when any excess power is unknown, their large power changes used during calibrations, the marked endothermic behavior following topping up of their cells with D_2O, and their use of small electrodes in large electrolyte volumes that would minimize the detectability of any excess power effect as well as contribute to poor stirring and possible H_2O contamination in these large cells. Furthermore, the unfavorable geometry of various cathodes (beads, ribbon, bar) would not provide for uniform electric fields and symmetry required for high deuterium loadings. These numerous error sources call into question any calorimetric conclusions stemming from the Harwell experiments.

5. Conclusions

The early cold fusion calorimetric results by several major laboratories in 1989-1990 contain serious errors that will ultimately undermine the acceptance of these studies as credible electrochemical calorimetry. These publications by N. Lewis, D. E. Williams, D. Albagli and others, however, serve to illustrate important calorimetric principles, problems, and sources of error relating to attempts to measure excess power in the $Pd\text{-}D_2O$ system. Electrochemical calorimetric measurements accurate to within ±1 mW require the integration of the differential equation governing the calorimeter as well as careful control of external experimental conditions such as the ambient laboratory temperature.

6. Acknowledgments

We thank Drs. Vesco C. Noninski and Joseph L. Waisman for helpful discussions relating to the calorimetric results reported by various laboratories.

7. List of Symbols/Nomenclature

a = $K_t (T_b - T_R)$, power intercept for $\Delta T = O$, W
C_p = Heat capacity at constant pressure, $JK^{-1}mol^{-1}$
E_H = Thermoneutral potential, V

$E(t)$ = Measured cell potential at time, t, V
F = Faraday constant, 96485 C mol^{-1}
h = Apparent heat transfer coefficient due to conduction, K/W
I = Cell current, A
K = Apparent calorimetric cell constant due to conduction, W/K
K_b = Calorimetric cell constant for heat flow from the cell into the bath, W/K
K_t = Calorimetric cell constant for heat flow out of the top of the cell, W/K.
L = Enthalpy of evaporation, J mol^{-1}
M^o = Heavy water equivalent of the calorimetric when topped up, mol
P = Partial pressure, Pa
P^* = Atmosphere pressure, Pa
P_{calor} = Rate of enthalpy change within the calorimeter, W
P_{EL} = Power input due to electrolysis, W
P_{gas} = Rate of enthalpy transport by the gas stream, W
P_{Re} = Power input due to calibration heater, W
P_X = Excess power, W
T_b = Temperature of bath, K
T_{cell} = Temperature measured at the outer wall of the electrolysis cell, K
T_R = Temperature of room (ambient), K
ΔT = $T_{cell} - T_b$, K
β = Dimensionless term allowing for D_2O losses by evaporation or other means besides electrolysis
γ = Current efficiency for D_2O electrolysis
σ = Standard deviation for series of measurements

8. References

1. Albagli, D. et. al., 1990, J. Fusion Energy, 9, 133.
2. Fleischmann, M. and Pons, S., 1992, J. Electroanal. Chem., 332, 33.
3. Fleischmann, M. et. al., 1990, J. Electroanal. Chem., 287, 293.
4. Lewis, N. S. et. al., 1989, Nature, 340, 525.
5. Miles, M. H. et. al., 1990, J. Electroanal. Chem, 296, 241.
6. Miles, M. H., Hollins, R. A. et. al., J. Electroanal. Chem. (accepted for publication).
7. Noninski, V. C. and Noninski, C. I. (personal communications and unpublished manuscripts).
8. Miskelly, G. M. et. al., 1989, Science, 246, 793.
9. Stilwell, D. E. et. al., 1990, J. Fusion Energy, 9, 333.
10. Thomas, L. C., 1992, "Heat Transfer," Prentice Hall, New Jersey, pp. 16-18.
11. Williams, D. E. et. al., 1989, Nature, 342, 375.
12. Wilson, R. H. et. al., 1992, J. Electroanal. Chem., 332, 1.

Tritium and Excess Heat Generation during Electrolysis of Aqueous Solutions of Alkali Salts with Nickel Cathode

M. Srinivasan, A. Shyam, T.K. Sankaranarayanan, M.B. Bajpai, H.Ramamurthy, U.K.Mukherjee, M.S.Krishnan, M.G.Nayar and Y.P.Naik

Bhabha Atomic Research Centre
Trombay, Bombay 400 085, India

ABSTRACT

A number of open cell electrolysis experiments of the Mills and Kneizys type using Nickel as cathode, Pt wire as anode and aqueous solutions of carbonates of Potassium, Sodium and Lithium (natural and enriched) as electrolyte have been carried out in three different laboratories at Trombay. The cells were fabricated out of commercial dewar vacuum flasks. The difference in temperature at equilibrium between the operating cells and that of an identical dummy reference flask was measured to deduce excess heat. The cells were calibrated using resistance heaters. In all, studies have been carried out so far in 29 electrolytic cells with various electrolytes. In some cases a mixture of H_2O and D_2O was used. The cells were operated for a few weeks at a time and excess heat up to a maximum of 70% appears to be present in most cells when the input joule power is upto a watt or two. The current density was less than 40 mA/cm^2.

Electrolyte samples before and after electrolysis were analysed for tritium content after microdistillation to eliminate chemiluminiscence effects. Samples from 18 out of 29 experiments analysed have indicated tritium levels varying in the region of 46 Bq/ml to 3390 Bq/ml. One cell with enriched Li_2CO_3 solution in H_2O which was monitored continuously for over a month indicated that tritium generation is continuous. Although the highest amount of tritium produced so far was with a K_2CO_3 in 25% D_2O cell, the generation of tritium in cells containing only H_2O is a new finding.

1. Introduction

Mills and Kneizys were the first to report observation of excess heat in a light water electrolytic cell using a cylindrical cathode made of Nickel sheet, Platinum wire anode and a solution of 0.57 M K_2CO_3 in H_2O as electrolyte. These authors however did not attribute their excess heat results to the occurrence of any nuclear reactions but claimed instead that it was due to the

FRONTIERS OF COLD FUSION

formation of "shrunken" hydrogen atoms involving "fractional quantum numbers" (Mills and Kneizys, 1991). The theoretical model of Randell Mills (1989) predicted that excess heat would be obtained with an aqueous solution of K_2CO_3 but not of Na_2CO_3, and they reported (Mills and Kneizys, 1991) that in fact their experiments had confirmed this prediction. They have since reported (Mills and Good, 1992) measuring excess heat margins of several hundred percent, with a scaled up version of their light water cell concept at input joule powers of several tens of watts. Further when intermittent d.c. was applied to the electrodes, the margin of excess heat significantly improved. More importantly they claim that their excess heat observations are much more reproducible than that obtainable with Pd–D_2O cells of the Fleischmann–Pons type (Fleischmann and Pons, 1989).

Shortly after Randell Mills preprint became available, Noninski (1992) announced that he had independently verified their experimental findings. These startling reports of excess heat generation in ordinary water cells appear to have been informally discussed among participants at the Como Cold Fusion meeting of June 1991. Speculating that the source of excess heat in aqueous K_2CO_3 solutions could perhaps be nuclear transmutation reactions of the type

$$^{1}p_1 + {}^{39}K_{19} \longrightarrow {}^{40}Ca_{20} + 8.3 \text{ Mev},$$

Robert Bush of California integrated this into his Transmission Resonance Model (TRM) (Bush, 1991) of cold fusion (which he has since begun referring to as Alkali–Hydrogen Fusion) and proceeded to verify his ideas experimentally by setting up Mills type light water cells with Nickel cathodes. The preliminary results of their excess heat and calcium build–up measurements seem to have confirmed his initial conjecture, but with the difference that Bush measured excess heat with solutions of other alkali carbonates also, such as Na_2CO_3 and Rb_2CO_3, besides K_2CO_3 (Bush, 1992). They also reported observing a proportionate increase in calcium concentration in the electrolyte following electrolysis when K_2CO_3 was used and of strontium level when Rb_2CO_3 solution was used, the magnitude of increase being commensurate with the observed excess heat.

It was at this point that we decided to initiate attempts to verify these claims independently in view of its potential importance and significance to the whole field of cold fusion. The first crude cell with a copper constantan thermocouple inserted into the cell and reading to an accuracy of 0.5^0C, was set up in January 92 at the Process Instrumentation Systems Division (PISD) of BARC. At the end of January 92 we learnt from Jed Rothwell (Rothwell, 1992) that six other groups in the world had confirmed the generation of excess heat in such Ni–H_2O cells. This communication also contained a recommended protocol for achieving success in such experiments, based on the experience of the successful groups. In March 92 a second group, located at the Purnima Laboratories of BARC began experimenting with cells constructed out of commercial dewar flasks (double walled silvered vacuum jacketed glass dewars). Since preliminary experiments (Shyam, 1992) had indicated that porous Nickel cathodes fabricated by the Desalination Division of BARC appeared to give higher levels of excess heat than rolled Nickel sheets, all experiments since April 92 have mostly used porous Ni as cathode material. In May 92 a third group belonging to the Chemical Engineering Division and

located at Hall No. 5 in Trombay joined the search.

2. Description of Cells

All the cells were of the open type with the electrolytic gases escaping through the top plug. Most of the cells were constructed using commercial 300 ml dewar flasks, although some of the early experiments at PISD used a 110 ml flask. The most recent cells set up at Hall–5 employ 500 ml flasks. While the initial experiments used cylindrical geometry for the electrode assembly (1 cm dia x 6 cm long) all subsequent cells have deployed a flat plate geometry (2 cm x 6 cm in size, 0.3 mm thick). The platinum anode which encompassed the Ni cathode was made of 0.15 mm or 0.2 mm dia Pt wire wound over a teflon holder. The lead wires to the electrodes were covered with teflon sleeving upto the top plug so that no portion above the solution level is exposed bare to the electrolytic gases. This is to minimise recombination effects giving rise to errors in calorimetry.

The electrolytic solution was either $\simeq$ 0.57 M K_2CO_3 or 0.57 M Na_2CO_3 or 0.1 M Li_2CO_3. In some experiments carbonates of enriched Li^6 (25% or 54%) were used in place of natural lithium. While most experiments were carried out with H_2O solutions, some runs used a mixture of H_2O and D_2O with the D_2O concentration being 25% or 50% or even 100%. The volumes of the electrolytic solution were 98 ml, 200 ml and 300 ml respectively for the 110 ml, 300 ml and 500 ml flasks.

To speed up data accumulation recent experiments have used banks of five electrolytic cells (flasks) connected in series. A sixth flask served as dummy or reference cell, for the DT (differential temperature between electrolytic cells and the reference cell) measurements. Highly stabilized constant voltage power supplies (0 to 30 V adjustable) with negligible ripple were employed to drive the cells. All cells had a built–in resistor or resistance wire (manganin or nichrome) encased in teflon sleeving or tape besides the Ni–Pt electrode assembly, for calibration purposes.

3. Instrumentation and Technique of Calorimetry

One of the main differences between Pd–D_2O cells and Ni–H_2O cells lies in the current densities involved and hence power inputs dealt with, which in Ni–H_2O cells, are over an order of magnitude lower. This, coupled with the fact that excess heat margins in terms of percentage of joule heat input are much larger here, has a significant bearing on the design of the cells, as well as instrumentation requirements for calorimetry.

The difference in temperature (DT) at steady state between the test electrolytic cell and the dummy cell containing identical volumes of electrolytic solution was taken as a measure of the steady heat generation rate in the test cell. It is well known however that this simple principle of calorimetry is subject to several sources of error which can lead to incorrect results. Some of these are: (a) Role of temperature gradients, if any, within the cell; (b) Effect of fluctuations of ambient temperature; (c) Variation of calibration constant due to changes in solution height in the dewars following evaporation/electrolysis; (d) Errors due to differences, if any, in the heat transfer characteristics between electrolysis runs when bubbles are present and resistance heating runs where no bubbles are present; (e) Inadequate waiting

time leading to non attainment of steady state. These and other sources of error arising in calorimetric measurements have been discussed exhaustively in cold fusion literature, ever since the failure of many groups in the world to reproduce the original results of Fleischmann and Pons. However before blindly applying all these arguments to the present experiments, one has to keep in mind the differences between Ni–H_2O cells and Pd–D_2O cells pointed out earlier. In most of the experiments of this paper the input joule power was typically < 2 W.

Amongst the three groups, the best instrumented system for calorimetry at present is that assembled by the PISD group. This has evolved over a period of about 6 months. In the initial series of experiments (designated as X–series) conducted by this group with a 110 ml flask, a 12 point, 0–10 mV range Honeywell recorder (Model Electronik – 15) calibrated for 0–4 mv range (corresponding to 0–100°C for ANSI type T thermocouple) was used to record all parameters, viz. temperature of the electrolytic solution, voltages applied to the cell and heater coil as well as their corresponding currents. The recorder was calibrated using a Keithley 4 $^1/_2$ digit Digital Voltmeter (DVM). For recording currents the voltage drops across two manganin wire resistors were measured. The resistance of these resistors used as standards were in turn determined accurately with the help of a 'decade box'. Manganin wire of 2.2 ohm per meter resistance insulated with teflon was used to make the heaters used for calibration of the cells.

In the X–series of experiments only one thermocouple was used for cell temperature measurement. Room temperature was measured with a calibrated Pt100 RTD (Resistance Temperature Detector). Appropriate correction was applied for the non–linear response of the copper–constantan thermocouples and for cold junction compensation. An accuracy of ± 0.5°C was achieved in differential temperature measurements.

In the second series of experiments with 300 ml flasks currently being conducted by the PISD group (designated as XA–series), a more sophisticated instrumentation system based on a Yokogawa hybrid recorder HR–2500 E (Model 3880), having 30 input channels, 60 channels for computing results and 60 channels for storing constants is being used. In the XA–series each cell has two calibrated ANSI type T thermocouples one immersed upto the bottom of the cell and another dipping just below the surface of the solution, which facilitate monitoring the uniformity of temperature within the solution. It was ensured by this method that no gradient more than ± 0.15°C existed within the solution, inspite of the fact that no stirrer was used. Cold junction compensation for the thermocouples was automatic. The ambient temperature in the perspex enclosure in which the six flasks were housed was measured by means of an RTD. Parameters such as total heat input to cells and DT between average cell temperature and average reference cell temperature (of the two thermocouples) was computed continuously (every 2 seconds) for each cell. Trend recording of the measured parameters such as individual cell/heater voltage as well as the common currents in the electrolysis and heater circuits and computed quantities was carried out at intervals of one minute with a chart speed of 15 mm/hr. The initial and finally stabilised values of all the measured and computed quantities were printed out on the same chart used for trend recording. The accuracies obtained in the various measurements were as follows : For temperatures: ± 0.1°C, for voltages and currents: ± 0.05%.

formation of "shrunken" hydrogen atoms involving "fractional quantum numbers" (Mills and Kneizys, 1991). The theoretical model of Randell Mills (1989) predicted that excess heat would be obtained with an aqueous solution of K_2CO_3 but not of Na_2CO_3, and they reported (Mills and Kneizys, 1991) that in fact their experiments had confirmed this prediction. They have since reported (Mills and Good, 1992) measuring excess heat margins of several hundred percent, with a scaled up version of their light water cell concept at input joule powers of several tens of watts. Further when intermittent d.c. was applied to the electrodes, the margin of excess heat significantly improved. More importantly they claim that their excess heat observations are much more reproducible than that obtainable with Pd–D_2O cells of the Fleischmann–Pons type (Fleischmann and Pons, 1989).

Shortly after Randell Mills preprint became available, Noninski (1992) announced that he had independently verified their experimental findings. These startling reports of excess heat generation in ordinary water cells appear to have been informally discussed among participants at the Como Cold Fusion meeting of June 1991. Speculating that the source of excess heat in aqueous K_2CO_3 solutions could perhaps be nuclear transmutation reactions of the type

$$^{1}p_1 + {}^{39}K_{19} \longrightarrow {}^{40}Ca_{20} + 8.3 \text{ Mev},$$

Robert Bush of California integrated this into his Transmission Resonance Model (TRM) (Bush, 1991) of cold fusion (which he has since begun referring to as Alkali–Hydrogen Fusion) and proceeded to verify his ideas experimentally by setting up Mills type light water cells with Nickel cathodes. The preliminary results of their excess heat and calcium build–up measurements seem to have confirmed his initial conjecture, but with the difference that Bush measured excess heat with solutions of other alkali carbonates also, such as Na_2CO_3 and Rb_2CO_3, besides K_2CO_3 (Bush, 1992). They also reported observing a proportionate increase in calcium concentration in the electrolyte following electrolysis when K_2CO_3 was used and of strontium level when Rb_2CO_3 solution was used, the magnitude of increase being commensurate with the observed excess heat.

It was at this point that we decided to initiate attempts to verify these claims independently in view of its potential importance and significance to the whole field of cold fusion. The first crude cell with a copper constantan thermocouple inserted into the cell and reading to an accuracy of 0.5^0C, was set up in January 92 at the Process Instrumentation Systems Division (PISD) of BARC. At the end of January 92 we learnt from Jed Rothwell (Rothwell, 1992) that six other groups in the world had confirmed the generation of excess heat in such Ni–H_2O cells. This communication also contained a recommended protocol for achieving success in such experiments, based on the experience of the successful groups. In March 92 a second group, located at the Purnima Laboratories of BARC began experimenting with cells constructed out of commercial dewar flasks (double walled silvered vacuum jacketed glass dewars). Since preliminary experiments (Shyam, 1992) had indicated that porous Nickel cathodes fabricated by the Desalination Division of BARC appeared to give higher levels of excess heat than rolled Nickel sheets, all experiments since April 92 have mostly used porous Ni as cathode material. In May 92 a third group belonging to the Chemical Engineering Division and

PISD (X–series) conducted with the 110 ml flask, reasonable stability appeared to be attained (as evident from the temperature trace on the Honeywell chart recorder) within about 6 to 8 hrs. While these results are still good, there is considerable scatter in these data points and in retrospect we feel it was possibly due to inadequate waiting times. In several experiments both electrolysis and resistance heating was simultaneously carried out, a procedure referred to in literature as "on the fly calibration".

Table I presents a summary of 18 experiments carried out so far wherein the variation of DT with input joule power was studied. The maximum cell current, input power range and other relevant parameters for each experiment are given in the Table. The input joule power is computed as $(V - 1.48) * I$ for H_2O cells and $(V - 1.54) * I$ for D_2O cells and appropriately weighted relations for mixtures of H_2O and D_2O. Figs. 1 to 7 present the calorimetric results in the form of DT vs input joule power (P_j) plots for a few selected experiments of Table I. The least squares fitted quadratic calibration curves pertaining to each of the experiments are also shown plotted. The DT points corresponding to electrolysis runs in all these figures are clearly above the calibration curves indicating the generation of excess heat of 20 to 70% by these cells.

Interestingly, out of all the experiments in which calorimetry has been carried out so far, there is only one cell, namely cell XA–1 (K_2CO_3 in H_2O) which did not show any excess heat at all. This cell was also a Ni–Pt cell similar to others with a flat plate porous Ni cathode but the size of the cathode was slightly smaller being only 2 x 3 cm^2 in area. It was reconstituted from a previously used electrode assembly and not much care appears to have been exercised in handling this electrode assembly. This was the only cell in which the electrolysis and heater calibration points have all fallen on the same curve. In contrast cell XA–2 which was basically a Pt–Pt cell (also K_2CO_3 in H_2O) was expected to yield a single curve showing no excess heat. However surprisingly this cell has also shown some excess heat. Later we learnt that the material of the cathode–mesh used in this cell is not pure Pt but is an alloy of Pt–10% Rh. The anode of XA–2 however was made of standard Pt wire as in all other cells.

The first four rows of Table II summarise the results of some early excess heat measurements carried out at Purnima (Shyam, 1992). Some of these indicated excess heat of 60 to 70% at an input joule power level of $\simeq$ 110 mw.

5. Tritium Level in Electrolytic Solutions

The magnitude of tritium activity in the electrolytic solutions was determined at the end of the electrolysis runs through standard liquid scintillation counting techniques. For this 10 ml samples of the electrolytic solutions were drawn and carefully transferred into clean fresh sample bottles and sent for analysis to the Isotope Division. Microdistillation of every sample was carried out prior to counting to eliminate chemiluminiscence effects. The distillation apparatus was thoroughly washed three times with different reagents and finally rinsed with distilled water and dried to avoid cross contamination. Washed water was counted and the washing process continued until it stopped giving counts. Also the apparatus itself was discarded after use for a few tens of samples. Pipettes, counting vials etc were disposed off after each use. The counting vials were made of glass of low K^{42} content. A digital

pipetting system with disposal tips capable of 0.001 ml accuracy was used to measure out exactly 1.000 ml of distilled sample for mixing with 10.0 ml of Dioxane based scintillation cocktail for counting. As a further measure of abundant caution, the vials containing cocktail plus distilled sample were kept in a dark cabinet for several hours for allowing for chemiluminiscence cooling prior to counting.

A Packard Tri–Carb model 3255 liquid scintillation spectrometer was employed and five minute counts were recorded for each sample. A standard tritium sample was also counted with each batch of samples to deduce counting efficiency. Blanks in the form of distilled water, tap water, unelectrolysed alkali solutions etc were also sent to the analysis group in a blind fashion to check for overall reliability of the distillation procedure and counting methodology. It was confirmed that the activity counted is in fact that of tritium and not some other radioactivity, by measuring the pulse height spectrum and comparing it with that of a standard tritium sample. In all over a hundred samples have been distilled and counted for tritium to date. The results of the tritium in electrolyte measurements for the experiments wherein excess heat was investigated systematically are summarised in the last Column of Table I. Table II summarises the tritium data for the other experiments. These data have not been corrected for electrolytic enrichment. This is because the volume reduction of the electrolyte during the whole course of the experiments was less than a factor of 1.5, in most cases. Hence the correction for electrolytic enrichment is quite small.

One point which needs to be commented upon is the apparently high tritium level of the blanks and control samples. This is because of the relatively high background of the counting instrument which is routinely used for counting a variety of samples from different groups in BARC. Even Dioxane based cocktail alone indicated counts equivalent to a few Bq/ml. Hence to be on the conservative side, only values above 10 Bq/ml (twice background value) were regarded as reliable evidence for tritium generation in the present paper.

It is seen that the measured tritium levels in the electrolysed solutions vary from 46 Bq/ml to as much as 3390 Bq/ml. On the whole 15 experiments out of 29 have indicated tritium levels significantly above background values so far. These include K_2CO_3 in 25% D_2O, Li_2CO_3 in 50% D_2O, K_2CO_3 in H_2O as well as Li_2CO_3 in H_2O combinations. Surprisingly most of the natural lithium carbonate in ordinary–water–cells run so far have generated detectable amounts of tritium whereas some enriched Li_2CO_3 in H_2O cells have not. For other combinations also for every successful case there has been atleast one cell with that particular combination which has not yielded tritium. While the maximum amount of tritium generated has been in a K_2CO_3 in 25% D_2O cell (3390 Bq/ml), the second highest (1454 Bq/ml) was with a Li_2CO_3 in H_2O cell. No "magic formula" has emerged for generating high levels of tritium so far. But perhaps the most surprising finding of these studies is that tritium has been generated, possibly for the first time in a light water electrolytic cell.

6. Evidence for Continuous Generation of Tritium

During the series B experiments conducted at Hall 5, samples of electrolyte were collected from the 5 cells of the series and sent for analysis

periodically. These results are summarised in Table III. It may be seen that cells B1 and B2 (Li_2CO_3 in H_2O) did not give any tritium throughout. However cells B3, B4 and B5 have indicated tritium in each of the 4 samples taken. Between the 2nd and 3rd sample the cells were operated in reverse electrolysis mode. The cause for the big jump in the tritium level shown by cell B3 in the 4th and final sample is not clear.

In order to study the temporal variation of build–up of tritium during electrolysis systematically, a special cell # OM–3 made of a separating funnel was set up. A porous nickel flat plate electrode assembly, similar to the ones described earlier was used. The evolved electrolytic gases were led into a glass trap containing Pt catalyst for recombination of the gases into H_2O, at room temperature. The re–formed H_2O condensed in the cooler parts. An oil trap isolated this system from the atmosphere. This cell was driven by a pulsed (intermittent d.c) power supply of the type described by Mills and Kneizys (1991). 5 ml samples of electrolyte were drawn once every few days and sent to the Isotope Division for tritium analysis.

In this experiment an attempt was also made to monitor tritium build–up on–line using a system developed by the Environmental Assessment Division of BARC. The on–line monitor comprises of a small scintillation chamber containing solid plastic scintillator fibres in the form of a sponge, with a pair of photomultiplier tubes viewing the chamber and connected to a coincidence circuit. A peristaltic pump was used to continuously circulate the electrolyte through the chamber of the detector assembly. The system was calibrated prior to start–up using Li_2CO_3 solutions containing a known quantity of tritium. An unexpected problem however arose during the investigations with the on–line monitor, in the sense that there was a 'spurious' increase in count rate as soon as the electrolysis was switched on. It appears that some unknown mechanism gives rise to scintillations in the detector assembly when electrolysed alkali carbonate solution is circulated through it. This interference was found to be lesser in the case of 0.1 M Li_2CO_3 electrolyte as compared to 0.57 M K_2CO_3 solutions' presumably because the alkali concentration is lesser in the lithium carbonate case. This was the reason for selecting Li_2CO_3 as electrolyte in cell # OM–3.

Fig.8 shows the continuous build–up of tritium in cell # OM–3 over a period of about 5 weeks. The authors believe that this result presents strong evidence for the continuous occurrence of some nuclear phenomenoa in light water electrolytic cells. The recombined H_2O (about 3 ml) from the electrolyte sample during the first three days of operation of this cell indicated 42.3 Bq/ml of tritium activity .

7. Summary and Conclusions

Measurements of excess heat and tritium production in light water cells of the Mills and Kneizys type have been carried out using Nickel as cathode material, by three different groups at Trombay. The electrolytes used were mostly 0.57 M K_2CO_3 (natural and enriched) dissolved in H_2O or a mixture of H_2O and D_2O. A few experiments were also done with an aqueous solution of 0.57M Na_2CO_3. The current densities employed were < 40 mA/cm2 and input joule powers typically < 2 W. The measured temperature difference (DT) at steady state between a cell undergoing electrolysis and an identical 'reference' cell was compared with the corresponding DT obtained in a calibration run

during which a resistance heater immersed in the electrolyte was switched on in place of electrolysis. In all but one of 18 such experiments carried out so far, the DT measured during electrolysis was invariably higher by between 20% and 70% than that measured during corresponding calibration run. Possible differences in heat loss characteristics of a flask with bubbles present, as during electrolysis, and one where no bubbles are present, as in a heater calibration run, cannot be the source of this "excess power". This has been confirmed by measuring the calibration constant several times when electrolysis was underway by simultaneously switching on the resistance heater (so called 'on the fly' calibration). This is also reinforced by the calibration data obtained during reverse electrolysis of several cells.

The other possible source of "excess power" could in principle be partial recombination of H_2 and O_2 in the gas plenum region in the flasks, above the electrolytic solution. For this a few Faraday efficiency measurements were carried out by measuring the total volume of electrolytic gases generated and comparing the same with the expected volume based on ampere–hours or coulombs of charge passed. Such measurements carried out with a simple make shift apparatus indicated a Faraday efficiency of atleast 90%. In this context it is worth noting that if a fraction, f, of the electrolytic gases were to recombine within the flask it could lead to an apparent excess heat of

$$[f * (1.48) / (V - 1.48)] = f/[(V/1.48 - 1)].$$

Hence if the applied voltage is more than 2.96 V, (as in most of our experiments) in order to generate an apparent excess power of say 50% the recombination fraction has to be more than 50%. Thus excess heat margins of 50% or more measured in some of our experiments, particularly in the low input power range, cannot be explained away on the basis of recombination effects.

The quantum of excess power, expressed as a fraction of input power, was in general lower at higher input power levels. The apparent scatter in the electrolysis data points may possibly be due to a "structure" in the excess heat data as observed by Bush (1992) using a flow calorimeter.

The two Na_2CO_3 cells studied by us also appear to have generated some excess heat. This tends to agree with the experimental observations of Bush (1992) but contradicts the results of Mills and Kneizys (1991) as well as Noninski (1992) both of whom have not detected excess heat in Na_2CO_3 experiments.

As for tritium generation only tritium concentrations above a threshold value of 10 Bq/ml have been accepted as reliable in the present paper. In spite of the relatively high background levels involved in the tritium analysis, it can be stated confidently that tritium has been generated in majority (> 50%) of the cells studied by us. Two cells have yielded 4 digit levels of Bq/ml, 8 cells have given 3 digit levels and rest in the 2 digit regime. It is possibly for the first time that significant quantities of tritium is found to have been generated in a light water electrolytic cell.

The results of the B series of experiments with deuterated lithium carbonate solutions (Table III) and the results of the on–line monitor cell # OM–3 (54% enriched $^6Li_2CO_3$ in H_2O) which has operated for more than a month, clearly indicate that tritium generation is continuous in time (see Fig.8). The amount of tritium carried away by/with the electrolytic gases has

however not been quantified by us so far. But it is reasonable to assume that it would constitute a non–negligible fraction of the overall quantity of tritium generated.

Since tritium seems to be generated both with K_2CO_3 and Li_2CO_3 with or without the presence of D_2O, we are unable to derive any clue from the results as to the mechanism of tritium generation. There does not appear to be a one–to–one correlation between excess heat and tritium generation. In the experiments where both tritium and excess heat have been measured, the quantity of tritium produced is far below what can be expected, if the same nuclear reactions were to be the cause of excess heat also. Thus, as observed in Pd–D_2O cells of the Fleischmann–Pons type also, tritium generation is obviously a secondary reaction in the context of excess heat production. However the relatively high success rate of detection of tritium in these light water cells clearly signals the occurrence of some nuclear phenomena in them.

The authors agree with other researchers who have experimented with such light water cells using Nickel cathodes, that this type of cells are much less "frustrating" to deal with than Pd–D_2O cells. Also the excess heat results are much more reproducible and success rate fraction higher. Excess heat, if present, is detectable within the first day of electrolysis. However great care needs to be taken in ensuring clean surfaces and avoidance of impurities, to get successful results.

8. References

1. Bush, R.T., 1991, Fusion Technol, 19, 313.
2. Bush, R.T., 1992, Fusion Technol, 22, 301.
3. Fleischmann, M and Pons, S., 1989, J. Electroanal Chem. 261, 301.
4. Mills, R.L and Farrell, J.J., 1989, The Grand Unified Theory, Science Press.
5. Mills, R.L and Kneizys, K., 1991, Fusion Technol., 20, 65.
6. Mills, R.L and Good, W.R., 1992, Paper submitted for publication.
7. Noninski, V., 1992, Fusion Technol. 21, 163.
8. Rothwell, J., 1992, Personal Communication, dated 28th Jan. 1992.
9. Shyam, A. et. al., 1992, Internal Report, dated 30th April 1992 (Unpublished).

Table I. Experiments Where DT was Measured for Various Input Power Levels.

Srl No.	Expt. No.	Date Comp–leted	No. of days	Alkali Type	Sol–vent	Max. Input Power P_j(w)	Max. Excess Power (%)	Tritium Content in Elect. (Bq/ml)
PISD GROUP (CYL. & PLANAR GEOMETRY; SOLID & POROUS Ni)								
1	X–8/12*	May,1	44d	K_2CO_3	H_2O	2.0w	40%	NIL
2	X–14†	Jun,3	16d	Li_2CO_3	H_2O	3.5w	30%	177
3	X–15†	May,21	10d	K_2CO_3	25%D_2O	1.6w	130%	3390
4	XA–1‡	Oct,20	30d	K_2CO_3	H_2O	1.2w		NIL
5	XA–2‡	Oct,20	30d	K_2CO_3	H_2O	1.0w		NIL
6	XA–3‡	Oct,20	30d	K_2CO_3	H_2O	1.3w	23%	NIL
7	XA–4‡	Oct,20	30d	Li_2CO_3	H_2O	1.0w	70%	NIL
8	XA–5‡	Oct,20	30d	Na_2CO_3	H_2O	0.8w	35%	NIL
HALL 5 GROUP (CYLINDRICAL GEOMETRY : POROUS Ni)								
9	A1	Jun,29	21d	K_2CO_3	25%D_2O		36%	NIL
10	A2	Jun,29	21d	K_2CO_3	25%D_2O		28%	NIL
11	A3	Jun,29	21d	K_2CO_3	25%D_2O	0.23w	28%	NIL
12	A4	Jun,29	21d	K_2CO_3	H_2O		24%	46
13	A5	Jun,29	21d	Li_2CO_3	H_2O		70%	1454
14	B1	Aug,25	28d	*Li_2CO_3	H_2O		40%	NIL
15	B2	Aug,25	28d	*Li_2CO_3	H_2O		58%	NIL
16	B3	Aug,25	28d	*Li_2CO_3	50%D_2O	0.3w	46%	513
17	B4	Aug,25	28d	Li_2CO_3	50%D_2O		49%	69
18	B5	Aug,25	28d	*Li_2CO_3	D_2O		53%	195

* Cylindrical Geometry, Solid Nickel Cathode
† Cylindrical Geometry, Porous Nickel Cathode
‡ Planar Geometry, Porous Nickel Cathode
* Enriched lithium (54%)

Table II. Other Excess Heat and Tritium Experiments.

Srl No.	Expt. No.	Cathode	Alkali	Solvent	Excess Power (%)	Tritium Level (Bq/ml)
1	NtPD–1	Solid Ni	K_2CO_3	25% D_2O	< 5%	88
2	NtPD–2	Por. Ni	K_2CO_3	H_2O	65%	NIL
3	NtPD–3	Solid Ni	Na_2CO_3	25% D_2O	72%	NIL
4	NtPD–4	Solid Ni	Li_2CO_3	H_2O	68%	NIL
5	TiB–1	Ti Button	Li_2CO_3	H_2O	10%	205
6	TiB–2	Ti Button	Li_2CO_3	H_2O	10%	124
7	TiF–1	Ti Foil	LiOD	D_2O	*	147
8	KSR–1	Por. Ni	K_2CO_3	H_2O	*	NIL
9	FP–1	Por. Ni	K_2CO_3	H_2O	*	310
10	OM–1	Por. Ni	K_2CO_3	25% D_2O	*	74
11	OM–3	Por. Ni	$^6Li_2CO_3$	H_2O	*	223

* Not measured

Table III. Variation of Tritium Level (Bq/ml) in Cells B3, B4 and B5 (Porous Ni Cathode).

Cell #	B3	B4	B5
Alkali	Li_2CO_3	Li_2CO_3	Li_2CO_3
Enrichment of Lithium	54%	7% (natural)	54%
Solvent	50% D_2O	50% D_2O	100% D_2O
12th day	28.8	28.6	61.6
16th day	64.1	30.6	79.2
(Reverse electrolysis done for 4 days)			
19th day	36.8	56.9	53.8
33rd day	513	69	193

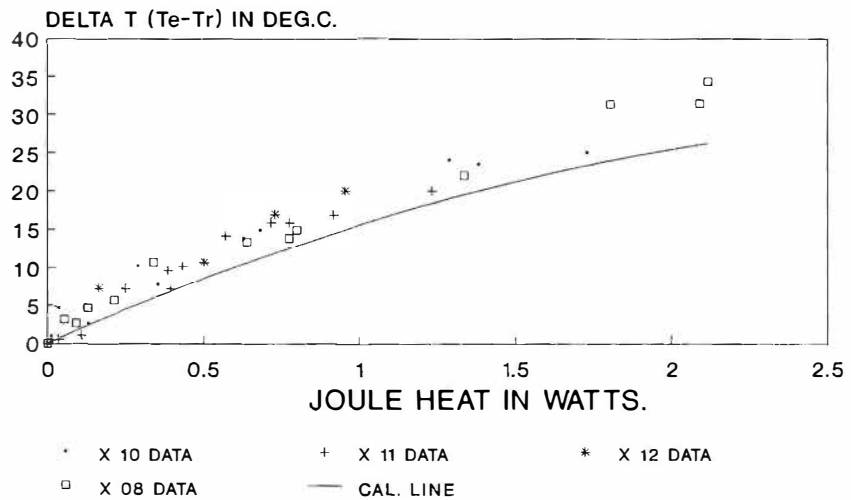

Figure 1. Expt. X 8/12: K_2CO_3 in H_2O; Solid Ni Cathode.
(March 16 to May 1, 1992)

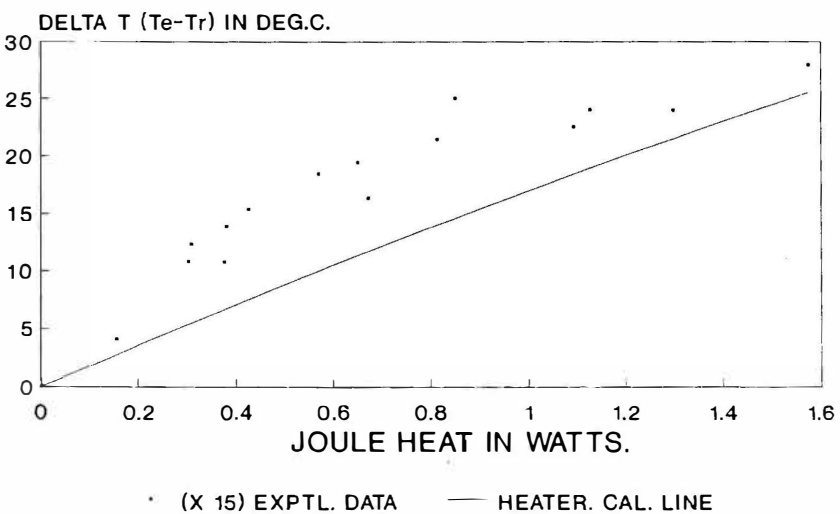

Figure 2. Expt. X 15: K_2CO_3 in 25%D_2O; Porous Ni Cathode.
(March 11 to March 21, 1992)

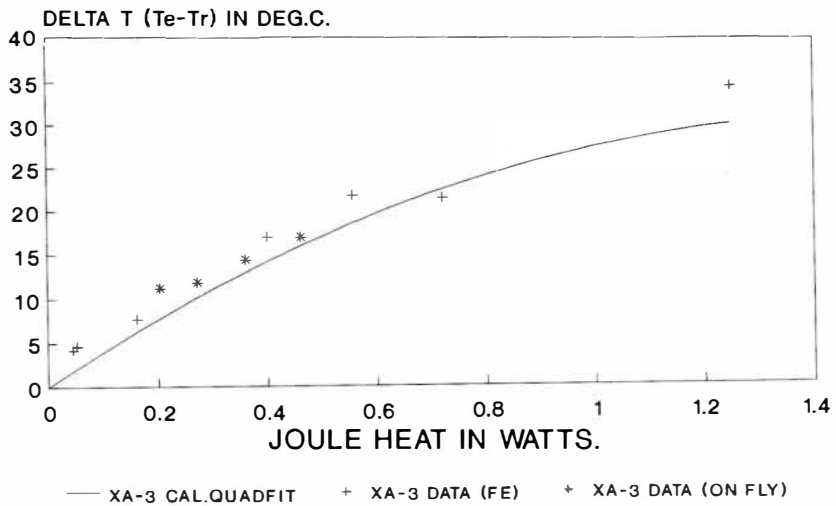

Figure 3. Expt. XA–3: K_2CO_3 in H_2O; Porous Ni Cathode. (September 11 to October 20, 1992)

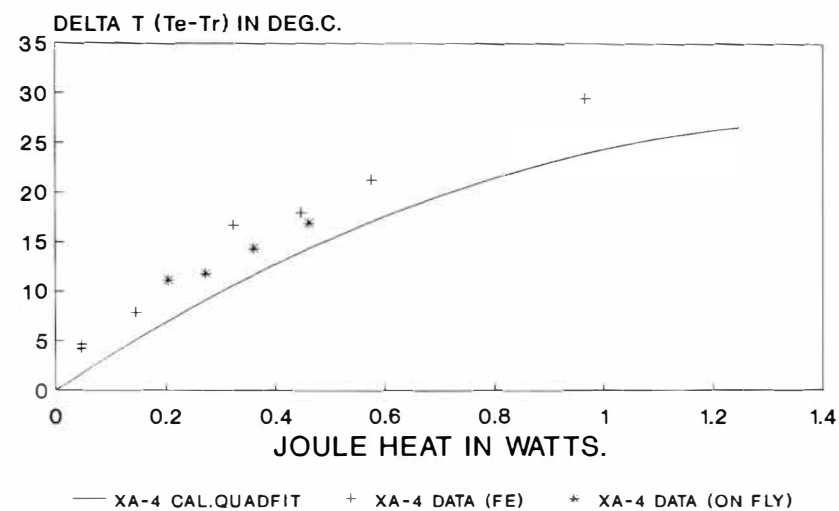

Figure 4. Expt. XA–4: Li_2CO_3 in H_2O; Porous Ni Cathode. (September 11 to October 20, 1992)

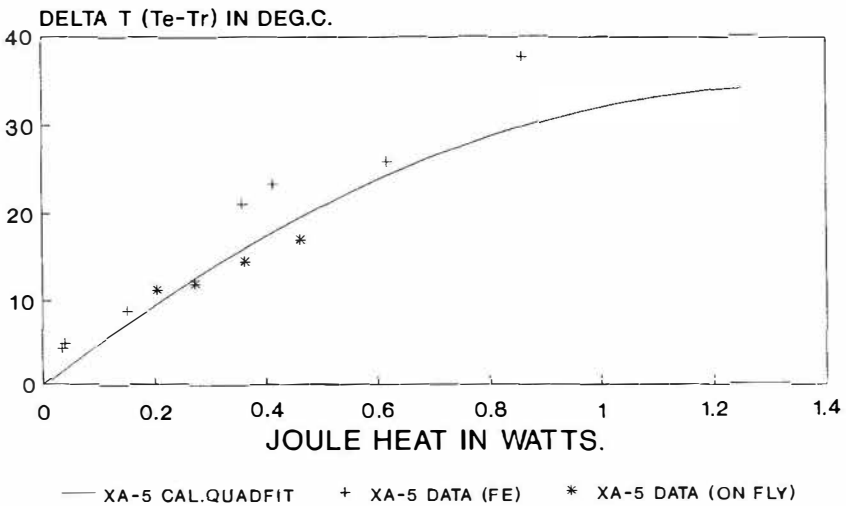

Figure 5. Expt. XA–5: Na_2CO_3 in H_2O; Porous Ni Cathode.
(September 11 to October 20, 1992)

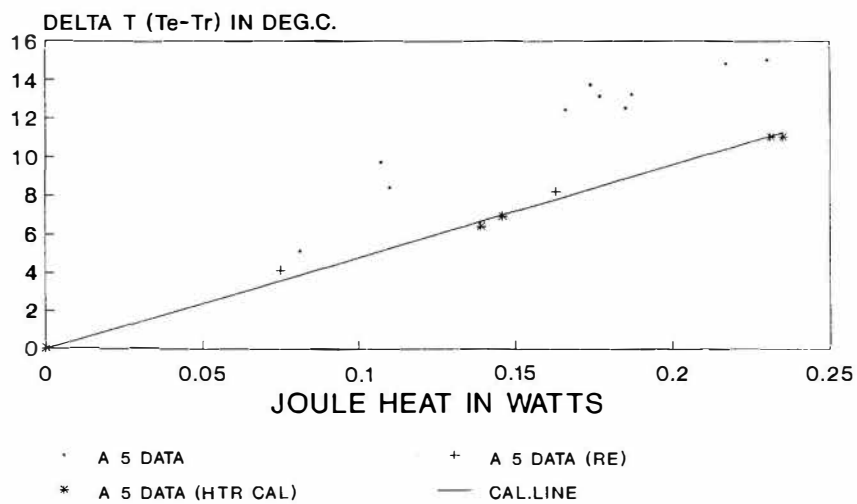

Figure 6. Expt. A 5: Enriched Li_2CO_3 in H_2O; Porous Ni Cathode.
(June 10 to June 29, 1992)

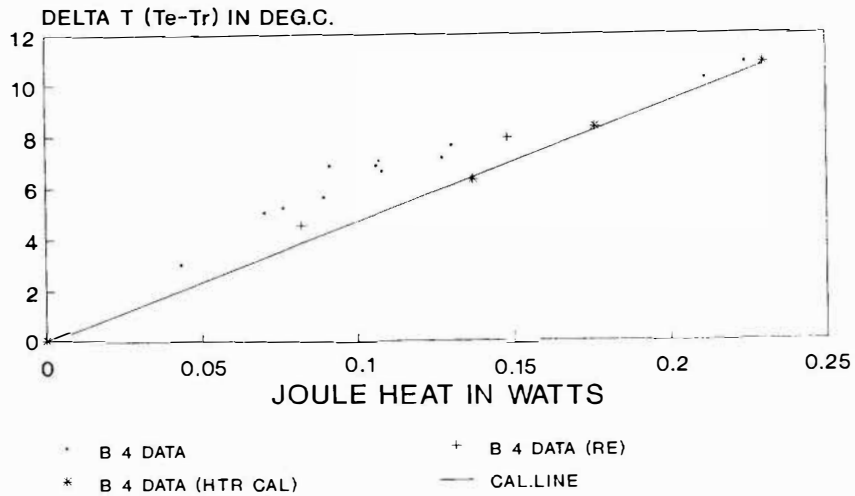

Figure 7. Expt. B 4: Li_2CO_3 in 50% D_2O; Porous Ni Cathode.
(July 24 to August 25, 1992)

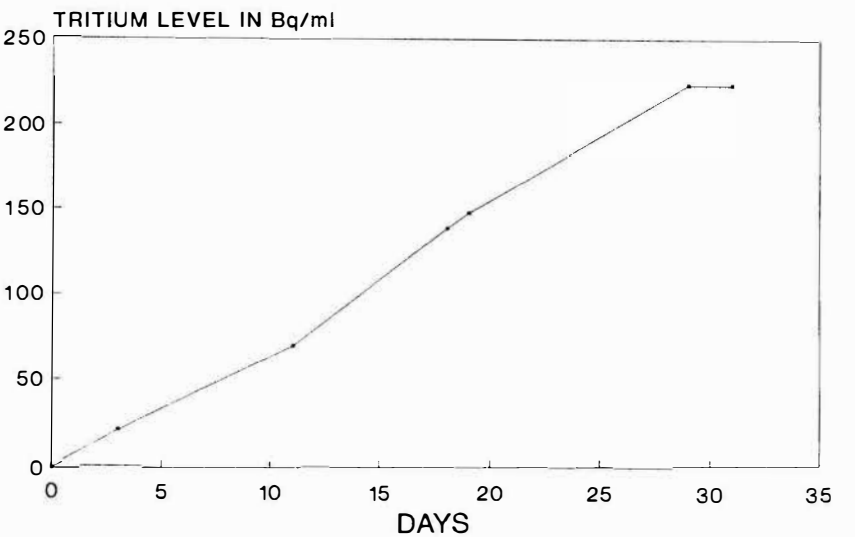

Figure 8. Expt. OM 3: Tritium Build–up.
(September 5 to October 6, 1992)

The January 2, 1992, Explosion in a Deuterium / Palladium Electrolytic System at SRI International

S.I. SMEDLEY, S. CROUCH-BAKER, M.C.H. McKUBRE
and F.L. TANZELLA
SRI International
333 Ravenswood Avenue
Menlo Park, CA 94025
USA

ABSTRACT

This paper reviews the accident that occurred at SRI International on January 2, 1992. A plausible explanation for the cause of the accident is proposed, and recommendations are made pertaining to the safety of future experiments. These recommendations relate to the design of electrolysis experiments, and to the behavior of recombination catalysts, and may provide useful guidelines for other workers in the field.

INTRODUCTION

On January 2, 1992, an electrochemical cell exploded during an experiment at SRI International in Menlo Park, California.[1] There was no major structural damage, fire, or release of toxic or radioactive materials, but one scientist, Dr. Andrew Riley, was killed when he was hit by a six-inch-long steel cylinder (a part of the cell container) which was propelled upward after the cell burst. Three other scientists were slightly injured by flying glass and other debris.

A diagram of the cell, which was placed inside a flow calorimeter, is shown in Figure 1. On January 1, it was noticed that gas was leaking from the tube which joined the cell to the pressure transducer; the tube was cut and a Swagelok union and endcap was fitted loosely using PTFE ferrules to the remainder of the gas tube.

FRONTIERS OF COLD FUSION

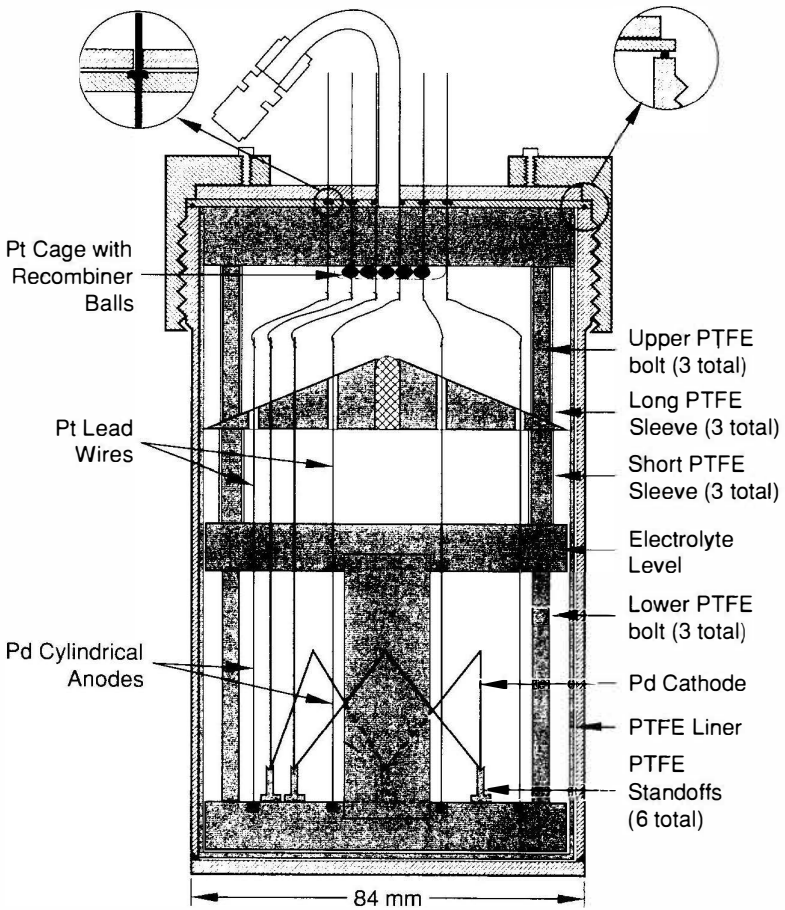

Figure 1. Cell before explosion (actual size).

The assembly was returned to the bath, subsequent to more complete repair the next day.

On January 2, another leak was observed. Dr. Riley first removed the clear acrylic top of the calorimeter and then lifted the calorimeter out of the water bath, set it on the edge of the bath, and was waiting for the water to drain back into the bath when the explosion occurred.

THE INVESTIGATION

Immediately after the accident, checks were made to determine whether nuclear products were associated with the event. Tests were performed on the dosimeters worn by the experimenters, wipes taken from the accident area, fluids from the area, and various internal components of the cell, for evidence of radiation. All showed radiation levels at background values. From these determinations, it was concluded that there was no measurable release of radiation at the time of the accident.

Metallurgical And Mechanical Examination

In order to assess the energy and pressure changes associated with the explosion, the deformation of the cell recovered from the accident was measured and modeled with SRI's proprietary computational codes.[2] The circumference of the cell was measured at several axial locations as shown in Figure 2. The maximum circumferential strain was 12.5% and was located in the top half of the cell, which, during use, contained mostly gas.

SRI's "L2D" code was used to model the effects of the explosion. This code was specially designed to calculate the effects of explosions on materials and structures. The stainless steel was modeled as an elastic-plastic material with work hardening, the PTFE components were generally modeled with zero strength, and the water and gas were modeled by appropriate equations of state.

Two types of scenarios were calculated with the L2D code. In the first type, thermal energy was taken to be deposited in the electrolyte over a short time, creating a high pressure steam bubble in the liquid. The results showed that the largest shell deformation was produced in the lower half of the cell, i.e., in that part of the cell containing the liquid. This

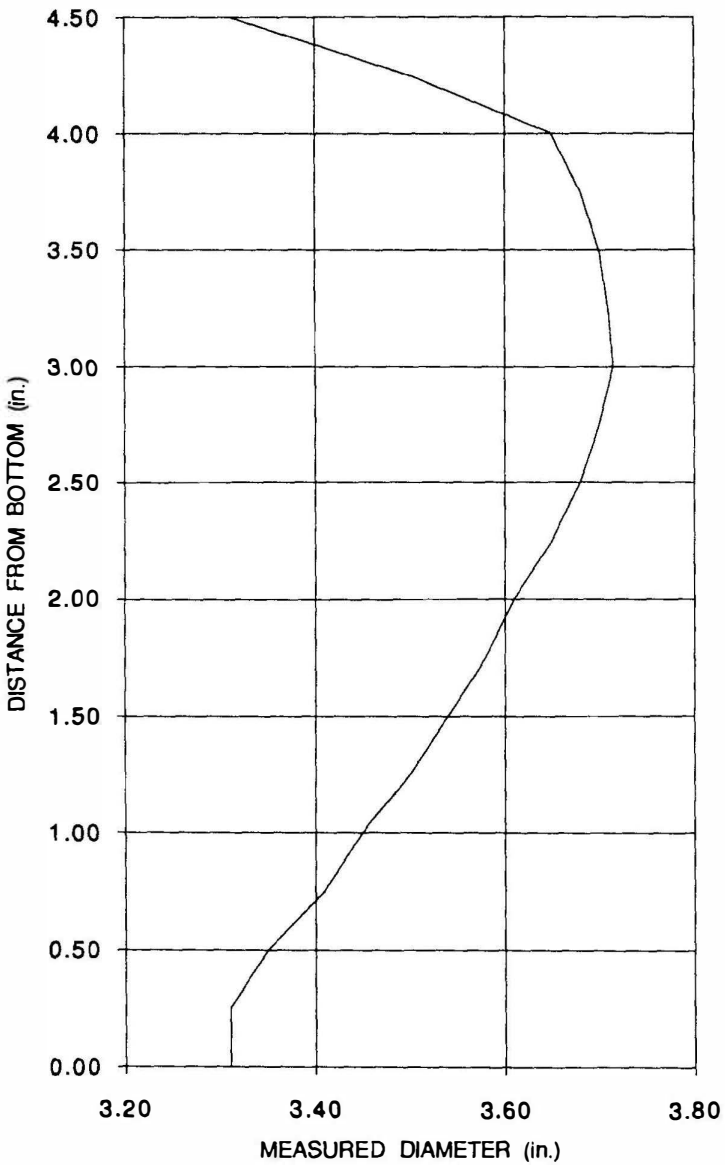

Figure 2. Measured deformation of cell diameter.

disagreement between the calculated location of the region of peak deformation and the actual observation on the cell, led us to conclude that a steam explosion did not substantially contribute to the accident.

In the second scenario, the case of a deuterium-oxygen explosion in the upper part of the cell was considered. In all calculations the initial pressure after detonation was taken to be 10 times the gas pressure before detonation or one half the Chapman-Jouget pressure. Comparison was made of the deformation calculated for a detonation initiated at the bottom (and at the top) of the gas volume and propagating at a velocity of 800 m/s, with that calculated for a constant volume (instantaneous) explosion. The calculated deformations for the two cases were identical. Therefore, all subsequent calculations were performed with constant volume explosions and with the equation of state of the polytropic gas.

A series of calculations were made for different initial gas pressures that produced different final deformations. The final deformation that most closely corresponds to the observed deformation is shown in Figure 3. The initial pressure in this calculation was approximately 300 atm, which corresponds to a pressure of approximately 30 atm before detonation. Comparison of Figures 2 and 3 shows that the calculated shape of the cell matches the observed shape reasonably well. In particular, the location and amplitude of the peak strain agree. For this case, the velocity imparted to the upper part of the cell which induced the fatality was calculated to be 25 m/s.

Table 1 shows the partitioning of the energy during the explosion. The format of this table is such that the shaded terms in each section are partitioned into the components shown in the next lower section of the table.

Conditions in the Cell at the Time of the Explosion

A comprehensive set of data was recorded for the cell over the entire 865 hr duration of the experiment (designated C1).[3] At 780 hr (event A in Figure 4), the pressure transducer recorded a rapid transient down to nominally 1 atm. The calorimeter net output power curve at 780 hr (event A in Figure 5) moved in the endothermic direction by about the correct power (0.16 W) for loss of the heat of recombination as a result of the loss of gas. This event is likely to be a transient leak of unknown origin.

Table 1. Energy partitioning (in J).

BEFORE EXPANSION	Total Internal Energy in gas		39700
PARTITIONING OF TOTAL INTERNAL ENERGY AFTER EXPANSION	PV work done on cell		3700
	Internal Energy of gas at time of venting		36000
PARTITIONING OF PV WORK DONE ON CELL	Strain Energy Absorbed		
	Shell	1620	
	Cover	110	
	Other	240	1970
	Energy to shear weld		100
	Kinetic Energy of cell		
	Top	760	
	Bottom	750	
	Cooling fins & water	140	
	Other	20	1670
			3740
	Energy absorbed by head impact		300–700
	Energy to reach ceiling		50
PARTITIONING OF KINETIC ENERGY OF TOP OF CELL	Energy to deform top of cell		10
	Energy to deform concrete		10
	Total		370–770

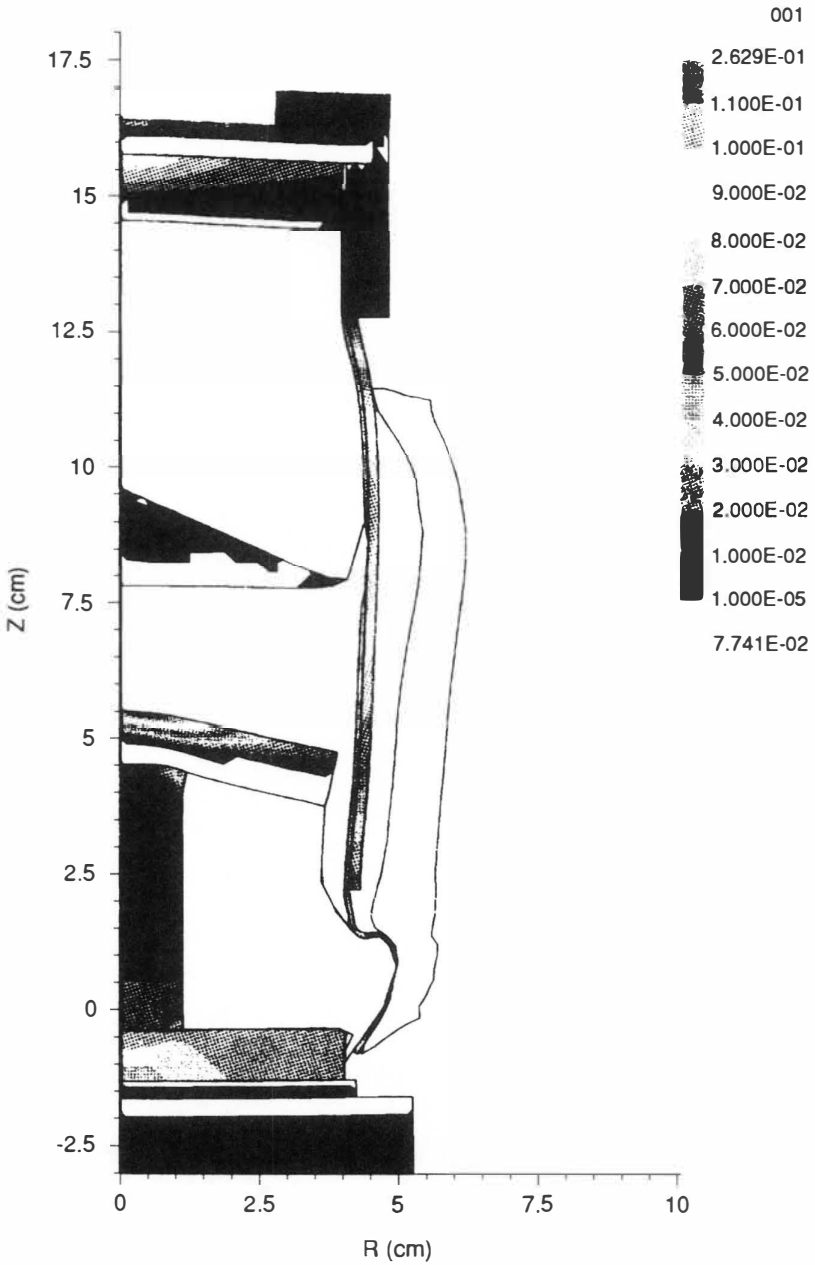

Figure 3. Computed deformed shape and contour plots of permanent strain from explosion of deuterium-oxygen at 30 bars.

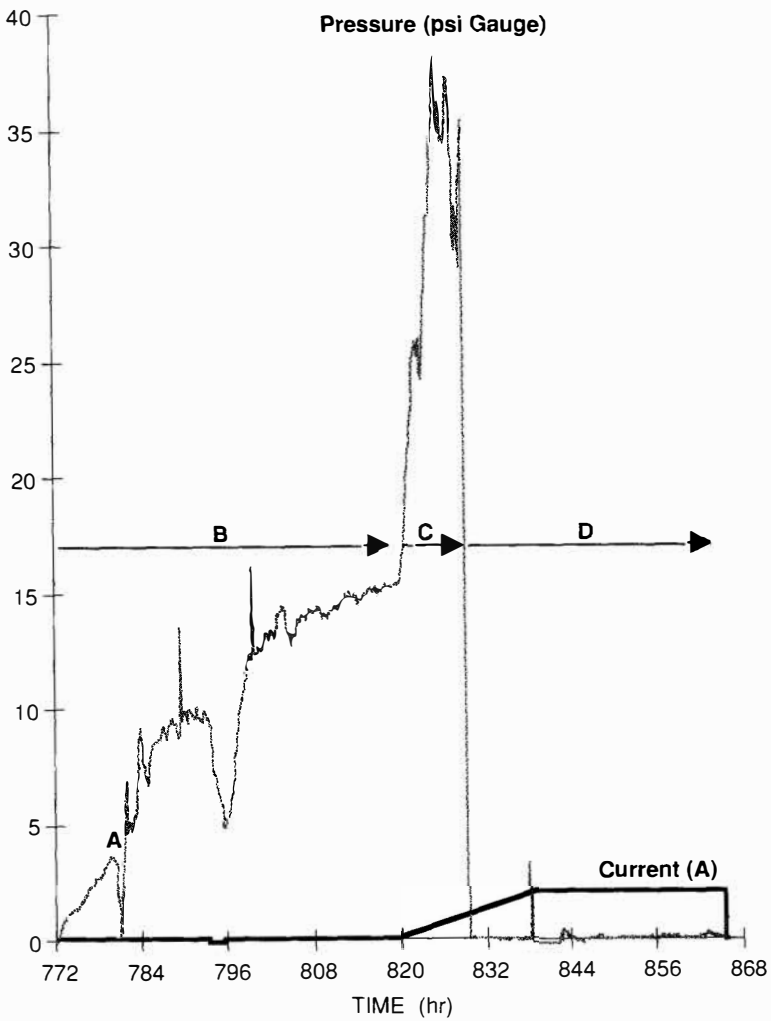

Figure 4. Current and gauge pressure at times following current step down.

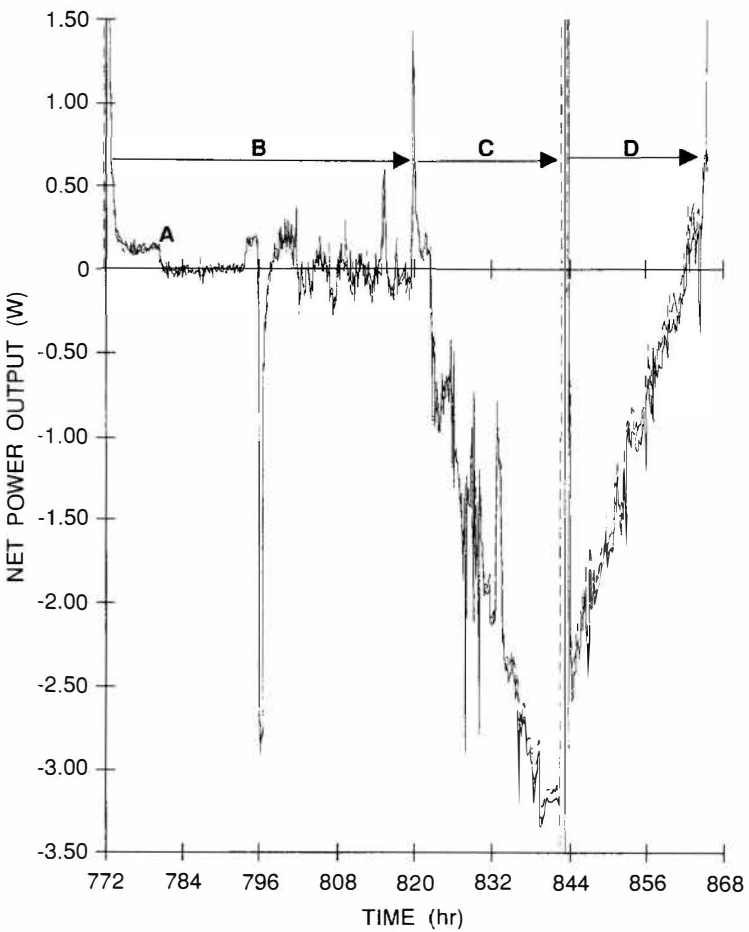

Figure 5. Excess power (W).

The pressure recovered at rates consistent with the electrolysis rate, but the power curve did not recover, suggesting that the catalyst cooled during the pressure transient and never recovered its initial activity. The pressure after 772 hr, until the obvious development of a major leak in the transducer/gas inlet tubing at 829 hr, increases, indicating that the activity of the recombination catalyst remained low. The net power record shows increasingly endothermic heating rates from 820 to 844 hr (event C in Figure 5), consistent with loss of recombination and the evolution of about 0.5 liters of stoichiometric gas.

The net power record following repair of the gas leak at 844 hr (event D in Figure 5), is hard to understand. The gradual, increasingly exothermic, progression of the net power suggests that, for this period, recombination was occurring in direct proportion to the pressure. Assuming that all leaks were effectively plugged, the rate of pressure increase inside the cell would have continued at about 4 atm/hr upon repair at 844 hr, decreasing to 0 atm/hr at 862 hr. This would indicate that the cell was pressurized with about 30 atm of stoichiometric gas (deuterium/oxygen) on the morning of January 2.

Several observations remain unexplained by the above scenario. The slow, almost linear, increase in recombination rate over the final 20 hr operation at a current of 2.1 A is not representative of normal recombination catalyst behavior. Under very high pressures of stoichiometric gas, increases in catalyst temperature caused by the highly exothermic reaction lead inevitably to rapidly accelerating rates. The observed behavior is more consistent with phenomena expected if the reaction quickly becomes limited by mass transport, e.g., if the active surface area was very small, such as a Pt wire surface, or if the active regions were in thermal contact with the cell wall, e.g., flakes or fragments contacting the wall or oxides on the wall surfaces. Alternatively, if the pressure reached 30 atm, the dissolution of gas in the electrolyte could lead to sufficient flux of oxygen to the cathode (and conversely deuterium to the anode) where recombination might occur.

CONCLUSIONS

The computed shape of the deformed cell for energy releases in the electrolyte with a range of pressures and locations, show that deformation would be concentrated in the bottom of the cell, unlike the deformation observed in the accident. In contrast, the

computed shape for a 30 atm mixture of deuterium-oxygen that detonates in the gaseous portion of the cell agrees approximately with the observed deformation.

Observations and calculations of the physical evidence from the explosion are largely consistent with the hypothesis that, over a period of time, a stoichiometric mixture of deuterium and oxygen built up in the cell, to a pressure of approximately 30 atm, and a detonation was initiated in the gas causing an approximately stepped pressure rise to about 300 atm. The detonation may have been initiated by physical effects associated with removing the cell from the water bath.

This hypothesis is not immediately consistent with the following observations:

Mass balance considerations show that a leak from the cell of about 0.1 cm^3/s would ensure no net pressure rise in the interval 843-865 hr; the cell was observed at 864 hr, and later, to have a leak that appeared to be sourced from a volume not significantly above 1 atm, at a rate that has been estimated to be between about 0.1 and 0.3 cm^3/s.

For the electrolysis of water, the pressure coefficient of cell voltage is not less than about 45 mV/decade of pressure. The cell voltage immediately preceding the accident was smaller than it had been at 844 hr at which time the cell had apparently been opened to ambient pressure. This indicates that, if anything, the pressure had gone down before the accident and not up. However, note that for a cell reaction which involves the simultaneous oxidation of D_2 and reduction of D_2O deuterium, the pressure coefficient of voltage is lower.

For several hours before the accident, recombination had been occurring, apparently at a rate of approximately 3.5 W, and presumably near the pressure of the explosion, thought to be 30 atm. It is not obvious how such extensive recombination could occur for an extended period without rapidly consuming essentially all available reactant. It is not our experience that a recombiner can function partially and stably. The experimentally determined catalytic function for deuterium/oxygen recombination at 40°C of a catalyst sphere recovered from the explosion, was indistinguishable from that of unused catalyst; its catalytic function apparently was not impaired.

These facts can largely be accommodated by supplementing the hypothesis described above with the condition that the pressure in the cell at 844 hr, when

it was apparently open to the ambient, would have to have been in the range 10-30 atm.

The preexistence of an elevated pressure provides an inventory of gas to source the leak and still provide approximately 30 atm at 865 hr; substantially decreases the sensitivity of cell voltage as a monitor of cell pressure since such changes are determined mostly by $\ln(P/P^{o})$; and accommodates a more obvious recombiner function, since recombination can be assumed to occur by two competing mechanisms.

The issue of how and when the elevated pressure came into existence and why it was not observed, remains to be addressed. One plausible explanation is that the PTFE disk at the top of the cell was forced up against the top plate through which the electrical and pressure feedthroughs passed, acting as a seal that became increasingly effective as the internal pressure rose. Initial closure may have been accomplished after a rupture occurred in the pipe, thus providing a pressure gradient that would force the PTFE disk against the cell top.

Safety In Future Experimentation

As a result of our experience we currently base our experiment design philosophy on the following concepts:

(i) Passive metal recombiners should not be relied on to perform in any regular fashion, and must be presumed to operate at any time fully and stably, partially or intermittently.

(ii) All electrolysis cells should be placed in an explosion shielded environment that can withstand the effects of a hydrogen/oxygen explosion which results in a final pressure of at least ten times the maximum sustainable hydrostatic pressure of the cell; this includes protection from the blast and any fragmentation projectiles.

(iii) No cell shall be removed from the shielded environment until the cell has been shown to be at an internal pressure of 1 atm of an inert gas; in this respect, relying on a pressure gauge alone, is insufficient.

A cell design that meets the requirement in (ii) is shown in Figure 6.

REFERENCES

1. SRI Scientific Investigative Committee, 1992, The January 2, 1992, Explosion in a Deuterium/Palladium Electroytic System at SRI International.
2. Colton, J. and Jones, R., 1992, Metallurgical/Mechanical Aspects of Accident Investigation.
3. Crouch-Baker, S., McCarty, J., McKubre, M., Smedley, S., Tanzella, F., 1992, Chemical, Thermodynamic and Electrochemical Aspects of Accident Investigation.

Nuclear Products

Experiments with Global Detection of Cold Fusion Byproducts

Daniele GOZZI[‡], Pier Luigi CIGNINI[*], Riccarda CAPUTO[‡], Massimo TOMELLINI[#], Giovanni BALDUCCI[‡], Guido GIGLI[‡], Evaristo CISBANI[†°], Salvatore FRULLANI[†°], Franco GARIBALDI[†°], Mauro JODICE[†°] and Guido Maria URCIUOLI[†°]

ABSTRACT

On the line of the previous experiments carried out in a multicell electrochemical system, we will present the results obtained with an improved experimental apparatus recently assembled. In the present experimental configuration, we have a 60 ^{3}He tubes neutron counter from Jomar/Canberra (Los Alamos, NM) in which the ten cells system is located. In this way the efficiency of the neutron detection has been increased from 5×10^{-5} to 0.22. The sixty tubes are divided in twelve groups to localize which cell is generating neutrons owing to the counting of the twelve separated scalers. ^{4}He determination by mass-spectrometry is another feature recently added to our experiment.

Preliminary results confirm what we already obtained and presented at ACCF2 last year. They are essentially the production of excess heat up to 43% without any appreciable neutron and tritium excesses compared to the respective backgrounds. A carefull check of the neutron data, through the analysis and dating of the single pulse shape, is still in progress to identify if intense spikes observed in the R+A count are due to a real *in situ* nuclear phenomena or background or artifact effects.

[‡]Dipartimento di Chimica, Università La Sapienza, P.le Aldo Moro 5, 00185 Roma
[†]Laboratorio di Fisica, Istituto Superiore di Sanità, V.le Regina Margherita 299, 00161 Roma
[°]INFN sez.Sanità, V.le Regina Margherita 299, 00161 Roma
[*]CNR-Centro di Termodinamica Chimica alle Alte Temperature, c/o Dipartimento di Chimica, Università *La Sapienza*
[#]Dipartimento di Scienze e Tecnologie Chimiche, Università Tor Vergata, 00100 Roma

FRONTIERS OF COLD FUSION

1. Introduction

Since 1989 the activity on *cold fusion* is mostly oriented to understand the true nature of the observed phenomena: if they are due to artifacts and/or known chemical and physical effects or they belong to a category of new phenomena which open a very interesting window in the physics of the condensed matter.

The continuous improvement done on our experimental set-up is a clear evidence that our activity follows this guideline. In this framework, we moved and are still moving to design an experiment in which as many as possible independent variables can be measured *in situ* and at the same time in a multicell F&P-like experiments.

Aim of this contribution is to show our recent results obtained in an improved experimental set-up which has been modified expecially in the parts of neutron detection and treatment of electrolysis gases before sampling for ^4He mass-spectrometric determination.

2. Methods

We will limit to describe only the parts which were changed or added with respect to our previous experiments reported in literature[1-2].

The flow-chart characterizing each cell is reported in figure 1 below.

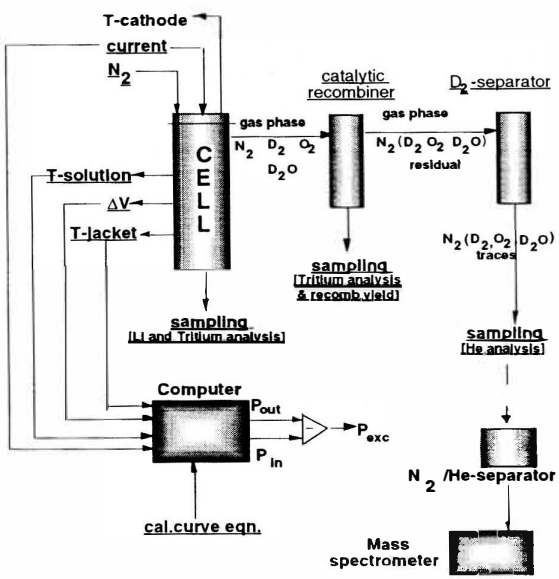

Figure 1. Flow-chart of one cell apparatus.

Electrochemical Cells

Heat excess is measured in a non-adiabatic calorimeter-electrochemical cell through the comparison with the thermal and electrochemical calibration curves obtained, using Au or Pt cathodes, in the same experimental conditions in which the experiment is then carried out. Cell geometry and carrier gas bubble stirring allow to

take into consideration only the thermal gradient on the plane orthogonal to the z-axis, so the calibration curve, obtained as a sequence of stationary states at constant input power values, P_{in}, is linear according to equation $\Delta T = P_{in}/k$. $\Delta T = T_s - T_j$ and T_j is the temperature of the thermostated water circulating in the torus-shaped bath. The heat excess is given by $P_{exc} = P_{out} - P_{in} = k\Delta T - P_{in}$ where ΔT is now the value measured in the experiment.

Features of such cells as calorimeters are:

- Materials- body: glass, cap: teflon
- Dimensions- inner ø 22 mm x 245 mm height
- Minimum heat detectable: 0.5 ÷ 1 W
- Maximum Input Power: 50 W
- Time constant: ≈ 350 s
- Continuously fluxed under N_2 (from LN_2) at controlled flow-rate

Features as electrochemical cells are:

- Electrolytic solution: 0.2 M LiOD(LiOH) in $D_2O(H_2O)$
- Anodes: Pt wire ø1mm shaped as cylindrical coil (10 mm inner ø x 20 mm height)
- Cathodes: pure Pd centered in the z-axis of anode. Mostly shaped as ø3mm rods subjected to different thermal and/or mechanical treatments according to the procedures indicated below:

A. Heated under $1x10^{-6}$ mbar at 1050 °C for 24 h and cooled at 0.5 °C/min
B. Screw dislocated by 3 rotations at room temperature
C. Screw dislocated by 3 rotations in LN_2
D. Screw dislocated (0.5 mm ø wires) by 11 rotations at room temperature
E. As received
F. Edge dislocated under 10^4 kg for 15 h at room temperature
G. Edge dislocated under 10^4 kg for 30 min in LN_2

Table 1 shows some characteristics of the cathodes used in the experiment here reported. Cells #1 and #8 were used as blanks; the first one had a Au cathode and in the second one the electolytic solution was LiOH in H_2O. Figure 2 shows, as typical, the calibration curves obtained both in thermal and electrochemical mode. As

Table 1. Characteristics of the cathodes

# Cell	Dimensions/mm ø x h	S.Area to Volume Ratio/cm^{-1}	Treatment& material
1	3 x 31	13.6	E&Au
3	3 x 28	13.7	AC&Pd
5	0.5 x 28*	8.1	D&Pd
7	3 x 30	13.7	EC&Pd
8	3 x 30	13.7	A&Pd
9	3 x 26**	10.0	F&Pd

*23 wires gold-soldered at one end to form a single cathode

**Starting dimensions of the road. After treatment F, dimensions were 6x1 (thick) x 26(height)

already discussed[2], in principle, both the calibration curves should be superimposed. Slight differences can be observed due to the different location in the cell of the heat sources (heater in the thermal mode, electrodes in the electrochemical one). Each cell indicated in Table 1 was calibrated in both the modes and in all the cases straight lines, $\Delta T_i=(a_i\pm\Delta a_i)+(b_i\pm\Delta b_i)P_{in}$, were obtained.

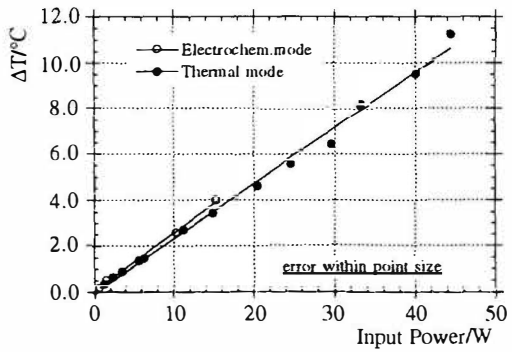

Figure 2. Typical calibration curves obtained in thermal and electrochemical mode

In Table 2, the averaged coeffients between the two modes were reported for each cell.

Table 2. Coefficients of the calibration curve equations

#Cell	$(a_i \pm \Delta a_i)$/°C	$(b_i \pm \Delta b_i)$/°CW^{-1}	R
1	0.05±0.06	0.128±0.004	0.9982
3	0.02±0.05	0.213±0.002	0.9996
5	-0.04±0.09	0.250±0.007	0.9977
7	-0.02±0.07	0.228±0.004	0.9977
8	0.08±0.02	0.297±0.001	0.9998
9	0.09±0.02	0.299±0.001	0.9999

^{4}He Detection Procedure by Mass-Spectrometry

In this section details are given for a procedure which is under development in order to detect ^{4}He in electrolysis gases. Present data refer to synthetic mixtures modelling the expected ones. The Mass Spectrometer used is a Nuclide Analysis Associates HT 7 (60°,12" radius) equipped with an electron impact ionization source and a sixteen stages Cu/Be electron multiplier. The Knudsen cell molecular source has been removed and replaced with a flange carrying an inlet system *via* a Balzers UDV 235 gas valve. The sample gas flows through the valve and a quarz tubing inserted into the ion source; the resulting flux is colinear to the ion path. The typical settings of the mass spectrometer main parameters are:

- electron ionization energy 100 eV
- electron emission current 1.0 mA
- ion accelerating potential 4510 V
- electron multiplier gain (mass 28) 2.0×10^5

For a given mass spectrometer, sensitivity is mainly affected by, on one hand, the partial pressure of ^{4}He realized in the ionization chamber and, on the other hand, the resolving power needed in order to discriminate between D_2 and ^{4}He peaks. A compromise must be reached. Indeed high partial pressures of ^{4}He admitted to the mass spectrometer imply, due to N_2 and D_2 in the carrying gas, an overall high pressure in the ionization chamber. As a consequence broadening of the mass peaks occurs. This requires an increase of the resolution to be used which, in turn, reduces the mass spectrometer sensitivity.

Neutron detector

A new high efficiency neutron detector has been used in the present experiment. It has been designed and manufactured, according to our specifications, by Jomar Systems Division of Canberra Industries Inc. Its design derives from detectors developed for the passive assay of plutonium in solid waste drums through non-destructive measurement system[3] in the advanced version used by H. Menlove also for cold-fusion experiments[4]. Complete description of the detector with its performances, experimental results and Monte Carlo simulations will be reported in a paper in preparation; here we summarize the main characteristics. The new neutron detector consists of 60 ^{3}He-proportional tubes of 41 cm active length, 2.54 cm diameter and 6 atm gas pressure. These tubes are embedded in a cylindrical polyethylene moderator. The detector is segmented in twelve independent counters consisting of five tubes each, arranged in inner and outer rings of six counters. The positions of the central tubes of each counter are stacked of half counter length between the inner and outer ring (see Fig. 3). The torus containing the ten electrochemical cells is surrounded by the detector and the localisation of the cell at the origin of the neutron emission can be obtained through the analysis of the pattern of the counts registered by the different twelve counters.

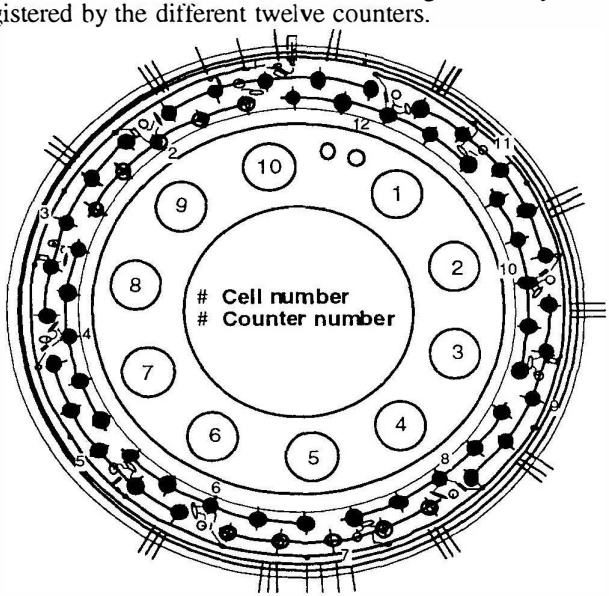

Figure 3. Neutron detector. Location of counters and cells.

If the emission is burst-like, the time correlated counts (with time correlation consistent with the die-away time of the detector) should affect contiguous numbered counters of the inner and outer rings facing the cell where the emission has occurred.

The efficiency of the detector measured with a source of Californium-252 placed in the different positions of the ten cells is 22%. The dependence of the efficiency on the cell position is limited to less than 1%. The counts are essentially distributed among three or four contiguous numbered counters shared between inner and outer rings. This distribution should allow the identification of the emitting cell if bursts of neutrons occur or if random generated emissions of neutrons happen at a

rate substantially higher than the background. In the present conditions of the experiment the background of the whole detector is about 1 count/s that means about 0.3 counts/s in a group of four contiguous numbered counters. The signals from eacl group of five tubes are processed by an AMPTEK A-111 hybrid charge-sensitive pre-amplifier/discriminator[5] that gives then, as output of the counter, both the digital and the linear OR of the five tubes. The scheme of the electronics used to derive and acquire the information from the detector is shown in Fig. 4. Digital output of each counter is sent to two scaler one of which is read and reset at fixed time interval and the other is read and reset only at the end of a run lasting several days.

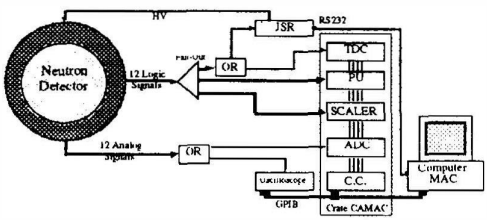

Figure 4. Simplified scheme of neutron detector electronics

In parallel it is sent to a Pattern Unit in order to detect all the counters hired within the time allowed by the acquisition cycle time (at present of the order of 1 ms) Moreover it is used to have a logical OR of all the twelve counters. The logical OR i: elaborated in order to measure with a TDC, for each neutron detected, the time interval between it and the following one. The logical OR is also sent to the Jomar JSR-12 Neutron Coincidence Analyzer[6]. The main purpose of the JSR-12 is to act a: a filter in order to enhance the capability of detecting time-correlated counts through its scaler R. In fact, each time a neutron is detected, a scaler T (Total) is incremented by a single count and two intervals of time are opened. the first one starting few μs after the detection and the second after about 1 ms. In the first gate both random neutrons and neutrons correlated with that one that has allowed the gate to be opene(are expected, while in the second gate only random neutrons are waited due to the large interval of time elapsed in respect to the die-away time of the detector. The counts in the first gate increment in non-linear way the R+A (Real + Accidentals) scaler of JSR-12; while those in the second one increment the A scaler. The two gate are opened for each neutron detected, then the increment of R+A is equal to the sum of the neutrons detected in each opened gate. When N neutrons are emitted in a very short time interval and all detected within the time interval of a single gate, the increment of the R+A scaler is equal to N(N-1)/2. The comparison of R+A and A scalers allows to estimate the number of correlated neutrons. The background value of this R+A scaler during the experiment was about 0.5/min, i.e., about a factor hundred less than the background value of total counter T. These counts are due essentially to cosmic rays spallation neutrons. The background value of the A scaler was a factor hundred less than the R+A value.

The twelve analogic signals from the twelve counters are amplified and then sent to a linear fan in-fan out from which two linear OR of these signals come out. The first one goes to a wave form digitizer, a digital oscilloscope, which permits to acquire the information on each pulse including the absolute time (given with a precision of ns) and the wave form; the second goes to an ADC that digitizes its integral and sends the value obtained directly to a histogramming memory. Scaler , pattern unit, TDC, ADC and histogramming memory are CAMAC modules and are

read through CAMAC BUS by a crate controller driven by a Macintosh II personal computer through a GPIB IEEE port that drives also the oscilloscope. The computer reads the pattern unit at each occurrence of CAMAC Look At Me (LAM) signal and reads the histogramming memory and the scalers each ten minutes. The (LAM) signal is emitted when the pattern unit has received at least one logic pulse from the detector. Besides, in order to minimize the time spent in readout, the computer does not read the oscilloscope until this has acquired a fixed number of pulses (block). This number is limited by the storing capability of the oscilloscope and depends on the choice of the number of points by which the pulse is digitized. Typical figures are: 100 points for each pulse and 1000 waveforms/block acquired before the computer reads the oscilloscope.

3. Results

Calorimetry

In order to give a synthetic view of the calorimetric data, we will use Table 3 to summarize the results obtained in all the cells and the related plots, assumed as typical, will be shown only for cell #5.

During the experiment, lasted more than 650 h, the current applied to the cells, which are connected in series, was changed both in step-fashion and modulated high-low according to a square-wave.

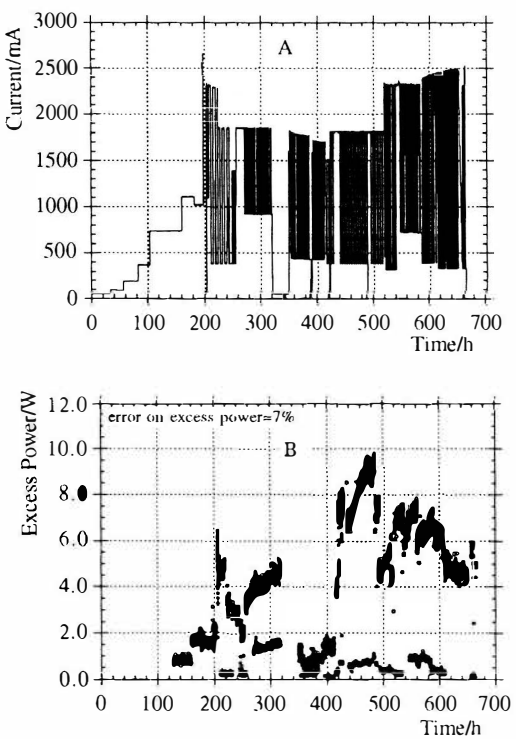

Figure 5. A. Profile of the current throughout the experiment. B. Excess power measured on cell #5.

Figure 5 shows the profile of the current applied to the cells and the measured excess power (cell #5) throughout the entire experiment.

The same excess power reported in fig. 5 is correlated with the input power in figure 6 below. In the same figure, the inset gives the ΔT trend with respect to the same power input range.

In Table 3 below, the integrated heat, Q, is calculated for 535 h where the heat production was at sufficient rate. The column, $(P_{exc}/P_{in})\%$, has to be intended as the maximum yield found and, in column P_{in}, the corresponding input power. For cells #1 and #8 any appreciable excess power was found.

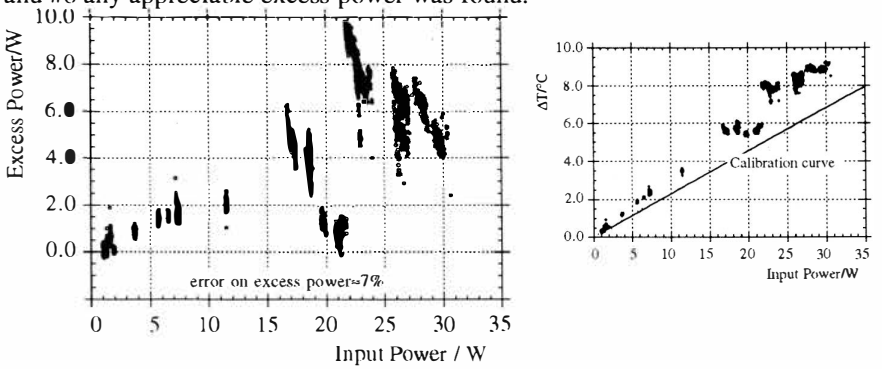

Figure 6. Excess power as a function of input power, P_{in}, at cell #5. In the inset, $\Delta T=T_S-T_j$ *vs* P_{in} compared with the calibration curve of cell #5.

Table 3. Summary of excess data found

#Cell	$(P_{exc}/P_{in})\%$	P_{in}/W	Q/MJ
1	-	-	-
3	32.2 ± 0.2	25	4.0
5	43.3 ± 0.4	22	6.0
7	42 ± 1	20	4.3
8	-	-	-
9	38 ± 1	21	3.1

$^4He/D_2$ separation tests

At present, the best sensitivity has been attained by valving off pumping in the ionization region; pressure in this region, during measurement, was $4x10^{-5}$ mbar . Typical resolution used, as from the half height measurement, is $M/\Delta M = 930$. Attempts are currently being made in order to increase the ratio between ^4He and the other gases admitted to the mass spectrometer by employing selective membranes. Recent data confirm that our procedure allows to eliminate D_2 from the electrolysis gas mixture at least in the limit of the mass spectrometer resolution. More details will be given in a paper in preparation.

Tritium measurements

As reported elsewhere[1,2], our procedure allows to determine tritium both in the solution and in recombined gases. Figure 7 shows both the trends throughout the

experiment. To compare with respect to electrolytic enrichment, data are plotted against the charged, $\int Idt$, passed through the cell at time t.

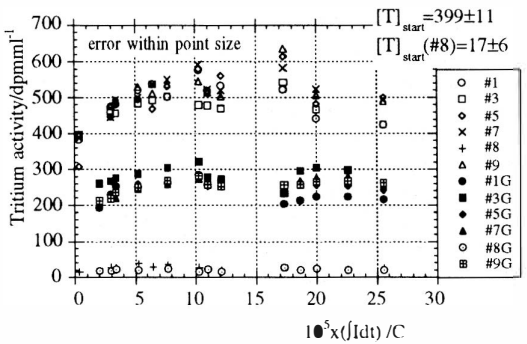

Figure 7. Tritium activity as measured throughout the experiment. Lower points correspond to the activity measured in recombined gases.

Neutron measurements

The analysis of all the information acquired during the experiment is still in progress. No evidence of neutron emission has been found in the analysis of the total counts integrated in 10 minutes time intervals. Even if our background level is very high, we can exclude the occurrence in the present experiment of events generating flux of thousands neutrons per second, seen in some previous experiment, lasting even few seconds.

The analysis of the correlated neutron events (R scaler) with the parallel analysis of the pulses wave form has shown the occurrence of several events whose pulse lasts for several hundreds of μs with overlapping of pulses and which give a big increment of the R scaler. The characterization of such anomalous events is still underway, aiming to check the digitized waveform of all the pulses acquired during all the ten minutes time intervals in which a value of R different from the background value has been found. Such analysis is extended also to characterize sporadic events occurred during the background acquisition with abnormal R scaler increment, in order to asses or reject a possible different nature between the events occurring when the electrolysis process is active from those occurring when the process is stopped.

4. Discussion

We briefly discuss the main aspects emerging from the above results. A more detailed discussion will be given elsewhere. Concerning the heat excess, we observe that we found, in a quite reproducible way with respect to our previous findings[2], a strict correlation of heat excess from the applied input power. As it appears from Fig. 6, the excess power is an increasing function of the input power. This behaviour is broken all the times the current is set to zero (see also Fig. 5). This seems to be in agreement with the hypotheses that *cold fusion* is feasible only if the D/Pd ratio is above a certain critical value and the loading of Pd by D is a process occurring under a gradient of electrochemical potential, as already pointed out in literature[7]. We can also observe that the maximum value of the excess power yield is located in the input power range from 20 to 25 W (see Table 3) and this is associated both to the

maximum excess power and a given current modulation, as reported for cell #5, in fig.5A,B. In fact, from the same figure, we can observe that excess power is particularly enhanced from the period of the current modulation instead of its amplitude. This is consistent with D diffusion time into Pd, $\approx x^2/d$ ($x=\phi/2$ in our samples, d=diffusion coefficient). Therefore, in the procedure adopted, we obtained that the maximum of excess power as well as the maximum ΔT did not correspond to the maximum value of the input power. This, if further confirmed, seems to be promising to develop the principles for practical applications of the *cold fusion.*

Concerning the production of nuclear particles, the present preliminary results seems to confirm both our previous results[2] and the general trend of *cold fusion* experiments in which the nuclear particles are not systematically observed as expected by the scheme of the plasma fusion reactions, if compared to the excess heat found. This is still the main question to which a satisfactory answer has not yet given. As shown in this Conference and in literature further experiments are still needed to confirm ^4He production associated to the excess heat. Our efforts are also oriented to give contributions accordingly.

Acknowledgments

The authors gratefully acknowledge the technical support of F. Giuliani, M. Gricia, M. Lucentini, L. Pierangeli and F. Santavenere of the Physics Laboratory of the Istituto Superiore di Sanità and INFN-Sanità and G. Gervasoni and S. Simonetti of the Department of Chemistry and CNR-Centro di Termodinamica Chimica alle Alte Temperature. The skill of M. Sabatini (Physics Laboratory of the Istituto Superiore di Sanità) in computer preparing drawings and materials for the poster presentation has been also of invaluable help.

References

1. Gozzi D. et al., 1992, J.Fusion Technology, 21, 60
2. Gozzi D. et al., Multicell Experiments for Searching Time-Related Events in Cold Fusion, Proc. 2nd Int. Conference on Cold Fusion, Villa Olmo, Como, June 29 - July 4, 1991, 1991, Conference Proceedings 33, 21, Società Italiana di Fisica, Bologna
3. Birkhoff G., Bondar L., Ley J., Berg R., Swennen R., Busca G., " On the Determination of the Pu-240 in Solid Waste Containers by Spontaneous Fission Neutron Measurements. Application to Reprocessing Plant Waste." Joint Nuclear Research Center Ispra Establishement, 1975, EUR 5158e; Bohnel K., "Die Plutoniumbestimmung in Kerbrennstoffen mit der Neutronen Koinzidenzmethode." Kernfoschungzentrum Karlsruhe, 1975, KfK 2203
   Krick M.S. and Menlove H.O., "The High-Level Neutron Coincidence Counter (HLNCC): User's Manual." Los Alamos Scientific Laboratory, 1979 LA-7779-M
4. Menlove H.O. and Miller M.C., 1990, Nucl.Instr. and Meth. A299, 10
5. Swansen J.E., 1985, Nucl.Instr.and Meth. B9, 80
6. Swansen J.E., Collinsworth P.R. and Krick M.S., 1980, Nucl.Instr.and Meth. , 176, 555; Menlove H.O. and Swansen J.E., Nucl.Techn. 71, 497
7. Tomellini M. and Gozzi D., 1990, J. Materials Science Lett., 9, 836

Possible Nuclear Reactions Mechanisms at Glow Discharge in Deuterium

A.B. KARABUT, Y.R. KUCHEROV, I.B. SAVVATIMOVA
Scientific Industrial Association "Luch"
Zhelesnodorozhnaya str.,24, Podolsk, Moscow region, Russian Federation 142100

ABSTRACT

Experimental results of impurity concentration measurements in palladium cathode by different methods before and after glow discharge in deuterium experiments are presented. Some very strange elements which we could not find in discharge environment can be seen. An attempt to understand this situation on the basis of fission and fusion in Pd-d system is presented.

1. Introduction

One of the main problems of the "cold nuclear fusion is the discrepancy between experimentally obtained ammount of heat and amount of nuclear products. Let us summarize some known experimental facts [1,2]:
1. Excessive heat is generated with output a few times larger than input.
2. Weak neutron signals with intensity $10\text{-}10^{7}s^{-1}$
3. Weak gamma-radiation with intensity $<10^{5}s^{-1}$
4. Characteristic X-rays with intensity $<10^{9}s^{-1}$.
5. Tritium formation.
6. Helium isotopes, mostly ^{4}He with intensity$<10^{8}s^{-1}$.
7. Charged particles have high energy, up to 10MeV and more.

As we noted in [2], to explain excessive heat we must assume that either charged particles have small energy (E<1MeV), or they are heavy (heavier than ^{4}He). This situation cannot be explained in terms of "hot" or "micro hot" fusion, because in this case cross-sections

of nuclear reactions are well known and branching of nuclear reactions - neutrons to tritium and 14 MeV neutron group to 2.45 MeV group does not correspond to thermal d-d reaction.

An interesting data appears with material science results. Earlier we considered only helium and tritium aspects of cold fusion, though we could see anomalies with other impurities for some time.

2. Initial material

We used pure 99.99 grade palladium as a cathode material. the bulk impurities content was defined by spark mass-spectrometry for all the elements of the Periodic Table. The analyses were made in the mass-spectrometry laboratory of GIREDMET analytical center. The method resolution was 10^{-8} atomic %, with standard deviation 0.15-0.30 for different elements.

3. The investigation of cathode material composition

For cathode material element and isotopic composition investigation X-ray microprobe (SEM "Hitachi S-800" with Link Analytical "LZ-5" detector) was used (A.D. Senchukov's group, SIA "Luch"), and secondary ion mass-spectrometry (SIMS) in I.P. Chernov's group (Tomsk polytechnical institute) and in A.G. Lototski's group (GIREDMET). Impurities in discharge environment (Mo, SiO_2, Al_2O_3) which could be transported to the cathode in the discharge were also investigated.

As a result such elements as Na; Mg; Al; Si; S; Ca; Ti; Cr; Fe; Ni; Zn; Ge; Br; Sr; Mo can be seen in the Pd after glow discharge experiments, sometimes up to 0.1% in the upper 1 micron layer of the cathode. Especially large is the contents of Na; Mg; Br; Zn; S; Mo; Si. The last two elements can appear due to sputtering. The appearance of other elements we can't explain. Wholly unexpected is the presence of germanium. The distribution of the impurities over the cathode surface was measured by the microprobe. The comparison of the distribution with SEM photos shows that most of the impurities are localized along the palladium crystalline boundaries. We must note that this method resolution is about 10^{-2}% and it doesn't show any impurities in the initial material. On an adjacent to palladium Mo-cap only silicon can be seen.

The data on isotopic composition obtained in a different groups varies and we'll discuss it in our next paper.

4. Discussion .

Let us look at a possible nuclear reactions which can lead to heavy charged particles (A>4) formation. We can extract reactions that don't contradict known data. Reactions can be written as follows:

$$A_1 + A_2 + A_3 + \ldots + A_n \rightarrow B_1 + B_2 + \ldots + B_n \quad (1)$$

in the left side are the reacting particles and reaction products are in the right side. As sharp peaks can be seen on charged particles spectrum, the pulse of reaction products must be fixed and there are no more than two reaction products in each act. It means that (1) can be written as:

$$A_1 + A_2 + \ldots + A_n \rightarrow B_1 + B_2 \quad (2)$$

For the discharge in deuterium with palladium cathode left side can look like: d+d; d+d+d; nd; Pd; d+Pd; 2d+Pd; 3d+Pd ets. Variant d+d in form of d(d,^{3}He)n and d(d,t)p, judging from neutron and c.p. spectra is not the main reaction.

For nuclear reaction to take place conservation laws must take place : energy, pulse, charge, barion charge,spin,isotopic spin,eveness. The deviation from these laws usually asks for too much energy and in case of "cold" reaction can be put aside. If we put aside Coulomb barrier problem, which is the main problem at "cold fusion", it appears that there is a rather limited number of nuclear reaction for which conservation laws are fulfilled. The amount of possible reactions goes down dramatically it we assume that only stable isotopes are formed. This statement must be true because palladium sample's radioactivity is very weak after the experiment. Than the list of a possible reactions will look like:

$$^{46}Pd \rightarrow (^{36}Kr + ^{10}Ne);\ (^{35}Br + ^{11}Na);\ (^{34}Se + ^{12}Mg);\ (^{32}Ge + ^{14}Si);\ (^{30}Zn + ^{16}S);\ (^{28}Ni + ^{18}Ar);\ (^{26}Fe + ^{20}Ca);\ (^{24}Cr + ^{22}Ti). \quad (3)$$

$^{46}Pd + {}_1d$ - all forbidden. (4)

$$^{46}Pd + 2^2d \rightarrow (^{87}Sr + ^{22}Ne);\ (^{73}Ge + ^{36}S). \quad (5)$$

$$^{46}Pd + 3^2d \rightarrow (^{95,97}Mo + ^{19}F);\ (^{98\text{-}104}Ru + ^{10}B). \quad (6)$$

$$\rightarrow (^{46}Pd + ^{6}Li). \quad (7)$$

It should be noted that the only allowed "catalytic" reaction is with ^{6}Li formation. From this point of view the following elements can be expected in palladium: ^{6}Li; ^{10}B; F; Ne; Na; Mg; Si; S; Ar; Ca; Ti; Cr; Fe; Ni; Zn; Ge; Se; Br; Sr; Mo; Ru.

The order of the energy in these reactions ~1MeV for group (3) - fission, ~20MeV for group (5) and ~30-40MeV for groups (6) and (7) - "fusion-fission". For excessive heat release in our experiments (~10kJ) this corresponds to ~10^{16} reactions in one experiment for the sample with the volume 10^{-3} cm^3, or 10^{-4}-10^{-3} at.%, which is higher than resolution threshold for the most analytical methodes. If the reaction takes place in a thin layer this only increases the local impurities concentration. If this layer is about 1 micron thick, reaction product concentration can reach ~0.1%.

5. Conclusion

In assumption that mechanisms allowing to overcome nuclear barriers exist, fusion and fission reactions for which conservation laws are fulfilled are taken into account. The analyses of the impurities, appeared in pure palladium after glow discharge experiments, give suspicious correlation with predicted elements. The given results are still difficult to call final, but if they will be confirmed on the basis of larger statistics they will ask for a new approach to the problem. The unique role of the deuterium will be questioned because the same think can be constructed for other gases and metals. It'll also initiate the search for long-living resonances of nuclear shell of Pd, exited by inelastic scattering of discharge ions (of the type of the laser effect).

6 References

1. Storms, E., Review of experimental observations about the cold fusion effect., 1991, Fusion Technology, 20, 433.
2. Karabut, A., Kucherov, Ya., Savvatimova, I., Nuclear product ratio for glow discharge in deuterium., 1992, Physycs Letters A, 170, 265.

Experimental Studies on the Anomalous Phenomenon in Pd Metal Loaded with Deuterium

Wang Dalun, Chen Suhe, Fan Daxiao, Chen Wenjiang, Li Yijun
Fu Yibei and Zhang Xinwei
Southwest Institute of Nuclear Physics and Chemistry
P. O. BOX 525-74, Chengdu 610003 P. R. China

ABSTRACT

The anomalous phenomenon in metal loaded with deuterium has been studied, using the electrolysis and the cycle method of temperature and pressure (CMPT). In the report, the experimental results are introduced, including the explosion occurred, and nuetron and tritium measured in electrolysis experiment. The sensitization phenomenon of X- ray film was found in CMTP experiment. It is considered that the reason of sensitization is derived from the chemical reaction and the anomalous effect in metal loaded with deuterium.

1. INTRODUCTION

Since M. Fleischmann, S. Pona[1] and S. E. Jones[2] published the experimental results on cold fusion in march, 1989, we have studied the phenomenon of cold fusion. In electrolysis experiment of April 21, 1989, we had measured neutron by the fission chamber, and tritium by the dual-channel liquid scintillation counter[3]. Since 1991 the phenomenon of cold fusion has been studied by electrolysis and CMTP[4]. The experimental results are briefly expressed below.

2. ELECTROLYSIS EXPERIMENT

2.1 Measurement of D/Pd

A Pd tube, $\Phi 1.67 \times \Phi 1.07 \times 80$(mm), was used to electrolyze heavy water, 99.5% in purity, with 0.1mol ^{6}LiD. The Pd tube is treated, including excluding oxygen and air, cleaning, anneal and activation. Variation of D/Pd with electrolytic time was determined by weighing. The experimental result of the variation is shown in Fig. 1.

2.2 Explosion Phenomenon in Electrolysis

Two sets of electrolytic cell exploded one after another in

FRONTIERS OF COLD FUSION

electrolysis experiment at end of April, 1991. The explosion may be derived from sudden release of a large amount of heat which was in a micro-zone of PdDx.

2.3 Measurement of Neutron

The Pd rod, $\Phi 5 \times 30$ (mm), was put into heavy water with 0.1mol ^{6}LiD to absorb deuterium by electrolysis. The electrolytic current was from 20mA/cm^2 to 100mA/cm^2. The temperature of cooling water was from 10 °C to 40°C. After 24 hours, the current rose to 100mA/cm^2, and the temperature of electrolyte was higher than 30°C. At this time counts of neutron were measured. The neutron detectors were two sets of parallel BF_3 counters as shown in Fig. 2.

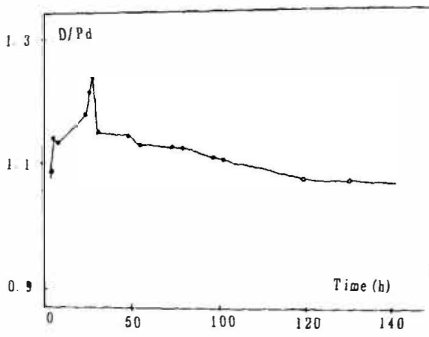

Fig 1. Variation of D/Pd with electrolytic time

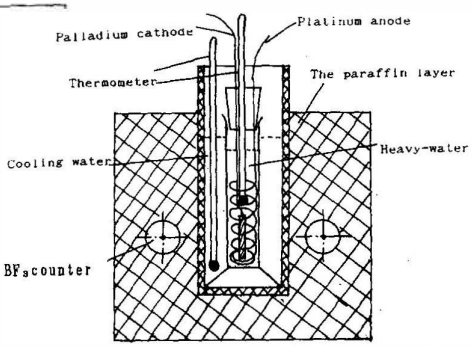

Fig. 2. Set-up of an electrolytic cell and neutron detectors

An Am-Be neutron source was used to calibrate BF_3 counters which efficiency was about 0.7%. The neutrons in cold fusion were detected by BF_3counters. A multichannel analyzer was used to record counts of neutron. The pulse height spectra recorded are shown in Fig. 3.

Fig. 3. indicates that there are differences between characteristic spectra of $^{10}B(n, \alpha)^{7}Li$ reaction produced by neutrons from Am-Be neutron source and cold fusion reaction.

(1) There are indistinct two peaks in the characteristic spectrum of Am-Be source neutrons. The two peaks may be due to overlap of pulses which are produced by charged particles of $^{10}B(n, \alpha)^{6}Li$ reaction and γ-ray of Am-Be source.

(2) The plane and long trail is in the rear of characteristic spectrum of neutrons from cold fusion. The trail may be produced by burst neutrons. It indicates that neutrons from cold fusion reaction may be burst ones and repeatedly emitted. In the experiment, a scaler was used to record neutron count and to measure variation of neutron count with time as shown in Fig. 4.

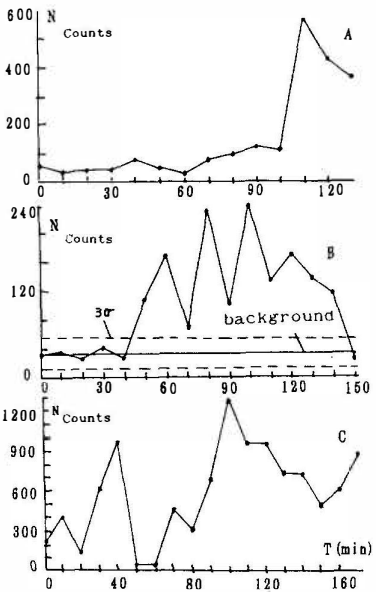

Fig. 4. Variation of neutron count with time

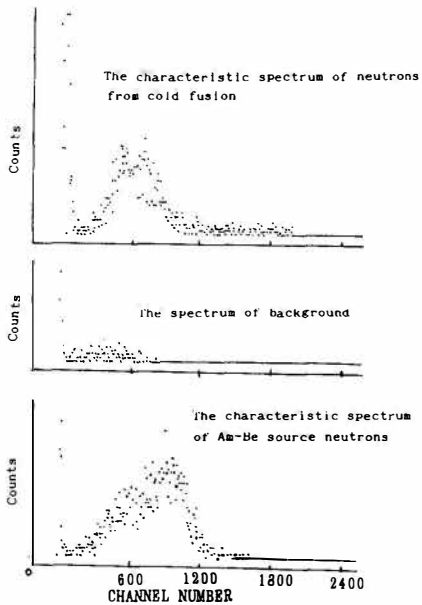

Fig. 3. The pulse height spectra of $^{10}B(n, \alpha)^{7}Li$ reaction

2.4 Measurement of Tritium

The results of measurement are listed in table 1.

Table 1. βactivity of tritium

No. of cell	cathode material			βcounts (n/min)
	size (mm)	purity (%)	weight (g)	
1	Φ5 Pd rod	99.95	7.0800	125±6
2	Φ5 Pd rod	99.95	7.0286	147±7
3	Φ3×0.5 Pd tube	钯银合金	2.8812	145±7
counts of background (n/min)				103±5

3. EXPERIMENT BY THE CYCLE OF TEMPERATURE AND PRESSURE

3.1 Experimental Conditions

a) Sample

Three kinds of metal slices were used to perform the experiment: (1) Pd slice 0.5mm in thickness; (2) Ti slice 0.1mm in thickness; (3) Pd slice of which Ti 0.5μm in thickness was evaporated on two surfaces.

b) Process of Experiment

Metal slices having been treated were sealed into copper vessel which vacuum was $10^{[-4]}$ torr to $5x10^{[-6]}$ torr. The vessel was put into liquid nitrogen ($LN_{[2]}$) and filled with deuteriulm gas of 10atm in order to perform the cycle of temperature and pressure. After the cycle, to reach vacuum in the vessel deuterium gas was exhausted. The samples were preserved in vacuum more than 48 hours.

3.2 Measurement

By the cycle of temperature and pressure, the sensitization results of X-ray films are stated as follows:

Films were sensitized in full area. But there was a image of Pd slice in full background of sensitized films which were in contact with Pd slice as shown in Fig. 5.

The experimental result indicates that there is a image of Pd tube on films as shown in Fig. 6.

Fig. 5. An image of Pd slice

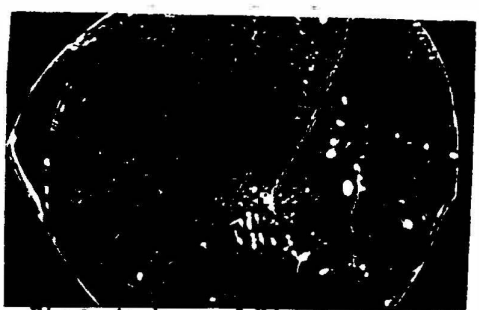

Fig. 6. An image of Pd tube

Several experiments with and without Pd slice and tube have been done. Two reasons of sensitization on films are found. One is that the reaction of deuterium with Br in a film produced DBr and Ag ion was displaced out. Another one is that an anomalous effect in Pd metal loaded with deuterium sensitize films, further studies will be carried out.

REFERENCES

1. M. Fleischmann and S. Pons, J. Electroanal. Chem. 261, (1989) 301
2. S. E. Jones et al, Nature 338 (1989) P737
3. 王大伦等. 低温核聚变(湿法)研究的阶段报告, 1990年5月冷聚变学术交流与对策研讨会 北京。(in Chinese)
4. A. De Ninno et al Europhys lett. 9 (1989) 221

Energy of the Neutrons Emitted in Heavy Water Electrolysis

Mutsuhiro NAKADA*, Takehiro KUSUNOKI, and Makoto OKAMOTO
Tokyo Institute of Technology, Reserch Laboratory for Nuclear Reactors
2-12-1, O-okayama, Meguro-ku, Tokyo 152
JAPAN

ABSTRACT

The Low/High pulse mode electrolysis has been introduced to carry out the experimental study to clarify the dependency of the L/H pulse modes operation of electrolysis on the neutron emission from the Pd cathodes. Among 6 runs of the electrolysis of L/H pulse mode operations, 3 of them gave appreciable neutron emission. The neutron energy spectra were found to have the two compornents (2.45 MeV peak and a broad band in higher energy region). The intensity of the 2.45 MeV neutron is smaller than that of the higher energy.

1. Introduction

To elucidate the mechanism of the neutron emission in the heavy water electrolysis, we have carried out a series of experiments for 3 years [2,3]. In the series, the constant current electrolysis of the heavy water was employed with different shapes of Pd cathode. In some cases, the anomalous neutron bursts were observed. But the reproducibility has been found to be very poor.

In the present study, the Low/High pulse mode electrolysis reported by Takahashi has been employed [4]. He reported that the L/H pulse mode elestrolysis gave the weak neutron emissions with a high reproducibility and the energy of neutrons consists of a 2.45MeV neutron component and a higher energy component. This pulse mode electrolysis has been introduced to carry out the experimental study to clarify the dependency of the neutron emission from the Pd cathodes on the L/H mode operation of electrolysis. The L/H pulse mode employed in the present work was modified from Takahashi's mode in the pulse repetition period and in the current density, and different shape of the Pd cathode was also employed.

* Present address : HOKURIKU Electric Power Co. Ltd

FRONTIERS OF COLD FUSION

2. Experimental

The electrolysis cell is shown in Fig. 1-a. The cell was made of quartz, and its capacity is about 170 cm^3.

Pd cathodes were preloaded with D_2 gas before use. After annealing of the Pd sheet, D_2 gas absorption was carried out repeatedly. After this process, the Pd sheet was placed into the cell and the electrolysis was initiated. In the present experiments, D/Pd ratios were estimated in two methods, one is mass difference method and another is pressure difference method between before absorption D_2 gas and after. The electrolyses were mainly operated with the rectangular pulse mode with rather short repetition period of one hour.

The arrangement of the cell, neutron detectors, and the shielding materials are shown in Fig. 1-b. Enclosing the test cell, three neutron detection systems are employed. One is composed of six ^{3}He counters, the second is three ^{3}He counters, and the last is the NE213 liquid scintillation counter (5x5 inches) to measure recoil-proton enrgy spectrum for the fast neutron events with a multichannel analyzer. The background neutrons were slowed down and captured in the solution of borric acid and in a polyethylene shield with cadmium sheets.

An example of the raw data obtained from the three neutron counting systems is shown in Fig. 2. The upper chart shows the signals from the two ^{3}He counter systems and the lower chart is for the neutron energy spectrum from the NE213 counter. The relation between the neutron energy and the channel number of the multichannel analyzer has been calibrated by use of O5S code [1].

The signal intensities from the two ^{3}He counter systems are so small, as shown in Fig. 2, to identify the occurence of the neutron emission. In the spectrrum obtained from NE213 spectrometer shown in the lower part, a small but appreciable

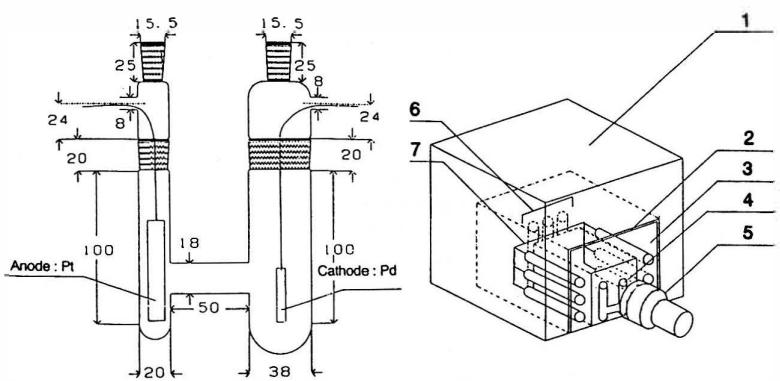

Figure 1. (a)Electrolysis cell.
(b)Arrangement of cell, neutron detectors, and shielding materials.
1. Solution of borric acid. 2. Cadmium sheet. 3. Polyethylene shield. 4. Cell. 5. NE213 detector. 6. ^{3}He counter(channel 1) 7. ^{3}He counter(channel 2)

edge of the recoiled protons was found at around 2.45 MeV. This edge has not been detected in the background run. The data obtained from NE213 spectrometer were analyzed statistically to evaluate the neutron emission throughout the present study. Even so, the signals obtained by the NE213 detector were so weak to evaluate the neutron energy directly from the spectrum as shown in the figure. The same statistical analysis method reported by Takahashi [5] is employed to evalutate the neutron energy spectrum from the present data. In this analysis, the foreground /background ratios were calculated in each 29 bins for 1024 channels of the PHA. The background data were obtained from the light water electrolysis. When the ratio is over unity, it is concluded that the neutron emissions were detected by the NE213 detector.

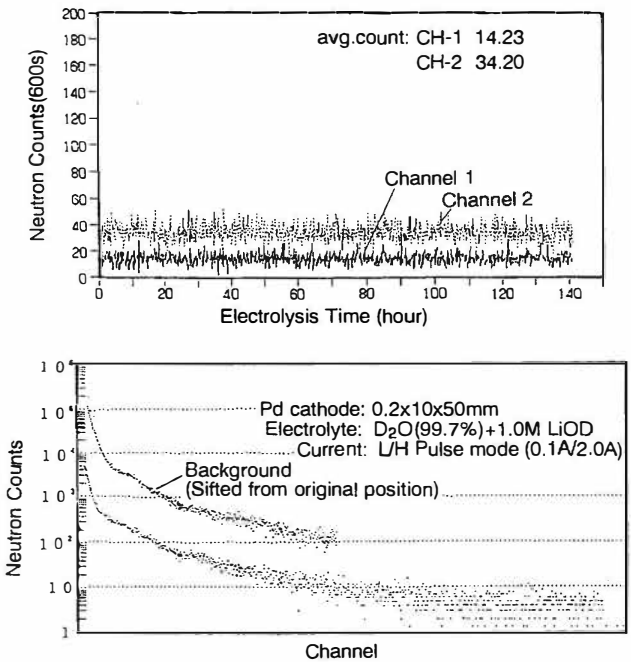

Figure 2. Examples of the neutron counting raw data.
Upper chart : Signal from the ^{3}He counter system.
Lower chart : Neutron energy spectrum from the NE213 detector

3. Results and Discussion

Table 1 shows the summary of the experimental condition - D/Pd ratio, Pd cathode's size, and the current density. The shapes of all Pd cathodes are plate. Among 6 runs of the electrolysis, 3 of them gave appreciable neutron emissions. We confirmed that run 1, run 2, and run 4 were positive experiments.

Table 1. Experimental Condition and Results

Run Number	Size(mm)	L/H Current Density (mA/cm^2)	D/Pd	Neutron Emission
1	0.2x10x50	10/200	2	Yes
2	0.1x10x50	10/200	0.8	Yes
3	0.2x50x50	2/40	0.74	No
4	0.2x10x50	10/200	0.77	Yes
5	0.5x10x50	10/200	0.64	No
6	0.5x10x50	10/300	0.60	Yes

The analyzed data for run 3 are shown in Fig. 3. This run is approximately even in the neutron counts between background and foreground. The abscissa of the graph represents the recoiled proton energy (channel number). The ordinate represents the pulse-height ratio of NE213. In this graph, the ratio is about 1. This indicates that this run was negative.

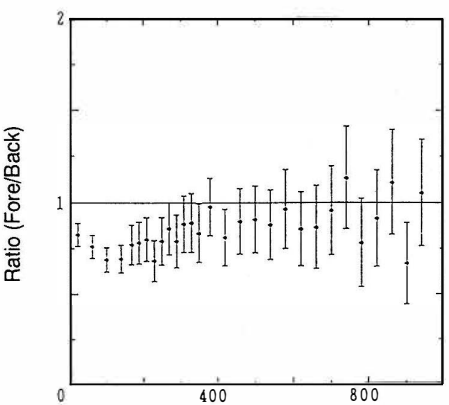

Figure 3. The analyzed data of NE213 detector from run 3

The analyzed data for run 2 are shown in Fig. 4. This run was positive. Lower channel peak indicates the 2.45MeV neutron emission, and higher channel peak indicates the higher energy neutron emissions. The analyzed data for run 1 are shown in Fig. 5-a. This run is also positive. It is seen in these two runs that the neutron emissions at 2.45MeV are smaller than that of the higher energy neutrons. The analyzed data for run 4 are shown in Fig. 5-b. This run is also positive. In this graph, the peak of 2.45MeV neutrons is clear, but the peak of higher energy neutrons is not so clear.

In the present study, we detected the weak neutrons emissions. The energies of the neutrons are 2.45MeV and higher. The relation betweens the neutron emissions and the experimental conditions are shown in Table 1. The relation between emissions and the D/Pd ratio indicates that the D/Pd ratio over 0.77 is necessary to observe Cold Fusion.

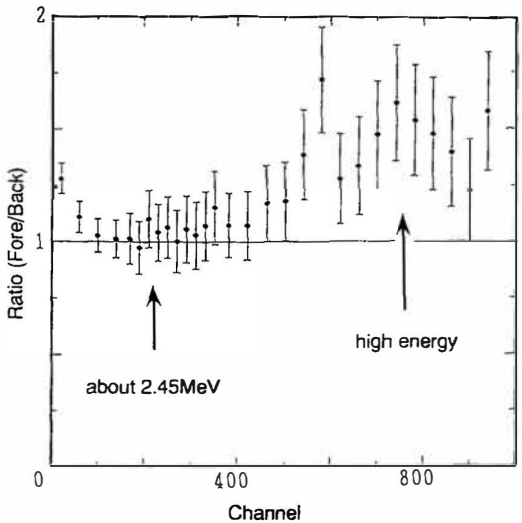

Figure 4. The analyzed data from NE213 detector in run 2.
Data collection for 144 hours after electrolysis started.

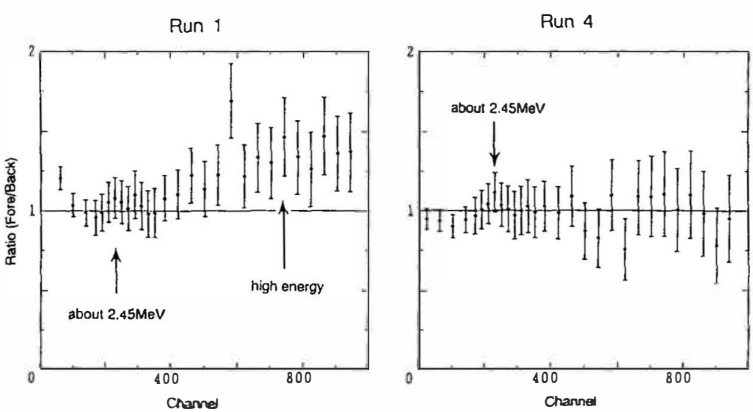

(a) (b)

Figure 5. (a)The analyzed data from NE213 detector in run 1
(Data collection for 144 hours after electrolysis starts).
(b)The analyzed data from NE213 detector in run 4
(Data collection for 152 hours after electrolysis starts).

Concerning the relation between emissions and the current density, it is concluded the current density over 120mA/cm^2 is necessary to observe Cold Fusion. D/Pd ratios of run 1 are the extreme case. We observed two compornents of the neutron energy. This fact suggests the possibility of the existence of the unknown nuclear process in the present electrolysis.

4. Conclusion

We performed the heavy water electrolysis with Low/High pulse mode to improve the reproducibility. In this experiment, the reproducibility was 50 percents. The weak neutron emissions with energy of 2.45 MeV and the higer (3-7 MeV) were observed. The intensity of 2.45 MeV neutrons is smaller than that of 3-7 MeV. To observe "Cold Fusion", the high D/Pd ratio (in our study : over 0.77) and the high current density (over 200 mA/cm^2) are needed. The present study completely comfirms the findings on the neutron energy reported by Takahashi et al. [4,5].

5. Acknowledgements

The authors would like to express their highest gratefulness to Tanaka Kikinzoku for the kind supply of Palladium used in this work. We would like to also acknowledge the advices of Prof. H. Sekimoto and Dr. T. Shimizu given in the measurement using NE213 scintillation counter.

6. References

1. Johnson, R.H. et.al., 1977, Nucl.Instr. and Meth., 145, 337
2. Okamoto, M. et.al., 1991, Fusion Technolgy, 19, 337
3. Okamoto, M. et.al., 1991, Proceeding of the second Annual Conf. on Cold Fusion, COMO, 81
4. Takahashi, A. et.al., 1990, J.Nucl.Sci.Technol., 27, 663
5. Takahashi, A. et.al., 1991, Fusion Technolgy, 19, 380

Direct Evidence for Nuclear Fusion Reactions in Deuterated Palladium

YAMAGUCHI Eiichi and NISHIOKA Takashi
NTT Basic Research Laboratories
3-9-11 Midori-cho, Musashino-shi, Tokyo 180, JAPAN

ABSTRACT

Using our own "*in vacuo*" method with a heterostructure of deuterated Pd (Pd:D), we have succeeded in the first highly reproducible and "*in situ*" detection of ^{4}He production. The real time observation has been performed by high-resolution quadrupole mass spectroscopy (0.001 amu at 4 amu). The amount of ^{4}He gas produced was closely correlated with the evolution of excess heat, and it increased with the loading ratio of D to Pd. At the highest loading ratio of D to Pd, we have also observed T production by detecting HT. The amount of HT increased in the final stages of ^{4}He production. The system of H-loaded Pd (Pd:H) heterostructure, on the other hand, produced neither ^{4}He nor T. Furthermore, the energy spectrum of charged particles detected during these experiments has revealed that α particles with an energy of 4.5–6 MeV and protons with an energy of 3 MeV were emitted from the oxide surface of Pd. The amount, however, was extremely small in comparison with that of ^{4}He detected. These results indicate that a new class of nuclear fusion occurs in the Pd:D and Pd:H systems.

1. Introduction

After Fleischmann, Pons and Hawkins[1] claimed in 1989 that electrolyzing heavy water with a palladium cathode released energy from nuclear fusion at room temperature, much effort has been made to reinvestigate the possibility of the electrolytically induced nuclear fusion in condensed matter. Many researchers have recently reproduced the evolution of heat by electrolysis of D_2O, but none have yet proved that this heat is caused by nuclear fusion nor even obtained definite evidence for the so-called "cold fusion" in solids.

By the lack of neutrons consistent with the excess heat, Fleischmann *et al.* presumed that "the bulk energy release is due to a hitherto unknown nuclear process or processes," specificaly[2]

$$d + d \longrightarrow {}^4\mathrm{He}\ (76.0\ \mathrm{keV}) + \mathrm{photons/phonons}\ (23.8\ \mathrm{MeV}). \qquad (1)$$

FRONTIERS OF COLD FUSION

In comparison with the normal reactions

$$d + d \longrightarrow t\ (1.01\ \text{MeV}) + p\ (3.02\ \text{MeV}) \quad (2)$$

$$\longrightarrow {}^3\text{He}\ (0.82\ \text{MeV}) + n\ (2.45\ \text{MeV}), \quad (3)$$

this reaction has negligibly small probability (10^{-7}), and should be accompanied by an emission of 23.8-MeV γ-ray. Consequently, their suggestion of "cold fusion" has been profoundly controversial. Schwinger[3], however, supported their claim, and furthermore, suggested that, because of the decrease in the Coulomb barrier between hydrogen nuclei and because of the asymmetry of the $p + d$ situation in contrast to the symmetry of the $d + d$ situation, the reaction

$$p + d \longrightarrow {}^3\text{He}\ (5.35\ \text{keV}) + \text{photons/phonons}\ (5.49\ \text{MeV}) \quad (4)$$

is more likely than that described by Eq. (1),

Other groups have suggested other mechanisms. Takahashi *et al.*[4] reinvestigated the experiment of Fleischmann *et al.*, and not only found slight peaks near 2.45 MeV in the neutron energy spectra, but also found one-order-of-magnitude-weaker broad peaks at 4–6 MeV. They conjectured that multibody reactions such as

$$d + d + d \longrightarrow {}^4\text{He}\ (7.95\ \text{MeV}) + d\ (15.9\ \text{MeV}) \quad (5)$$

$$d + d + d \longrightarrow {}^3\text{He}\ (4.76\ \text{MeV}) + t\ (4.76\ \text{MeV}) \quad (6)$$

$$p + d + d \longrightarrow {}^4\text{He}\ (4.77\ \text{MeV}) + p\ (19.08\ \text{MeV}) \quad (7)$$

etc. produced high energy deuterons (Eq. (5)), which then fused to produce neutrons with energies ranging from 4 to 6 MeV. Hagelstein suggested other multi-body mechanisms due to weak interactions[5].

Since the reality of cold fusion cannot be established simply by the observation that excess heat is released, it is necessary to determine the presence or absence of nuclear products. As shown in Eqs. (1)–(7), there are three kinds of possible nuclear products: (1) neutrons; (2) charged particles with high energies; and (3) ^{4}He, ^{3}He, or T compounds (such as T_2, HT or DT) in the gas phase.

With regard to the production of neutrons, a few groups have reported that neutron spectra show slight peaks at 2.45 MeV during the electrolysis of D_2O. These spectra, however, inevitably include background signals from space as well as from fissionable sources in the laboratories. The background contribution usually fluctuates so much that the observation of neutron emissions that are at most one order of magnitude greater than the averaged background has never given a definite answer. Anderson *et al.*[6], for example, found weak peaks near 2.45 MeV in background spectra without electrolysis.

Tritium measurement has encountered the same problem, because the heavy water used in the electrolysis experiments contains various amounts of contaminating T_2O. Although several groups have reported to have found large amounts of T when using radioactivity measurements to analyze the water after the electrolysis, their results have not yet persuaded sceptics.

Only the following two methods can produce evidence proving the presence or absence of cold fusion phenomena:

1. Mass spectroscopy for ^{4}He, ^{3}He and T in gas phase, with the background reduced to zero throughout all measurements. To investigate the correlation between the production of those gases and the excess heat, the measurement must be performed "*in situ*" and in real time. For instance, with a nominal mass 4 amu, there are 4 possible species: ^{4}He (4.00260 amu), HT (4.02388 amu) , D_2 (4.02820 amu), and DH_2 (4.02975 amu). It is therefore possible to distinguish between ^{4}He and the others by using a high-resolution mass spectrometer.

2. Energy spectroscopy of emitted charged particles, with the sensor under a pressure of less than 10^{-4} Torr. Background signals from cosmic rays can be zero within a tight chamber having sufficiently thick walls. The measurement must be also performed "*in situ*" in real time.

Even in the electrolysis measurements developed by Fleischmann *et al.*, mass spectroscopy can be used to analyze gas samples extracted from the closed electrolysis cell[7-9]. The existence of ^{4}He, ^{3}He, and T in the air and water, however, provides substantial background signals, so this analysis cannot give unambiguas evidence. Furthermore, real-time mass spectroscopic measurements are impossible in this kind of experiment. In fact, Morrey *et al.*[7] found that there was so much ^{4}He in the unused Pd that its production in the electrolyzed metal could not be established. The energy spectroscopy of charged particles is also difficult or impossible in the electrolysis type experiment.

We have therefore developed a new, "*in vacuo*," method[10-12] for inducing cold nuclear fusion in solids. This technique has enabled us to observe gigantic burst of neutrons and, at the same time, both the explosive release of D_2 gas and excess heat from deuterated Pd (Pd:D) plates and a biaxial plastic deformation of the samples[10]. We have for the first time reproduced the evolution of excess heat[11].

The key technology of this method is to form a layer of D accumulated at solid Pd:D surfaces by using hetrostructures, formed under He-free and T-free conditions, to control the out-diffusive transport of D atoms. One side of these Pd:D surfaces is covered with a thick Au-film that prevents leakage of D atoms from that side, and the other side of the surface is covered with an oxide (MnO_x, SiO_x or AlO_x) that provides a surface barrier to out-diffusing D atoms. A layer of D atoms therefore accumulates in the Pd near the Pd/oxide interface. The β phase formation at this interface expands the lattice two-dimensionally and then the Gorsky effect enhances the out-transport of D atoms toward the interface. As a result, a D-rich layer accumulates at the Pd surface.

The purpose of the present work is to demonstrate the results both for the high resolution mass spectroscopic analysis of released gases and for measuring the energy spectroscopy of emitted charged particles, using our "in vacuo" method. In Sec. 2, we explain the details of sample preparation and of the measuring technique. Section 3 presents experimental results showing the the first definite evidence of cold nuclear fusion. Section 4 summarizes our conclusions.

2. Experimental

Samples with a MnO_x/Pd:D(H)/Au heterostructure were prepared as follows.

First, after Pd plates ($3\times3\times0.1\ cm^3$) with purity of 99.9 % were rinsed with a mixture of HCl and HNO_3 (3:1 by volume) for 10 seconds, an electron-beam evaporator was used to deposit a 200-Å-thick film of MnO_x on one surface of the Pd plates at room temperature.

Second, the samples were set in a stainless steel vacuum chamber (Vieetech Inc., 61.37 l), and annealed at 300–400 °C for 18–22 hours under vacuum (final pressure $< 5 \times 10^{-7}$ Torr) to completely degas the samples. With the heater kept on, 99.9% pure D_2 was introduced up to a pressure of 400 Torr. For some samples, H_2 gas or the mixture of D_2 and H_2 gases were used instead of pure D_2 gas. Then the temperature was decreased at -2°C/min to room temperature.

Third, after keeping the samples under the H_2, D_2, or D_2–H_2 mixture for 60 hours, the chamber was evacuated to less than 10^{-4} Torr and within 15 min., a 2000-Å-thick film of Au was deposited on the other surface of Pd plates. Note that these second and third procedures eliminate any chance of He or T being left in Pd lattices.

The samples were taken out of the vacuum chamber and weighted to the nearest 10 μg. The samples were also weighted after the measurement procedure, and since all D or H atoms in the Pd were completely out-diffused after the measurement, the average loading ratio of D or H to Pd could be estimated from the weight difference. This ratio varied between 30 to 60%. Two of the samples were then attached to a sample holder equipped with electrodes and Si-SSDs (solid state devices) and were set in the same vacuum chamber used for D loading. Measurements were started after reducing the chamber pressure to less than 10^{-5} Torr.

Measurement setup is shown schematically in Fig. 1. The chamber was evacuated by a turbomolecular pump (550 l/s). Part of gases around the samples was drawn through a 25-cm-long rambling stainless steel tube (1/8 inches in diameter) to the mass-sensing chamber equipped with one high-resolution quadrupole mass (Q-mass) sensor (Extrel: EXM25) and two independent low-resolution Q-mass sensors (Spectramass: Selector). This differential evacuation system made it possible to keep the pressure in the mass-sensing chamber one order of magnitude lower than that in the main chamber.

The signal from the high-resolution Q-mass sensor was analyzed with a controller (Extrel: C50): where the optimized resolution in the mass number at nominal mass 4 was 0.001 amu, and the sensitivity with which ion current was measured was 1 pA . Figure 2 shows the calibration data obtained after the measurements when the high-resolution Q-mass spectrometer was loaded with D_2 gas and with ^{4}He gas while no samples were in the main chamber. This figure shows that the D_2 gas used in this experiment did not contain detectable amounts of ^{4}He.

The system for measuring the energy spectrum of charged particles consisted of two independent sets made up of an Si-SSD (Canberra: PD-450-19-700-AM; active area= 4.5 cm^2, active thickness=700 μm), a preamplifier (EG&G Ortec: 142B), an amplifier (EG&G Ortec: 575A), and an AD converter (Canberra: 8713). Both sets were connected to a multichannel analyzer

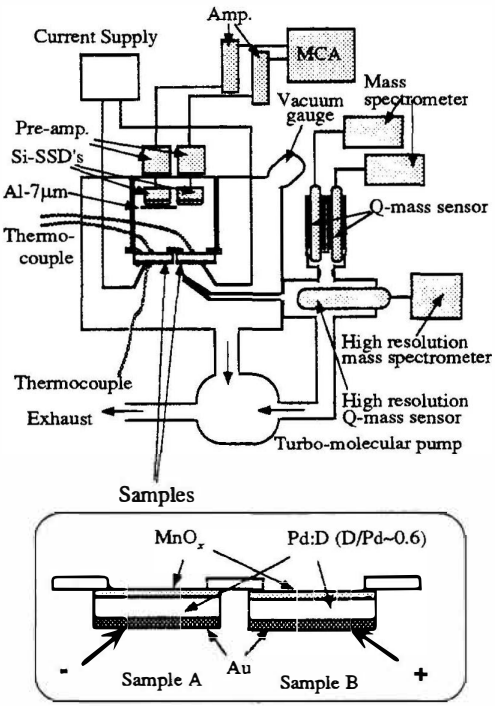

Fig. 1: Schematic diagram of the measuring apparatus.

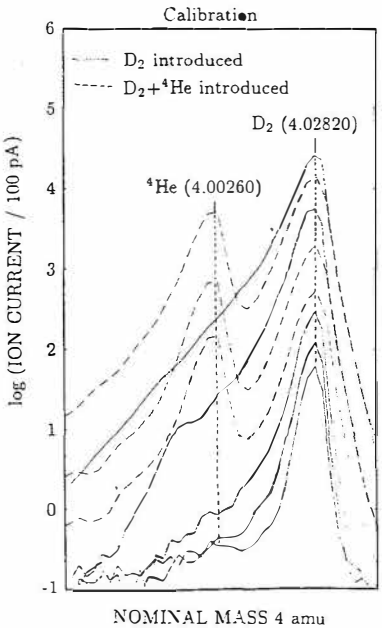

Fig. 2: Calibration data for high-resolution Q-mass spectrometer.

(Nuclear Data: 556-AIM), and both SSDs were 6.0 cm from the MnO_x surface of the Pd plates. One of the SSDs was covered by a 7.0-μm-thick piece of Al foil to identify the species of the charged particles. Time-resolved data from MCA was outputted to a workstation (DEC: VS3100-M76) running special software (Nuclear Data: GENIE system). The energy calibration was performed by using ^{241}Am (5.484 MeV) and ^{244}Cm (5.805 MeV). To avoid detecting background photons, the vacuum chamber was completely darkened throughout the measurement.

A constant current/voltage supplier (HP: 6032A) supplied electric current to the samples through tungsten needles. As shown in the inset of Fig. 1, two equivalent samples were reversely biased in order to find out whether the out-transport of D atoms in Pd was enhanced by electromigration. The sample surface temperature was measured by K-type thermocouples. Strain gauges were sometimes put on the Au surfaces, but never before attempts to detect ^{4}He production. This measurement setup thus provided a perfect system free of background ^{4}He.

3. Results and Discussion

Our previous papers[10,11] have shown that the following three events always occur chaotically within 1–3 hours of starting to pass electric current through the samples:

(1) Explosive release of gas from the samples, during which the ratio of partial pressure for molecules with mass 3 to that for molecules with mass 4 or 2 increases markedly.

(2) Evolution of excess heat (0.5–2 W for 10^3 seconds). This follows the explosive gas release.

(3) Uniform biaxial bending of the samples. This plastic deformation begins suddenly at the peak of gas release and it ends within 10 seconds.

We have also found that two equivalent samples (A and B) arranged as shown in the inset of Fig. 1 exhibit these phenomena. This means that the out-transport of D or H atoms in Pd lattices is due not to electromigration but to the temperature gradient perpendicular to the surface (heat of transport). Thus, the electric current turns out to work for heating the samples.

The present paper shows experimental results for four typical samples with MnO_x/Pd:D(H)/Au heterostructures. Samples 1 and 4 were respectively made by immersing the Pd plates in D_2 and H_2 at 400 Torr; the loading ratio of D to Pd was 48 % for sample No. 1 and the loading ratio of H to Pd was 56 % for sample No. 4. Samples 2 and 3, on the other hand, were made by immersing plates in the mixtures of D_2 and H_2 gases (D_2:H_2 volume ratio=7:1 for No. 2; 1:1 for No. 3), each with a total pressure of 400 Torr. In each of the four measurements, two equivalent samples A and B configured as shown by the inset in Fig. 1 were heated by a continuous pulsed current (5 A/7 A at 50 Hz).

The results of time-resolved mass spectroscopic analysis of gases collected during experiment No. 1 (Pd:D) are shown in Fig. 3(a). This figure clearly shows that only D_2 is detected initially but a peak attributable to ^{4}He gradually appears. This is the first definite evidence for ^{4}He production because there is no background ^{4}He in this experimental method. In the final stages of ^{4}He production, a peak attributable to HT appears and increases with the time. Since there is also no background T in this system, this experiment also gives definite evidence for T production.

The mass spectra from experiments No. 2 (Pd:D/H) and No. 3 (Pd:H/D), Figs. 3(b) and 3(c), also show clear ^{4}He peaks at 4.00260. As shown in Fig. 4(a), this ^{4}He production is clearly correlated with the excess heat released by the sample B in experiment No. 3. The maximal intensity of the ^{4}He peak, however, as well as the total amount of ^{4}He produced, were lower for experiments No. 2 and No. 3 than for experiment No. 1. This indicates that the ^{4}He production decreases with the amount of D_2 loaded in the Pd.

The time-resolved mass spectra for experiment No. 4 (Pd:H), shown in Fig. 3(d), show only a single small peak at 4.02820 amu. This peak is due to D_2 contamination from the H_2 bottle or the inner wall of the chamber, or both. We can therefore conclude that Pd:H systems exhibit ^{4}He production nor T production. This figure also shows that there is no background ^{4}He in these experiments.

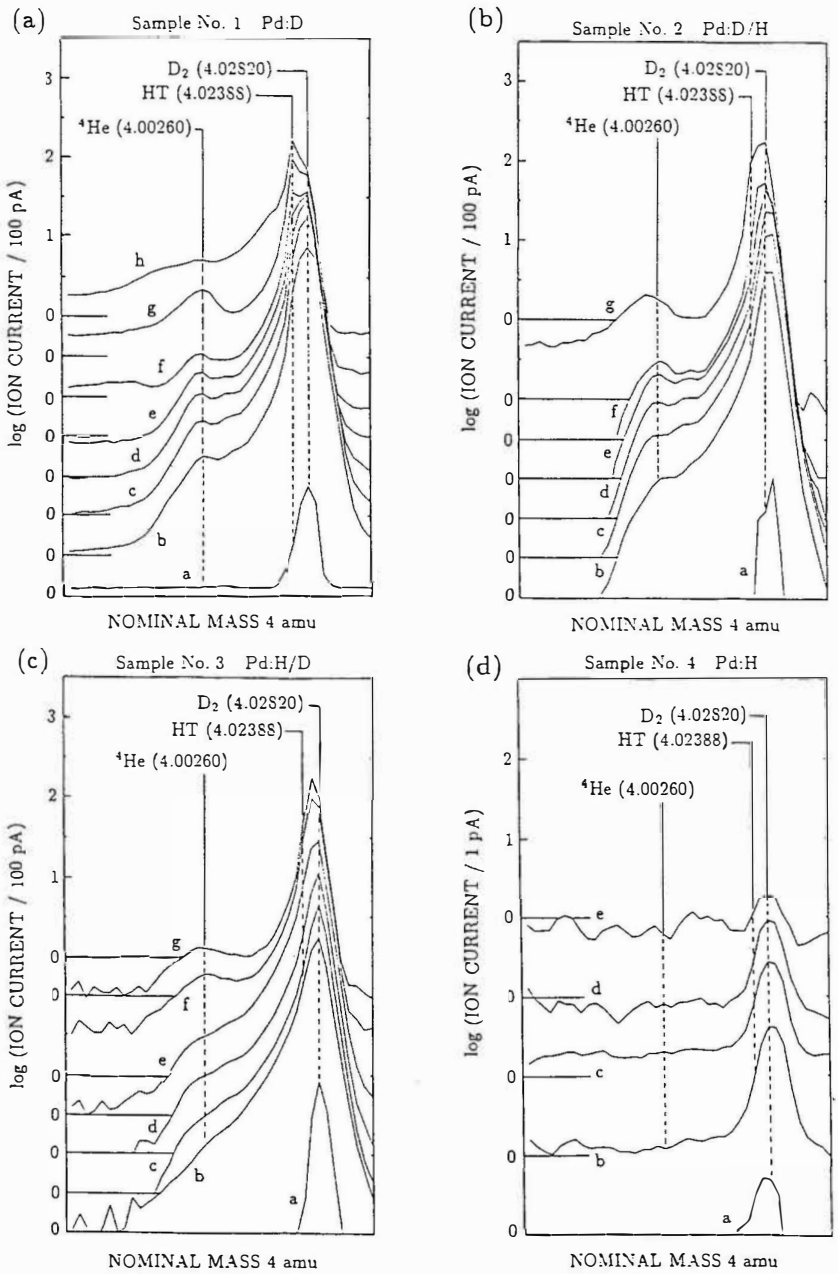

Fig. 3: The experimental results of mass spectroscopy at nominal mass 4 for released gases from (a) sample No. 1, (b) No. 2, (c) No. 3 and (d) No. 4, where each spectra from (a) to (h) were taken at every 72 min. for sample No. 1, 28 min. for No. 2 and 3, and 55 min. for No. 4.

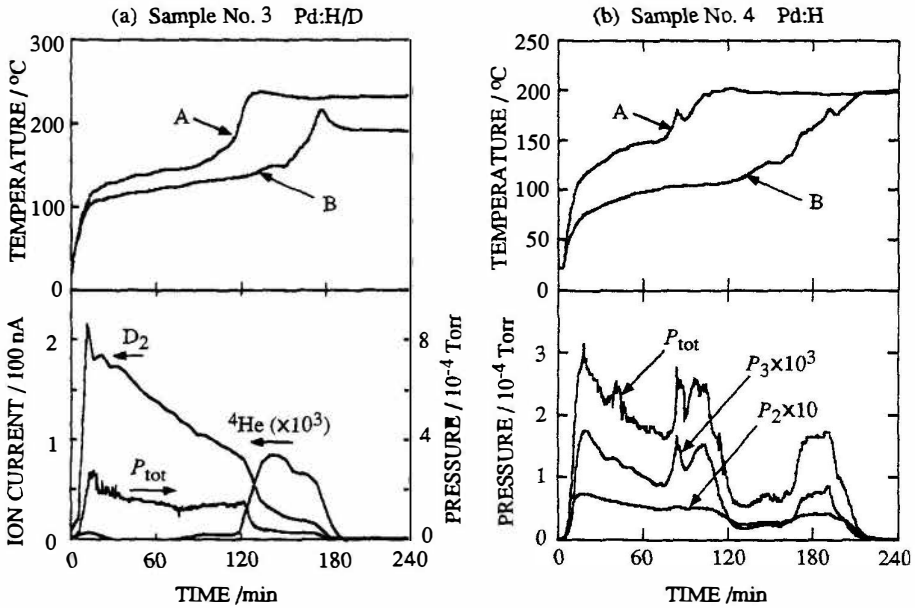

Fig. 4: Time dependence of the surface temperatures for the sample A and B, the total pressure, P_{tot}, of the main chamber, the ion current for D_2 and ^4He (or the pressure for mass 2, P_2, and mass 3, P_3) in the (a) measurement No. 3 and (b) measurement No. 4.

As shown in Fig. 4(b), however, the Pd:H system nevertheless chaotically produced excess heat in both the A and B samples. At those sudden increases in temperature, at 80–120 min. for sample A and at 160–200 min. for sample B, the ratio of P_3 to P_2 increases dramatically. Similar increases in P_3 have also been observed in experiments No. 1–3.

If the mass 3 gas were HD or H_3, the time dependence of the partial pressure P_3 should be proportional to P_2 and the pressure for D_2. Since the amount of T is negligible, as shown in Fig. 3(d), it is most likely that this dramatic increase in P_3 is due to ^3He production. To test Schwinger's conjecture, it will be necessary to use the high-resolution Q-mass system to observe the time-resolved mass spectra at nominal mass 3 amu.

While measuring the mass spectra described above, we simultaneously made two independent measurements of the energy spectrum of charged particles. It must be noted here that since the Si-SSD used in this experiment has a 700-μm-thick depletion layer, we can detect p, d, t, ^3He, and α emission at energies up to 10, 13, 14, 35, and 40 MeV, respectively. The amplifier and AD converter were set to detect, with a resolution of 7 keV, any charged particle of the energy up to 28 MeV.

Each sample spectrum was taken after starting the current injection, where the live time is 508 min. for No. 1 and 203 min. for No. 2–4. The sum is shown in Fig. 5. The spectrum shown in Fig. 5(a) has clear peaks at 3 MeV and a broad range of peaks from 4.5 to 6 MeV. These peaks probably correspond to

the peaks at 2.2 MeV and from 3.5 to 4.5 MeV in Fig. 5(b). From this energy loss resulting from the 7μm of Al foil, we can conclude that the emission at 3 MeV is attributable to protons and that the peaks around 4.5–6 MeV are attributable to α or ^{3}He particles. Our data shows that that there is no signal above 10 MeV.

The proton emission at 3 MeV is probably due to the reaction specified in Eq. (2). The origin of the higher energy emission, however, cannot be stated with certainty, because the background itself has an extremely low probability of containing α emissions at an energy of 5–6 MeV. Since January 1991, we have measured the backgound data of charged particle emissions 50 times, each with a live time of 810-812 min. Two of these sets of background data showed α particle emission with an energy of 5.7–5.9 MeV. This is perhaps due to fissionable sources in the stainless steel. The 4.5- to 6-MeV emission shown in Fig. 5, however, is almost ten times the highest background levels. More detailed and lengthy work will be needed to clarify the origin of this 4.5–6 MeV emission of α or ^{3}He.

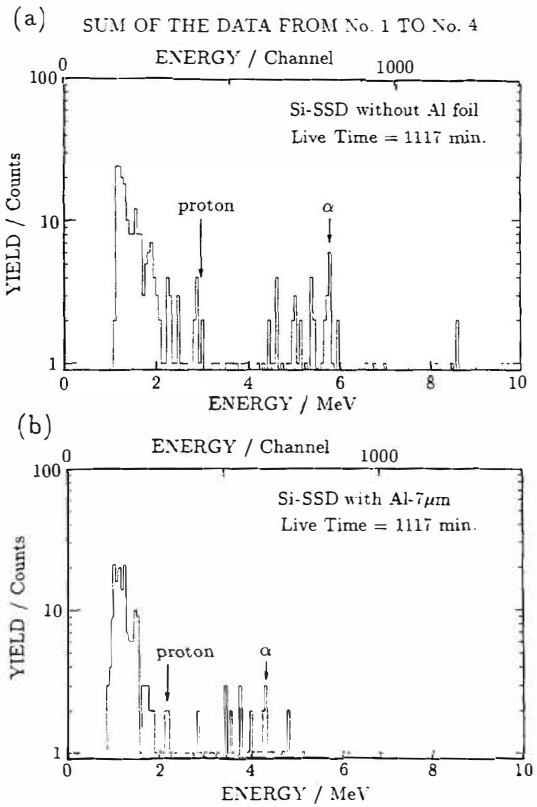

Fig. 5: The experimental results of energy spectroscopy for charged particles detected by Si-SSD (a) without Al-foil and (b) with Al-foil (thickness=7μm), where ths sum of the data from sample No. 1 to No. 4 are shown.

4. Conclusion

We have for the first time succeeded in detecting ^{4}He production "*in situ*" and with high reproducibility. Our "*in vacuo*" method gives the first definite evidence for the reality of "cold nuclear fusion" in solids. The real-time observation of fusion products has been performed by quadrupole mass spectroscopy with high resolution (0.001 amu at 4 amu). The amount of ^{4}He gas produced was closely correlated to the evolution of excess heat, and it increased with the loading ratio of D to Pd.

At the highest loading ratio of D to Pd, we also detected HT. The amount of HT produced increases in the final stages of ^{4}He production. The system of hydrogen loaded Pd (Pd:H), on the other hand, produces neither ^{4}He nor T.

This system nonetheless evolves the excess heat at the same time that 3-amu gas is explosively released.

Furthermore, the energy spectrum of charged particles emitted during these experiments has revealed that α particles with an energy of 4.5–6 MeV and protons with an energy of 3 MeV were released from the oxide surface of Pd. The amount of these particles, however, was extremely small in comparison with the amount of ^{4}He detected. These facts suggest that the reaction $d + d \longrightarrow {}^4\mathrm{He}$ + photons/phonons is strongly enhanced in the system Pd:D, and that the reaction $p + d \longrightarrow {}^3\mathrm{He}$ + photons/phonons is strongly enhanced in the system Pd:H/D.

Acknowledgments

We are grateful to Profs. IKEGAMI Hideo and MATSUMOTO Osamu for stimulating discussions. We also thank Drs. KIMURA Tatsuya, HORIKOSHI Yoshiji and OTSUKA Kenju for their advice.

References

1. Fleischmann, M.*et al.*, 1989, J. Electroanal. Chem., **261**, 301.
2. Walling, C. and Simons, J., 1989, J. Phys. Chem., **93**, 4693.
3. Schwinger, J., 1990, Z. Phys. D, **15**, 221.
4. Takahashi, A. *et al.*, 1991, AIP Conf. Proc., **228**, 323.
5. Hagelstein, P. L., 1991, AIP Conf. Proc., **228**, 734.
6. Anderson, R. E. *et al.*, 1991, AIP Conf. Proc., **228**, 43.
7. Morrey, J. R., 1990, Fusion Tech., **18**, 659.
8. Bush, B. F. *et al.*, 1991, J. Electroanal. Chem., **304**, 271.
9. Liaw, B. Y. *et al.*, 1992, J. Electroanal. Chem., to be published.
10. Yamaguchi, E. and Nishioka, T., 1990, Jpn. J. Appl. Phys., **29**, L666.
11. Yamaguchi, E. and Nishioka, T., 1991, AIP Conf. Proc., **228**, 354.
12. Yamaguchi, E. and Nishioka, T., 1991, Elsevier Studies in Applied Electromagnetic in Materials, **3**, 21.

Search for Anomalous Effects Involving Excess Power and Helium during D_2O Electrolysis Using Palladium Cathodes

Melvin H. MILES and Benjamin F. BUSH
Chemistry Division, Research Department
Naval Air Warfare Center Weapons Division
China Lake, CA 93555-6001 USA

ABSTRACT

Eight electrolysis gas samples collected during episodes of excess power production in two identical cells showed the presence of ^4He. Six control samples gave no evidence for helium. Various studies of helium diffusion into our Pyrex glass sample flasks established a minimum helium detection limit of 3 x 10^{13} ^4He/500 mL (3 ppb) for our experiments. This places our rate of ^4He production at 10^{11}-10^{12} $^4He/s \cdot W$ which is the correct magnitude for typical fusion reactions that yield helium as a product. Simultaneous evidence for excess power, helium production, and anomalous radiation was present in these experiments. Progress relating to helium measurements have been hindered by difficulties in obtaining large excess power effects.

1. Introduction

The low intensity of neutrons in cold fusion experiments has prompted proposals of nuclear processes that yield only heat and helium as products. We report here the results of electrochemical calorimetric experiments designed to detect helium in the effluent gases while rigorously excluding possible helium contamination from other sources. However, the diffusion of atmospheric helium into our Pyrex glass flasks during the time period between sample collection and analyses (22-61 days) could be significant. We have therefore investigated the atmospheric helium diffusion rate for our flasks when filled with either nitrogen, hydrogen, or deuterium-oxygen electrolysis gases. These studies yield revised helium detection limits that place our rate of ^4He production in the range of 10^{11}-10^{12} atoms/s per watt of excess power.

2. Methods

The eight round-bottom Schlenk flasks (500 mL Pyrex) used for the collection of electrolysis gas samples were vacuum leak tested prior to use. All

FRONTIERS OF COLD FUSION

glass joints were carefully lapped for a concentric fit and lubricated with silicon grease (Dow Corning, High Vacuum). The average glass wall thickness determined volumetrically was d = 1.8 mm. The electrolysis gas samples collected at China Lake were sent to the University of Texas for analysis by mass spectrometry. Details of the electrochemical experiments and helium analyses are reported elsewhere by B. F. Bush et. al. and by M. H. Miles et. al. Two commercial laboratories (Helium Field Operations, Department of the Interior, Amarillo, Texas, and Rockwell International, Canoga Park, California) were used for studies of the rate of atmospheric helium diffusion into these flasks.

The detection of anomalous radiation involved the use of a thin end window Geiger-Mueller (GM) alpha-beta-gamma detector (Ludlum, Model 44-7) positioned about 20 cm from the tops of the electrochemical cells and connected to a scalar rate meter (Ludlum, Model 2200 and printer (Casio HR-8A). Dental X-ray film (Kodak Ultra-Speed, DF-58) placed near the outside surface of the electrochemical cell was also used for the detection of any radiation. There was no direct contact of the film with the electrolysis gases (D_2, O_2) which exited the system through an oil bubbler about 1 meter from the cell.

3. Results

Table 1 presents results from two different laboratories relating to atmospheric helium diffusion into three of our flasks when filled with nitrogen. These measurements yield a mean diffusion rate of $3.2 \pm 0.6 \times 10^{12}$ atoms/day that is in good agreement with the theoretical value as defined by S. Dushman

$$q = \frac{K \cdot P}{d} = 2.6 \times 10^{12} \text{ atoms/day} \qquad (1)$$

for Pyrex flasks with A = 314 cm^2 and d = 1.8 mm. This experimental agreement indicates that these three flasks were quite uniform. Measurements by the two laboratories were done several months after our helium measurements were completed, hence any effects due to deuterium or hydrogen saturation of the glass would have likely dissipated.

Table 1. Experimental Helium Diffusion Rates in Nitrogen-Filled Flasks (500 mL Pyrex, A = 314 cm^2, d = 1.8 mm).

Time (days)	Measured ^4He (atoms)	Diffusion rate (atoms/day)
14[a]	47×10^{12}	3.4×10^{12}
44.6[b]	167×10^{12}	3.7×10^{12}
65[a]	170×10^{12}	2.6×10^{12}

[a] Helium Field Operations, Amarillo, Texas.
[b] Rockwell International, Canoga Park, California.

Measurements of atmospheric helium diffusion into our flasks when filled with hydrogen or deuterium-oxygen electrolysis gases are shown in Figures 1 and 2. These four flasks yield a mean helium diffusion rate of 1.9 ± 0.3 x 10^{12} atoms/day suggesting that the inward diffusion of atmospheric helium is somewhat slower for flasks containing hydrogen or deuterium as postulated by Miles et. al. Flask uniformity is again indicated by the good agreement of helium diffusion rates for these four flasks. A total of eight flasks were used in our heat/helium studies, but one flask was broken during shipment, hence Table 1 and Figures 1 and 2 present helium diffusion results for all seven remaining flasks. A very important result from these helium diffusion studies is that there is absolutely no evidence for any leakage of air into our flask in any of these experiments. Additional studies by the Amarillo, Texas laboratory indicated that the rate of atmospheric helium diffusion into our flasks is 2-3 times slower for flasks that contain deuterium instead of nitrogen.

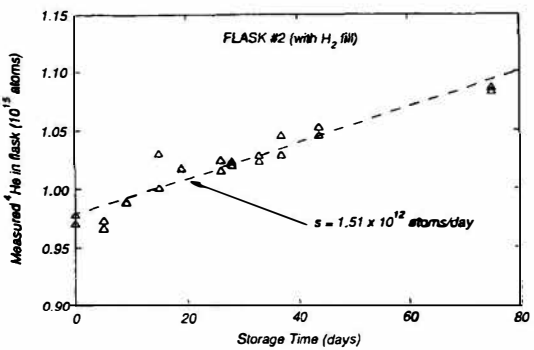

Figure 1. Experimental rate of atmospheric helium diffusion into one of our Pyrex flasks when filled with hydrogen.

The excellent agreement between experimental and theoretical rates for the diffusion of atmospheric helium into our nitrogen-filled flasks allows us to determine a minimum value for our ^{4}He detection limit. As reported by M. H. Miles and R. A. Hollins et. al. four of our flasks filled with nitrogen were analyzed for helium by our usual procedures after 9 days of storage. One flask showed the presence of ^{4}He at the detection limit while no helium could be detected in the other three flasks. Based on the mean helium diffusion rate of 3.2 x 10^{12} atoms/day established experimentally in Table 1, our helium analyses for the nitrogen-filled flasks yields a minimum ^{4}He detection limit of 3 x 10^{13} atoms/500 mL or 3 ppb. This detection limit compares favorably with the ±1 ppb error range reported by a commercial laboratory (Amarillo, Texas) for the analysis of our gas samples. Helium detection limits of 1000 ppb (1 ppm) reported by N. S. Lewis et. al. and D. Albagli et. al. are far too insensitive to detect any ^{4}He fusion product in the effluent gases of Pd/D_2O electrolysis cells.

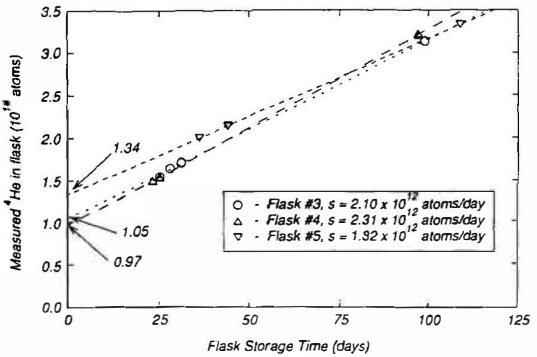

Figure 2. Experimental rate of atmospheric helium diffusion into three of our Pyrex flasks when filled with D_2-O_2 from Pd/D_2O electrolysis.

Table 2 presents results for the calorimetric measurements of excess power that were time-correlated with the collection of electrolysis gas samples for helium analysis. Since $X = P_{OUT}/P_{IN}$, the input power (P_{IN}) can be calculated from $P_{IN} = P_{EX}/(X-1)$. The numerical values for ^{4}He are based on the revised detection limit of approximately 10^{13} atoms/500 mL. The time

Table 2. Helium Production During D_2O Electrolysis: Revised Detection Limits.

Sample	P_{EX} (W)	X	^{4}He Atoms/500 mL[a]
12/14/90-A	0.52b	1.20[b]	10^{15} (large peak)
10/21/90-B	0.46	1.27	10^{15} (large peak
12/17/90-A	0.40[b]	1.19[b]	10^{14} (medium peak)
11/25/90-B	0.36	1.15	10^{15} (large peak)
11/20/90-A	0.24	1.10	10^{14} (medium peak)
11/27/90-A	0.22	1.09	10^{15} (large peak)
10/30/90-B	0.17	1.12	10^{13} (small peak)
10/30/90-A	0.14	1.08	10^{13} (small peak)
10/17/90-A	0.07	1.03	$< 10^{13}$ (no peak)
12/17/90-B	0.29[b,c]	1.11[b,c]	$< 10^{13}$ (no peak)

[a] No ^{3}He was detected. Mass spectrometer always at highest sensitivity.

[b] I = 250 mA/cm^2. All other experiments used I = 200 mA/cm^2.

[c] Possible calorimetric errors due to low D_2O solution levels.

required to generate 500 mL of electrolysis gas is 4440 seconds at 200 mA/cm^2 for our electrode area (A = 2.6 cm^2), laboratory temperature (23°C), and pressure (700 torr). For the experiments yielding 10^{15} ^{4}He atoms per 500 mL of

electrolysis gas, the rate of helium production is 10^{11}-10^{12} ^{4}He/s•W. This is the correct magnitude for typical fusion reactions listed in Table 3 that yield ^{4}He as a product.

Table 3. Low-Energy Deuteron Fusion Reactions Producing Helium.

Reaction	Energy (MeV)	Reactions/second/1 W output
$^2H + {}^2H \rightarrow {}^4He + \gamma$	23.8	2.6×10^{11}
$^2H + {}^3H \rightarrow {}^4He + n$	17.6	3.6×10^{11}
$^2H + {}^6Li \rightarrow 2\ {}^4He$	22.4	2.8×10^{11}
$^2H + {}^7Li \rightarrow 2\ {}^4He + n$	15.1	4.1×10^{11}

The amount of helium observed versus the flask storage time for each electrolysis gas sample is shown in Figure 3. Results for the four nitrogen-filled flasks are also included. Since Table 1 and Figures 1 and 2 show that the flasks are reasonably homogeneous with respect to helium diffusion, any significant diffusion of atmospheric helium into our flasks should yield helium levels that increase linearly with the flask storage time. No such effect exists in Figure 3. For the D_2O-LiOD experiments, high and low helium levels occur at both short and long storage times that ranged from 22 to 61 days. In fact, linear regression

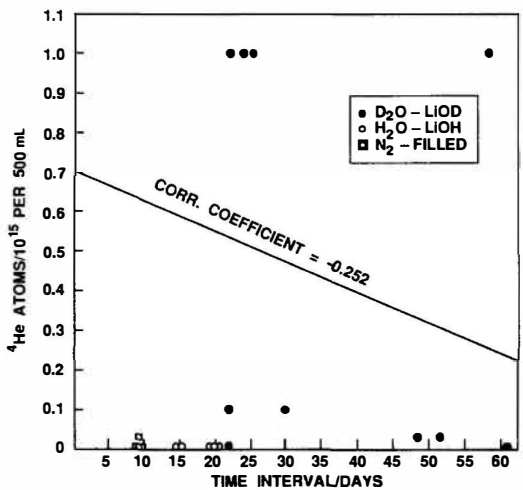

Figure 3. Amount of helium observed versus the flask storage time interval between gas collection and helium analysis. The results for the N_2-filled flasks establish a minimum helium detection limit for our experiments of 10^{13} atoms/500 mL.

shows a negative correlation if any exists at all. Ignoring the heat/helium relationship (Table 2), the simple yes or no detection of helium in 8 out of 8

experiments producing excess power and the absence of helium in 6 out of 6 control experiments (1 in D_2O and 5 in H_2O) implies a chance probability of only $(1/2)^{14}$ = 1/16,384 or 0.0061%. Atmospheric helium contamination, therefore, does not provide a likely explanation for our ^4He measurements.

The exposure of dental films during episodes of excess power has been reported elsewhere by Miles et. al. During this same time period our GM-detector recorded anomalous high radiation count rates as shown in Figure 4. Several following experiments involving Pd/D2O + LiOD electrolysis and using new Pd cathodes yielded near-normal radiation counts as shown in Figure 5. These electrolysis experiments also failed to produce significant excess power and showed no exposure of dental films. Furthermore, the passing of the electrolysis gases directly into our GM-detector did not yield anomalous radiation count rates. Several later electrolysis experiments also failed to produce any anomalous radiation counts as shown in Figure 6. This series of studies were used to establish a mean and standard deviation of 31,296 ± 275 counts per 12-hours for our GM-detector. Radiation monitoring continued as shown in Figure 7 for periods of electrolysis studies as well as for time periods with no experiments in operation. Normal radiation counts were always observed, and no excess power was detected. The anomalous radiation counts shown in Figure 4 have proven to be nearly as elusive as the excess power effect.

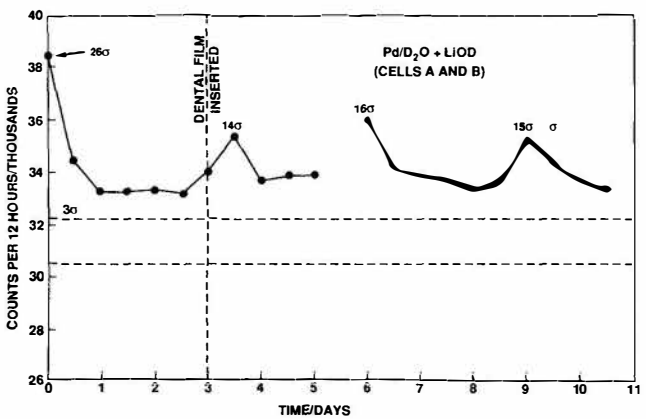

Figure 4. Anomalous radiation counts observed with the GM-detector during the time period December 15-25, 1990. During this same time period, gas sample 12/17/90-A showed the production of helium (Table 2) and dental films in cells A and B became blackened.

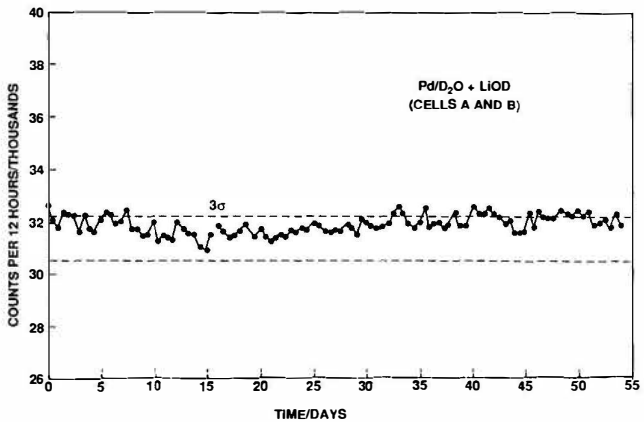

Figure 5. Radiation counts observed with the GM-detector during Pd/D_2O + LiOD electrolysis for the time period March 14-May 6, 1991. The electrolysis experiment began on February 25, 1991.

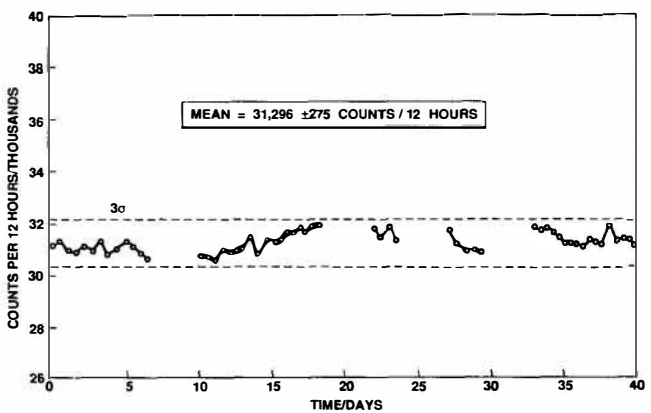

Figure 6. Radiation counts observed with the GM-detector for the time period July-September 1991. Various Pd/D_2O experiments were conducted but no significant excess power was detected. These radiation counts were used to establish the mean background of 31,296 ±275 counts per 12 hours.

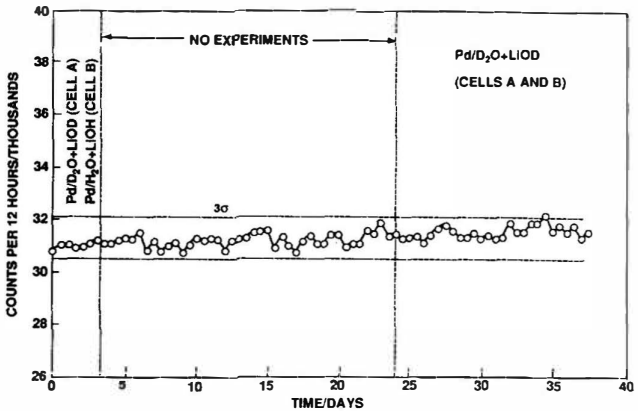

Figure 7. Radiation counts observed with the GM-detector for the time period October 15-November 21, 1991. Periods of Pd/D_2O + LiOD and Pd/H_2O + LiOH electrolysis as well as a period of no experiments are shown.

The plateau determination for our GM-detector is shown in Figure 8 for our normal background as well as for ^{55}Fe and ^{137}Cs sources. No unusual

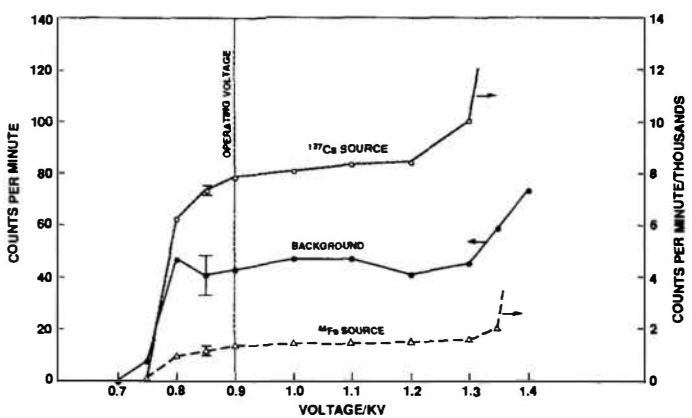

Figure 8. Plateau determinations for our GM-detector using ^{137}Cs and ^{55}Fe sources as well as the background counts. Normal behavior is observed.

behavior was observed. At the instrument setting of 0.9 kV suggested by the manufacturer, small voltage changes would not produce high count rates for this detector. The problem of reproducibility has hindered further studies of this anomalous radiation effect. However, several more recent experiments with the

GM-detector placed closer to the Pd/D_2O + LiOD cells (5 cm) have shown sporadic periods of elevated counts as reported by M. H. Miles, R. A. Hollins et. al. Furthermore, the variation of the distance between the cell and detector traces the radiation source back to the electrolysis cell. Similar detections of radioactive emissions have been reported by H. Uchida et. al.

4. Discussion

Factors that may affect the reproducibility of the excess power effect during Pd/D_2O + LiOD electrolysis include the palladium metallurgy, the handling or conditioning of the palladium, the extent of deuterium loading, the cell configuration and symmetry, the current density profile, the electrolyte; impurities in the cell components, palladium, D_2O or lithium; atmospheric contaminations such as H_2O or CO_2 as well as the time span of the experiments. Our experience suggests palladium metallurgy as a possible critical factor for excess power. Two of our palladium rods have given excess power in seven of eight experiments. Experiments using eight new palladium rods have all failed to give any large excess power effect. Our results suggest that palladium rods that yield excess power may be used repeatedly.

Experimental processes that could yield excess power effects include the exothermic formation of PdD_n where $n \leq 0.6$ and the exothermic deloading of the palladium for $n \geq 0.6$ as reported by J. Balej and J. Divisek. The exothermic formation of $PdD_{0.6}$ in our experiments would yield an excess power less than the detection limit of our calorimeter (± 0.020 W) as reported by M. H. Miles, R. A. Hollins et. al. The exothermic deloading of the palladium cathode represented by

$$PdD_{0.8} \rightarrow PdD_{0.6} + 0.1\ D_2,\ \Delta H = -3050\ \text{J/mol Pd} \qquad (2)$$

yields an excess power effect of 0.012 W for our experiments (0.0416 mol Pd) when averaged over a 3-hour period required by our calorimetry (time constant $\approx$ 25 minutes). This exothermic deloading effect for our cells, therefore, yields an excess power that is again less than the detection limit of our calorimeter.

Another possible explanation for the excess power observed is the Joule-Thomson effect for deuterium compressed into the palladium. The Joule-Thomson coefficient is expressed thermodynamically as

$$\mu = \left(\frac{\partial T}{\partial P}\right)_H = \frac{T(\partial V/\partial T)_P - V}{C_P} \qquad (3)$$

From the Van der Waals' equation of state, the Joule-Thomson coefficient for hydrogen is

$$\mu = \frac{2a/RT - b}{C_P} = -0.02331\ \text{K/atm} \qquad (4)$$

A similar value would be expected for deuterium. Thus for 1 cm^3 of Pd containing $PdH_{1.0}$ (0.0565 mol H_2), a pressure change for hydrogen of $\sim 10^5$ atm averaged over a 3-hour time period would yield an excess power effect of 0.35 W. This is approximately the excess power that we have observed as seen in Table 2. However, there are several major problems with this Joule-Thomson explanation for excess power. Since a net enthalpy balance is required by the First Law of Thermodynamics, periods of excess power due to the release of deuterium under pressure must be balanced by periods of power shortfalls when deuterium is compressed into the palladium. Furthermore, the Joule-Thomson effect could not sustain excess power over long time periods as observed experimentally. In addition, excess power based on the Joule-Thomson effect would be expected for both H_2O and D_2O experiments. Finally, any Joule-Thomson derived excess power would not correlate experimentally with any helium production as reported in Table 2.

Progress relating to helium measurements at our laboratory has been hindered by experimental difficulties in obtaining large excess power effects. However, small excess power as well as anomalous radiation was detected when the electrolysis samples shown in Figure 2 were collected. Flasks 3 and 5 were collected at the same time from cells A and B, respectively. An anomalous radiation count of 38,668 per 12 hours (27 σ) was observed during this time period. Flask 4 was collected 4 days later from cell B during a time period of normal radiation (31,240 counts per 12 hours). The experimental excess power was 0.08 W for flask 5 and about 0.02 W for both flasks 3 and 4. As seen from Figure 2, the extrapolated amount of helium initially present is largest for flask 5 (1.34×10^{14} atoms/500 mL) that showed the largest excess power effect. Smaller amounts of helium that are nearly identical were measured for the other two flasks (1.05×10^{14} and 0.97×10^{14} atoms/500 mL) where the excess power was near the detection limit of our calorimeter. Although these excess power measurements are marginal, the differences in detected helium and observed power for flasks 3 and 5 or for flasks 4 and 5, nevertheless, yields 10^{11}-10^{12} atoms/s•W. This is in good agreement with our previous studies. Furthermore, these were double blind experiments since neither Rockwell International nor our laboratory knew the correlation of excess power and helium measurements until after all results were reported to a third party.

5. Conclusions

Simultaneous evidence for excess power, helium production, and anomalous radiation suggests that nuclear reactions do in fact occur in Pd/D_2O + LiOD electrolysis experiments. Reproducibility remains a major problem in defining these effects.

6. Acknowledgments

We thank David L. Miles for computer assistance in the analysis and display of the experimental data. We also thank Dr. Brian M. Oliver (Rockwell International) and Tom Davidson (Helium Field Operations, Department of the Interior) for measurements relating to helium diffusion into our flasks.

7. List of Symbols/Nomenclature

a = Van der Waal's gas constant, L^2 atm mol^{-2}
b = Van der Waal's gas constant, L mol^{-1}
C_P = Heat capacity at constant pressure, JK^{-1} mol^{-1}
d = Average thickness of glass, mm
H = Thermodynamic enthalpy, J
K = Permeability for helium diffusion through glass
P = Thermodynamic pressure, atm
ppm = Parts per million
ppb = Parts per billion
T = Thermodynamic temperature, K
V = Volume, liters (L)

8. References

1. Albagli, D. et. al., 1990, J. Fusion Energy, 9, 133.
2. Balej, J. and Divisek, J., 1989, J. Electroanal. Chem, 278, 85.
3. Bush, B. F. et. al., 1991, J. Electroanal. Chem, 304, 271.
4. Dushman, S., 1962, "Scientific Foundations of Vacuum Technique," 2nd ed., John Wiley and Sons, Inc., New York, pp 491-500.
5. Lewis, N. S. et. al., 1989, Nature, 340, 525.
6. Miles, M. H. et. al., 1992, in "Proceedings of the Symposium on Hydrogen Storage Materials, Batteries, and Electrochemistry," Vol. 92-5, Corrigan, D. A. and Srinivasan, S., Editors, The Electrochemical Society, Pennington, NJ, pp. 287-297.
7. Miles, M. H. et. al., 1991, in "The Science of Cold Fusion, Conference Proceedings," Vol. 33, Bressani, T., Del Giudice, E., and Preparata, G., Editors, Italian Physical Society, Bologna, Italy, pp. 363-372.
8. Miles, M. H., Hollins, R. A. et. al., J. Electroanal. Chem (accepted for publication).
9. Uchida, H. et. al., 1992, "The Third International Conference on Cold Fusion," Nagoya, Japan (post deadline abstract). See also Uchida, H. et. al., 1991, J. Less Common Metals, 172-174, A40.

Deuteron Fusion Experiment with Ti and Pd Foils Implanted with Deuteron Beams

Toshiyuki IIDA, Morio FUKUHARA, Hiroaki MIYAZAKI,
Yasuhiro SUEYOSHI, SUNARNO, Jun DATEMICHI and Akito TAKAHASHI

Department of Nuclear Engineering, Faculty of Engineering,
Osaka University, 2-1 Yamada-oka, Suita, Osaka 565, Japan

ABSTRACT

In order to examine the "cold" deuteron fusion reaction, we have tried making deuteron implantation experiments on Ti and Pd foils. A 20 cmΦ x 24 cm cylinder-type vacuum chamber was installed at the end section of a 240 keV deuteron accelerator. In the center of the chamber, a Ti or Pd foil sample was set to face toward 3 nsec pulsed deuteron beams collimated with a 3 mmΦ aperture. A Si-SSD was placed behind the foil sample for the measurement of high energy charged particles emitted from the foil by the supposed deuteron fusion reactions.

During the deuteron implantation for a 19 μm thick Pd foil, almost all signals came from the well-known D-D reaction but an unusual peak was measured around 5 MeV after the implantation, i.e., without deuteron beams. Also an inexplicable 8 MeV helium peak was measured during the deuteron implantation for 20 μm thick Ti foils with aluminum-oxide layer on their surface. These 5 and 8 MeV peaks seem to suggest the following three-body fusion reaction which A. Takahashi proposed as a hypothetical explanation of the mechanism of the cold fusion phenomena : 3D → d(15.9 MeV) + α (7.9 MeV), t (4.75 MeV) + ^{3}He (4.75 MeV). Further implantation experiments on characterized foil samples and more detailed measurements for the identification of the 5 MeV particles and for the precise detection of the 15.9 MeV deuteron correlated with the 7.9 MeV α and others are needed to prove the 3D fusion reaction.

FRONTIERS OF COLD FUSION

1. Introduction

Since M. Fleischman and S. Pons[1] and S. Jones[2] announced on the cold nuclear fusion, many scientists in the world have made every effort[3][4] to reproduce and explain the amazing phenomena. A. Takahashi proposed a bold multibody fusion model[5][6] for explaining the large excess-heat produced in the D_2O/Pd electrolysis experiments[1][7][8]. And in order to directly detect more energetic particles from the multibody fusion reactions, A. Takahashi and his group have tried making deuteron implantation experiments besides electrolysis experiments by modifying a deuteron accelerator OKTAVIAN[9], which has been used to produce D-T neutrons. Vacuum environment in the beam experiments is suited for the identification of nuclear reactions in Ti and Pd foil samples, or for the exact measurement of the type and energy of the nuclear charged particles emitted from the foils.

The purpose of the present deuteron implantation experiments is to find out energetic charged particles except those from normal D-D and related secondary D-T and D-^{3}He reactions. At first this paper describes the experimental method and apparatus and then shows some preliminary results obtained for Ti and Pd foil samples implanted with 240 keV deuteron beams.

2. Experiment

A 20 cmΦ x 24 cm cylinder-type vacuum chamber was installed at the end section of the deuteron accelerator. In the center of the chamber, a Ti or Pd foil was set to face toward the deuteron beam collimated with a 3 mmΦ aperture. The configuration of the experimental apparatus is shown in Fig.1. The central portion of a foil sample was implanted with 3 nsec pulsed deuteron beams, whose repetition frequency was 2 MHz. The average beam current was 2-10 μA. To examine the nuclear charged particles from the foil, a silicon semiconductor detector (Si-SSD) was set behind the foil, which was for the avoidance of a large number of backscattered deuterons. Therefore, the thickness of sample foils was controlled to be penetrated by not deuteron beams but more energetic nuclear particles. In such a foil sample, 240 keV deuterons are perfectly decelerated and many low energy deuterons should be between lattice atoms excited by the repeated pulsed-beams. The Si-SSD was commercially available, had the effective window area of about 35 mm^2 and the depletion layer depth of about 150 μm and analyzed energy till about 15 MeV for α-rays and about 4 MeV for protons. The distance between the foil sample and the Si-SSD was 15-30 mm. Also to examine the type of the energetic charged particles, another Ti foil was occasionally placed between the sample foil and the Si-SSD. Discrimination between hydrogen, helium and others can be made from the difference in their energy loss rate in the screen foil.

Samples for the deuteron implantation were 5-20 μm thick Ti (99.5%) and 5-25 μm thick Pd (99.95%) foils. As for some of the sample foils, moreover, we formed about 1000Å thick aluminum-oxide layer on their surface by an evaporation process. The preparation of these foils was based on the suggestion by

E. Yamaguchi[10][11], A. Takahashi[12] and others; a thin metal oxide layer on Pd plate may play an important role in enhancing the excess-heat production. Three types of Ti and two types of Pd foil samples were prepared to examine the aluminum-oxide layer effect. They were a 20 μm thick unprocessed Ti foil, the same foil whose surface was covered with 0.1 μm thick aluminum-oxide layer, the same foil with one sided aluminum-oxide layer, a 12.5 μm thick bare Pd foil and the same Pd foil with both sided aluminum-oxide layer. The formation of the aluminum-oxide layer on the surface of the samples was made at the same time by an evaporation process. Therefore, the constitution of the aluminum-oxide layers should hardly differ between the samples. A series of the deuteron implantation experiments on these samples was carried out under the same conditions of deuteron beams, the measuring system and others.

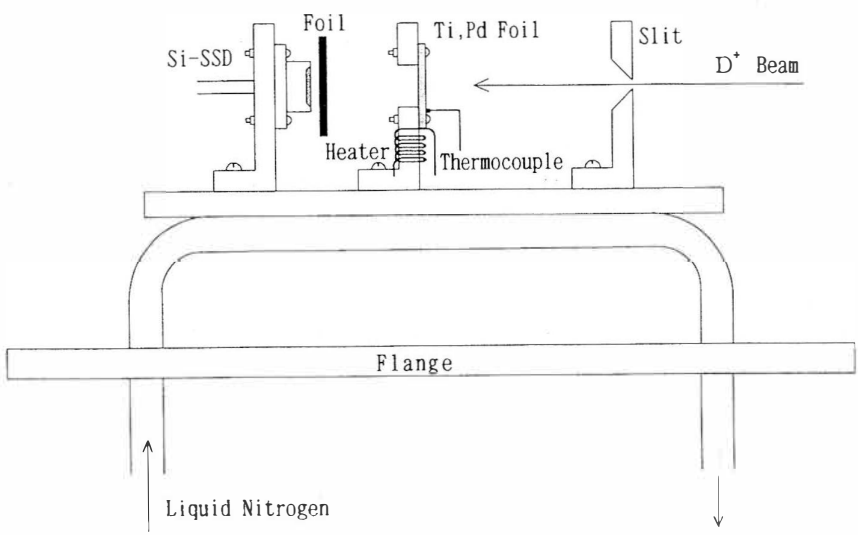

Figure 1. Configuration of experimental apparatus

3. Result and Discussion

It is about a year since we began the deuteron implantation experiments and so far (before using the foil samples with aluminum-oxide layer) we have obtained some unusual data showing a few but significant counts in the energy region over the highest energy of protons from the normal D-D reaction. However, statistics of the data were too low to discuss the relation to the nuclear particles expected from the multibody fusion model.

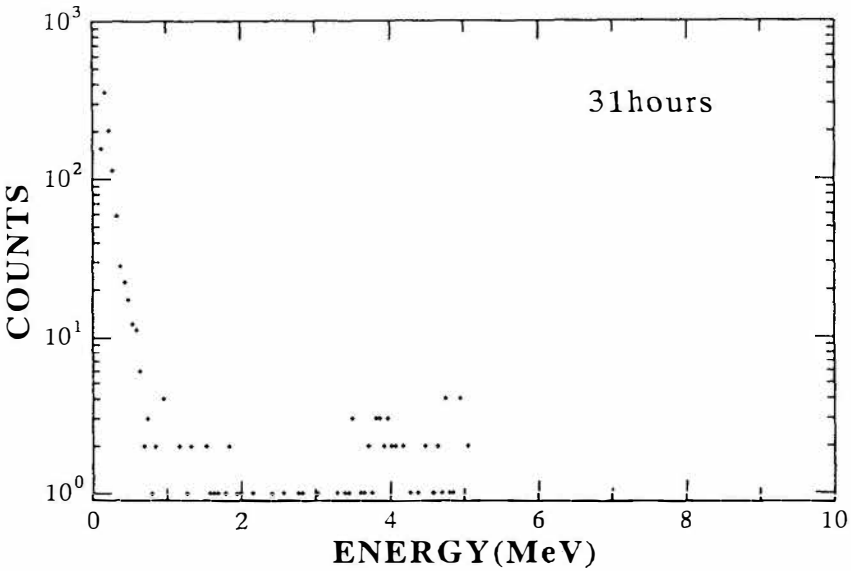

Figure 2. Typical example of inexplicable energy spectra of charged particles measured for 19 μm Pd foil in deuteron implantation experiments

Figure 2 shows a typical example of inexplicable energy spectra of charged particles measured for a 19 μm Pd foil. In the spectrum counts were stored for 31 hours after finishing a five-hour deuteron implantation. During the deuteron implantation, almost all signals came from the well-known D-D reaction but a weak peak was measured around 5 MeV after the implantation, i.e., without deuteron beams, and it may have something to do with the 4.75 MeV T and ^{3}He which are expected from the following three-body fusion reaction[5][6]: 3D $\rightarrow$ d(15.9 MeV) + α (7.9 MeV), t (4.75 MeV) + ^{3}He (4.75 MeV). This uncommon but interesting result also seems to be similar to experimental results which G.Chambers et al.[13] obtained by 350 eV deuterium bombardment of a 1 μm thick Ti film evaporated onto 500 nm Au on a 3.8 μm thick Ni foil, although the peak in Fig.2 is not so clear as that by G.Chambers et al. They have described that the particle in the 5 MeV peak looks like the triton.

In accordance with Takahashi's suggestion, we quite recently made similar deuteron beam experiments using sample foils with aluminum-oxide layer on their surface. Figure 3 shows a typical energy spectrum of charged particles measured for the 20 μm thick Ti foil with 0.1 μm thick aluminum-oxide layer bombarded by 240 keV deuteron beams. Besides the normal proton peak from the well-known D-D reaction, some small peaks were measured in the energy region higher than the proton peak. And in the similar measurements with the screen foil in front of the Si-SSD, we observed that the 22 μm Ti screen foil caused large energy reduction and broadening of the 8 MeV peak in Fig.3 and moreover that the 40 μm

Ti screen foil removed almost all 8 MeV signals. It is simply given from the well-known Bethe formula that 8 MeV hydrogen can easily penetrate the 40 μm thick Ti foil but 8 MeV helium suffers large energy loss in the 22 μm Ti foil and can not penetrate the 40 μm foil. From these measurements, the particle of the 8 MeV peak looks like helium, which may be 7.9 MeV α expected from the 3D fusion reaction. The 15.9 MeV deuteron correlated with the α can not be analyzed with the Si-SSD with thin depletion layer depth (150 μm). As for the peaks in the energy range of 3-5 MeV, the type of the particles could not be identified because the peaks with low statistics were too near the proton peak from the D-D reaction. Therefore, the interpretation on the 3-5 MeV peaks is unsatisfactory.

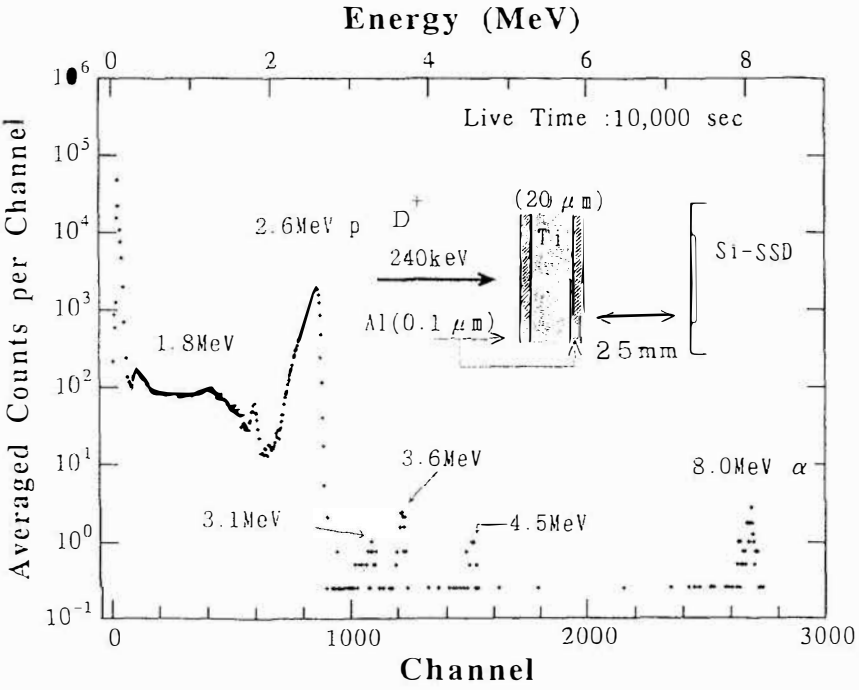

Figure 3. Typical energy spectrum of charged particles measured for the 20 μm thick Ti foil with 0.1 μm thick aluminum-oxide layer bombarded by 240 keV deuteron beams

Table 1 summarizes results of the series of the experiments on the foils with the aluminum-oxide layer. As for the three cases (1),(2) and (3) concerning the Ti foils with aluminum-oxide layer on their surface, the similar unusual 8 MeV and some 3-5 MeV peaks were measured and their spectral figures were on the whole the same, although the counting rate of the peaks fairly differed. On the other hand,

these peaks were not observed for the bare Ti and Pd foils [case(4),(6)]. In addition the similar 8 MeV peak was measured for the Pd foil with aluminum-oxide layer [case(5)]. It is clear from these results that the aluminum-oxide layer should have something to do with the unusual 8 and 3-5 MeV peaks. Also in the case (3) the similar uncommon spectrum was measured for the foil with one-sided aluminum-oxide layer behind the deuteron beams, which means that the direct reaction between deuteron beams and aluminum-oxide layer or impurities in it is low possibly related to the unusual peaks.

Table 1. Unusual peaks of charged particles measured for Ti and Pd foils in deuteron implantation experiments

Case	Foil type	Aluminum-oxide layer	3-5 MeV peaks	8 MeV peak
(1)	Ti (20μm)	Both-sided	Three clear	Clear
(2)	Ti (20μm)	One-sided*	Two clear	Clear
(3)	Ti (20μm)	One-sided**	One clear	Clear
(4)	Ti (20μm)	None	None	None
(5)	Pd (12.5μm)	Both-sided	One weak	Weak
(6)	Pd (12.5μm)	None	None	None

*: facing toward beams, **: behind beams

4. Conclusion

In order to examine the "cold" deutron fusion reaction, Ti and Pd foils were implanted with 240 keV, 3 nsec pulsed deuteron beams. The energetic charged particles from the foils were measured with the Si-SSD which was placed behind the foil.

During the deuteron implantation for a 19 μm thick Pd foil, almost all signals came from the well-known D-D reaction but an unusual peak was measured around 5 MeV after the implantation (i.e., under beam off). Also an inexplicable 8 MeV helium and some weak 3-5 MeV peaks were measured during the deuteron implantation for 20 μm thick foils with aluminum-oxide layer on their surface. These 5 and 8 MeV peaks seem to suggest the following three-body fusion reaction which A.Takahashi proposed as hypothetical explanation of the mechanism of the cold fusion phenomena : 3D $\rightarrow$ d(15.9 MeV) + α (7.9 MeV), t (4.75 MeV) + ^{3}He (4.75 MeV). The present experiments have been preliminarily started and have given rather qualitative data. Further implantation experiments on foil samples characterized with appropriate surface analyzers and more elaborate measurements with enough statistics for the identification of the 5 MeV particles and for the precise detection of the 15.9 MeV deuteron correlated with the 7.9 MeV α and others are needed to prove the 3D fusion reaction or to explain the unusual spectra. Moreover, such a simple experiment is incapable of explaining the process leading to the fusion reaction and the aluminum-oxide layer effect on the reaction. We have many problems to be solved.

[References]

(1) Fleischmann, M, and Pons, S., 1989, J. Electroanal. Chem. 261, 301.
(2) Jones, S. et al., 1989, Nature, 338, 737.
(3) Provo, Proc. Anomalous Nuclear Effects in Metal/Deuterium System, 1990.
(4) The Science of Cold Fusion, Proc. ACCFZ, Como, 1991.
(5) Takahashi, A., 1989, J. Nucl. Sci. Technol., 26 [5], 558.
(6) Takahashi, A. et al., 1991, Fusion Technology, 19, 380.
(7) Takahashi, A., 1992, Proc. Int. Symp. Nonlinear Phenomena in Electromagnetic Fields, Nagoya, 5.
(8) Takahashi, A. et al., 1992, Int. J. Appl. Electromag. Materials, 3, 221.
(9) Sumita, K. et al., 1990, Nucl. Sci. Eng., 106, 249.
(10) Yamaguchi, E. and Nishioka, T., 1990, Jpn. J. Appl. Phys., 29, 2666.
(11) Yamaguchi, E. and Nishioka, T., 1990, Proc. Anomalous Nuclear Effects in Metal/Deuterium Systems, 354.
(12) Takahashi, A. et al., 1992, "Anomalous Excess Heat by D_2O/Pd Cell under L–H Mode Electrolysis", this Conf. (ICCF3, Nagoya).
(13) Chambers, G.P. et al., 1991, NRL Memorandum report 6927.

Observation of High Energy Protons Emitted in the TiD_x + D Reaction at E_d = 150 keV and Anomalous Concentration of ^3He

J. Kasagi
Laboratory of Nuclear Science, Tohoku Univ., Mikamine, Sendai 982, Japan

K. Ishii
Cyclotron and RI Center, Tohoku Univ., Aramaki, Sendai 981, Japan

M. Hiraga and K. Yoshihara
Department of Chemistry, Tohoku Univ., Aramaki, Sendai 981, Japan

Abstract

Energetic protons were observed up to ~ 17.5 MeV in the bombardment of 150-keV deuteron on highly deuterated Ti rods. It has been shown that these protons are originated from the D+^{3}He reaction. The observed spectrum can be explained very well by the sequential reaction process, except for the three cases which require anomalous concentration of ^{3}He in TiD_x. The concentration, which is severely limited at some particular places in TiD_x and seldom occurs, is considered to occur before the bombardment.

1. Introduction

Since a possibility of the so-called cold fusion was indicated by Fleischman and Pons[1] and Jones et al.[2], considerable efforts have been made to confirm their results, especially to clarify whether the nuclear reaction can really occur in the condensed matter at the room temperature. Up to the present, however, the situation is still unclear.[3] In this paper, we report on observation of energetic charged particles emitted in deuteron bombardment on highly deuterated Ti, because the analysis of the spectrum clearly shows anomalous concentration of ^{3}He in TiD_x, which is considered to have occurred before the bombardment.

2. Experiment

Target samples were prepared as follows. D_2 gas was absorbed into various Ti rods (10, 8, and 6 mm in diameter and 30 mm in length) and plates (10 mm x 30 mm x 2mm), which were manufactured by Nippon Mining Co., Ltd. A cylindrical vessel (16 mm in inner diameter and 10 cm in length) made of inconel metal was used for the gas absorption, and was set in an electric oven. The vacuum line, to which a high-pressure D_2 gas container, a 500-cm^3 reservoir, a vacuum gauge and a pressure gauge were connected, was made of stainless steel and was evacuated by a

FRONTIERS OF COLD FUSION

turbo molecular pump. Before admitting D_2 gas, a plate or a rod of Ti was loaded in the vessel and degassed by heating the vessel at around 800 °C in vacua of 10^{-5} Pa for at least 20 hours. After that, the temperature of the vessel was lowered to about 600 °C and then the vessel as well as the reservoir was filled with the D_2 gas of 3 atm. The absorption speed increased gradually; for example, for a rod of 10 mm in diameter and 30 mm in length, it took about 30 min. that the pressure decreased from 3 to 1 atm for the first fill but a few min. for the second fill. Then, it decreased rapidly after the third fill. The system was refilled with the gas again and again until the absorption was saturated; we usually took more than 24 hours to stop the gas loading. In our experience, the gas can be absorbed into a rod much more than into a plate, probably because the plate is easily bent due to the non-uniformly absorption and stops the absorption. Average atomic ratio D/Ti was obtained by weighing before and after the D_2 gas loading.

The bombardments have been performed with a deuteron beam obtained from a Cockcroft-Walton accelerator at Department of Chemistry at Tohoku University. Deuterons were ionized in an RF-type ion source and accelerated up to 150 keV. After passing through the acceleration tube, the beam was bent by 30 degree by a dipole magnet in order to select the D^+ beam. The targets were set at the center of a small chamber (10 cm in radius). The beam passed through a collimator of 3 mm in diameter, set at the entrance of the chamber. Since the beam is stopped in the target, the electric current from the target was monitored and integrated during the run. Typical intensity of the beam was about 2 μA.

3. Charged particle spectra

Charged particles emitted in the bombardment were detected with either a surface barrier Si detector of 2 mm in thickness and 25 mm^2 in area or a Li-drifted Si detector of 5 mm in thickness and 100 mm^2 in area, placed at a distance of 1.5 - 2 cm from the target and at angles of 110° and 135° in respect to the beam direction. Energy resolution of the detectors was checked with an ^{241}Am source and was about 30 keV for 5.48 MeV. A 15-μm thick Al foil was placed in front of the detector to prevent δ-electrons from hitting the detector.

Up to the present, more than 20 plates and 10 rods have been bombarded. The average atomic ratio D/Ti of them ranges from 0.3 to 1.9. In the bombardment on TiD_x with small x (< 0.9), only protons from the D(d,p)T reaction were observed. To our surprise, however, very energetic charged particles were observed in the bombardment for larger x (> 1.2). In Fig. 1(a) is shown such a spectrum measured at 135° in the bombardment on the rod A. A huge peak appearing at about 2.45 MeV, whose actual energy is 2.75 MeV, is attributed to protons emitted in the D(d,p)T reaction. Although a simple kinematical consideration requires a broader peak between 2.74 and 3.02 MeV, the observed peak is not broad because of the steep fall of the reaction cross section for lower incident energies. Events due to the double and the triple pileups of the protons are distributed up to about 4.9 and 7.5 MeV, respectively, where sharp edges are clearly seen in the spectrum.

In addition to these normal events, events up to about 17.5 MeV are also seen. They are neither pileups nor events produced in the detector as proved in Fig. 1(b), which shows the spectrum measured with the same condition but putting a 200-μm thick Al foil in front of the detector to stop protons from the D(d,p)T reaction. As seen, the huge proton peak and the pileups disappear, but still remain the similar structure at the high energy region. Observed energy difference for these spectra clearly indicates that these high energy particles are protons emitted in the target. The

characteristics of the proton spectrum are a broad bump ranging from 12.5 to 16.5 MeV, and a sharp peak at E_p = 14.1 MeV. We have to add, furthermore, that the sharp peak at 14.1 MeV does not always appear; we have had only three cases which show the peak clearly, out of more than 50 bombardments on various places of the rods and plates. By contrast, the bump always appear in any measurements on TiD_x as far as x > 1.

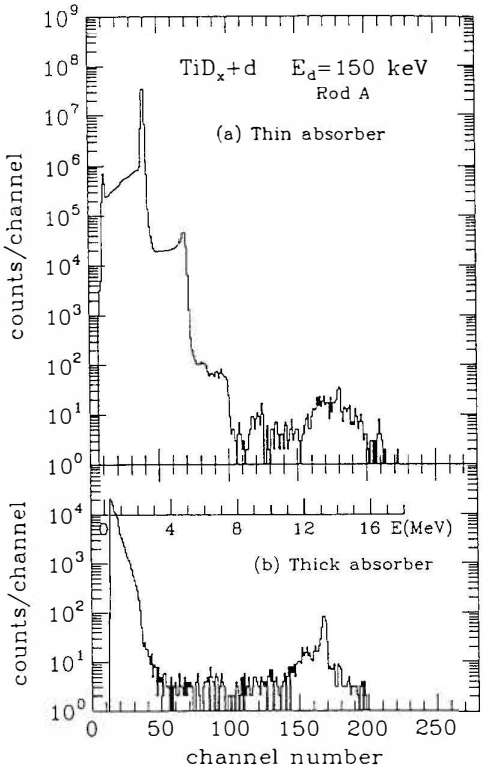

Fig. 1. Charged particle spectra obtained in 150-keV deuteron bombardment on TiD_x (x=1.3) at 135° with a 15-μm thick Al absorber (a) and a 200-μm thick Al absorber (b). The energy scale represents energy of charged particles after passing through the absorber.

The origin of both the broad bump and the sharp peak has been considered to be the D+^{3}He->p+^{4}He reaction, since no other reactions with deuterons can emit such high energy protons. For the broad peak, protons are interpreted to be emitted in the D(^{3}He,p)^{4}He reaction which sequentially occurs following the primary D(d,^{3}He)n reaction. In this case, the ejected ^{3}He particle reacts with deuterons at rest

in the target, and thus the protons cannot make a sharp peak, because of the spread of energy and direction of the ejected ^{3}He. In order to verify this situation quantitatively, we have calculated the spectral shape of protons emitted in the sequential reaction. For the calculation, an excitation function of the cross section and angular distributions of the primary D(d,^{3}He)n reaction for E_d < 150 keV were taken from ref. 4. Angular distributions of the secondary D(^{3}He,p)^{4}He reaction were assumed to be isotropic in the CM frame for $E_{^3He}$ < 1.33 MeV (the maximum incident energy for the secondary reaction), and cross sections were estimated from the differential cross sections[5] and reported S-factors[4]. Values of energy loss of deuteron and ^{3}He in Ti were taken from ref. 6. In Fig. 2, spectra measured at 110° and 135° are compared with the calculations. The calculations can explain the spectral shape very well for both angles. Therefore, we conclude that the broad bump is due to the sequential D(^{3}He,p)^{4}He reaction.

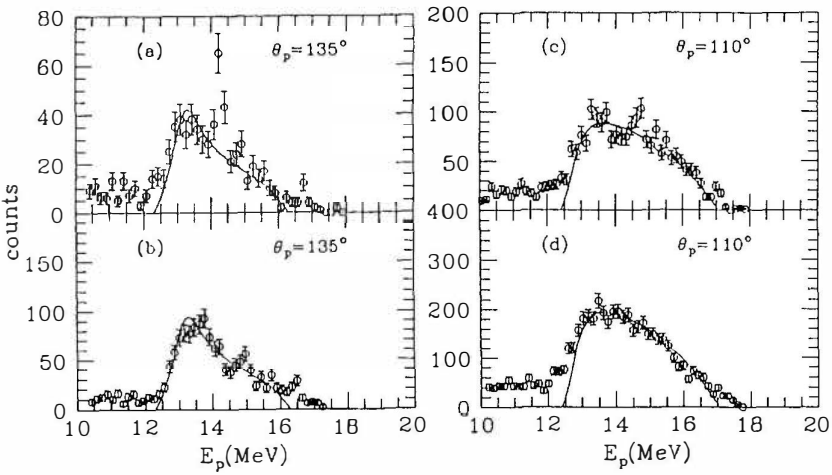

Fig. 2. Comparison of observed proton spectra with the calculations (solid lines) for the detection angles of 135° ((a) and (b)) and 110° ((c) and (d)). The sharp peak does not exisit in (b) and (d); it is seen unambiguously in (a), whereas ststistical fluctuations can also explain the structure in (c).

The yield of the sequential reaction is proportional to the square of deuteron density in the target; this explains why the bump was not observed for the targets with smaller D/Ti ratio (< 0.9). The value of D/Ti at the bombarded region of the target can be deduced accurately from the ratio of the yield of the broad peak to that of the peak of the D(d,p)T reaction; the ratio is proportional to D/Ti. For this purpose, the calculated ratio of the yield of the sequential reaction to that of the primary D(d,p)T reaction at the detected angles was compared with the measured one. The value of D/Ti mentioned below is the one deduced with this method, which generally agrees with the averaged one obtained by weighing.

The sharp peak at 14.1 MeV in the spectrum measured at 135• is naturally interpreted as the protons emitted in the ^{3}He(d,p)^{4}He reaction, where the deuteron

beam directly interacts with ^{3}He at rest, since the peak energy exactly coincides with the kinematical prediction. However, up to the present, we have had only three rods (rod A, B and C) with which the peak was observed unambiguously; we could find only one place in each rod in random bombardments. The rod A is the first case; the spectra for the rod A are already shown in Fig. 1 (and also in Fig. 2(a) which shows the same one as in Fig. 1(a) but with the linear scale). The spectra were obtained in the bombardments on the same place but at different time; the spectrum in Fig. 1(a) was obtained at the bombardment 45 days after the one for Fig. 1(b). The yield ratio of the peak at E_p = 14.1 MeV to the one at E_p = 2.75 MeV is proportional to the atomic ratio of ^{3}He/D. It is 8.5×10^{-7} for Fig. 1(a) but 5×10^{-6} for Fig. 1(b). This decrease is probably due to diffusion of ^{3}He, which is much smaller than the usual one in Ti because of high density of deuteron. In the second and the third cases, we obtained the spectra with much larger peak. They are shown in Fig. 3 as for rod B and C whose D/Ti ratios are 1.7 and 1.9, respectively. The yield of the 14.1-MeV peak is quite large so that the bump underlying the peak is hardly seen in both spectra; ratios of the peak yield to that of 2.75-MeV peak are 4.5×10^{-5} and 8×10^{-5} for rod B and C, respectively. Values of the cross sections of the ^{3}He(d,p)^{4}He reaction are almost similar with those of the D(d,p)T reaction for $100 < Ed < 150$ keV[4]. This indicates that the atomic ratio of ^{3}He/D at the bombarded area is the order of 5×10^{-6} to 8×10^{-5}, and thus the atomic ratio of ^{3}He/Ti is 3.8×10^{-6} to 4.5×10^{-5}. In other words, the number of ^{3}He, at least in the volume of about 7 mm^2 x 0.2 μm (area of beam spot times effective depth), is the order of 5×10^{11} to 10^{13}.

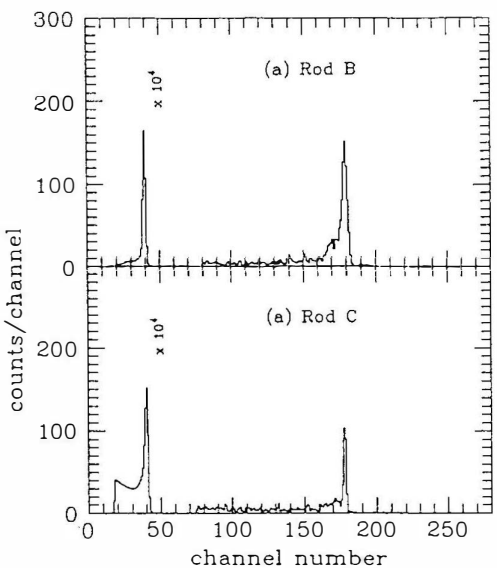

Fig. 3. Proton spectra measured at 135° for the rod B (a) and C (b). Only the sharp peak at E_p = 14.1 MeV is seen because of higher concentration of ^{3}He.

4. Discussion

The fact that the concentration of ^{3}He is severely limited to some particular places in the Ti rod is a characteristic of the observed anomalous phenomena and is quite difficult to understand. It is impossible to consider that ^{3}He was concentrated in the manufacturing process, for the following reasons. Natural abundance of ^{3}He is 1.3×10^{-6}. Therefore, if the observed concentration of ^{3}He is due to He bubbles which might be formed during a manufacturing process, the number of He required in the area of the beam spot is 3×10^{17} to 8×10^{18}. However, He gas was never used in the whole manufacturing process from rutile to Ti rods, at Nippon Mining Co., Ltd. How could it be happened that the He atoms in 5×10^4 cm^3 of air can be concentrated in the small region of the Ti rods ?

The effects of contamination of ^{3}He in D_2 gas should be considered, also. Since no information on the ^{3}He contamination in the D_2 gas was available, the upper limit of ^{3}He is assumed to be equal to the quantity of tritium; the T/D ratio in the D_2 gas was less than 10^{-14}. In the D_2 gas loading process, about 4000 cc of gas was absorbed into a Ti rod. The number of ^{3}He atoms in the gas is, then, less than 10^9, that is again far below the required number. The number of ^{3}He in the residual gas in the D_2 gas loading system after pumping is estimated, from the quantity of ^{3}He in air, to be less than 10^5 atoms.

^{3}He nuclei that are produced and stop in the target as the reaction residues of the D(d,n)^{3}He reaction cannot contribute to the yield of the sharp peak at all, since a dueteron bombardment of 10 mC in electric charge on the target with D/Ti=2 only produces 7×10^9 atoms of ^{3}He which is far below the required number of 10^{13}. In fact, we have lots of targets with which the 14.1-MeV peak cannot be seen at all.

Finally, we have inferred that the ^{3}He concentration was produced by nuclear transmutation during the D_2 gas loading, *i.e.*, by the so-called cold fusion, since, as discussed above, neither the normal production in the bombardment, nor the existence in D_2 gas and Ti can explain the ^{3}He concentration. The occurrence of cold fusion is not widely accepted, mainly because of the lack of reproducibility. In the present work, we found only three rods of TiD_x having particular spots of the dense ^{3}He area, out of 12 rods; this indicates again the poor reproducibility. Although we have not yet specified conditions under which ^{3}He is produced in Ti, the following is common to the three cases showing the sharp peak: (1) The TiD_x rod with $x > 1.3$ was bombarded. (2) A peripheral region of the split section of the rod was bombarded. (3) The peak disappeared when the beam position was changed to a central region of the split section.

5. Conclusion

In conclusion, the sharp proton peak, observed in the 150-keV deuteron bombardment on highly deutarated Ti, is attributed to anomalous ^{3}He concentration which is considered to be produced during the D_2 gas loading into Ti, *i.e.*, "cold fusion". The present observation shows that the concentration of ^{3}He is severely limited to some particular places and seldom occurs.

The author would like to thank to Mr. Kawasaki for developing the D_2 gas loading technic in the early stage of the experiments.

References

1. M. Fleischmann and S. Pons, J. Electroanal. Chem., 261 (1989) 301
2. S.E. Jones, E.P. Palmer, J.B. Czirr, D.L. Decker, G.L. Jensen, J.M. Thorne, S.F. Taylor and J. Rafelsji, Nature, 338 (1989) 737
3. References on cold fusion compiled by E. Storms, Fusion Tech., (1992) to be published
4. A. Krauss, H.W. Becker, H.P. Trautvetter, C. Rolfs and K. Brand, Nulc. Phys., A465 (1987) 150
5. J.L. Yarenell, R.H. Lovberg and W.R. Stratton, Phys. Rev., 90 (1953) 292
6. J.F. Ziegler, The Stopping and Ranges of Ions in Matter, Vol. 3 and 4, Pergamon Press, 1980

Evolution of Tritium from Deuterided Palladium Subject to High Electrical Currents

T.N. Claytor, D.G. Tuggle, and S.F. Taylor
Los Alamos National Laboratory, MS-C914
Los Alamos, NM 87545, USA

ABSTRACT

An increase in the tritium level was detected in deuterium when various configurations of palladium foil or powder and silicon wafers or powder were subject to a high pulsed current. The deuterium, at over one atmosphere pressure, was circulated in a sealed loop containing the cell and an ionization chamber to measure the tritium increase as a function of time. Over 4800 hours of data, spanning 10 cells (including deuterium and hydrogen controls), were collected with this system. Average tritium production has varied from 0.02 to 0.2 nCi/h. Due to experimental constraints we have not been able to measure neutron output with these cells while simultaneously measuring the tritium increase. The question of tritium contamination in the palladium has been primarily resolved by the development of techniques that allow the palladium powder or foil to be reused. Various methods for increasing the tritium production, such as, increased current density, surface modifiers, and higher deuterium loading, will be discussed.

1. INTRODUCTION

The anomalous appearance of small amounts of tritium has been repeatedly observed in electrolytic and solid state gas loading experiments[1,2,3,4,5]. Some of these results were obtained with gas loaded discharge tubes operated at 25 kV, some with voltages as low as 50 V in electrolytic cells and some with only cyclic hydriding and dehydriding of metal. The only readily

FRONTIERS OF COLD FUSION

common features in all the experiments are the presence of palladium (or other metal), deuterium and a disequilibrium condition for the deuterium. We will report on our tritium generation results from the Pd-Si-D cell when it is subjected to periodic unipolar current pulses. The primary advantages of this experiment are that it is reproducible, produces readily detectable tritium levels in a few hours or days and offers the possibility that it could be much more efficient. In our previous work, all tritium data was obtained in a batch mode, here we will, primarily, discuss our latest tritium results with a new, more sensitive, on-line tritium monitor.

Some have criticized[6] the detection of tritium because the signals are insignificant, tritium is seemingly omnipresent, and the palladium metal is subject to possible tritium contamination. We will briefly discuss the possible avenues for contamination and show that each is negligible in the experiments described. The magnitude of the signals discussed in this paper are multi-sigma and are often over a hundred times the tritium background in the supply gas. Furthermore, tritium may be the most sensitive and rapid indicator of anomalous nuclear behavior in deuterided metals. As such, it is well suited for rapid parametric investigations.

2. MATERIALS

The detailed analysis of our materials (Pd,Si,D2) has been described previously[1]. For this work we used, exclusively, either the Liquid Carbonic or Cryogenic Rare Gases deuterium that has less than 0.15 nCi/l of tritium. The major impurity in the deuterium is H_2 (0.6%). Major impurities in the Engelhard palladium are oxygen (980 ppm) Chlorine (80 ppm), Nitrogen (65 ppm) and Carbon (47 ppm). All other major impurities are (each) under 35 ppm by weight. A total of 159.3 g of palladium powder was used in our recent experiments described in this paper. Of that amount, 38.5 g was used in various control experiments to test for tritium contamination. A total of 43.2 g of palladium foil (99.9%) from Johnson and Matthey was used in the foil cells; 0.44 g of this foil was checked for tritium contamination.

The 220 micron thick foils were always annealed at 850 C for 2 h at 10^{-6} torr before use. These foils have been hydrided, dehydrided and annealed seven times and show neither a monotonic decrease nor increase in tritium production. Palladium powder can also be reused in experiments once it has been reoxidized at 623 K.

Tritium contamination in the palladium was tested by three independent methods: dissolution and scintillation counting[7], hydriding and dehydriding and measurement[8] of ^3He. By these means we can assign an upper limit on tritium contamination of 0.005 nCi/g (i.e., no tritium detected within experimental error).

The silicon powder is a conchoidally fractured ,monosized, sieved, intrinsic silicon with a particle size of 10 to 20 μm. Added to the silicon powder was 3% (wt) of either PVA or Dow XUS 40303 binder. These binders, ethanol solvents and silicon powder were tested for tritium contamination. No tritium could be detected over background. It has been found that the Dow binder contains a significant (300 ppm) amount of sulfur. The binder can be reduced during cell operation releasing the sulfur.

In this report, cells 39 and 40 were made of alternating layers of palladium foil and silicon wafers, while cells 41, 42 and 46 were constructed with palladium and silicon powder. A typical cell, made with powders, might contain 12 to 21 grams of palladium in eight layers and 6 to 8 grams of silicon distributed between seven layers. The palladium powder for cell 46 was pressed (11.2 MPa, 2000 psi) into disk form and then oxidized, in air, at 623 K for 2 hours (weight gain of 0.37%).

3. APPARATUS

Shown in Figure 1 is the stainless steel gas analysis loop containing a three liter ion gauge and a 310.9 cc calibration volume. The pressure gauges, ion gauge and sample and room temperatures are recorded on a computer log at 110 s intervals. In operation, a solid state cell would be attached to the loop and hydrided in situ with deuterium or hydrogen or a mixture of gas. The pressure drop during hydriding indicates the stochiometry of the PdD_x. The environmental chamber also enables us to heat (500 K) and cool (200 K) the sample allowing various levels of stochiometry.

The Femtotech ion gauge rejects pulse type radioactive events that effectively discriminate against radon and cosmic ray ionization. Prior to this study, the Femtotech background was usually between 1.8 and 2.2 nCi/l and had a low drift, initially (0.006 nCi/l-hr). It should be noted that the present instrument was calibrated with a gamma source so that the intrinsic drift rate of the loop would be as low as possible. Two 2 micron filters are installed at the inlet of the ion gauge and at the outlet of the cell to

eliminate spurious responses due to particulates.

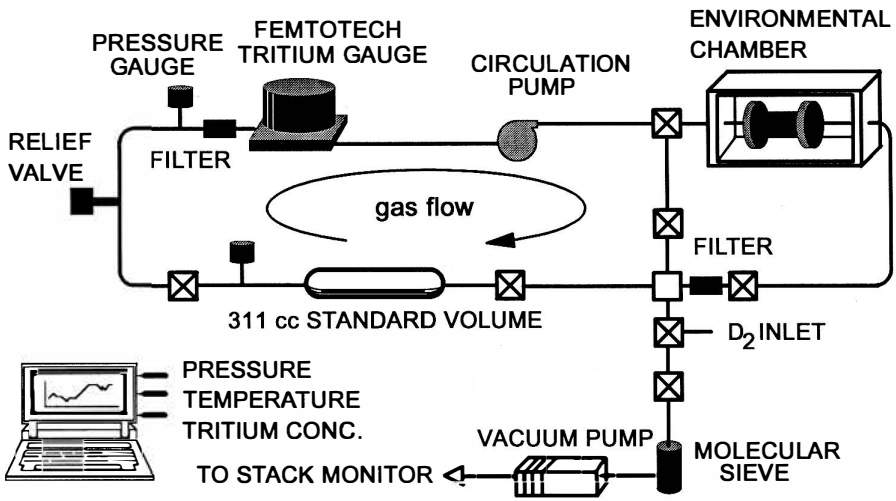

Figure 1. Tritium analysis system used in this study.

4. PROCEDURE

The procedure for hydriding a cell was to first fill the 3 l loop with deuterium gas at 600 to 1200 torr and measure the background tritium concentration, if possible. The gas would then be circulated around the loop for several days to determine if the apparent background rate is increasing. If the drift rate was less than 0.06 nCi/h then the loop was judged sufficiently clean to initiate a new powder-powder cell experiment. With the loop drift rate measured, fresh deuterium was introduced into the loop and the cell hydrided slowly with the deuterium flowing in the loop.

After the cell had been hydrided, the gas was circulated with the cell in place from 15 minutes to several days to again determine the background drift rate. Repetitive voltage pulses were then applied to the cell at 100 pps with a width of 200 us. Typically, the foil-wafer cells were run at 200 V and currents up to 25 A, while the powder-powder cells were run at 800 V at 1 A.

To dehydride the samples, the environmental chamber temperature was increased to 473 K. This caused the majority of deuterium to be released from the palladium. A final dehydride could be accomplished by closing off the cell evacuating the loop and then opening the hot cell to vacuum. The last 6-10% of the deuterium could be recovered by this method.

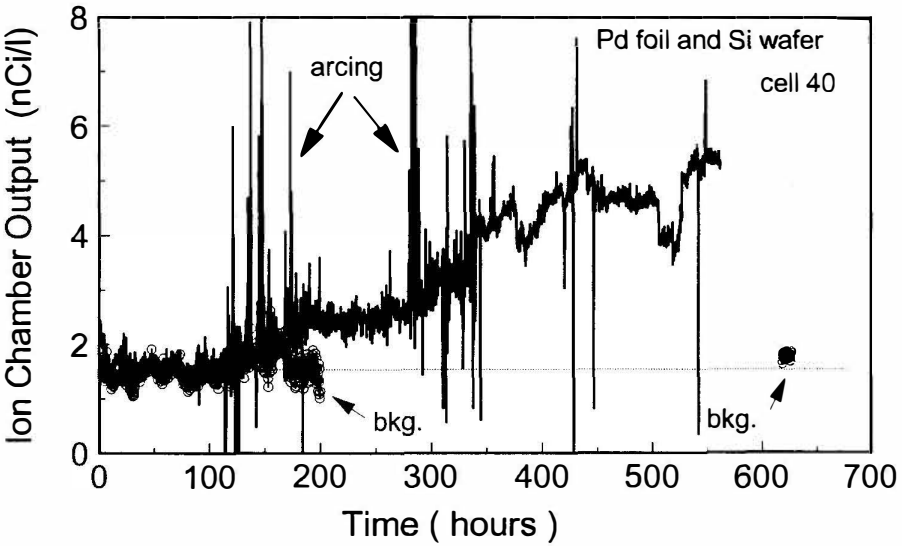

Figure 2. Comparison of background and foreground results with palladium foil.

5. RESULTS

Shown in Figure 2 is the time evolution of tritium from the first palladium foil cell (40) to be run in the system after the Femtotech was connected to the computer. Figure 2 shows the background (open circles) level (prior to run 40) and the foreground level, with cell 40 but without current excitation, for nearly 110 h. The curves are nearly identical. After 110 h the cell was pulsed at 170 V at 5 A. The onset of the pulsing is indicated by the large current spikes due to ionized gas that entered the ion chamber. During this time the tritium output increased until about 200 hours when the voltage was turned off. The pulsing was halted because it was unclear what effect the large ion pulses were having on the background tritium level. However, at 200 hours there is a clearly different tritium level for the background and for the cell. The background run only extends contiguously from 0 to 200 hours because it was taken prior to the running of Cell 40 and it was unknown how long experiment 40 would continue. From 200 to 290 hours the current was off and the tritium level remained relatively constant. At 290 hours the voltage pulsing (400 V at 12.5 A) was again resumed resulting in large current spikes. After about 350 hours the cell stopped arcing; however, the tritium level continued to increase. The Femtotech was rezeroed at 375 hours

resulting in a sudden drop in the reading. After 450 hours the current was discontinued. Finally at 560 hours the cell was dehydrided. Immediately after the dehydride, the old deuterium was pumped out and replaced with fresh gas. The background tritium level with the fresh gas is seen to be within 6% of the initial value. The total amount of tritium in this cell was then determined to be about 10.2 nCi or 0.043 nCi/h. Prior to this, the loop drift rate was less than 0.006 nCi/h. Therefore, the generation rate with the cell was about a factor of 7 over the background.

A summary of the next series of experiments is shown in Figure 3. Cell 41 was run immediately after cell 40 and was a control cell consisting of 20 g of palladium powder (native oxide) and 10 g of silicon powder pressed into disks and placed in a cell to be deuterided but not pulsed. The first 24 h after cell 41 was hydrided showed no increase in tritium level at room temperature. Therefore, in an attempt to outdiffuse any intrinsic contamination out of the loop, cell or palladium, it was decided to heat the cell to determine if the tritium level would increase. An immediate rise in tritium level was noted when the cell was heated. This was not unexpected because hot gas and water vapor emanating from the cell causes deadsorption of tritium on the walls of the system loop. After 210 h cell 41 was completely dehydrided resulting in a total increase of 7.2 nCi or 0.034 nCi/h or slightly less than the foil cell. However the foil cell was run near room temperature (308 K) rather than 423 K. After cell 41 was removed and the old deuterium pumped out, fresh deuterium was introduced into the loop at 600 torr and circulated in the loop (no cell) at room temperature for 210 h. The drift rate with this gas was 0.006 nCi/h (lower curve Figure 3).

Next, cell 42 was prepared as a standard (native oxide) 8 layer Pd-Si cell and was hydrided with fresh gas. The gas was circulated through the loop and the cell for 15 minutes to let the Femtotech stabilize and then the current was applied resulting in an almost immediate rise in the tritium level as shown in Figure 3. The temperature of the cell did not rise enough (5 °C) to notice any significant dehydriding of the palladium. The pulsing conditions were initially 1000 V, 0.1 A (chosen to mitigate the possibility of breakdown of the cell). As the experiment continued, the voltage and current were increased slowly (to 1200 V). After 210 h the voltage was discontinued and the cell dehydrided by raising the temperature to 200 C. The excess tritium in the cell and the average rate of generation was 25.1 nCi and 0.11 nCi/h respectively for

the gas (DT).

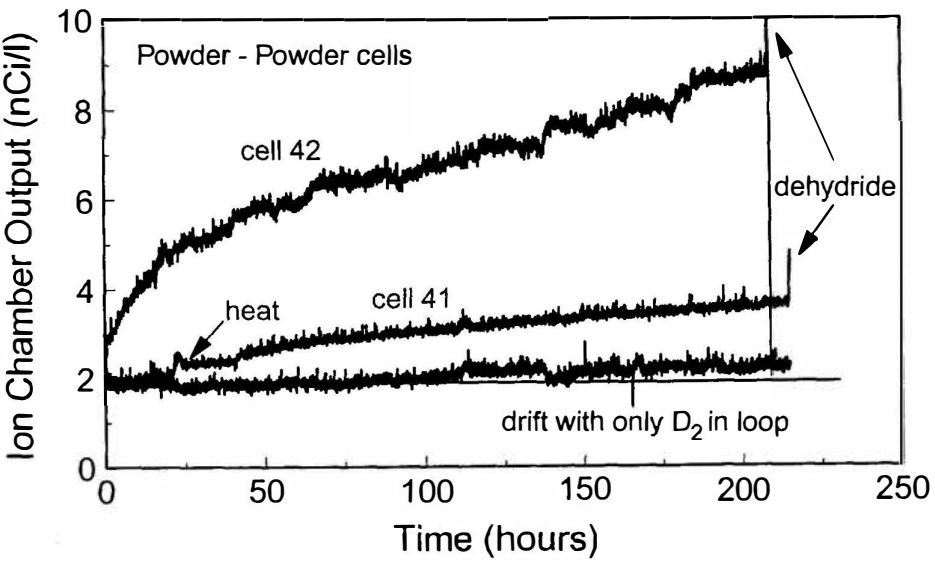

Figure 3. Comparison of background, hot control cell and active powder cell.

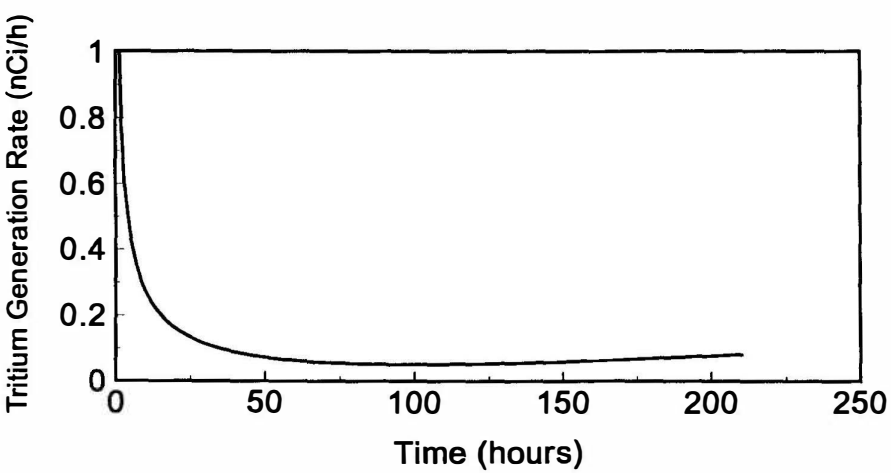

Figure 4. Tritium generation rate from cell 42.

Figure 4 shows the tritium generation rate for cell 42 as a function of time. Two features are evident, the initial rate of tritium evolution can be

as much as 10 times the average rate and the rate at long times increased slightly perhaps due to the increased pulsing current. The nonlinear slope is directly observable in Figure 3. The slope for the control cell, by comparison, appears to be approaching an asymptote typical of a source of tritium diffusing out of the wall of the vessel.

After cell 42, it was found that the loop was severely contaminated with TDO and the drift rate with hydrogen or deuterium in the loop was nearly the same as with cell 42. Repeated flushes and heating of the system were required to clean up the loop. If we attribute all the post run tritium to cell 42 we find that the cell produced a total of 173.8 nCi (1.08 nCi/h). Ultimately, the drift rate of the system could be reduced only to about 0.03 nCi/h, much higher than the 0.006 nCi/h drift rate found prior to cell 42.

The experimental run with cell 46 clearly illustrates the problems that the tritiated water generated in these cells can cause in the loop. Shown in Figure 5 is a comparison of the tritium output from cell 42 and 46.

Cell 46 was hydrided at 258 K to retain any water vapor that might be generated during the exothermic hydride process. After about 5 hours the liquid nitrogen dewar ran empty and the temperature rose releasing the water vapor resulting in a quenching of the ion gauge and an apparent decrease in output. However, the ion gauge reading recovers after about 10 hours. At the time indicated in the figure, the pulser was started, resulting in a further increase in the tritium level.

At 140 hours the current was raised abruptly to 1 A. The generation rate of tritium increased after this change. After 210 h the experiment was terminated and the cell was dehydrided resulting in 21 nCi detected in the gas. The cell was then dehydrided and was disconnected from the loop. Once the cell had been disconnected, the gas flow rate in the loop greatly increased due to the removal of the palladium and silicon powder plug. The increased flow caused the ion chamber output to swing negative and then positive. The chamber output eventually stabilized at 29 nCi/l or a total of 81 nCi.

It should be noted that the powder used in cell 46 was reused from a hydrogen control cell (43). Because cell 43 was run after cell 42 and the contamination from 42 was not fully appreciated, the drift rate on the hydrogen control was unacceptably high (0.095 nCi/h) but the reused powder from cell 46 still exceeded this value if only the TD is taken (0.136

nCi/h) and very much exceeded the value if all the tritium (TD+TDO) detected is taken into account (0.47 nCi/h).

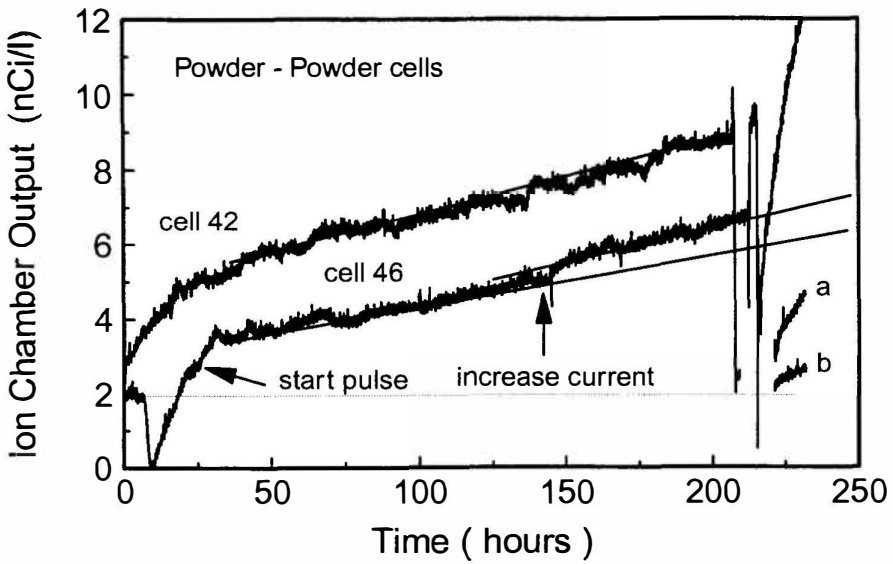

Figure 5. Tritium generation from cell 46 and 42.

Also shown in Figure 5 is the background and drift rate in the loop with just hydrogen immediately after cell 46. A section of this curve is labeled "a". As can be seen, the background is elevated from the nominal value of 2 to about 2.8 nCi/l and the drift rate of the loop is much higher than any of the backgrounds without cells. After 2 hot flushes of hydrogen the drift rate and background are as shown in segment "b". It is seen that the drift rate has decreased and the initial background is nearly equal to the "normal" value of 2 nCi/l. This is very strong evidence that cell 46 put tritium into the system. It was found that 7 or more flushes were required to return the loop to a low drift state with dry hydrogen. However, with wet (0.1% H_2O) hydrogen four or more additional flushes are necessary before the source of tritium seemed to be exhausted.

6. DISCUSSION

Tritium has been detected in these Pd-Si systems when excited by unipolar pulses. There are four

plausible sources for the excess tritium. The tritium could be contamination in the palladium, silicon or binder, the tritium could be hiding in the loop, the tritium could be coming out of the cell container and finally the tritium could be generated in the palladium.

Since no tritium could be detected in any of the materials the possibility that the loop or the cell body is contaminated has to be considered. The cell bodies were heated to 473 K in deuterium with all constituent parts except for the powder. No excess tritium could be detected in this test.

The next most likely source of excess tritium is from hideout in the loop itself. The loop has been previously exposed to tritium for calibration purposes and other cells have generated copious amounts of tritium that may have diffused into various parts of the system. In one test, (during the cleanup after cell 42) the Femtotech was valved off from the rest of the loop and showed no drift (< 0.02 nCi/h) but when the valves were opened to the loop the tritium level immediately rose and the drift rate increased to 0.12 nCi/h. The loop was heated to 423 K for this test to promote cleanup.

Another possibility is that the ionization gauge may be directly affected by some agent originating in the cell such as water vapor, CO_2 or carbon deposits caused by the arcing. It is unlikely that the carbon deposits could have migrated to the ion chamber to cause enhanced leakage since the background after cell 40 was very close to the initial value. It is also very unlikely that there would have been enough of a change in the composition of the gas to change the ionization efficiency by any significant amount since additions of CO_2 (1 to 5 torr out of 1200 torr) are undetectable by the ion chamber. The fact that the chamber did not drift with the valves closed yet the system was drifting indicates that contamination of the ion chamber itself is not the primary factor. Furthermore, it is apparent that the ion chamber can be quenched by the presence of water, but we have no evidence that leakage current due to adsorbed water on the probe insulator will give anything other than a negative reading.

From what has been discussed above it should be apparent that the loop contains various reservoirs for TDO hideout and storage. We believe the storage is of TDO rather than TD based on our extensive experience with similar systems that have been exposed to high levels of gaseous tritium. These systems can be cleaned up quickly and without the problems we have

experienced here.

The TDO is released slowly over a period of days as the material exchanges with normal water or is deadsorbed from the surfaces of the loop. Many flushes of hydrogen or deuterium are required to remove the water and to return the loop drift rate to a low level.

Cell 41 and 42 should be viewed as cells that were run with a relatively clean system containing very little adsorbed TDO. The drift rate as seen in Figure 3 was low initially and after cell 41 but very high after cell 42. We attribute this to the formation of TDO in cell 42 and also in cell 46 due to the oxide layer on the powder. Foil cells have no oxide and did not exhibit this effect.

Since the TDO was not present in the loop initially, it must have come from the powder. The TDO had to be generated in the cell because the powder has no detectable tritium. It is not clear at this point if this implies a faster reaction at the surface (near the oxygen), but clearly the TDO was generated in the first 24 to 50 hours of operation. After that, the apparent rate of tritium generation is influenced by the exchange and deadsorption rate of the TDO.

7. CONCLUSIONS

A reproducible method of tritium generation has been demonstrated. The tritium output scales with the current applied to the cells. The tritium yield is found to depend strongly on the type of palladium metal used (powder or foil). Various tests for tritium contamination confirm that there is no initial tritium contamination in the powder, foil, or other materials used in this study.

Annealing of the palladium seems to be necessary to reactivate foils after a deep dehydride. Lower values of stochiometry or lower gas pressures are less efficient for the generation of tritium. In the experiments conducted to date, tritium production is not enhanced by increasing the concentration of hydrogen in the deuterium gas.

On the basis of an analysis of all our experiments and those of others[9] it appears that the tritium is produced during the dehydriding of palladium deuteride with a surface impurity layer. The layer in the case of the powder and the foil may be an oxide or a monolayer of adsorbed CO. Other impurity layers such as metals may be much more effective. The main effect of the current is to dehydride the palladium by heating. Only a small area near the surface is important to this process. The foil is less productive than the powder

because of smaller surface area and the fact that the surface barrier is largely absent. In the powder cells, the rapid decline in tritium production at the start of the experiment may be due to the depletion of the favored oxygen sites at the interface. The only purpose of the silicon is to provide a non ohmic heat source near the palladium surface. Arcing is less efficient than cyclic heating because the arcing essentially melts the palladium resulting in a complete dehydride, the material then would have to be reannealed to become active. However, partial dehydriding within the two phase region preserves the activity of the material.

If our conclusions are correct, it should be possible to construct much more efficient cells with less material. More robust partially permeable surface modifiers are available and microfabrication of the palladium would allow rapid hydride-dehydride cycles.

8. REFERENCES

1. Claytor, T. N., Tuggle, D. G., Menlove, H. O., Seeger, P. A., Doty, W. R. and Rohwer, R. K. Tritium and Neutron Measurements From Deuterated Pd-Si, AIP Conference Proceedings 228, Anomalous Nuclear Effects in Deuterium/Solid Systems, Jones, S., Scaramuzzi, F. and Worledge, D., (Eds) Provo Ut., 1990, p 467.

2. Claytor, T. N., Tuggle, D. G., Menlove, H. O., Tritium Generation and Neutron Measurements in Pd-Si Under High Deuterium Gas Pressure, Conference Proc. Vol 33, The Science of Cold Fusion, Bressani, T. et. al. (Eds.), SIF, Bologna, 1991, p 395.

3. Bockris, J. O'M., Chein, C., Minevski, Z., Tritium and Helium Production in Palladium Electrodes and the Fugacity of Deuterium Therein, Contained in these proceedings.

4. Wada, N. and Nizhizawa, K., 1989, Nuclear Fusion in Solid, Japanese Journal of Applied Physics, Vol. 28, No. 11, p L 2017.

5. Lanza, G., Bertolini, V. Vocino, E., Parnisari, E., and Ronsecco, C., Tritium Production Resulting From Deuteration of Different Metals and Alloys, Conference Proc. Vol 33, The Science of Cold Fusion, Bressani, T. et. al. (Eds.), SIF, Bologna, 1991, p 151. See also Adachi, G. in these

proceedings.

6. Huizenga, J. R., Cold Fusion Scientific Fiasco of the Century, University of Rochester Press, ISBN 1-878822-07-1, 1992.

7. Cedzynska, K., Barrowes, S. C., Bergeson, H. E., Knight, L. C., and Will, F. W., 1991, Tritium Analysis in Palladium With an Open System Analytical Procedure, Fusion Technology, Vol 20, No 1, p 108, and private communication.

8. Pohts, J., December 1992, private communication.

9. Yamaguchi, E., Nishioka, T., 1990, Cold Nuclear Fusion Induced by Controlled Out - Diffusion of Deuterons in Palladium, Jpn. J. Appl. Phys., Part 2, Vol 29, No 4, p L666.

Tritium and Helium Production in Palladium Electrodes and the Fugacity of Deuterium Therein

John O'M. BOCKRIS
Chun-Ching CHIEN
Dalibor HODKO
Zoran MINEVSKI

ABSTRACT

An account is given of the massive production of tritium at a Pd electrode. Production continued for ~ 750 hours after which time it was arbitrarily curtailed. Production of T was found to cease every few days but could be resuscitated by increasing the overpotential of the electrode reaction. A logarithmic relation between the rate of tritium production and the overpotential of the electrode reaction was established. The Will-Cedzynska method of examining T contamination in specimens has shown that nothing above the background of T was detected if no D_2O had been electrolytically evolved on the Pd specimens concerned.

Helium production was found to accompany that of T. The He was analyzed by thermal expulsion and mass spectroscopy. No He^3 was found but He^4 was measured in nine specimens out of ten examined. Voids were also detected ~ 1 micron within the electrode. The excess tritium production on Pd co-deposited with deuterium was found.

Cracking and spreading of cracks is shown. An attempt was made to calculate the amount of hydrogen trapped in cracks and to calculate the standard free energy of trapping.

1. Introduction

For the studied phenomena it is desirable to make a set of simultaneous measurements of heat, neutrons, tritium, helium, x-rays and gamma rays. However, economic considerations have made it necessary to measure only one or two of these quantities.

The most obvious proof of cold fusion is the production of tritium from deuterium and we have gone principally in this direction. Recently, our group has observed an electrode which yielded T at ~ 10^4 times above the background. This paper deals with the production of tritium which continued for three weeks and was intentionally interrupted. Also, it was found that T production is accompanied with He production. Further, possible excess tritium production on Pd co-deposited with

FRONTIERS OF COLD FUSION

deuterium is considered as well as the speculations on the mechanism of reaction and conditions favorable to reach high fugacities inside the Pd electrode. Cracking of Pd electrode and trapping of hydrogen is also considered.

2. Methods

The principal method used in this investigation was a potentiostic one. The total potential applied to the cell was controlled and measured by a d.c. power supply. Cell potential, Pd electrode potential and current were measured by using Digital Multimeters and continuously monitored on XY-t recorders.

3.1. Production of tritium and helium

Experimental. The palladium electrodes were pre-treated by etching in dilute nitric acid and then treated electrochemically by applying a positive potential. The liquid scintillation counter was used for tritium measurements which was equipped with a chemiluminescence counter and indicated its own efficiency.

Helium analysis were done on palladium samples, which had shown tritium production. Also, analysis were done on platinum anode samples and non-electrolyzed Pd electrode samples. These were packed in solid CO_2 and sent to Rockwell International, Los Angeles, California for He^3 and He^4 analysis by mass spectrometry.

Results and Discussion. The usual procedure, for the initiation of tritium production was to charge the Pd electrode cathodically, at -0.05 V (vs. RHE) after the anodic pre-treatment. As shown in Fig. 1. there was no increase in tritium activity. The increase in cathodic direction triggers the reaction and a steady increase in tritium activity was observed. The initial, almost linear, relationship between tritium activity and time, is shown in Fig. 1, and this represents the results of two cells, A and B, run in parallel. The maintenance of a continuous increase in tritium activity, triggered by small increases in applied potential, has not been recorded previously though, T activity in a burst-like manner has been observed.

Tritium production reached its maximum of $3.8 \cdot 10^7$ T atoms s^{-1} cm^{-2} after 327 h of electrolysis, Fig. 2. The reaction was quenched at 406 h, when D_2O was added. Tritium production restarted again at 471 h of electrolysis with no potential increase.

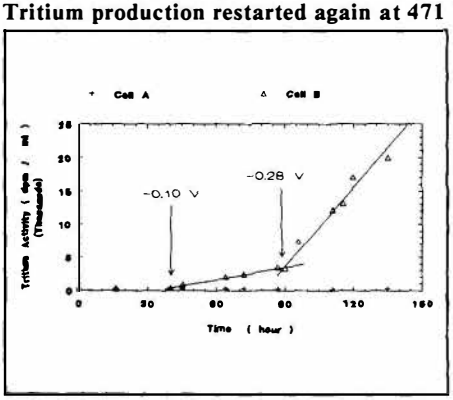

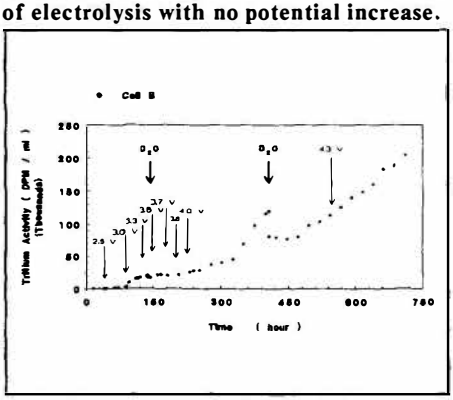

Figure 1. Tritium activity measurements vs. time at the initial stage of electrolysis: Cell with no (+) T in excess and ( ) high levels of T production.

Figure 2. Recording of the tritium events during one month of continuous tritium production in cell B. Arrows indicate voltage adjustments.

After the addition of heavy water tritium production ceased for two days. The reaction was quenched for the second time after 406 h of electrolysis and the decrease in T activity was observed due to dilution. An incubation period of 65 h was needed for the reaction to restart again.

From Figs. 1. and 2., four intervals of constant rate of tritium production may be recognized. A relation between overpotential and the rate of tritium production is shown in Fig. 3. The value of the slope is 4.5 ($F/(2 \cdot 2.303 \cdot RT) \sim 8.2$). In the sense of a Tafel slope, then, the present result $-\frac{4RT}{F}$.

Tritium contamination of Pd virgin material was also examined. A summary of results is shown in Table 1. For this purpose virgin Pd was dissolved in aqua regia and liquid scintillation analysis of distilled samples were done. The method used, was the one developed by F. Will and K. Cedzynska and both, the closed apparatus for dissolution of Pd as well as the one for distillation were similar to those described in ref. [1].

Table 1. Tritium analysis of the bulk of virgin Pd rod.

Sample # 01	Sample # 02	Sample # 03
$4 \pm 3 \cdot 10^8$ T-atoms/g Pd	$3 \pm 3 \cdot 10^8$ T-atoms/g Pd	$4 \pm 3 \cdot 10^8$ T-atoms/g Pd

It is important to note that tritium measurements before the start of electrolysis were also done and the results are shown in Table 2. No increase in T activity was observed in the electrolyte after anodic pre-treatment.

Table 2. Typical tritium activity analysis of the 0.1 M LiOD electrolyte before and after anodic pretreatment.

T-activity before anodic pretreatment DPM / ml	T-activity after anodic pretreatment DPM / ml
12 ± 3	12 ± 3

An attempt was made to restart T production after ceasing the electrolysis. All tritium results are summarized in Table 3. However, no further T production was found.

After intentionally stopping the electrolysis, a Pd electrode, which produced tritium, was transferred into liquid nitrogen and was kept there for one week. Then it was removed and cut into 5 pieces for further analysis. Fig. 4. shows how the Pd electrode was cut and the position of cut discs used for He^3 and He^4 analysis as well as for some other analysis.

Disc #5 was cut for He^3 and He^4 analysis.

All samples, with and without thermal treatment showed positive findings of He^4. The data in Fig. 5. represent the amounts of He^4 released by the specimens that exceeded the average amount released or desorbed during the analysis of the Rockwell control specimens. Excess of He^4 was observed in 9 out of the 10 electrolyzed palladium samples from electrode which produced tritium. In the case of He^4 there was no interference as far as the production of an HD artifact is concerned. However, an HD artifact interfered with the signal for He^3. It is assumed that the interference with He^4 does not occur because of better resolution between He^4 and hydrogen isotope signals.

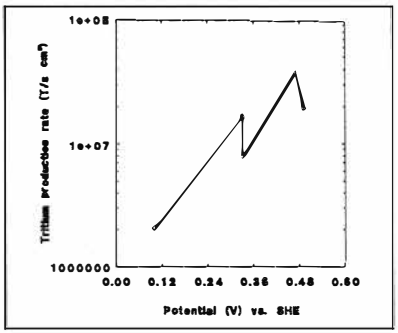

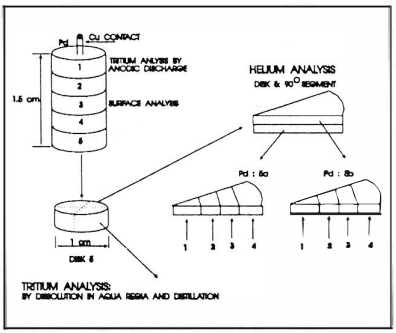

Figure 3. Tritium production rate dependence on electrode overpotential.

Figure 4. Pd electrode which produced tritium: cutting diagram and annotation of samples used in subsequent analysis.

Table 3. Summary of tritium results.

T_{total} in ELECTROLYTE	T in GAS PHASE (assuming $T_g/T_l=5$)	T in Pd (by dissolution in aqua regia)	T in Pd (by anodic discharge method)
$1.6 \cdot 10^{14}$ T-atoms or $1.5 \cdot 10^{13}$ T-atoms/g or $2.5 \cdot 10^{13}$ T-atoms/cm^2	$8.1 \cdot 10^{14}$ T-atoms or $5.4 \cdot 10^{13}$ T-atoms/g or $1.2 \cdot 10^{14}$ T-atoms/cm^2	$5.1 \cdot 10^{9}$ T-atoms/g Pd (or total in Pd=$7.6 \cdot 10^{10}$ T)	$8 \cdot 10^{9}$ T-atoms/g Pd (or total in Pd=$1.2 \cdot 10^{11}$ T)
TOTAL AMOUNT OF T PRODUCED (ELECTROLYTE, GAS, BULK)		~ 10^{15} T-atoms or $6.9 \cdot 10^{13}$ T-atoms/g or $1.5 \cdot 10^{14}$ T-atoms/cm^2	

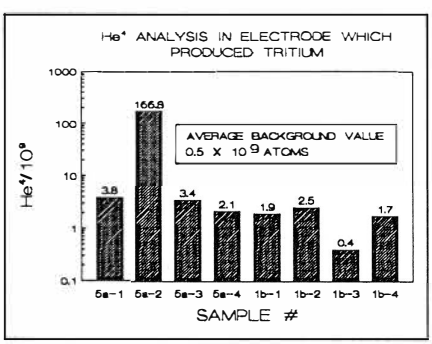

Figure 5. He^4 analysis in electrode which produced tritium.

Thus, were needed samples were thermally pre-treated prior to analysis. In this way mass spectra collected were free from any interference of residual hydrogen isotopes.

3.2. Tritium produced on Pd co-deposited with deuterium

Experimental. Another type of experiment was performed in order to check the possible excess of tritium production. The electrolysis started at low current densities of 2.5 mA cm^{-2} in order to avoid a too fast Pd dendrite growth. Within the next 5 hours the current density was increased to 25 mA cm^{-2}, which was followed by a large potential change from c. -0.02 V to -0.8 V vs. RHE.

Results and discussion. If the obtained results are compared with previously published data for deuterium evolution on Pd [2] it is then obvious that Pd deposition took place with simultaneous deuterium evolution at high overpotentials. Also within the first 40-50 hours of electrolysis a highly dendritic layer of Pd was visible at the electrode and was approximately 2-3 mm thick.

It is known that a change in tritium concentration occurs due to the additions of fresh D_2O containing background levels of T and due to the removal of tritium by electrolysis. The later depends on the isotopic separation factor of tritium and deuterium, S, [3]:

$$\frac{n_T(t)}{n_T(0)} = S - (S - 1)\exp(-\frac{t}{\tau}) \qquad (1)$$

This equation assumes that the amount of tritium added to the solution is equal to the rate of tritium removal by electrolysis. In equation (2) .. is the tritium build-up time constant given with the following expression:

$$\tau = \frac{S n \cdot V}{R} \qquad (2)$$

where n is the concentration of D_2O in mole dm^{-3}, V is the volume of the cell in dm^3 and R is the rate of deuterium production in the solution, R = I/2F. The D/T separation factor on Pd is in the range of 1.7 to 2.2, and in this case a value of 2 was taken.

Fig. 6., shows the change in tritium concentration, both for the liquid and gas phases during the two weeks of electrolysis. For comparison, theoretical lines as calculated from equations (1) and (2) are also shown in this figure. A burst type of excess tritium production was observed in the gas phase. At the same time or with the delay a burst in the solution phase occurred. A summary of T production observed in four out of six investigated cells is given in Table 4. The only cell which did not demonstrate excess tritium production is cell E shown in Fig. 7.

It is important to note that in both cells where no excess of T was found, a Cambridge D_2O was used. However, in previous cold fusion-positive results an Isotech D_2O was used [4] as in the cells A, B and C.

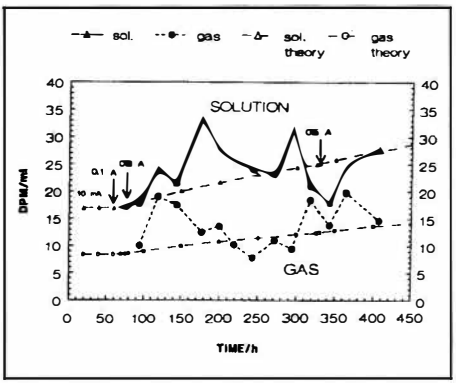

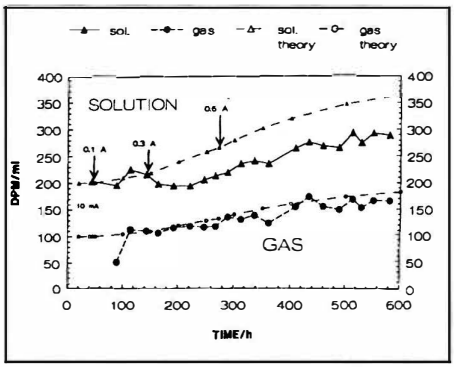

Figure 6. CELL A: T bursts in the liquid and gas phases during 2 weeks of electrolysis in 0.05 M $PdCl_2$/0.3 M LiCl; dashed lines-theoretical values.

Figure 7. CELL E: T bursts not observed during the two weeks of electrolysis.

Table 4. Summary of excess tritium findings in cells A, B, C and D.

CELL	INITIATION TIME hours	BURST #	BURST DURATION hours	GAS PHASE $T_g/T_{g,b}$	SOLUTION $T_s/T_{s,b}$	RATIO T_g/T_s	COMMENT
A	35	1	120	2.1	1.6	0.83	bursts in gas phase preceed bursts in solution
		2	80	1.8	1.3	0.93	
B	32	1	140	2.4	2.1	0.67	both gas and liquid above T_{th} during whole experiment
		2	70	1.6	1.7	0.51	
C	17	1	130	2.1	1.7	0.80	gas phase constantly ca 80% above T_{th}
		2	90	1.6	1.2	0.91	
D	25	1	135	1.5	1.0	1.52	T bursts both in gas and liquid phases; decreased with time of electrolysis

3.3. Presence of D in voids

Experimental. The potentiostatic current proportional to the rate of deuterium permeation is measured in a specially constructed permeation cell. Here, deuterium is evolved on the cathodic side of a bi-electrode, Pd membrane, and the permeating deuterium is oxidized, anodically on the other side.

Results and discussion. Working on the permeation of deuterium through the Pd metal as a function of time, results, have been observed, which indicate the embrittlement and damage of Pd. Time variation of the current is interpreted in terms of changes in the metal structure caused by absorption of deuterium. This method allows the determination of permeation current, P, diffusion coefficient, D, and the solubility of hydrogen corresponding to a certain fugacity which in turn corresponds to the overpotential according to following equations:

$$D = \frac{0.693 \cdot L^2}{t_{\frac{1}{2}}} \qquad (3)$$

$$P_{\infty} = \frac{FD(C_0 - C_L)}{L} = \frac{FDC_0}{L} \qquad (4)$$

Fig. 8. shows spreading of cracks. The first and the second micrograph are taken after 2 and 4 hours of electrolysis on the mirror polished Pd disc, from the outer area of the electrode inward. The rate of crack spreading corresponds to the diffusion coefficient of deuterium into the Pd metal. The third one shows the appearance of cracks after etching in nitric acid.

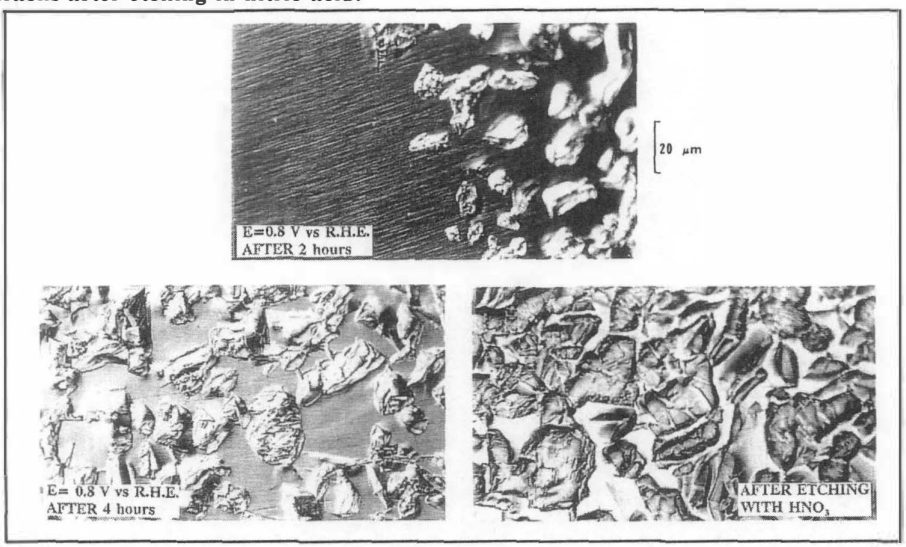

Figure 8. Micrographs, obtained by differential interference contrast microscopy, of mirror polished Pd after 2 and 4 hours of hydrogen evolution, and after etching in HNO_3.

In Fig. 9. the permeation of deuterium as a function of applied potential in the solution of pH=13. Each point represents the steady state current obtained at the corresponding potential. The increase in permeation current is observed with the subsequent increase in potential. A decrease in permeation current is seen from Fig. 8. and this clearly indicates that at higher overpotentials the permeation of deuterium is associated with the onset of deuterium embrittlement.

The permeation-time transients below and at critical potential are shown in Fig. 10. At lower potentials a typical permeation-time transients are obtained, without any noticeable difference except in the permeation value. These transients are reproducible. However, it was found that there is a threshold value of the deuterium potential when the permeation-time transient exhibits a maximum, Fig. 10., and when an attempt to repeat a transient has failed.

The question what happens at this so-called critical potential has already been addressed [5] and it is assumed that at this potential a critical concentration of D is dissolved and as this level is reached, some kind of change in metal lattice occurs. Taking in account the fugacity of D_2 in the metal, it seems reasonable to conclude that the process corresponding to the maximum of the permeation-time relationship is the spreading of microcracks.

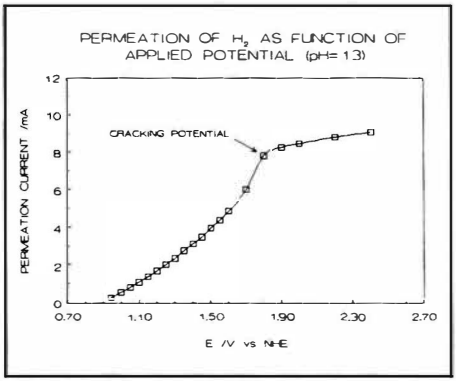

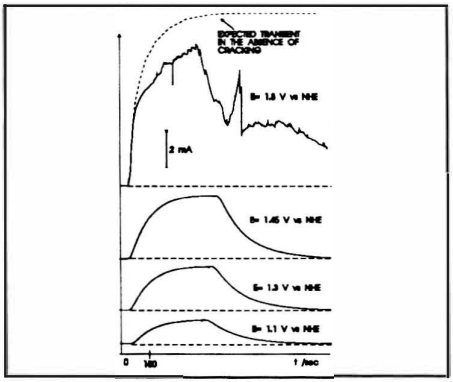

Figure 9. Permeation of H_2 as a function of applied potential.
Figure 10. Permeation-time transients exhibiting normal behavior and cracking.

By following the model of Bockris and Subramanyan [6] of this anomalous permeation it is possible to determine the quantity of trapped hydrogen and the standard free energy of trapping. The trapping reaction can be represented as

$$D + \square \rightarrow D_{tr} \tag{5}$$

and the equilibrium is attained when

$$C_{D,tr} = K^1 C_{\square} C_{D,L} \tag{6}$$

where $C_{D,tr}$ and $C_{D,L}$ is the concentration of D in traps and in the lattice sites, respectively. C.. is the concentration of unfilled traps, while K^1 is the equilibrium constant. For a given concentration of lattice D, the number of filled traps at equilibrium will be proportional to $C_{D,L}$ and so

$$C_{D,tr} = KC_{D,L} \qquad K = K^1 C_{\square} \tag{7}$$

The differential equation which describes the lattice diffusion with trapping is based on the fact that diffusion from one trapping site to another does not occur by direct jump without the intermediate stage of diffusion through the lattice sites:

$$\frac{\partial C_{D,L}}{\partial t} + \frac{\partial C_{D,tr}}{\partial t} = D\frac{\partial^2 C_{D,L}}{\partial X^2} \tag{8}$$

and by taking in account previous equations for $C_{D,L}$ and $C_{D,tr}$ it follows that

$$\frac{\partial C_{D,L}}{\partial t} + \tau K\frac{\partial C_{D,L}}{\partial t} = D\frac{\partial^2 C_{D,L}}{\partial X^2} \tag{9}$$

and

$$\frac{\partial C}{\partial t} = \frac{D}{(1 + \tau K)}\frac{\partial^2 C}{\partial X^2} \tag{10}$$

The last equation can be solved assuming that the entry of D into the lattice is a fast process and that the trapped D will always be in equilibrium with lattice dissolved hydrogen (C_0) and hence the numerical constant τ is 1. The boundary conditions are:

$$at\ X=0,\ for\ t>0,\ C = (1 + K)C_0 \tag{11}$$

and

$$at \quad X=L, \quad for \quad t>0, \quad C=0 \tag{12}$$

The solution is

$$C(X,t) = (1 + K)C_0 \,(A - B) \tag{13}$$

where

$$A = \sum_{n=0}^{\infty} (-1)^n \, erfc \, \frac{(X + 2nL\sqrt{1 + \tau K})}{2\sqrt{Dt}} \tag{14}$$

and

$$B = \sum_{n=0}^{\infty} (-1)^n \, erfc \, \frac{(-X + 2L + 2nL)\sqrt{1 + \tau K}}{2\sqrt{Dt}} \tag{15}$$

and the permeability is given as:

$$P_{tr} = \frac{DfC_0}{L} \frac{2}{\pi^{\frac{1}{2}}} \left(\frac{L^2}{Dt}\right)^{\frac{1}{2}} \exp\left(-\frac{L^2(1 + \tau K)}{4Dt}\right) \tag{16}$$

The last equation shows that at relatively short times the trapping permeation is smaller than normal permeation. Also, once the trapping is switched on the permeability decreases from the normal one and gives rise to the prominent hump in the build-up permeation transients, Fig. 10. From this figure it can also been seen what would be an expected normal transient if cracking did not occur (dashed line). The steady state permeability was obtained after 90 minutes.

In order to obtain the total amount of trapped deuterium the area between the extrapolated and the actual transient is calculated for charge. The trapping constant, K, is calculated by knowing the charge of trapped hydrogen, Q, the permeation area, A, thickness of the membrane, L, C_0 and C_{crit} which is the solubility of H calculated from the transient which does not and which exhibits the cracking, respectively. Thus, from

$$K = \frac{2\,Q}{AL(C_0 - C_{crit})} \tag{17}$$

and

$$C = \frac{PL}{zFD} \tag{18}$$

where P is permeation and D diffusion coefficient, $D=1 \cdot 10^{-6}$ cm^2 sec^{-1}.
It turns out that $C_0=2.38 \cdot 10^{-3}$ mole cm^{-3}, $C_{crit}=1.97 \cdot 10^{-3}$ mole cm^{-3}, Q = 45 C, A = 1 cm^2, L= 0.025 cm. And so the trapping constant is K=0.93.

Now, in order to get the equilibrium constant the concentration of traps is calculated assuming that the density of microcrack or Stroh cracks is 10^8/cm^2 [6]. Further from Fig. 8. the length and the width of the cracks is taken to be approximately 10^{-3} and 10^{-4} cm, respectively. Thus, the internal surface are of the crack and the number of metal atoms therein is calculated. Lastly, the density of traps per cm^3 and concentration of traps is calculated. So, the C of traps is $3 \cdot 10^{-6}$ mole dm^{-1}. Hence, the equilibrium constant is calculated to be $K^1=3.1 \cdot 10^5$. From here then the standard free energy of trapping is obtained as

$$\Delta G = - RT \ln K^1 = - 31.33 \; kJ \; mole^{-1} \tag{19}$$

which is equivalent to - 7.5 kcal mole^{-1}. This value seems to be in good agreement with the standard free energy of solubility of hydrogen in Pd found by Fullenwider to be - 4 kcal mole^{-1}, [7].

From C_{crit} and Sievert's low it is possible to calculate the critical pressure needed to expand a microcrack:

$$p_{D_2 crit}^{\frac{1}{2}} = \frac{C_{crit}}{K_s} \tag{20}$$

where K_s is Sievert's constant equal to $8.8 \cdot 10^{-9}$ mole$^{-1/2}$. Thus, for the above value of C_{crit} the value obtained for p_{crit} is $5 \cdot 10^4$ atm.

4. Discussion

It is not unusual to observe high Tafel slopes [2]. The logarithmic dependence of the rate upon overpotential and the rational slope indicates that the rate determining step for the passage of tritium into solution is a charge transfer mechanism which probably involves a reverse proton discharge mechanism. An explanation for the high tritium production on Pd, based on the influence of the amount and the type of impurities on the mechanism of deuterium evolution reaction on Pd surface has already been proposed [2,4,8].

It is important to note that according to the above calculations, deuterium is mostly located in voids and cracks and not in the bulk of the electrode. From the experimental results and Sievert's law it is shown that the critical pressure to expand the microcrack is $5 \cdot 10^4$. This is in good agreement with the critical pressure of $3 \cdot 10^4$ [8] used to calculate the fugacity in the order of 10^{17} atm. Thus, it is possible to obtain in the void space high fugacities, while the pressure remains below that for cracking.

There is evidence that the phenomena reported depend upon the surface structure. Thus, the surface structure would determine the path and rate-determining step of deuterium evolution and this in turn is known to determine the fugacity developed in voids. Thus, the high fugacity in voids theory connects up the times of waiting for switch-on, the sporadicity of the results, and the fact that clean solutions do not give good results but dirty ones sometimes do.

5. References

1. K. Cedzynska and F.G. Will, Investigation of Cold Fusion Phenomena in Deuterated Metals, Final Report, Technical Information Series PB91175885, Vol I, p. I-80.
2. J.O'M. Bockris, D. Hodko and Z. Minevski, Proceedings of the II Annual Conference on Cold Fusion, p. 337, June 29 - July 4, 1991, Como, Italy.
3. G.H. Lin, R.C. Kainthla, N.J.C. Packham, O. Velev and J.O'M. Bockris, Int. J. Hydrogen Energy, 15 (1990) 537.
4. C.C. Chien, D. Hodko, Z. Minevski and J.O'M. Bockris, J. Electroanal. Chem., in press.
5. W. Beck, J.O'M. Bockris, J. McBreen and L. Nanis, Proc. Roy. Soc., A290 (1966) 220.
6. J. O'M. Bockris and P.K. Subramanyan, J. Electrochem. Soc., 118 (1971) 1114.
7. M.A. Fullenwider, Thesis, University of Pennsylvania, Philadelphia (1969).
8. J. O'M. Bockris, D. Hodko and Z. Minevski, presented at 180th Meeting of The Electrochemical Soc., Oct. 13-18, 1991.

Reproducible Nuclear Reactions during Interaction of Deuterium with Oxide Tungsten Bronze

K.KALIEV, A.BARABOSHKIN, A.SAMGIN, E.GOLIKOV,
A.SHALYAPIN, V.ANDREEV, P.GOLUBNICHIY
Institute of High-Temperature Electrochemistry,
620219, Ekaterinburg
RUSSIA

ABSTRACT

The possibility of essential increase of rate of carring out nuclear reactions with participance of deuterium in solids representing solid electrolytes with cation-electronic conductivity has been shown in the paper. It is found out that strict maintenance of experiment parameters leads to completely qualitatively reproduced results: generation of neutrons and heat at introduction of deuterium into the system.

1. Introduction

Begining with the famous work of Fleischmann and Pons on cold fusion /1/ the investigators of anomalous nuclear phenomena in condensed matter did not succeed in getting 100 % reproduction of the results on observation of emission of nuclear reactions products. All these experiments were carried out with solids on the basis of systems metal-hydrogen, neither the structure nor crystallographic orientation being non controlled. Unlike all other experiments carried out earlier for achieving of high level of reproduction we used principally new materials as investigation objects: monocrystals of oxide tungsten bronzes (OTB) of non stoichiometric compounds, having general formula Na_xWO_3. The facet (100) of the crystal was a working surface and the channels of rigid W-O sublattice being perpendicular to it. Alkali metal cations are placed and can move in these channels. In dependence on the content of alkali metal in OTB in consequence of change of valent state

FRONTIERS OF COLD FUSION

of tungsten in sublattice W-O, electronic conductivity of OTB can very greatly. It allows to create structures with high gradients of composition and properties conditioned by it.

2. Methods

Natrium may be extracted from channels in surface layer of bronze crystal and replaced by hydrogen ions by electrochemical methods (anodic treatment in salt melts, water solutions or vacuum).

The main part of experimental installation is a hermetic chamber of stainless steel. Anode and cathode consisted of tungsten plates situated one over another are inserted into the chamber. Monocrystal of natrium tungsten bronze of $Na_{0.9}WO_3$ composition in the form of a plate 10 x 10 x 2 mm in size was placed on anode. The plate was cut out of monocrystal grown by electrolysis of polytungsten melt according to the technique worked out by us /2/ in such a way that natural facet (100) was a working surface. At mounting of the installation the gap of 2 mm between the working surface of crystal and cathode was kept.

The measurement of neutrons flow were taken by means of 2 independent channels: 2 blocks of 4 counters of SNM-42 type with paraffine retardant. These blocks were placed at both sides of the chamber, their signals being summed by digital recorder and were led out independently at the register tape. Summary efficiency of 2 blocks was about 1.4 %.

Crystal temperature was measured by chromel-alumel thermocouple made of wires 0.1 mm in diameter.

After placing the crystal on the surface of anode the chamber was hermetized and evacuated up to 10^{-6}-10^{-5} mm Hg. After that anode with the crystal was heated up to 720-760 °C and direct voltage 500-1000 V was switched on between anode and cathode and passing current was registered. Such anodic treatment lasted for 1-5 hours and suumary amount of electric charge was 0.1-1.0 C. After switching off current the crystal was cooled to room temperature and deuterium (or hydrogen) was introduced into the chamber till the pressure becomes 1 mm Hg. The introduction moment considered as a zero point of counting and was registered at the tapes of registration of neutrons flow and temperature. Restarting of digital neutron recorder was being produced at the same moment. In 10 minutes the chamber was vacuumed once more and registration of neutron flow and crystal temperature was going on.

Then the cycle was repeated. Up to 15 cycles were carried out at one crystal.

3. Results

Neutron flow intensity after deuterium introduction increase sharply and in 10-20 min registration does not exceed the background (fig. 1).

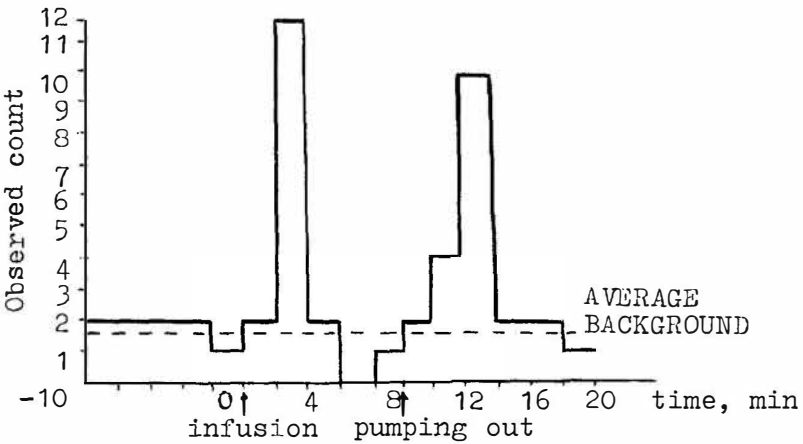

Figure 1. Typical observed neutron production

Always one can choose 2 minute interval during the first 5 min, when average intencity of neutron flow essentially in several times exceeds the background.

Just the same neutron impulse but with less intensity is observed after begining of pumping out.

Thus, for example, in one of the last series of 4 experiments with one and the same monocrystal (total) number of exceeded 100 those with positive results) average neutron emission was fixed during 2 min $(800\pm300)n$ at infusion and pumping out (650 ± 300) n at ratio of signal to the background 8 and 6 correspondingly. In one of control experiments the flow $(3.6\pm1.3)\cdot10^4$ N/min was fixed. In the experiments with hydrogen excess of neutron flow over the background was not uncovered.

The increase of crystal temperature takes place synchronically with introduction both hydrogen and deuterium. The front of temperature increase for deuterium is more steep, temperature jump (ΔT) varies in great limits, reacing sometimes 40-50 °C for deuterium. In the series of experiments at one and the same crystal, in which after deuterium infusion in repeated cycle

hydrogen infusion, was conducted, it was determined that temperature jump for deuterium is higher than that for hydrogen.

4. Discussion

The main result of the work is getting out to the level of qualitative reproduction of experiment, when performance successivness of operations with monocrystal of OTB described earlier leads to one and the same reply at predicted up to 1 min time: generation of neutrons and heat in the experiments with deuterium and neutron generation stops 10-20 min later. Thus single action causes the effect happenning only once.

If to suggest that the reaction generating neutrons occurs at the expense of deuterium, absorbed by the channels of crystal at introduction, that all current at anodic treatment is spent for natrium extraction and the number of deuterium atoms N, absorbed by the crystal is equal to the number of extracted natriun atoms (at passing of 1 C of electricity 0)

$$N = \frac{Q \cdot N_A}{F} \approx \frac{1(C) \cdot 6 \cdot 10^{23} \ (at/mol)}{96500 \ (C/mol)} \approx 6 \cdot 10^{18} \text{ D atoms},$$

(F - Faraday of electricity, N_A - Avogadro's number), thus the average neutron emission rate per deuteron pair (DD) at infusion

$$\Lambda = \frac{400/60 \ (n/s)}{3 \cdot 10^{18} \ (DD)} \approx 2 \cdot 10^{-18} \ n \ (S)^{-1} \cdot (DD)^{-1}.$$

5. Conclusions

The results of the work allow to come to a new level of experiment: determination of qualitative dependences between the process parameters, that will give the opportunity to find out the mechanism of the phenomenon observed and to discover the ways of realization of controlled process.

6. References

1. Fleischmann, M. and Pons, S., 1989, Electroanal. Chem.,261, 301.
2. Kaliev, K.A. and Baraboshkin, A.N., 1982, In: Oxide Bronzes.Moscow, 137.

Is Reported "Excess Heat" Due to Nuclear Reactions ?

David B. BUEHLER, Lee D. HANSEN, Steven E. JONES and Lawrence B. REES
Departments of Chemistry, Electrical Engineering and Physics
Brigham Young University
Provo, UT 84602

ABSTRACT

A portable X-ray detector has been developed to complement "cold fusion" studies. Our reasoning is that any set of nuclear reactions which produce measurable heat must also produce abundant secondary X-rays. However, at the Nagoya meeting and elsewhere, we found that errors and uncertainties in current experiments prevent unambiguous interpretation of claims of excess-heat generation. Hence, this paper also outlines criteria for establishing calorimeter performance for definitive measurements of "excess heat" in cold-fusion experiments.

PORTABLE X-RAY DETECTOR

Nuclear reactions are characterized by release of MeV-scale energies, hence their importance to power-production schemes. (Chemical reactions typically involve eV-energies, down by a factor of 10^6 from nuclear reactions.) But energy release at the nuclear level implies that secondary x-rays will be produced, since only tens of keV are required to generate x-rays. If nuclear reactions are indeed producing heat at the levels claimed ($>$ 1mW), then sufficient x-rays should be produced to be detectable. The x-rays arise from the ionizing effects of nuclear products on the materials in which the heat develops. Thus, x-ray measurements may provide a crucial test for the presence of heat-generating nuclear reactions.

Characteristic x-rays of Pd or Ni (for example) which result from K shell vacancies produced by fast nuclear products are readily detected using a 10mmX10mm photodiode. The energy of the x-rays provides information on what reactions are taking place. (For example, if the Ru K-alpha line at 19.2 KeV is strong, one may surmise the production of Ru.) A typical response spectrum for this detector is shown in Figure 1. Note that the noise level is well below the nickel K-alpha line (7.5 keV) and the Pd K-alpha energy (21.1 keV). The detector is small enough (2.8 cm-diameter X 3 cm long) to fit next to or even into an operating cell. Furthermore, it operates well near room temperature.

A Monte Carlo computer code was written in order to estimate the number of x-rays detected near an electrolytic cell in which one of several fusion reactions occur. The cell is assumed to be cylindrical in shape, to have glass walls, and to contain a cylindrical palladium (or nickel) electrode immersed in D_2O. The number of x-rays detected per fusion event is calculated.

FRONTIERS OF COLD FUSION

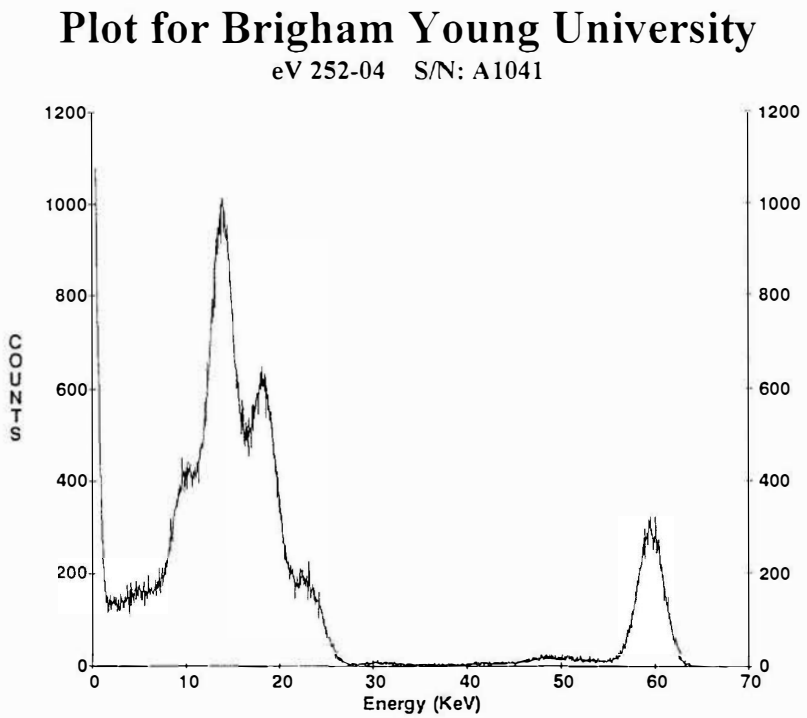

Source	^{241} Am
Photodiode Size	10 x 10 mm
Bias Voltage	+40 VDC
Shaping time	3 μsec
Oper. temp.	+20^{0} C
FWHM	4.4%

Fig. 1: Typical x-ray energy spectrum from small x-ray detector.

The input parameters are:
·rod radius and length
·thickness of the surface layer in which fusion events occur
·distance from center of cell to rod
·cell radius and height
·glass thickness
·reaction: d+d-->p+t, d+d-->n+^{3}He, d+^{6}Li-->2α, d+^{7}Li-->n+2α
·detector aperature (assumed to be square)
·distance from center of cell to detector
·quantum efficiency of the detector
After these parameters are determined, the program follows the charged particles event by event.

First a fusion site is determined. This site is randomly selected from points within the specified skin thickness of the palladium electrode. (End effects are neglected.) The skin thickness may be set to the electrode radius in order to model fusion events occurring uniformly throughout the volume of the electrode.

Then the direction of the first outgoing charged particle is randomly selected and the particle is stepped through the palladium rod. At each step the energy is calculated using the proton stopping powers of Zeigler, Biersack, and Littmark, *The stopping and ranges of ions in matter*, Pergamon Press, New York (1985). The stopping powers of other ions are determined from proton values by using Z^2 scaling. At each step, the K-shell ionization cross section is calculated using ECPSSR cross sections from Chen and Crasemann, *At. Data and Nucl. Data Tables*, **33**, 217, and Chen from Johansson and Campbell, *PIXE*, Wiley, New York (1988). The x-ray production cross section is then calculated by multiplying the ionization cross-section by the fluorescence yield. The cross section for ions other than protons is determined by taking Z^2 times the proton cross section for the same energy per nucleon.

From the cross section, an x-ray production probability is determined. Since the cross sections are very small, the probability is augmented by a suitable factor which is later divided out of the results. (This is equivalent to making each "event" correspond to a large number of identical fusion events.) On the basis of this probability, it is determined at each step whether or not an x-ray is emitted.

If an x-ray is emitted it is determined if the x-ray is a K-α or K-β x-ray on the basis of the β/α ratio. The direction of travel is then randomly chosen. The x-ray is followed along this direction through the electrode, D_2O, and glass to the detector. Each event is then given a weight corresponding to the overall attenuation factor. The sum of such weights then represents the total (fractional) number of detected x-rays.

Since K-α and K-β x-rays have different attenuation factors, they are summed separately so as to provide an estimate of the numbers detected in each peak.

Whether or not an x-ray is emitted at a given step, the ion continues its path through the electrode. Each ion is then followed until it stops or leaves the electrode, the possibility of x-ray emission being considered at each step. If more than one charged particle is produced in the fusion event, the second particle is tracked in a similar fashion.

EXAMPLE: Fusion occurs at the rate of 10^{11} events per second (10^{-1} W assuming d-d fusion) in the volume of a 1.0 mm diameter Pd wire, 3.0 cm long. The average path of x-rays through D_2O is 2.0 cm and through glass is 2.0 mm. The detector is 3.0 cm from the Pd wire.
5.86×10^5 K-α x-rays make it to the surface of the Pd each second.
The solid angle factor is 0.00774
Transmission through the D_2O is 0.307
Transmission through the glass is 0.378
Detector efficiency is 0.115
The product of the last four factors is 1.03×10^{-4}, so 60 K-α x-rays per second are detected. This is of order 10^2 above the sensitivity limit imposed by typical backgrounds.

We strongly encourage use of x-ray detectors in connection with cold-fusion experiments in order to determine the presence of nuclear reactions. Our detector including multi-channel analyzer board and portable computer cost only about $5,500 so that expense should not be a major obstacle to its use. This detector system was developed at the suggestion of Dr. Tom Passel of EPRI.

OUTLINE OF CRITERIA FOR ESTABLISHING CALORIMETER PERFORMANCE FOR MEASUREMENT OF "EXCESS HEAT" IN COLD-FUSION EXPERIMENTS

The calorimetrist has the responsibility to conclusively demonstrate the accuracy and precision of the heat measurements. Accurate heat measurement is far from trivial and nothing should be assumed without good justification. Experience shows that gross errors can occur from obscure and difficult to detect effects.

I. A precise and complete description of how the calorimeter functions must be given together with a detailed physical description of the instrument. The physical description must include materials and accurate dimensions for all calorimeter components. The functional description must include the method of heat measurement and a description of the calorimeter system and surroundings.

   A. There are three methods of heat measurement.

      1. In the heat conduction method, the temperature difference across a thermal path with constant thermal conductivity between the system and surroundings is measured. This temperature difference is linearly proportional to the rate of heat flow through the path (Newton's law of cooling). For accurate measurement as much as possible of the heat flow must be through the measurement path. All other heat flow paths must also have a constant thermal conductivity.

2. In the power compensation method, the heat rate is measured by the change in input power required to maintain a constant temperature in the calorimeter when the measured process occurs.

3. In the temperature change method, total heat is obtained by multiplying a measured temperature change in a known amount of material by the heat capacity of the material. If the material is flowing at a known rate, the heat rate is obtained.

B. The calorimeter surroundings may be one of two types.

1. In isoperibol calorimeters, the surroundings are kept constant.

2. In adiabatic calorimeters,the temperature of the surroundings is kept at the same temperature as the calorimeter system so no heat is exchanged.

C. The calorimeter may interact with the surroundings in ways other than heat exchange.

1. The calorimeter may be open and mass may be transported between the calorimeter system and the surroundings. An open system usually is operated at a constant pressure, i.e. atmospheric pressure. At constant pressure heat is equatable with enthalpy.

2. A closed system is also usually a constant volume system where heat is equatable with total energy.

II. Three kinds of experiments have been done in efforts to determine the "excess heat" that may be due to cold fusion.

A. Absolute heat measurements have been made by comparison of the heat effects of the reactions to the heat from an electrical heater. To be accurate, an absolute measurement must meet several criteria.

1. All heat generated in the heater must be transported to the calorimeter system. The amount of heat generated in and lost through the heater lead wires must be negligible or corrected for.

2. All heat transport paths between system and surroundings must be quantified, controlled, and accounted for.

3. The heat distribution in space and time produced by the heater must closely match that from the reactions.

4. Calibrations and tests must be alternated in time and done in approximately equal numbers.

B. Relative heat measurements have been made by comparison of the heat effects of the reactions in control (e.g. light water) and test (e.g. heavy water) systems. Precision is more important than accuracy in such measurements, thus the following criteria.

1. To assess random errors and detect any changes in calorimeter function, controls and tests must be alternated or simultaneous in time, approximately equal in number, and if possible done both in parallel and sequentially.

2. The thermal conductivities of all heat transfer paths must be shown to be the same for both controls and tests.

3. The heat distribution in space and time must be the same for controls and tests.

C. Some experiments have been designed to show that the "excess heat" effect is so large that no conceivable errors or chemical effects could possibly account for the results, and thus the observed heat must come from nuclear reactions. Such experiments require verification by sufficient and proper controls.

III. The calorimeter output signal must be consistent with the heat transfer characteristics of the calorimeter. For example the time constant for changes in the measured heat rate must be the same as the time constant for transport of heat from the calorimeter to the surroundings in a heat conduction calorimeter. Proper functioning of temperature sensors in the calorimeter environment must be verified. As an example, thermocouples are prone to errors caused by chemical corrosion of the junction and by stray electrical currents.

IV. Finally, to verify actual performance, the calorimeter must be tested with a reaction having an accurately known enthalpy change.

V. Because all electrochemical calorimetric experiments intended to demonstrate "excess heat" require correction for the heat of the electrolysis reaction, the expected reaction must be verified and quantified. Otherwise an incorrect value for the thermoneutral potential will be used in the correction. For example, deposition of an alkali metal under a silicate (or aluminate or borate)

coating on an electrode in aqueous solution possible at cell voltages near 3 volts. The thermoneutral potential for Li is about 2.9 volts, compared to 1.5 volts for hydrogen. A negative "excess heat" rate proportional to the rate of deposition of Li would thus be found if the reaction were assumed to be strictly generation of hydrogen. The accuracy of the thermoneutral potential must also be assessed. A value derived from a single source or type of the measurement cannot be considered reliable. Note also that if a lithium layer is deposited on an electrode under a coating (e.g., silicate, borate or aluminate coating) and later should the coating crack, then exothermic water-lithium reactions would result, producing "heat bursts".

"Excess heat" can only be proven to be nuclear in origin by showing that the products of the nuclear reactions are produced at the same time and rate as the heat and in amounts commensurate with the law of mass-energy conservation. X-rays would, however, be a strong indicator of nuclear (MeV-scale) reactions and would be an effective tracer of high-energy reactions when the precise nature of the processes remains hidden. Until such proof exists, application of Occam's razor demands that "excess heat" be regarded as having its source in ordinary chemical reactions.